UNIVERSITY OF PRETORIA
FACULTY OF ENGINEERING, BUILT ENVIRONMENT AND INFORMATION TECHNOLOGY
DEPARTMENT OF MECHANICAL AND AERONAUTICAL ENGINEERING

A Stochastic Hybrid Blade Tip Timing Approach for the Identification and Classification of Turbomachine Blade Damage

Student:
RG Du Toit (11028701)

Supervisor:
Prof PS Heyns
Co-supervisor:
Dr DH Diamond

November 2017

Submitted in Partial Fulfilment of the Requirements for the Degree
Master of Mechanical Engineering

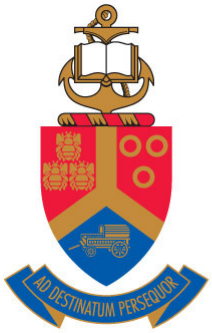

UNIVERSITEIT VAN PRETORIA
UNIVERSITY OF PRETORIA
YUNIBESITHI YA PRETORIA

In loving memory of my grandfather, Charl du Toit, who inspired me to become an engineer.

Summary

A Stochastic Hybrid Blade Tip Timing Approach for the Identification and Classification of Turbomachine Blade Damage

Author:	Ronald Graham du Toit
Student number:	11028701
Supervisors:	Prof PS Heyns and Dr DH Diamond
University:	University of Pretoria
Department:	Mechanical and Aeronautical Engineering
Degree:	Master of Mechanical Engineering

Industry is increasingly confronted by ageing turbomachines nearing their decommissioning dates. These turbomachines are especially prone to unexpected and catastrophic failure, which is often the consequence of rotating blade failures. Thus the failure of a single blade may result in immense safety and financial impacts. The aforementioned points raise further questions with regards to the optimal outage planning of turbomachines. The distinct need to monitor the conditions of turbomachine blades during operation was therefore identified. It was further identified that monitoring of the blade conditions should provide sufficient evidence as to when a blade damage threshold has been reached, therefore providing early warning of imminent blade failure.

Blade Tip Timing (BTT) has existed for many decades as an attractive vibration based condition monitoring technique for turbomachine blades. The technique is non-intrusive and online monitoring is possible. For these reasons, BTT may be regarded as a feasible technique to monitor the conditions of turbine blades. The processing of BTT data to find the associated vibration characteristics is, however, a non-trivial task. In addition, these vibration characteristics are difficult to validate, therefore resulting in questionable reliability of the various BTT techniques. The use of a hybrid blade condition monitoring approach is therefore proposed in this research project. This hybrid approach incorporates a stochastic Finite Element Model (FEM) modal analysis to supplement the BTT results, therefore creating a basis of comparison as the BTT results become available. The aim of this research is to test the ability of the proposed hybrid approach to perform the following processes: blade *damage identification* and *damage classification*.

The use of a new BTT technique based on Bayesian Linear Regression (BLR) was tested on an experimental setup, where the first bending mode of the blades in the rotor assembly were excited. BTT based on BLR assumes a Single-Degree of Freedom (SDOF) model to describe the blade tip displacements. The advantage of the BLR curve-fitting is that it solves for the parameters in this SDOF model as multivariate probabilistic quantities. More so, this technique solves these parameters for each revolution during the measured blade resonance conditions. The use of the multivariate probabilistic quantities in a Monte-Carlo Simulation (MCS) enables the amplitude and phase values of the blades to be derived (also as statistical quantities). The natural frequencies of the blades can then be determined by extracting features from the corresponding amplitude and phase results.

Incremental discrete damage was introduced to a particular blade to test the ability of the proposed technique to track the changes in the derived natural frequencies. Discrete damage was also introduced in the Finite Element Analysis (FEA). Slight variations in the material properties, operational conditions (centrifugal loads) and the geometry of the discrete damage were introduced in the FEA for each damage increment. This ensured that this analysis was stochastic rather than deterministic, thus enabling uncertainty to be modelled. The proposed *damage identification* requires that the change in natural frequencies of the BTT and FEA results as tracked as relative quantities. The changes in blade natural frequencies were inherently due to the increase in discrete blade damage.

The effects of varying blade temperatures and how this would affect the performance of the proposed hybrid approach was also tested. Experimentally, this required the heating of the blades to the desired temperatures, before and during the BTT tests. The FEA incorporated temperature effects by modelling uncertainty in the material properties. The proposed BTT technique was able to detect the decrease in the natural frequencies of the blades due to the increase in temperature. More importantly, the hybrid approach demonstrated that it is general enough to still be applicable with regards to the relative natural frequency tracking (blade damage identification) with varying temperature effects. The relative changes in the natural frequencies from the undamaged, or reference states, of the relevant blades were computed to infer the degree discrete damage as part of a probabilistic damage identification procedure. A probabilistic damage threshold for the damage identification procedure was proposed based on the following question: *What is the probability that the relative change in the natural frequency of the test blade is as large as what the FEM modal analysis (at a chosen discrete damage size) projected it to be?* This probabilistic damage identification procedure was demonstrated for various scenarios, therefore demonstrating the ability of the hybrid approach to infer the degree of blade damage for various scenarios.

The blade *damage classification* process relies on the use of *K-means* clustering. The clustering implementation offers the advantage of a single BTT measurement being sufficient as an indication of blade specific conditions. The FEM natural frequency results were used to initialise cluster centroids and the individual BTT points were assigned to clusters with the closest centroid (based on the amplitude and natural frequencies). The classification of a point to a certain cluster thus provides an indication of the severity of the blade damage. This was done for the BTT tests with and without the effects of varying the blade temperatures. The accuracy of the damage classification implementation seems promising. The decision of whether a damage threshold has been reached for this implementation is purely based on the damage classification of the individual points.

The BTT methodology incorporating BLR proved to be reliable when used as part of a hybrid approach. Furthermore, the advantages of the stochastic nature of the hybrid approach are highlighted in terms of quantifying uncertainty. The proposed hybrid methodology demonstrates the ability to identify and classify blade damage. In doing so, it was possible to determine that a blade damage threshold had been reached. It was therefore shown that the proposed stochastic hybrid approach may offer many short- and long-term benefits for practical implementation. The proposed method therefore offers a feasible turbomachine blade monitoring solution that provides early warning of imminent blade failure.

Keywords: Blade Tip Timing, Bayesian Linear Regression, Clustering, Damage Identification, Damage Classification, Finite Element Analysis, Stochastic, Hybrid Approach, Turbomachines

Acknowledgements

All glory to my Almighty Father who blessed me with the gift of knowledge, the ability to learn and for giving me the daily strength to complete my studies.

"I can do all things through Christ who strengthens me."
Philippians 4:13

The following people's direct contributions, guidance and assistance during the completion of this research project were invaluable:

- As my academic supervisor Prof PS Heyns provided an unrivalled insight into various topics of vibration-based condition monitoring and the vision for the Centre for Asset Integrity Management. It was a privilege working with a global leader in this industry, that not only exhibits a passion for the field, but equally for the people around him. Thank you for inspiring me and for providing me with the wonderful opportunity to pursue my post-graduate studies.
- It was a privilege working with my co-supervisor, Dr DH Diamond, who is an expert in the field of blade tip timing and a visionary of various technologies. I appreciate the time you took out of your busy schedule to share your knowledge and innovative ideas with me. Thank you for also performing the relevant BLR processing of the raw BTT time of arrival data. Without your guidance this research would not have been possible.
- The Eskom Power Plant Engineering Institute (EPPEI) for financial support of this research project. Without your support this project would not have been possible.
- Esteq (Pretoria) for allowing us to use their specialised data acquisition equipment.
- National Instruments (South Africa) for their interest to develop my ability to use their equipment and software.
- Thank you to Miss B Mokoka, the kingpin of the Centre for Asset Integrity Management, for your integrity and advice. I take my hat off to you for working with such diligence and precision while studying part-time. Thank you for your kindness and genuine interest.
- Mr G Breitenbach and Mr H Booysen, thank you for sharing your technical knowledge in the fields of rotating machinery, vibration-based condition monitoring and the relevant electronics.
- Thank you to Mr S Pienaar for introducing me to the LabVIEW environment and for offering insight into many spheres of the research project.

On a more personal note I would like the thank the following people:

- My parents, Dr GJ Du Toit and Mrs D Du Toit, thank you for your utmost interest and support in my academic and personal endeavours. Thank you for being generous, loving, kind parents and always having my best interests at heart. Thank you for your financial support and endless wisdom. This journey would not have been possible without you.
- My fiancée, Miss DJ Tarr, for being the biggest blessing in my life. You are an inspiration and I know God has big plans for your life. Thank you for the endless support, encouragement and excitement that you add to my life. This would not have been possible without you. I love you with a deep love.
- Thank you to my brothers for always keeping me on my toes and for challenging me. Thank you for all your support and for you insight into so many areas of my life.
- Lastly, thank you to all my friends for being the family that I get to choose. You are a crazy bunch, but without you life would be dull.

Note from Author

The text in the main document contains hyperlinked information (for the digital *.pdf* format only). Clicking on the hyperlinks will transfer the reader to the referenced information. The hyperlinks were selected as the same colour as the rest of the text in order to maintain a consistent look. The hyperlinks apply to the following sets of information:

- Preamble information: Table of contents (Chapters, sections and sub-Sections)
- In-text referenced information: Figures, equations, tables, citations, sections or chapters, abbreviations.

Contents

List of Abbreviations

AI Artificial Intelligence

ANNs Artificial Neural Networks

AoA Angle of Arrival

AR Auto-Regressive

BLR Bayesian Linear Regression

BTT Blade Tip Timing

BVMS Blade Vibration Monitoring System

C-AIM Centre for Asset Integrity Management

CBM Condition-Based Maintenance

CDF Cumulative Distribution Function

CFD Computational Fluid Dynamics

CFF Circumferential Fourier Fit

CPSM Casing Pressure Signal Methods

DAQ Data Acquisition Device

ELDV Eulerian Laser Doppler Vibrometry

EO Engine Order

FEA Finite Element Analysis

FEM Finite Element Modelling

FFT Fast Fourier Transform

FM Frequency Modulated

FRF Frequency Response Function

HCF High Cycle Fatigue

HPMs Hybrid Prognostic Models

IAS Instantaneous Angular Speed

IGV Inlet Guidance Vanes

LP Low Pressure

MCS Monte-Carlo Simulation

MPDF Multivariate Probability Density Function

MPR Multiple Per Revolution

NBM Needs-Based Maintenance

NDE Non-Destructive Evaluation

NSMS Non-Intrusive Stress Measurement Systems

ODE Ordinary Differential Equation

OPR Once Per Revolution

PCT Patent Cooperation Treaty

PM Preventive Maintenance

PSR Probe Spacing on the Resonance

RB Run-to-Break

RMSE Root-Mean-Square Error

RUL Remaining Useful Life

SBM Schedule-Based Maintenance

SDOF Single-Degree of Freedom

SG Strain Gauge

SHM Structural Health Monitoring

SPF Stator Passing Frequency

VCCT Virtual Crack Closure Technique

ToA Time of Arrival

VCM Vibration-Based Condition Monitoring

2PP Two-Parameter Plot

3D Three-dimensional

Nomenclature

English letters and symbols

A	BLR tip response equation parameter.
A_n	Response amplitude used in the AR method (mm).
B	BLR tip response equation parameter.
C	BLR offset parameter value.
D_{off}	DC offset in the AR method.
E	Young's modulus (GPa).
K	Reference to a particular discrete crack size.
N	Number of probes or measurements in the BLR derivation.
$p()$	Probability function.
r	Radius from the blade tip to the centre of the shaft (mm).
T	Temperature ($^{\circ}C$).
t	Time (s).
V	Voltage value of the raw signal (V).
x	Blade tip displacement (mm).
X_{dt}	Prescribed damage threshold probability.

Greek Symbols

Δ	Change in a particular value.
δ_{damage}	Difference between the independent BTT and FEM normal distributions.
γ	Angular distance between the first and last probes (radians).
μ	Mean.
Ω	Shaft rotational frequency or IAS (rad/s).
ω_f	Blade excitation frequency (rad/s).
ω_n	Natural frequency of the blade (rad/s).
ϕ_n	Phase at a particular engine order used in the derivation of the AR method (radians).
ρ	Material density (kg/m^3).
σ	Variance.
θ	Angular distance (radians).

Special Characters (Matrix, Vector and Statistical Symbols)

$\boldsymbol{\mu}$	Multivariate mean output of the BTT-BLR process.
$\boldsymbol{\Sigma}$	Multivariate covariance output of the BTT-BLR process.
$\ddot{\tilde{x}}$	Blade acceleration used for the AR method derivation.
$\dot{\theta}$	IAS derived from zero-crossing times (rad/s).
$\hat{\phi}$	Phase output from the MCS (radians).

$\hat{A}$	Response amplitude output from the MCS (mm).
$\mathcal{N}$	Normal or Gaussian distribution.
$\tilde{x}$	Blade tip displacement in the AR method.
$\mathbf{w}$	Vector of target parameters in BLR.

Subscripts

NV	Reference to non-vibrating blades.
i	Specific revolution.
n	Particular section of the shaft encoder.

Chapter 1

Introduction

1.1 Background

Industry is increasingly confronted by ageing turbomachines prone to unexpected and catastrophic failure. This raises questions with respect to safety and optimal outage planning [Mishra et al., 2014] therefore increasing the need for enhanced Remaining Useful Life (RUL) estimations [Liao and Köttig, 2014; Sikorska et al., 2011]. Turbomachine blades (generally low pressure steam turbine blades [EPRI, 1985]) undergo numerous excitations during normal operation. This commonly leads to reduced fatigue life, the risk of crack formation and ultimately an increased risk of blade failure. The most dangerous excitation frequencies should ideally be avoided during the operation of the turbomachines. However, this is not always possible as the turbomachine rotational speeds are ramped up through the blade resonant frequencies [Rigosi et al., 2017]. Traditional turbomachine blade monitoring techniques include metallurgical assessments or the application of strain gauges on blades normally in service for an extended period of time (usually close to or beyond the designated life). These approaches are nevertheless far from ideal as they are largely intrusive and result in undesirable turbomachine downtime [Salhi et al., 2009].

Blade Tip Timing (BTT) is presently considered as one of the most promising techniques for blade condition monitoring, mainly due to its associated low-cost, non-intrusive nature and potential for online application [Rigosi et al., 2017]. Furthermore, the use of BTT creates the possibility to measure the vibrational state of each blade on a particular row of a rotating disk. This is achieved by using a set of proximity probes placed circumferentially around the casing which sense when a blade passes.

The direct application of BTT for vibration monitoring has existed since the 1970s, yet this technology is still maturing [Rzadkowski et al., 2016]. Despite being considered promising, scepticism surrounding this method persists. Diamond et al. [2015] highlights that there is no consensus in published literature as to which BTT method performs the best and what the associated accuracies of these methods are. The reasons for this are related to the difficulty of measuring and validating turbomachine blade vibrations. Rao and Dutta [2012] speculate that unless a BTT technique is made simple and reliable to implement, power plants will not find it attractive to invest on upgrading to this monitoring technique to ensure the safe operation of turbomachines. The following requirements are therefore proposed as a prerequisite for BTT techniques to appeal to industry:

1. Simple implementation of the testing equipment and post-processing methodologies.
2. The chosen BTT algorithm needs to have a proven reliability in terms of its associated accuracy, robustness and generality.

From the aforementioned points it is firstly noted that there is a need for the online and non-intrusive condition monitoring of turbomachine blades. This condition monitoring technique, in essence, needs to provide early warning of imminent blade failure through the *identification* and *classification* of the associated blade damage. The brief background to BTT indicates that this may be a promising approach to doing so, however, a few challenges are associated with the use of this technique. The second need is therefore related to the BTT monitoring technique or approach. This approach needs to meet the criteria outlined by Rao and Dutta [2012] with regards to being simple to implement and having a proven reliability. This dissertation therefore proposes a stochastic hybrid BTT approach for the identification and classification of turbomachine blade damage. The remainder of this chapter motivates various aspects of the proposed methodology by presenting a literature review and the detailed scope of the research.

1.2 Literature Review

1.2.1 Overview

The focus of this study is to propose a practically implementable hybrid methodology incorporating BTT and Finite Element Modelling (FEM) modal analysis for blade damage identification and classification. The literature review aims to provide motivation for the choice of this methodology as well as establishing the theoretical framework for the research project by categorising a number of topics in a logical order. The thought-process behind the problem formulation and the desired research outputs are outlined in the various sections of this literature review. Figure 1.1 gives an overview of the conceptualisation of the research project in terms of the problem identification, the need or opportunity for further research and possible solutions for the problem area. The identification of a general problem area is merely used to provide context of where the proposed solution may be applicable. For the purposes of this study, turbine blades from the power industry are used as an example of a problem area. The need to develop a reliable methodology to prevent the unexpected and catastrophic failure of these turbine blades is then elaborated on. Essentially, the need for an online and non-intrusive blade condition monitoring technique is identified. Lastly, a review of various possible solutions to the outlined problem area and needs are discussed. The proposed solutions focus on the use of Vibration-Based Condition Monitoring (VCM) techniques. The advantages and disadvantages of various VCM are therefore elaborated on, in essence motivating why specifically BTT may be seen as a viable solution to the identified problem area. This framework, discussed above and shown in Figure 1.1, aims to ensure that the literature review remains concise, yet informative and relevant.

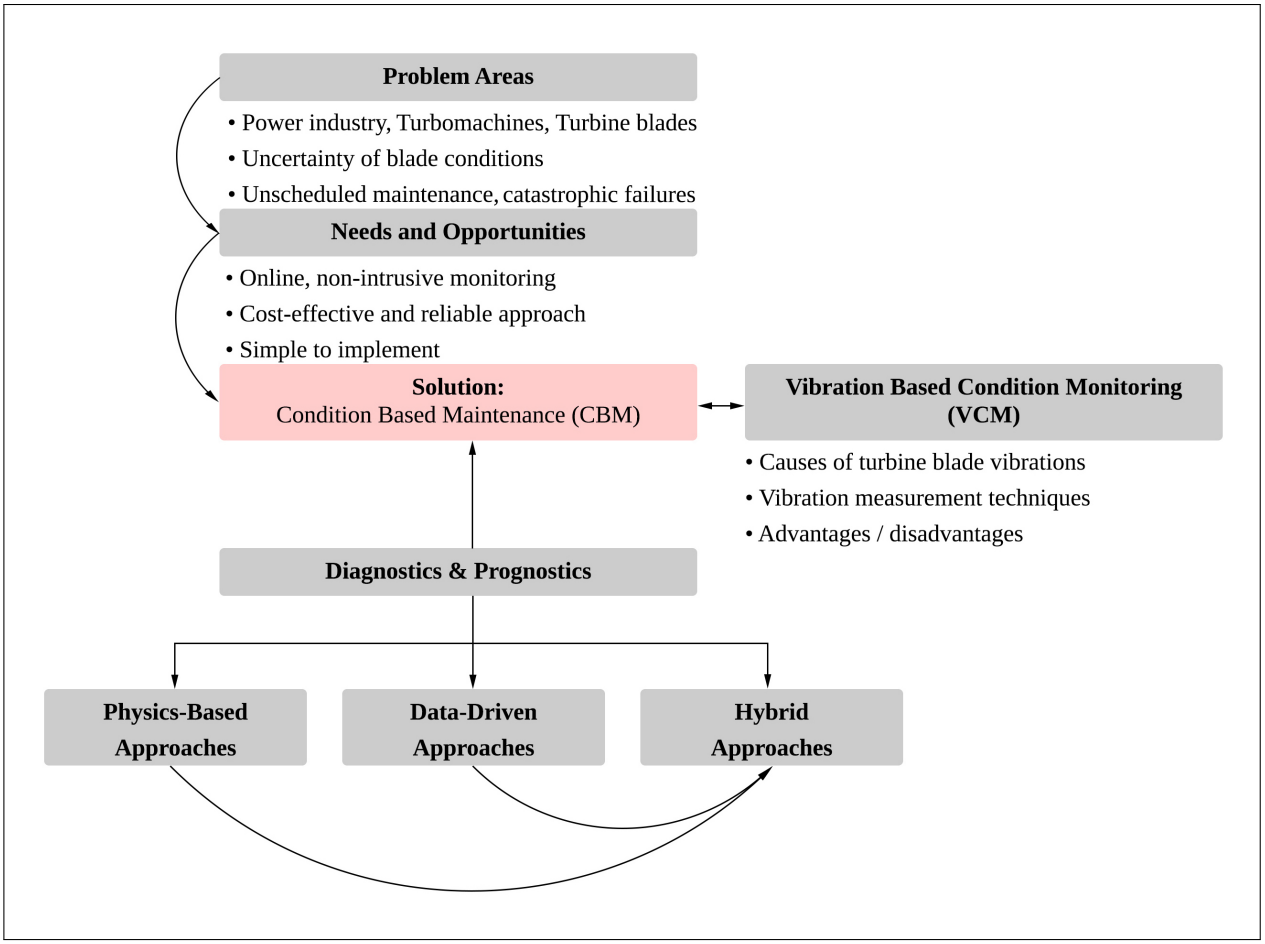

Figure 1.1: Overview of the literature review.

1.2.2 Problem Areas

The undesired downtime of power generation units is largely a result of turbine failures and poorly planned maintenance operations [McCloskey et al., 1999]. According to Gubran and Sinha [2014] the most common cause of failures in rotating machinery or turbomachines is related to blade failures. When considering gas and steam turbines similar conclusions may be reached. The occurrence of gas turbine failures due to blade failures is reported as roughly 42% [Al-Bedoor, 2002]. Diamond et al. [2015] indicate that steam turbines are almost equally susceptible to blade failures, with 75% of these blade failures being Low Pressure (LP) blade failures [EPRI, 1985]. Many mechanisms for blade failure exist, among which the following are reported as common: corrosion fatigue, stress corrosion cracking and fatigue Rao and Dutta [2012]. Turbine blades in the late stages of LP turbines are identified as the most vulnerable to failure as a result of these mechanisms [Das et al., 2003; Rao and Dutta, 2014]. It is highlighted that roughly 30% of LP blade failures are as a result of the accumulation of High Cycle Fatigue (HCF) during both steady and transient operating conditions EPRI [1985]. Diamond et al. [2015] further note that 40% of blade failures have unknown causes, implying they are not well understood and are therefore difficult to prevent.

Figure 1.2a gives three examples of fatigue cracking along the first hook serration in the LP blade roots. Fatigue cracking is deemed common in this area due to the accumulation of HCF damage as a result of transient operating conditions [Booysen et al., 2015]. Blade vibrations and resonance corresponding to critical speeds induce high dynamic cyclic stresses, which causes HCF damage. Figure 1.2b shows the failure of an LP turbine blade due to HCF damage resulting from transient operations. Branco et al. [2015] emphasise that the unexpected failure of a single turbine blade may have catastrophic consequences. Diamond et al. [2015] stressed that the loss of a single blade may result in significant financial and safety impacts. Booysen [2014] provides context for the related problems the South African power industry faces. South Africa's power industry is largely coal-driven, with most of the turbines being operated beyond their design lives or close to their decommissioning dates. This poses a risk of unexpected and catastrophic failures in line with the aforementioned failure mechanisms. The possible consequence of HCF due to various operating conditions is crack initiation on the affected blade [Murakami and Miller, 2005]. Crack propagation undoubtedly follows if the blade remains in service, ultimately resulting in the unexpected and catastrophic failure of the blade [Jono, 2005].

(a) Fatigue cracking in LP blade roots along the first hook serration.

(b) HCF failure of an LP turbine blade during transient operating conditions.

Figure 1.2: Consequences of fatigue cracking on LP turbine blades, adapted from [Booysen et al., 2015].

To avoid catastrophic blade failure, Church [2015] noted that a paradigm shift from Schedule-Based Maintenance (SBM) to Needs-Based Maintenance (NBM) for the early detection of blade damage is essential. The ability to detect a certain crack size, however, largely depends on the crack detection method. Non-Destructive Evaluation (NDE) techniques are conventionally used for life management and assessment of LP turbine blades prone to fatigue damage. NDE techniques typically involve inspecting the blades for cracks and replacing the blades as required [Booysen, 2014]. Some of the problems associated with these conventional NDE techniques are as follows:

1. Conventional NDE techniques are usually intrusive, thus disrupting the normal operation of turbomachines.
2. Online monitoring of blade conditions is not utilised, therefore increasing the risk of unexpected and catastrophic blade failures as blades near their design lives.
3. The monitoring of all the blades in a particular stage of the turbine is generally a tedious or difficult process. Due to this, only a select few blades are often evaluated.

Salhi et al. [2009] outlined the use of strain gauges as a conventional contacting blade vibration measurement technique. The use of strain gauges, along with the relevant signal processing, offers the potential of online and proactive VCM. Strain gauges are, however, largely intrusive due to the frequent installation disruptions of the normal operation of the turbomachines. Salhi et al. [2009] further highlight the following disadvantages of using strain gauges for VCM:

1. The installation of strain gauges is a very expensive process due to the need for high quality telemetry systems.
2. Strain gauges are only installed on selected blades and this installation process may be tedious. As a result, not all the blades are instrumented and monitored.
3. Strain gauges have a limited operating life as they are exposed to harsh on-engine conditions.
4. Strain gauges likely interfere with the aerodynamic and mechanical properties of the blades.

The use of strain gauges is therefore more suitable for a laboratory setup, ideally for cases where a methodology needs to be validated. When considering purely fatigue failures, Booysen et al. [2015] highlighted that this failure type in itself, is a complex process to understand. This is mainly due to a great deal of uncertainty and variability within the associated fatigue failure mechanisms. Further highlighted is the fact that information of the actual turbine blade material properties is not always readily available. It is therefore extremely difficult to predict blade conditions and, more so, to validate these predictions. An obvious solution to the problems outlined would be to avoid the root causes of the failure mechanisms. For example, blade vibrations or resonances which induce cyclic stresses should be avoided in order to prevent fatigue failures. However, run-up and -down operating speed profiles pass through critical speeds which excite blade resonances. This is typically unavoidable and may accumulate HCF damage [Rao, 1998].

It is therefore clear that the problem area outlined for the power industry may be identified on a component level as LP turbine blades experiencing unavoidable blade vibrations. Fatigue blade damage, specifically HCF, is identified as the common result of these blade vibrations induced during transient or steady operating conditions [Booysen et al., 2015]. The use of SBM strategies is discussed as posing a risk for unexpected and catastrophic blade failures. Immense financial and safety implications may be a result of catastrophic failures and should be avoided through the adoption of a more proactive blade monitoring approach.

A brief overview of conventional evaluation and monitoring techniques was given, which highlight that these techniques have many shortcomings. It was further mentioned that many uncertainties are associated with understanding fatigue blade damage and eventual blade failure. The problem area discussed in this section (Section 1.2.2) aims to give insight into the various topics which follow. Section 1.2.3 aims to elaborate the needs and opportunities to overcome the identified problems.

1.2.3 Needs and Opportunities

There is a need to avoid undesired downtime as result of turbine blade failures and poor maintenance operations of turbomachines [McCloskey et al., 1999]. It is essential that maintenance operations are performed in advance of unexpected and catastrophic turbine blade failures [Church, 2015]. The problem areas identified in Section 1.2.2 are now elaborated on in terms of the associated needs and opportunities:

1. There is a need to reduce the 42% of gas turbine failures reported by Al-Bedoor [2002], specifically due to LP turbine blade failures EPRI [1985]. Although this reported statistic may be slightly outdated or seen as a generalisation, the fact remains that a single blade may fail unexpectedly, thus emphasising the need for the online monitoring of turbine blades [Branco et al., 2015].
2. HCF is identified as a leading cause of LP turbine blade failure. HCF blade damage is a result of blade vibrations or resonances during transient and steady operating conditions, with these vibrations often being unavoidable [Booysen et al., 2015]. For this reason it is essential to monitor the condition of each blade in the desired stage of the turbomachine. This ultimately creates the opportunity for the early detection of blade damage.
3. Conventional blade NDE techniques limit the paradigm shift from SBM to NBM, where the conditions of the blades are continuously monitored [Church, 2015]. This is due to conventional NDE techniques relying on physical inspections of blades, therefore being intrusive and disruptive to the normal operation of turbomachines. These conventional NDE techniques are therefore non-ideal with regards to proactive condition monitoring. This serves as strong motivation for the implementation of an online and non-intrusive blade monitoring technique.
4. Booysen et al. [2015] emphasises that probabilistic principles are essential for modelling uncertainties associated with the condition monitoring of turbine blades. Brits [2016] further suggested the need for stochastic, rather than deterministic, analyses when modelling the physics associated with fatigue failures of turbine blades.

The above needs place emphasis on improved turbomachine maintenance practices. Mishra et al. [2014] outline that proper maintenance practices play an important role in terms of an extended useful life, reduced life-cycle costs, improved reliability and availability of the potential system. Furthermore, the need for a more proactive maintenance strategy is highlighted by the fact that maintenance technology more recently shifted from “failure” maintenance to “condition” maintenance. The use of diagnosis and prognosis technology is identified as a requirement to model the degradation process and associated prediction of the RUL of the machine. The accurate estimation of the RUL of a specific component or sub-component is, however, not always possible to determine. This is largely due to the many complexities associated with such an estimation and an inadequate understanding of the prognostics-diagnostics process [Mishra et al., 2014; Sikorska et al., 2011].

Figure 1.3 gives an overview of the prognostic-diagnostic process. Diagnostics involve detecting an abnormal operating condition, isolating the fault in terms of which a component is degrading or has failed, and identifying the nature or extent of the fault [Sikorska et al., 2011]. Thereafter a fault alarm may be triggered based on the outcome of the diagnostic analysis. Prognostics on the other hand is more concerned with the component damage that is yet to occur given the diagnostic information. Tobon-Mejia et al. [2010] describe prognostics as, “an estimation of time to failure and risk for one or more existing and future failure modes.” Figure 1.3 shows three distinct levels of prognostics, namely; providing an estimate of the RUL of the component / system as derived from the progression of each diagnosed failure mode (level 1), an evaluation of the likely future failure modes (level 2) and an evaluation of the effect of potential maintenances actions (level 3) [Sikorska et al., 2011]. Each successive level in this process adds increasing value in industry, however, the associated complexity increases substantially. This is largely due to the amount and quality of data required for each level following a similar trend down this process flow.

Obviously, the chosen maintenance strategy ideally needs to establish a balance between its industrial value or potential and associated complexity (as explained for the diagnostics and prognostics process flow in Figure 1.3). Rao and Dutta [2012] summarised the minimum requirements of diagnostic techniques to be attractive for the use in industry as follows:

1. Simple implementation of the technique.
2. Proven reliability in detecting machine or component faults.

The remainder of the literature review therefore aims to explore various maintenance strategies which offer a feasible solution to the needs outlined in this section (Section 1.2.3). The minimum requirements summarised by Rao and Dutta [2012] and attributes of the process flow shown in Figure 1.3 will form the basis of assessing the feasibility of different maintenance strategies.

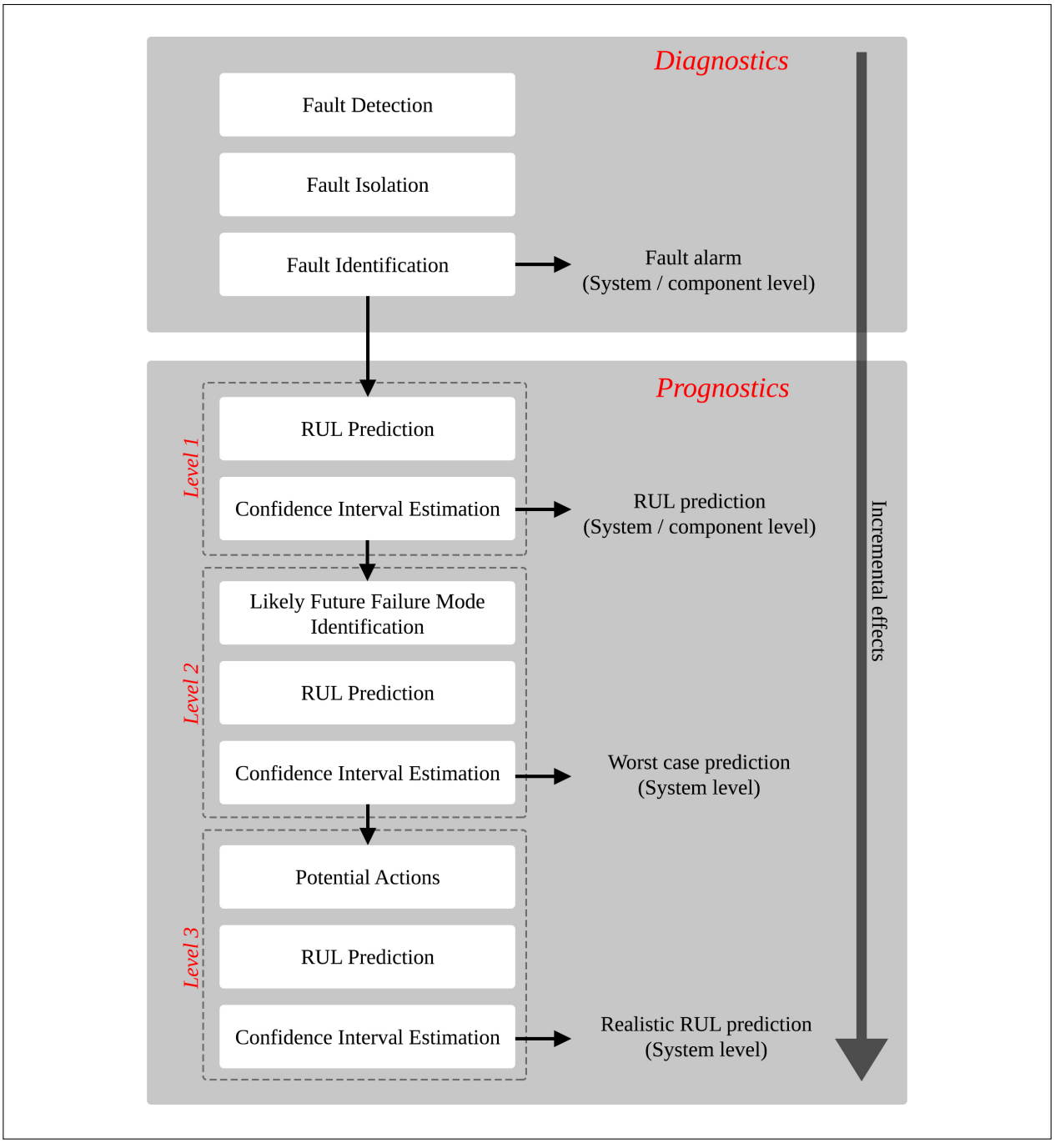

Figure 1.3: Overview of the prognostics and diagnostics process flow, adapted from ISO13381 [Sikorska et al., 2011; Tobon-Mejia et al., 2010].

1.2.4 Maintenance Strategies

For many companies, maintenance operations are traditionally seen as a cost centre, however, Al-Najjar and Alsyouf [2004] and Al-Najjar [2009] promoted the idea that proper maintenance strategies may transform maintenance operations into profit centres. It is therefore vital to select the appropriate maintenance strategy that may add financial value. Randall [2011] broadly categorised the available maintenance strategies as follows:

1. *Run-to-Break (RB):* Machines are typically run until they break. This strategy has many disadvantages, such as; catastrophic and unexpected failures, longer repair time between failures and higher maintenance costs. This strategy is more suitable to smaller machines in a production line where the loss of a single machine for a short time period is not critical.

2. *Time-Based or Preventive Maintenance (PM):* Maintenance is performed using a predetermined schedule or on regular intervals. The main benefit of this strategy is that maintenance operations may be planned in advance. The biggest disadvantages being that unexpected failures are not entirely prevented and high maintenance costs may be incurred because of unnecessary maintenance. There is also the possibility of replacing perfectly healthy parts. This is due to statistical predictions, as opposed to measured conditions, dictating the replacement of these parts.

3. *Condition-Based Maintenance (CBM):* This maintenance strategy is also referred to as "predictive maintenance" due to the condition monitoring of a machine enabling the prediction of potential breakdown. This technique has been used with great success for between 30-40 years. Neale and Woodley [1978] predicted in 1978 that maintenance costs in the British industry could be reduced by up to 65% for various industries. Vlok et al. [2002] and Sundin et al. [2007] presented a number of more recent cases where immense savings resulted due the implementation of Condition-Based Maintenance (CBM). CBM is even more attractive due to the fact that catastrophic and unexpected failures are greatly limited, since the current conditions of machines are continuously monitored to predict future conditions. Randall [2011] further explains that machine conditions may be monitored during operation, essentially using two main techniques:

   (a) *Vibration analysis:* This form of CBM is more specifically referred to VCM. Vibration analysis incorporates the observation that a machine or component has a distinct vibration signature during normal operation. During the development of a fault this associated signature may change. VCM may then track the change in this signature over time to make predictions or to give an indication of the machine or component condition.

   (b) *Lubricant analysis:* This form of CBM relies on the information carried by the lubricant from inside to outside the machine. Wear particles and chemical contaminants are common indicators of a fault present from within the machine. This form of CBM may be limited in the sense of quantifying associated levels of damage when compared to VCM.

From the above maintenance strategies and the needs outlined in Section 1.2.3, it is clear that CBM offers a viable solution to minimise unexpected and catastrophic failures of turbine blades. The remainder of the literature review only focuses on the topic of VCM, mainly because blade vibrations or resonances directly contribute to the accumulation of HCF blade damage [Booysen et al., 2015; Rao, 1998]. Understanding the cause and effect of the blade vibrations may give further insight into how the turbine blade conditions may be monitored. More specifically, possible solutions or techniques for monitoring the blade conditions are elaborated on. VCM techniques offer the potential to track the changes in the vibration signatures of turbine blades [Randall, 2011]. Analysing the changes in the vibration signatures may indicate the levels of associated blade damage. This may theoretically be the input for the diagnostics phases shown in Figure 1.3. Over time, prognostics information could be formulated and an RUL estimate could be made as an eventual result of VCM. RUL estimates are, however, not always possible [Mishra et al., 2014].

1.2.5 Turbine Blade Vibrations

Turbine blade vibrations have a multitude of causes, but are typically categorised as either *synchronous* or *asynchronous*. The main distinction between these classifications relate to whether the excitation frequencies are integer multiples of the shaft speed (engine-ordered). Equation 1.1 shows that the Engine Order (EO) is the ratio of the excitation frequency (ω_f) to the rotation frequency (Ω).

$$EO = \frac{\omega_f}{\Omega} \tag{1.1}$$

The differences between these classifications are discussed below:

1. *Synchronous:* This form of excitation phenomena is also referred to as *engine-ordered*, since these vibrations occur at frequencies which are integer multiples of the shaft speed [Rao and Dutta, 2012]. Lower EO excitations are generally caused by a variety of structural components directly in the fluid-flow path [Zielinski and Ziller, 2000]. This may include: stator vanes, diaphragms, moisture separators and structural components [Diamond et al., 2015; Rao, 2010]. Zielinski and Ziller [2000] further notes that the upstream and downstream stators of the rotor stage cause pressure fluctuations of higher integral engine orders. This associated excitation frequency is consequently called the Stator Passing Frequency (SPF). Figure 1.4 shows a schematic of the fluid passing over the stationary Inlet Guidance Vanes (IGV), onto the moving turbine blades, past the stator row and onto a second rotor stage. This fluid-flow path interaction with the rotating turbine blades generally results in synchronous blade vibrations. Non-concentric turbine casings, which affect the circumferential blade tip clearance, and irregular pressure distributions within the turbine are also contributors to this category of vibration [Zielinski and Ziller, 2000].
2. *Asynchronous:* This form of excitation is caused by aerodynamic instabilities which may include: self-exciting flutter (from an unfavourable interaction between blades and flow), rotating stall, acoustic resonance, compressor surging [Sabbatini et al., 2012; Zielinski and Ziller, 2000]. Asynchronous vibrations are non-integer multiples of the shaft rotational speed; i.e. not engine-ordered.

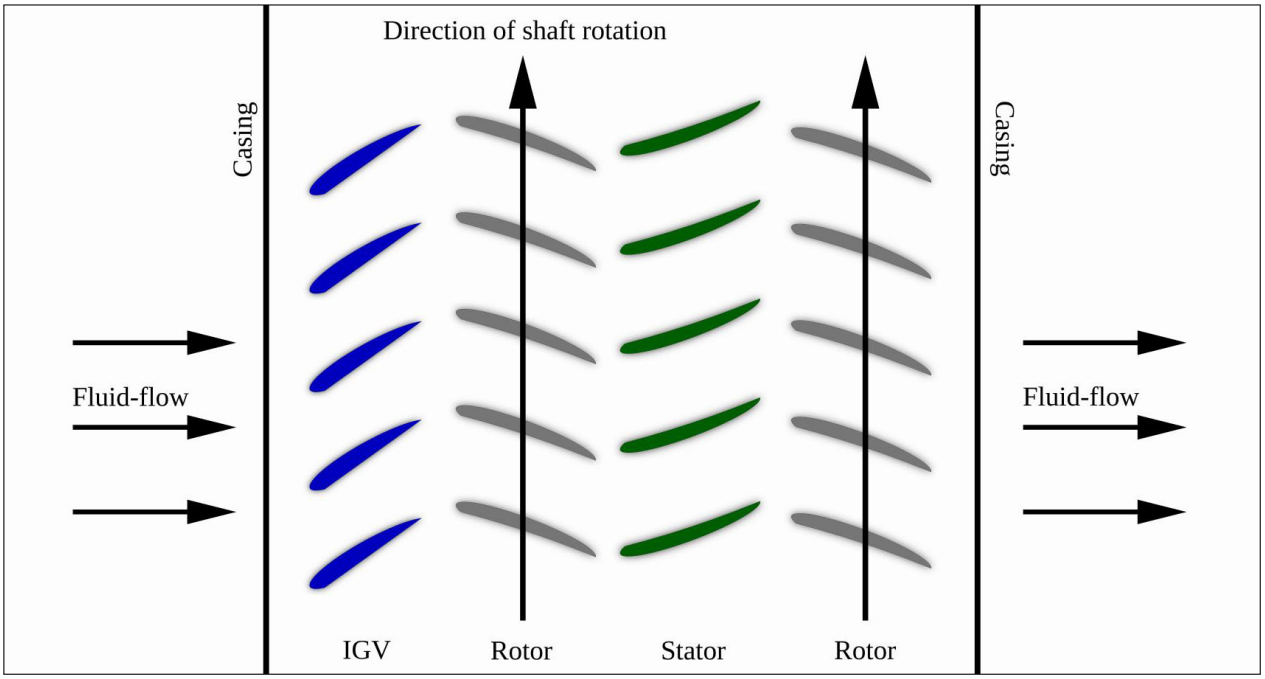

Figure 1.4: Schematic of turbine cross-section showing the fluid-flow path and direction of shaft rotation, adapted from Forbes and Randall [2013].

It is possible for multiple synchronous vibration modes to occur simultaneously, or for synchronous and asynchronous vibration to occur simultaneously. The designers of turbomachines design the rotor system such that the blade resonant frequencies do not coincide with integer multiples of the shaft speed during the common operating conditions. It is, however, a greater challenge to avoid synchronous vibrations during the run-up or run-down of turbomachines. The reason is that during run-up or run-down the transient operating speeds may pass through a critical speed which induces synchronous blade vibrations. This is limited by quickly passing through these critical speeds [Rao and Dutta, 2012]. Over time this process may result in an accumulation of fatigue damage and blade failure could be a consequence.

The mode shapes shown in Figure 1.5 are important to consider in terms of the effect it has on the fatigue life of blades. The basic blade mode shapes are categorised as either flexural (bending), torsional (twisting) or a combination of the two [Cookson et al., 2001]. In EPRI [2008], the mode shapes of a free-standing vibrating blade are outlined in greater detail. It is noted that bending modes are further categorised as flap-wise (about the weak axis) or edge-wise (about the strong axis). Thus, the mode shapes are categorised in terms of the relative direction of motion compared to the disk. Figure 1.5 gives an overview of some of the common mode shapes. The four fundamental mode shape classifications are discussed as follows [Booysen, 2014; EPRI, 2008]:

1. *Tangential:* A flap-wise movement of the blade occurs. This is shown in Figure 1.5 as the first flap mode.
2. *Axial:* An edge-wise movement of the blade occurs. This is not shown in Figure 1.5, however, the edges of the blades would translate in the axial direction.
3. *Torsional:* The ends of the blade are out of phase as the blade *twists*. This is shown in Figure 1.5 as the first torsional mode.
4. *Second bending modes:* The blade tip and body are out of phase. This is shown in Figure 1.5 as the second flap mode.

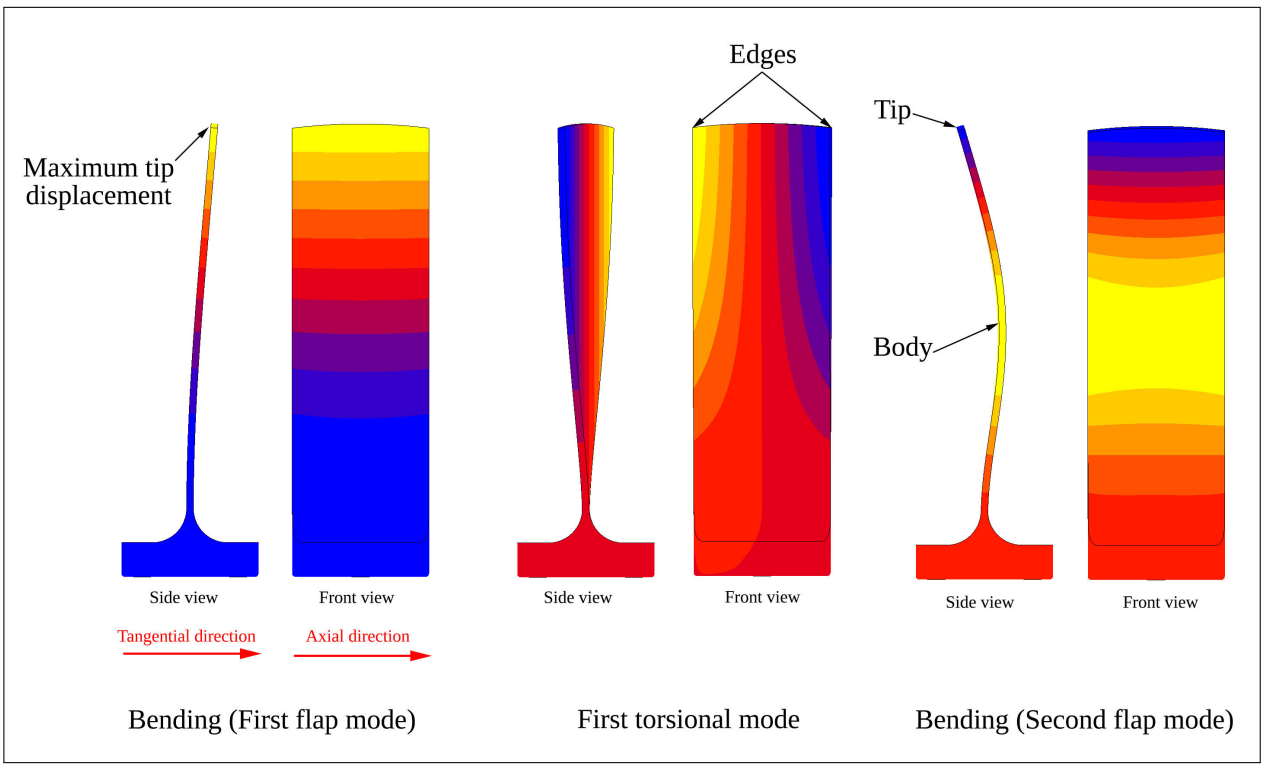

Figure 1.5: Simplified turbine blade mode shapes with contour bands showing the displacement profile.

The different mode shapes shown in Figure 1.5 result in different stress distributions on the turbomachine blades. In the study conducted by Booysen et al. [2015], pertaining to the probabilistic fatigue life prediction of LP turbine blades, it was concluded that only the first flap mode (bending mode) had a significant effect on the fatigue life of the test specimens.

The aforementioned paragraphs highlight the causes and effects of turbomachine blade vibrations. The first flap mode was specifically identified as a main contributor of fatigue in turbine blades. For practical applications the logical next step would be to determine at which operational speeds the first few blade resonances are excited. These critical operational speeds are generally identified on a Campbell diagram where the relationship between the shifting natural frequency of a particular mode (due to stress stiffening caused by the increasing operational shaft speed) and possible harmonic excitation from synchronous vibration mechanisms are shown [Battiato et al., 2017]. Figure 1.6 shows a Campbell diagram for an arbitrary blade in the first flap mode. The critical speeds are located where the first flap mode frequencies cross the EO lines. Exposing turbine blades to these operational speeds could result in synchronous blade vibrations and the accumulation of fatigue damage over extended periods of time.

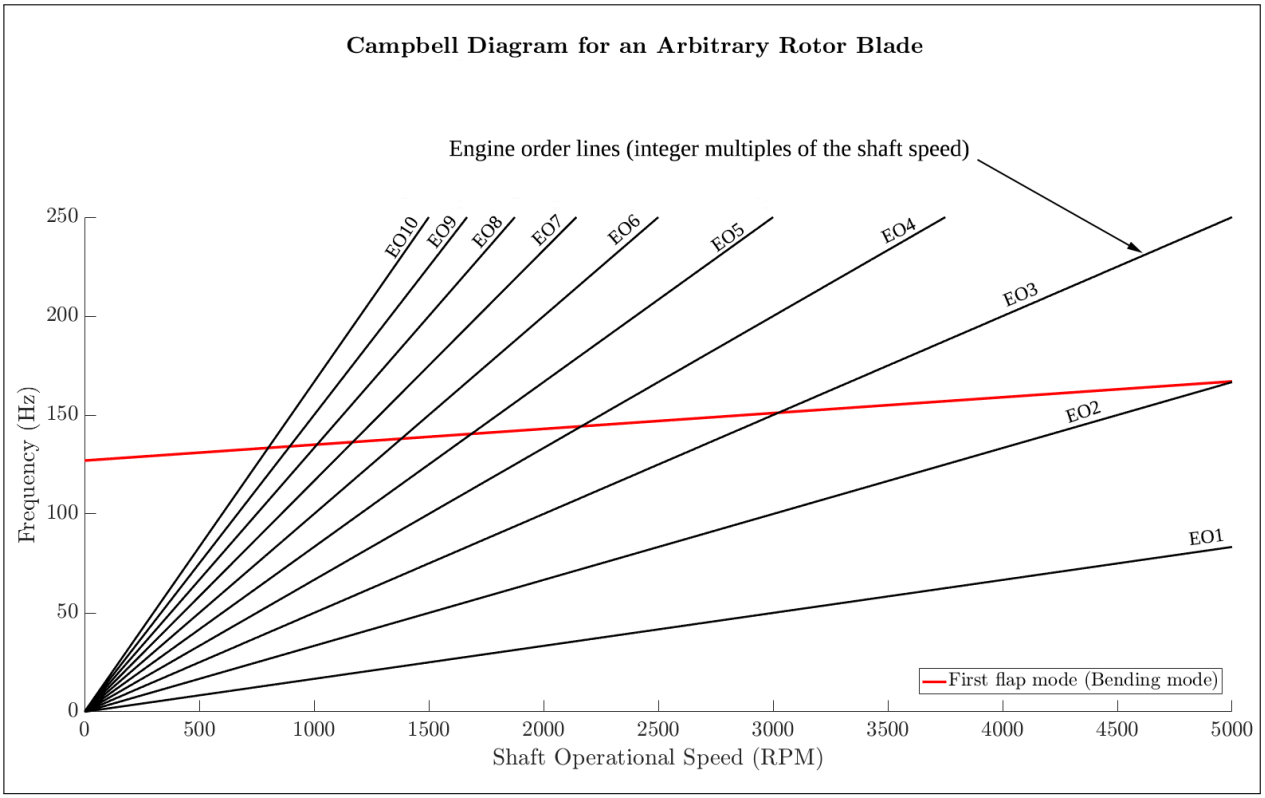

Figure 1.6: Campbell diagram for the first flap mode.

In princinple, employing VCM as a blade CBM monitoring technique can allow blade damage to be detected and tracked over time. VCM utilises the fact that machine components have a distinct vibration signature and a deviation from the expected vibration signature would be indicative of damage [Randall, 2011]. For example, a shift in the frequencies associated with the critical operating speeds (or natural frequencies for the particular mode) could indicate a change in the blade condition. Quantifying or tracking the change in natural frequencies over time could allow maintenance decisions to be made. This process importantly requires an indication of the associated healthy and critical damage vibration signatures of the blade. It is therefore essential to further investigate feasible VCM techniques which offer the practical requirements outlined by Rao and Dutta [2012], as discussed in Section 1.2.3.

1.2.6 Turbine Blade Vibration Measurement Techniques

This section discusses some of the traditional and more progressive turbomachine blade vibration measurement techniques. The advantages and disadvantages of each technique are also highlighted in an attempt to motivate why certain techniques are not ideal for rotor blade VCM. Traditional techniques used to measure blade vibrations include the Strain Gauge (SG) approach and the Frequency Modulated (FM) grid method [Sabbatini et al., 2012]. The discussion of these traditional methods are as follows:

1. The SG approach requires the attachment of SGs to the surface of a blade. Only the individual blades with SGs attached to their surfaces are monitored. The vibration response is captured during the normal operation of the turbomachine and signal processing techniques are used to extract associated vibration characteristics. Section 1.2.2 identified some of the difficulties and disadvantages of using the SG approach. Russhard [2015] emphasises that SGs are non-ideal for this purpose due to their low life expectancy and their exposure to harsh operating conditions. This results in a disruptive and intrusive installation process. The SG approach further requires costly high quality telemetry systems (either rotor mounted radio or slip ring systems) [Salhi et al., 2009; Russhard, 2015]. In Section 1.2.2 it was concluded that the use of the SG approach is more suitable for a laboratory setup where a vibration measurement technique or methodology needs to be validated. The SG approach is trusted in literature as an established and accurate approach for the aforementioned validation procedure [Gallego-Garrido et al., 2007a; Lawson and Ivey, 2005; Rigosi et al., 2017].

2. The FM grid method utilises the fact that a modulated alternating current can be used to determine the frequency of vibration of the blades [Sabbatini et al., 2012; Zielinski and Ziller, 2000]. This is done by mounting permanent magnets to the tips of a select few blades and embedding receiver wires in the casing of a particular rotor stage. As the magnets pass the embedded receiver wires, a modulated alternating current is induced. These modulations relate to the frequency of the blade response. Determining the frequency of the modulation may indicate what the blade frequencies of vibration are at a specific operational speed. Zielinski and Ziller [2000] mention that the drawbacks with the FM grid method are: it is a costly and complex implementation process. The fact that the blades are physically altered (by including magnets to the tips) also pose a number of issues.

Although the aforementioned traditional techniques facilitate online monitoring, many disadvantages exist. The FM grid method physically alters the turbomachine blades and using SGs are not an ideal long-term solution. There is thus a need for non-contact monitoring techniques. The remainder of Section 1.2.6 introduces two alternative techniques, namely Eulerian Laser Doppler Vibrometry (ELDV) and Casing Pressure Signal Methods (CPSM), which potentially overcome the disadvantages of the traditional techniques. These techniques are briefly discussed as follows:

1. Oberholster and Heyns [2009] presented a fixed reference frame or Eulerian implementation of Laser Doppler Vibrometry, coined ELDV. This implementation is specifically for the monitoring of axial-flow turbomachine blades where a fixed frame of reference with a stationary transducer and a moving target is established. In essence, this technique functions by focusing the laser at a fixed point in space. Measurements are taken for the required intervals; i.e. when the rotating blades are exposed to the fixed laser point. It was concluded from the experimental testing and FEM in the study that this measurement approach is feasible for online blade condition monitoring. The feasibility was in principle, determined for when phase angles at reference frequencies were monitored using a non-harmonic Fourier analysis. However, it was recommended that the proposed blade monitoring approach should be verified at higher rotational speeds and that measurements are necessary on a multi-bladed rotor to determine whether a distinction could be made between healthy and damaged blades.

2. Forbes and Randall [2013] presented a non-contact method to estimate the associated rotor blade natural frequencies by measuring the casing vibrations at a single operating speed. CPSM utilises the fact that the internal pressure of a gas turbomachine exhibits the response signature of vibrating blades. The vibrations of the blades occur as they move through the fluid, as well as other factors. The internal pressure profile may result in the excitation of the external casing and measuring this excitation may give an indication of the blade natural frequencies [Forbes and Randall, 2007, 2010]. Figure 1.7 gives an example of an in-plane pressure model without blade vibrations (with and without Gaussian noise) as shown by Church [2015]. Figure 1.7 indicates that a high pressure (HP) region occurs ahead of the rotating blades and a low pressure (LP) region behind the blades. The angular distance, θ_s, between the blades would change when the blades are vibrating and alter the resultant pressure profile. Importantly, an angular reference frame, θ, is established in order to quantify the changes in the pressure profile and to determine the frequencies of vibration of the blades.

   The study conducted by Forbes and Randall [2013] further introduced a blade fault on one of the rotor blades and it was concluded that the CPSM could successfully estimate the simulated natural frequency value. The natural frequencies in this study were, however, only conducted for constant operational speeds which may limit the applications of this method in industry. It was also noted that a reasonable amount of post-processing is required to extract the natural frequencies of the blades using CPSM. This adds a degree of complexity to using this methodology. In the study conducted by Church [2015], it was concluded that the feasibility and practicality of CPSM may be questioned. This concern was raised due to the need for the internal pressure sensors having to be both fast enough to capture the response, whilst also being robust enough to withstand the harsh internal casing environment. Lastly, it was noted by Forbes and Randall [2013] that the derived natural frequencies were merely estimates and that the accuracy of these estimates need to be determined.

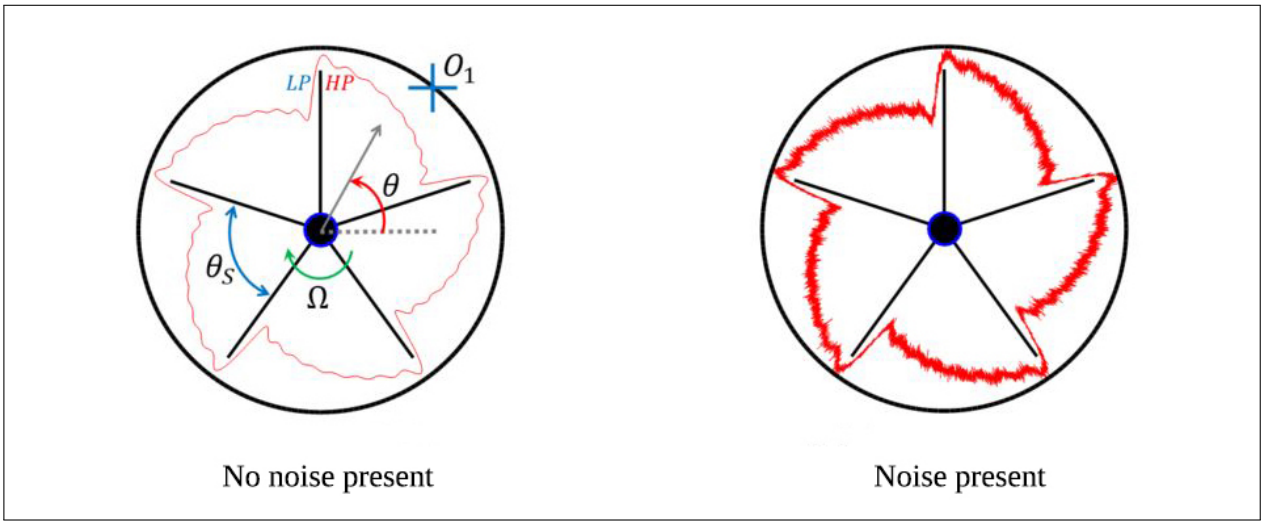

Figure 1.7: CPSM arbitrary pressure response, from Church [2015].

Forbes and Randall [2013] mentioned that the non-contact measurement of gas turbine rotor blade vibrations is a non-trivial task. More so, it needs to be emphasised that there is no non-contact VCM method available which has no significant drawbacks. It is therefore clear from the aforementioned discussions that a compromise needs to be made. This compromise is dependent on the type of method that is implemented. For example, a method that is simple and quite cheap to implement may result in an unacceptable measurement accuracy. The opposite may also be a scenario. It is therefore vital to determine what the main requirements are for the intended VCM technique and to what accuracy the response of a blade needs to be measured. Section 1.2.7 sets out to present a VCM technique which is believed to offer great potential for practical application.

1.2.7 Blade Tip Timing as a Solution

Background

Rigosi et al. [2017] regards BTT as currently the most promising technique for blade VCM. BTT boasts the possibility of online and non-intrusive (non-contact) measurement capabilities. Furthermore, it is possible to monitor each blade in a particular stage of the turbine individually [Rigosi et al., 2017]. Conventional VCM techniques generally only exhibit one or two of these advantages. The fact that all these advantages are present makes BTT very attractive for the practical condition monitoring of turbomachine blades. When considering the history of BTT it is quite intersting to note that the technique started getting academic attention in the early 1970s. However, Rigosi et al. [2017] note that this technology is still maturing to the present day. Rzadkowski et al. [2016] give a very thorough overview of the various contributions from authors in the BTT field; starting from the early stages and ending with more recent contributions. For 1970 two contributions are noted by Rzadkowski et al. [2016], namely:

1. The system patented by Robinson [1970] for measuring rotor vibrations.
2. The work performed by Zablotskiy and Korostelev [1970] entailing an integral vibration analysis using the ELURA device. Furthermore, inductive sensors, also referred to as speed pick-ups or variable reluctance sensors, were used for BTT in steam turbines.

The early work in the field of BTT or Non-Intrusive Stress Measurement Systems (NSMS) prioritised sensor development. The technology, in terms of the probes and data acquisition devices, has become much more advanced since the early stages of this field. These advancements have thus led to a greater interest in the practical application of BTT as a diagnostic tool. Rzadkowski et al. [2016] further noted that in 1989 the work by Kudelski and Szczepanik [1989] demonstrated the ability of NSMS to detect rotor blade crack growth. This was an fundamental advancement that arguably led to further interest and developments for the detection of blade crack growth using NSMS. For the historical period around 1999 and 2000 it was demonstrated by Kurkov and Dhadwal [1999] that NSMS is not limited to only detecting blade crack growth, but also hub crack growth. In this period Heath [1999] also presented a new technique for identifying synchronous resonances using BTT.

More recent work focused on the selection and performance of specific BTT algorithms used to determine the associated blade vibration response. Diamond et al. [2015] compared the performance of three BTT methods: the Auto-Regressive (AR), Circumferential Fourier Fit (CFF) and the newly implemented BTT method based on Bayesian Linear Regression (BLR). More detail of various BTT algorithms will follow in the subsequent sections. Rigosi et al. [2017] presented a method to extract the amplitude and frequency during blade resonance; the proposed method in this study revised the well-known Two-Parameter Plot (2PP) method. The thorough review of literature indicates that many BTT algorithms exist, however, there is no consensus in published literature as to which method performs the best or exhibits the greatest accuracy. Diamond et al. [2015] mentioned that this lack of consensus is partly due to the fact that turbomachine blade vibrations are notoriously difficult to measure and therefore difficult to validate. The difficulty in validating the measurements results in a lot of disagreement regarding the methods applicability in industry. In Gallego-Garrido et al. [2007b] it is mentioned that, “blade tip timing has the potential to overcome many of the limitations of currently well-established systems, providing more information at a fraction of the cost.” However, Rao and Dutta [2012] show scepticism towards the applicability of BTT for practical applications.

The remainder of Section 1.2.7 outlines the basic principles behind BTT, proving why this may be regarded as a feasible approach for rotor blade VCM. Details regarding specific BTT algorithms will also be discussed where applicable. Figure 1.8 presents a condensed overview of the history of BTT and foreshadows what this particular research will focus on.

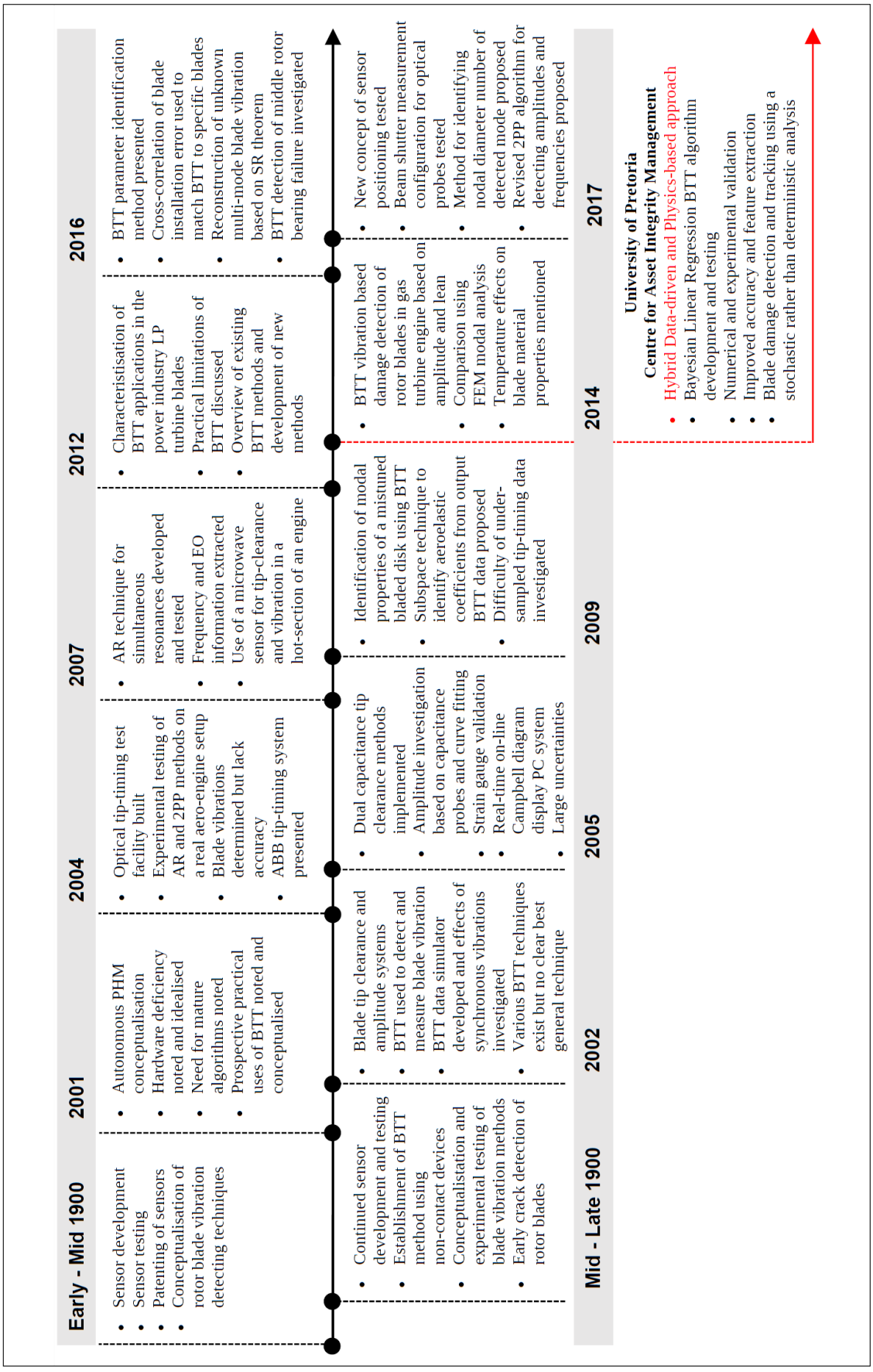

Figure 1.8: BTT timeline, adapted from Rzadkowski et al. [2016] and a collection of various sources presented in Section 1.2.7.

Basic Principles

BTT used proximity probes distributed circumferentially and mounted radially around the turbomachine casing for a particular row. The proximity probes are used to sense when blades pass the probes [Diamond et al., 2015]. The number, type and location of probes particularly depends on the intended use of the BTT data [Rigosi et al., 2017]. The fundamental principles behind BTT are relatively straightforward: the measured Time of Arrival (ToA) values of the blades passing a proximity probe is analysed to indicate the vibrational state of each blade. The ToA of a non-vibrating blade is completely dependent on the shaft angular velocity. For example, a non-vibrating blade would arrive at a single proximity probe in known time increments (ToA_{NV} based on the relationship shown in Equation 1.2, assuming that the rotational speed (Ω, in radians per second) remains constant for all the angular distances travelled by the rotor($\theta = 2\pi$ radians per revolution).

$$\text{ToA}_{\text{NV}} = \frac{\theta}{\Omega} \tag{1.2}$$

However, a vibrating blade arrives either earlier or later than expected at the proximity probe. This physically translates into the vibrating blade leading or lagging upon arrival at the proximity probe. These vibrating blades therefore arrive earlier or later than expected at the proximity probes. The blade tip displacement can be calculated from the change in Angle of Arrival (AoA) (ΔAoA) of a vibrating blade which may be derived by using a Once Per Revolution (OPR) pulse as a shaft reference position [Diamond et al., 2015]. The change in AoA values may then be used to find the tip displacement values. These tip displacements are then finally used to derive the vibration response features (amplitude, phase and frequency) associated with the individual blades in a particular row. The way that these features are extracted depends on the type of BTT algorithm that is implemented (this will be discussed in the remaining sub-sections). The types and accuracy of the features extracted from the BTT measurements may provide the necessary information for the desired VCM of turbomachine blades.

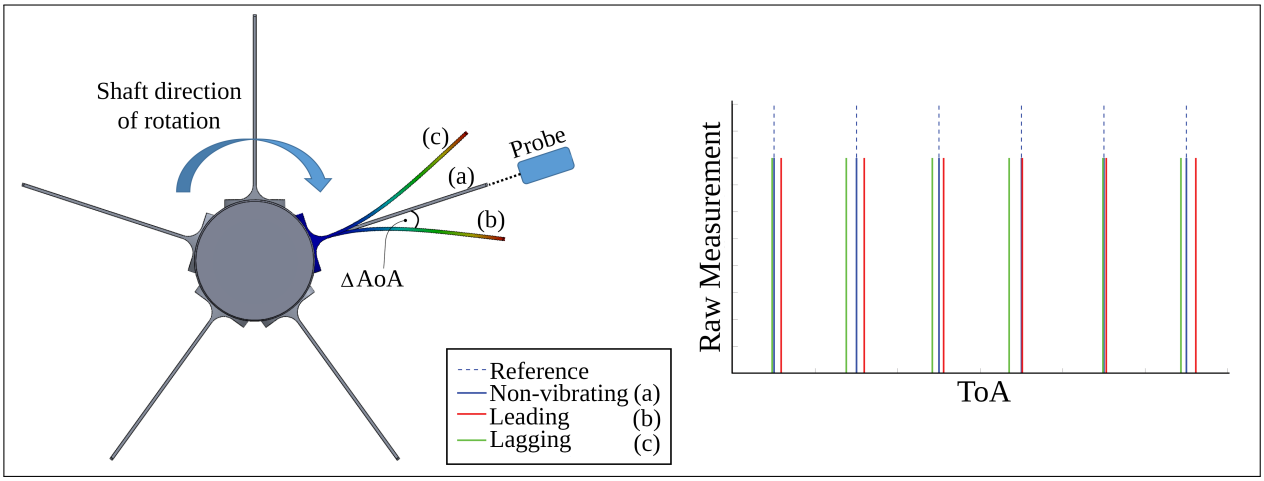

Figure 1.9: Basic BTT principles.

Figure 1.9 summarises the basic BTT principles in terms of what is physically measured using the proximity probe (left) and how these measurements are represented as a ToA (right). BTT may be considered as a three-step process Rigosi et al. [2017]:

1. Acquiring the ToA of the individual blades at each proximity probe.
2. Deriving the blade tip displacements from the ΔAoA.
3. Analysing this data and extracting the desired results for further post-processing.

The sampling of the blade tip displacement occurs at each proximity probe based on the difference between the ToA of a vibrating and non-vibrating (theoretical) blade. As a result this sampling rate depends entirely on three aspects [Diamond et al., 2015]:

1. The current shaft speed.
2. The number of proximity probes installed.
3. The spacing of the proximity probes.

Diamond et al. [2015] give an example; if the rotor is turning at 25 Hz and there are 4 proximity probes, the effective sampling rate is 100 Hz. This example demonstrates an associated difficulty with these measurements, namely, aliasing as a result of sub-sampling. Figure 1.10 gives an example of an aliased signal. Due to this difficulty associated with aliasing, conventional signal processing techniques such as the Fast Fourier Transform (FFT) have limited use [Diamond et al., 2015]. The

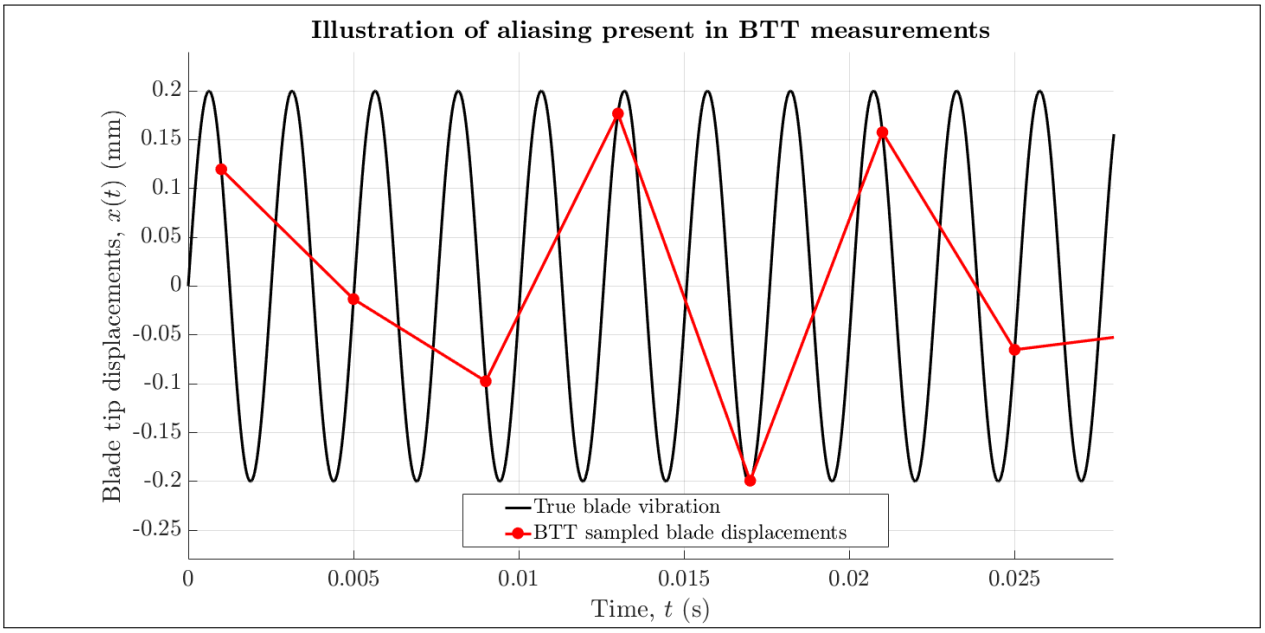

Figure 1.10: Comparison of the true vibration response and aliased BTT measurements, adapted from Diamond et al. [2015].

concept of the Probe Spacing on the Resonance (PSR) was formulated (specifically for the AR class of BTT models) due to aliasing inherently resulting in physical constraints on the positioning of the proximity probes. The PSR is described as the percentage of the response waveform captured by measurement probes during one oscillatory cycle of a blade [Gallego-Garrido et al., 2007b]. Gallego-Garrido et al. [2007b] describe the PSR as one of the most important considerations in BTT data analysis. The importance of this consideration is related to the errors in the estimation of the blade response frequency. For example, a PSR percentage that is too small will result in significant errors in the estimation of the response frequency. Similarly, a large PSR percentage will result in an under-sampling of the response and again lead to large errors. Equation 1.3 shows how the PSR is calculated in terms of the EO and the angular distance between the first and last probe (γ, expressed in radians). Figure 1.11 indicates the effects of having a low and high PSR with regards to the measurement of the *true* blade response. In Figure 1.11 roughly 1-EO resonance is sampled and it is assumed that there are 10 arbitrary proximity probes. Furthermore, from this figure it is clear that the low PSR data could incorrectly be representative of a straight line. On the other hand, the higher PSR results in measured points closer to the *true* sine wave response.

$$\text{PSR} = \frac{\text{EO} \cdot \gamma}{2\pi} = \frac{\omega_f \cdot \gamma}{\Omega \cdot 2\pi} \tag{1.3}$$

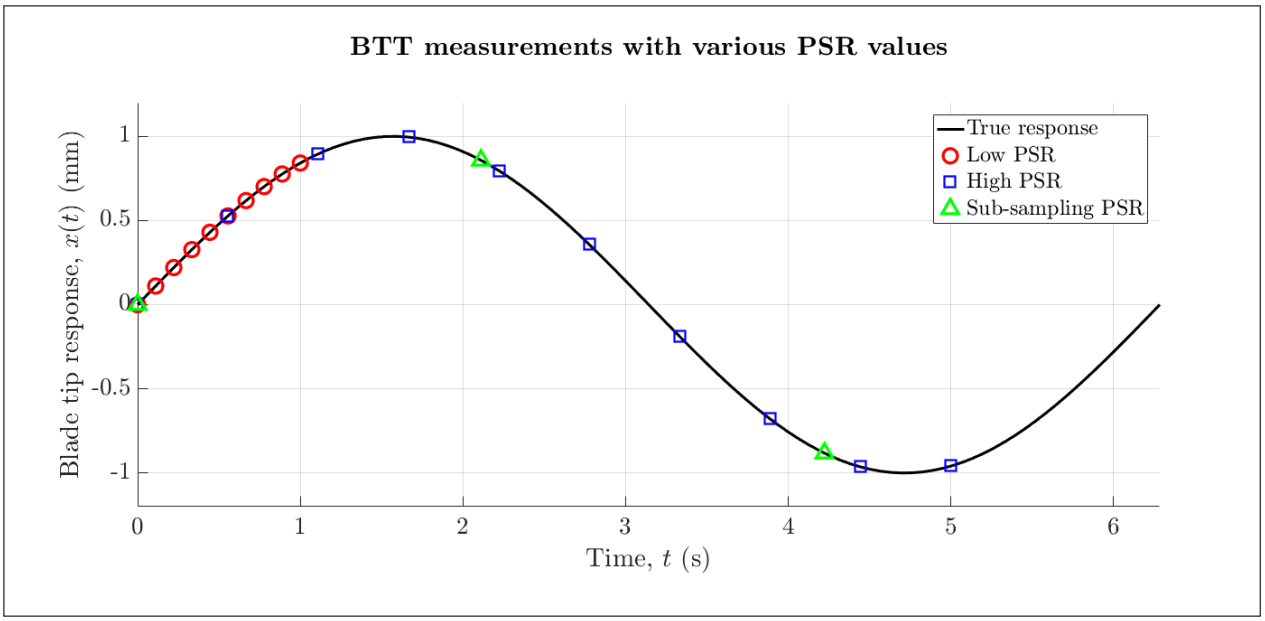

Figure 1.11: Comparison of BTT measurements with various PSR ratios present, adapted from Gallego-Garrido et al. [2007b].

The performance of the BTT technique in deriving the vibrational characteristics of the blades also largely depends on the chosen BTT algorithm. Numerous studies elaborated on the available curve-fitting techniques or algorithms applied to the direct synchronous BTT problem. In these studies the performance of each technique, based on both experimental and simulated data, was compared [Diamond et al., 2015; Gallego-Garrido et al., 2007a,b]. The next sub-section provides some detail about various BTT algorithms.

BTT Algorithms Overview

As previously mentioned, extracting blade vibration parameters is a non-trivial task. This is largely due to the measured signals being aliased or sub-sampled, therefore inhibiting conventional signal processing. Many BTT algorithms have been developed to overcome these difficulties and are divided into two main categories [Diamond et al., 2015; Rigosi et al., 2017]:

1. *Indirect methods:* These methods operate during transient operating conditions [Diamond et al., 2015]. The maximum amplitude and corresponding frequency, only at resonance, is determined. Indirect methods require that BTT data is collected across the entire resonance region of the blades. Carrington et al. [2001] note that this is achieved by sweeping the rotor operating speed over a range corresponding to foreseeable blade natural frequencies. The advantage of using indirect methods is that only one or two proximity probes are required.
2. *Direct methods:* These methods operate during steady state operating conditions [Diamond et al., 2015]. The main advantage of direct methods is that the blade response is found at each measured rotational speed and not only at resonance. Rigosi et al. [2017] suggest that at least four proximity probes are required to overcome the difficulty of synchronous blade vibrations, resulting in a single BTT measurement point always capturing the same blade displacement.

The remainder of the BTT algorithmic overview focuses on two examples of direct methods, namely: the AR method and recently developed BLR method. A number of BTT algorithms exist, however, the discussion of these specific algorithms aims to motivate the choice of algorithm used in this research. Both these methods solve the blade response as part of a curve-fitting exercise following a number of assumptions. The overview of these two methods and their formulation follow.

1. *The AR method:* The tip deflection under the AR approach is assumed to be a Single-Degree of Freedom (SDOF) sinusoid with a frequency equal to the blade natural frequency; i.e. $\omega_f = \omega_n$ [Carrington et al., 2001]. The Ordinary Differential Equation (ODE) shown in Equation 1.4 is used to set up the AR formulation of the BTT data analysis problem.

$$\ddot{\tilde{x}} + \omega_n^2 \cdot \tilde{x} = 0 \tag{1.4}$$

The solution to the ODE shown in Equation 1.4 above is given by Equation 1.5 with $\tilde{x}$, A_n, ω_n, ϕ_n and D_{off} representing the blade response displacement, amplitude, natural frequency, phase and DC offset respectively.

$$\tilde{x} = A_n \cdot \cos(\omega_n \cdot t + \phi_n) + D_{off} \tag{1.5}$$

The detailed formulation of the AR method is documented by Carrington et al. [2001]. The in-depth formulation of the AR method used to find the blade response, amplitude and natural frequencies is therefore not presented in this dissertation. However, it is important to note the difficulties or disadvantage associated with the AR method. Firstly, proximity probes are required to have an equidistant spacing between them [Carrington et al., 2001]. There is foreseeable difficulty in ensuring this equidistant probe spacing. Secondly, it is identified that biased AR parameters result if data points used in the formulation of the AR method contain experimental errors [Cooper, 1989]. In order to overcome this bias and other associated disadvantages of the simple AR method Carrington et al. [2001] considered two more advanced AR approaches. Lastly, the formulation of the AR method shown by Carrington et al. [2001] indicates that deterministic solutions of vibration characteristics are found. This is limiting as there is no indication of the uncertainty in the solutions of the vibration parameters.

2. *The BLR method:* This method was proposed by Diamond et al. [2015] and also assumes a SDOF model for the blade response, as expressed in Equation 1.6. An in-depth discussion of the BLR method is not given here as the BLR method is in the process of being commercialised and patented (refer to Section 1.4).

$$x_i(t) = A \cdot \cos(\omega \cdot t_i) + B \cdot \sin(\omega \cdot t_i) + C \tag{1.6}$$

$$\text{where} \quad \omega = EO \cdot \Omega \tag{1.7}$$

BLR is used to infer the values of the constants A, B and C as probabilistic quantities. The values in Equation 1.6 are solved for each revolution (indicated by the subscript i) at a corresponding angular velocity, Ω. One advantage of using a Bayesian based technique lies in the fact that prior assumptions of the solution influences the final inferred solution. It was mentioned by Diamond et al. [2014] that the BLR for this particular problem works best when the proximity probes are irregularly spaced. The fact that proximity probes do not need to have an equidistant spacing for the BLR method is a distinct advantage over the AR method. Secondly, the processed data considers the whole range of inferential solutions, therefore resulting in a stochastic solution. This allows the BLR technique to facilitate noise tolerant behaviour. The third advantage is related to the fact that the constants A, B and C of Equation 1.7 are inferred as probabilistic quantities. These values may then be used to find the amplitude and phase of blade vibration with a corresponding confidence interval derived from associated probability distributions.

It is clear that many BTT methods exist and that the applicability of a specific method depends on the desired application. Each method offers its own advantages and has its own disadvantages. For example, Diamond et al. [2015] claim that the newly developed BLR method boasts a higher accuracy than the AR and CFF (not discussed in detail) methods in most instances. However, cases were also reported by Diamond et al. [2015] where large frequency and amplitude estimation errors occurred. The BLR method is therefore a promising method with many advantages. However, due to a lack of consensus in published literature as to which method performs best, the discretion of the user is still required to determine which method is most suitable.

1.2.8 Hybrid Approaches

Liao and Köttig [2014] noted that there is no universally accepted best prognostics / diagnostics model, due to each model having its own advantages and disadvantages. It was further noted by Liao and Köttig [2014] that the right prognostics / diagnostics model may be case case specific. The prognostics / diagnostics model with the specific aim to prevent the catastrophic and unexpected failure of turbomachine blades, may ultimately be very case specific. Thus far, the use of BTT as a VCM technique has been suggested as a viable solution in preventing this sort of blade failure. The preceding sections (specifically Section 1.2.7) highlighted that the monitoring of the corresponding blade vibration signature may indicate the condition of a particular blade. Madhavan et al. [2014] specifically used a tip-timing methodology to detect abnormalities in the resonant amplitudes of specific blades. Based on the immense reduction in reported resonant amplitudes, it was then concluded that the blade stiffness reduced considerbaly. Madhavan et al. [2014] concluded that a limitation of this particular experimental investigation was that it only revealed that there was an initiation of blade damage. However, a fractographic analysis was still required to show what the cause of damage was and how to quantify this damage. The fractographic analysis required the premature disassembly of the bladed system. This disassembly would be impractical in industry unless there is enough evidence available to suggest that the blade damage is critical.

Furthermore, it is also essential that utmost confidence exists in the indication or prediction of the blade damage. In light of the proposed solution of using BTT it should be emphasised that there are also difficulties. Diamond et al. [2015] concluded that there is no consensus of which BTT method or algorithm performs the best in extracting blade vibrational characteristics. Furthermore, these characteristics were noted to be extremely difficult to validate. Recall the requirements of a diagnostics approach outlined by Rao and Dutta [2012]: "Unless a diagnostic technique is made simple to implement and whose reliability is proven, power plants will not find it attractive to invest on upgrade for safe operation of the machine." This statement hints at the possible downfall of using only a single diagnostics approach. For this reason the concept of a hybrid diagnostics / prognostics approach is introduced.

Liao and Köttig [2014] and Mishra et al. [2014] gave an elaborate overview of various conceptualised Hybrid Prognostic Models (HPMs). The advantages associated with using a hybrid approach were thoroughly discussed. In summary, it was noted that the use of a hybrid approach aims to alleviate the disadvantages of an individual analysis type while conserving its advantages [Liao and Köttig, 2014]. For example, combining FEM modal analysis with a BTT approach may help simulate expected blade conditions while also conserving the online and non-intrusive practical advantages of the BTT approach. Eventually, two strong individual pieces of evidence of the blade condition may be combined or compared to result in a more reliable prediction. Liao and Köttig [2014] outlined five combinations of models for hybrid approaches. These combinations are shown in Table 1.1 and will be discussed briefly in the remainder of this section. Before the discussion of the various hybrid approaches, the individual models are defined. The discussion of the individual models follows:

1. Experience-based models are commonly documented as *if-then* rules directly used by domain experts with specialised knowledge of the machinery in question. As a result, this prognostics model incorporates expert knowledge and experience of an observed situation to infer information based on historical measurements or events. This approach is therefore representative of how a human specialist solves a problem based on reasoning. The major downfall of this approach is that a heavy burden is placed on the capability of the domain expert to specify the rules of the system and the capability of developing rule-sets to represent the characteristics of the entire system. This model is proposed to rather supplement a data-driven or physics-based model as part of a hybrid prognostics implementation [Liao and Köttig, 2014]. The isolated use of this approach may consequently run the risk of human-error, affirming that such a model is not guaranteed to be reliable.

2. The functioning of data-driven models relies only on previously observed data to predict the trend or projection of the system state. In essence, similar patterns of the system operation is matched in order to infer further information about the system or component. Data-driven models typically incorporate a feature extraction process (vibration signals in the case of BTT) as an input to the data-driven model. Data-driven models often have the ability to model different health stages (normal, crack initialisation, growth and failure, in the case of fatigue damage) of machinery without the assumption of monotonic degradation. Importantly, the specific fault progression in each stage is not required, however, data collected or measured from different stages is required for training procedures. The downside of this approach is that large amounts of data, proportional to the respective health stages, is required for the training of the models. Furthermore, it is mentioned by Liao and Köttig [2014] that anomalies may not always be detected using this approach. The anomaly-detection capabilities moreover depend on the type of data-driven model that is implemented.

3. In physics-based models, knowledge of system failure mechanisms (crack-growth) is used to build a mathematical description of the degradation process. The system behaviour is quantitatively characterised using physics or first principles. Crucially, model parameters need to be identified using specifically designed experiments and extensive empirical data [Liao and Köttig, 2014]. These models may be very complex to formulate and case-specific.

The combinations of hybrid approaches are shown in Table 1.1, with a brief discussion of each following. The advantages and disadvantages of these combinations are summarised in Table 1.2.

Table 1.1: Overview of the various hybrid approach combinations.

Combination	**Model 1**	**Model 2**	**Model 3**
H1	Experience-based	Data-driven	-
H2	Experience-based	Physics-based	-
H3	Data-driven	Data-driven	-
H4	Data-driven	Physics-based	-
H5	Experience-based	Data-driven	Physics-based

1. *H1 - Experience-based and Data-driven:* H1 HPMs provide the flexibility of integrating domain knowledge into data-driven models for system state or health level estimation Liao and Köttig [2014]. However, the H1 approach still heavily relies on the expert to specify the underlying system behaviour.

2. *H2 - Experience-based and Physics-based:* The H2 category integrates both experience-based and physics-based models, where the output of the experience-based model is often used as an auxiliary to purely enhance the physics-based model prediction. Alternatively, the experience-based model can be utilised to estimate the system health state, resulting in a health (condition) level prediction [Liao and Köttig, 2014].

3. *H3 - Data-driven and Data-driven:* H3 HPMs use the direct integration of two data-driven prognostics methods. This is done in an attempt to eliminate some of the disadvantage of either model, ultimately improving the performance of the system health prediction. Approaches in the H3 category are described by Liao and Köttig [2014] to be two-fold, due to a duplication of similar underlying principles being incorporated.

4. *H4 - Data-driven and Physics-based:* H4 approaches are described by Liao and Köttig [2014] as the approach which has been extensively studied in the literature. Mishra et al. [2014] only mention the possibility of performing fault diagnosis and prognosis using three main approaches; either data-driven, physics-based or the combination of these in a hybrid approach. This type of hybrid approach is conceptualised in detail in the literature with a further four sub-categories being outlined. The four sub-categories specifically utilise the details outlined in points 4a. to 4d. as follows [Liao and Köttig, 2014].

(a) Using a data-driven model to infer a measurement model and use a physics-based model to predict the condition of the system or component.

(b) Using a data-driven model to replace a system model in a physics-based model.

(c) Using a data-driven model to predict future measurements and use a physics-based model to predict condition of the system or component.

(d) Using a data-driven model and a physics-based model for predictions, and fuse the results.

5. *H5 - Experience-based, Data-driven and Physics-based:* The incorporation of all three of the proposed prognostics models into a hybrid model is described as being the most advantageous [Liao and Köttig, 2014]. Consequently, the strengths of the data-driven, physics-based and experience-based models are amalgamated into a single model. This can however be very complex to implement.

The use of a hybrid approach will certainly be beneficial as it may assist in overcoming some of the difficulties associated with a purely BTT-based approach. There is clearly an abundant flexibility when it comes to specific hybrid approaches and how these approaches may be used to monitor the condition of turbomachine blades. From the aforementioned discussion and summary in Table 1.2 it is clear that the H4 hybrid approach may be the most advantageous and feasible in terms of the identified problem area. The criteria of a prognostic / diagnostic technique to be simple to implement therefore provides motivation for why the H4 hybrid approach is favoured instead of the more complex H5 approach.

1.2.9 Summary

Figure 1.12 summarises the various outcomes of the literature review for the topics outlined in Figure 1.1. The identified problem area is HCF of LP turbomachine blades, which potentially leads to catastrophic and unexpected blade failures. The literature study reveals that a distinct shift from SBM to CBM is required to overcome this problem. The VCM, using a newly developed BTT technique based on BLR, was identified to be promising with regards to monitoring turbomachine blades. This BTT technique allows online, non-intrusive and reliable monitoring, while also being relatively simple to implement. It is, however, identified that the use of a hybrid approach (incorporating a data-driven and physics-based approach) would be favourable in minimising some of the disadvantages of using a purely BTT-based approach. The details of the aforementioned will be outlined in the scope of this research project (Section 1.3).

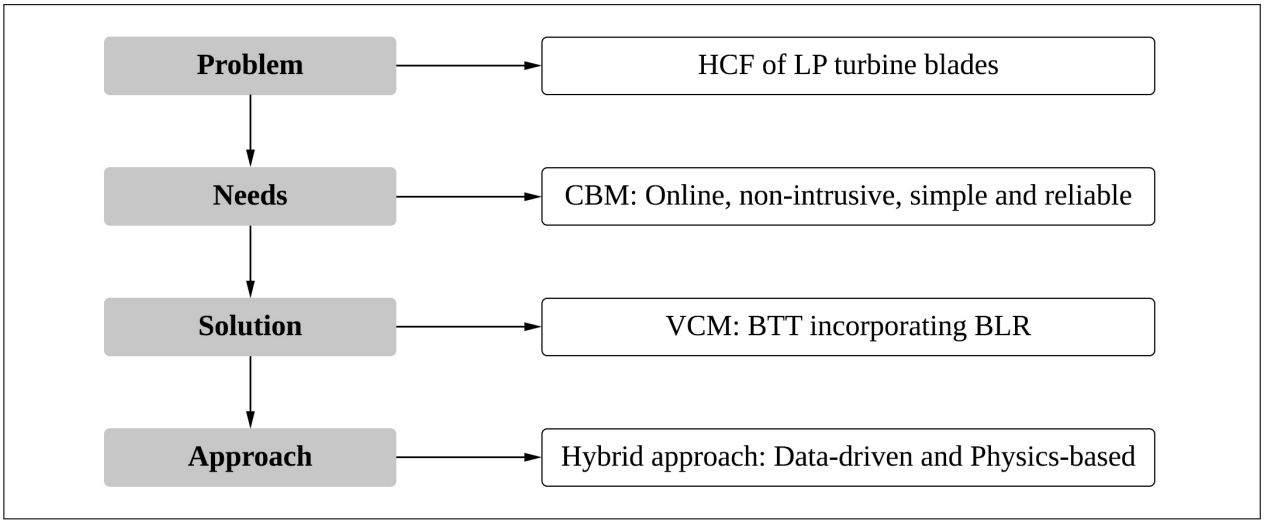

Figure 1.12: Summary of the various topics and outcomes of the literature review.

Table 1.2: Summary of the advantages and disadvantages of various hybrid approaches.

Model	Advantages	Disadvantages
H1	• Uncertainty is reduced from using a purely data-driven approach. • Adaptation of machine specific hypotheses in the absence of failure data. • Domain knowledge helps foresee the dynamics of degradation due to various operating conditions and failure modes. • Learning of machine nominal and faulty levels in absence of failure data.	• No guarantee of all the failure modes to be captured. • Lack of physics knowledge to support evidence of failure mechanisms. • Inability of expert knowledge capturing intermediate states may inhibit the interpolation capability of the reasoning system.
H2	• Physics-based models result in detailed and application specific models. • Physics-based model may be complex to initially set-up • Domain knowledge supports deterministic physics-based model.	• More accurate health prediction due to physics-based model. • Physics-based model may be computationally expensive. • Expert knowledge may not capture all failure modes.
H3	• Aggregation of data-driven models' results improve prediction performance. • Multiple data-driven models can help capture dynamics both in failure modes and operating conditions • Probabilistic answers are possible with regards to the RUL prediction.	• Using multiple data-driven models may be computationally intensive and impractical. • An abundance of historical data is required to train the data-drive models, which may not always be available. • The selection of an appropriate fusion mechanism is critical.
H4	• Mature approach with regards to the abundance of examples in literature. • Improved prediction accuracy due to the use of a physics-based model. • Possible to use a mathematically sound physics-based model to predict the system internal health, therefore making results easier to explain or post-process. • Various combinations and sub-models exist in the H4 hybrid approach therefore making it application specific.	• Selection of an appropriate fusion mechanism is critical. • An abundance of training data is required in order to initiate the data-driven models. • System model can significantly be affected by the alternating operating conditions, therefore affecting the capturing of fault propagation patterns. • The freedom in choosing an appropriate model within this category may add a degree of complexity.
H5	• Practically the most accurate method due to the heterogeneous nature of the predictions and diverse information-sets.	• May be extremely difficult and impractical to implement due to difficulties encountered by each type of model. • Fusion mechanism remains an issue. • Complexities associated with aggregating the results.

1.3 Scope of Research

This section refines the scope of the research project with regards to the identified problem areas, needs and proposed solution incorporating a hybrid approach. The scope is therefore discussed in terms of the outcomes from the literature review and the past contributions of research topics at the University of Pretoria (as shown in Figure 1.13). It was decided to discuss the past contributions of the Centre for Asset Integrity Management (C-AIM) due to the fact that this research project incorporates various aspects of previous work and in essence intends to build on this knowledge. In Figure 1.13 the alignment of the text-boxes (containing the information of the authors and topics) indicates whether the research was more concerned with data-driven, physics-based approaches or a combination of these approaches. Note that the contributions made by the Diamond of [Diamond et al., 2015] in the field of BTT were extensively used in this research (refer to Section 1.4). Figure 1.13 shows the long-term vision of C-AIM and indicates where the author of this research project makes further contributions in this field. Also note that the reference to the RUL estimation of turbomachine blades accounts for the long-term vision of the research in C-AIM and is by no means indicative of the outcome of this particular study.

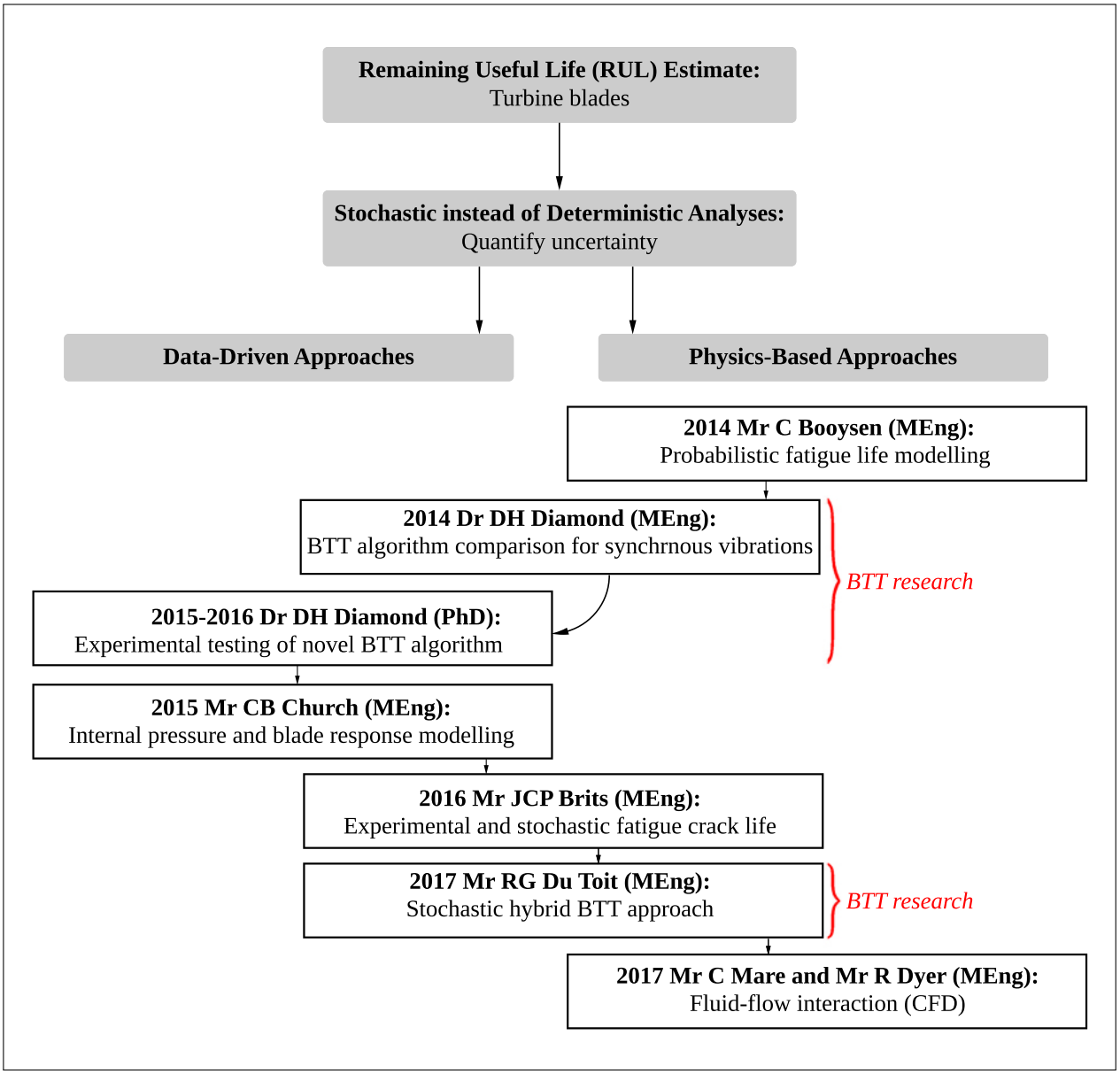

Figure 1.13: C-AIM contributions and vision.

The literature review starts off by identifying the main problem areas by using the power generation industry as an example. It is noted that the undesired downtime of power generation units is largely due to turbine failures and poor maintenance operations [McCloskey et al., 1999]. The most common cause of turbine failures is related to rotating blade failures [Gubran and Sinha, 2014] with roughly 42% of gas turbine failures being accredited to blade failures [Al-Bedoor, 2002]. Steam turbines are identified to be almost equally susceptible to blade failures, with 75% of these blade failures being LP blade failures [Diamond et al., 2015; EPRI, 1985]. The accumulation of HCF is specifically noted as one of the leading mechanisms of these blade failures, by roughly accounting for 30% of LP blade failures EPRI [1985]. It isemphasised that the unexpected failure of turbomachine blades may have catastrophic consequences. For the aforementioned reasons the damage related to turbomachine blades has been the focus of numerous research projects within C-AIM (as shown in Figure 1.13). The scope of this research therefore incorporates the following points related to the problem area:

- This study focuses on fatigue blade damage of turbomachine blades. The first bending mode of synchronous blade vibrations is focused on in terms of causing this fatigue damage.
- A rotor test setup is used for the experimental testing. The operational conditions excite the first bending mode of the blades.
- Incremental discrete blade damage is introduced to areas on the test blades where fatigue damage is most likely to occur. Discrete blade damage is introduced, as opposed to *naturally* propagating a crack, due to the difficulty of inducing natural cracks in the laboratory test rotor blades.

The literature review outlines a number of needs with regards to the aforementioned problem area. The distinct need to avoid catastrophic and unexpected failure of turbomachine blades is identified [Diamond et al., 2015; McCloskey et al., 1999]. The need to monitor the condition of turbomachine blades during the operation is therefore required, thus allowing an early warning of imminent blade failure. This could result in maintenance operations being scheduled based on the condition of the blades, therefore overcoming the need of undesired downtime due to unnecessary maintenance operations [Sikorska et al., 2011]. Booysen et al. [2015] emphasised the need for probabilistic principles to be incorporated in the monitoring techniques as this will enable uncertainties associated with the monitoring technique to be quantified. Brits [2016] further suggested the need for a stochastic analysis to be incorporated when modelling the physics associated with fatigue failures of turbomachine blades. The scope of this research project therefore incorporates the following points:

- The study focuses on avoiding catastrophic and unexpected failures of turbomachine blades. The study therefore also focuses on avoiding the unexpected downtime of turbomachines due to these failures.
- The study further focuses on the need for online and non-intrusive monitoring of these blades. Overcoming this need aims to enable the early warning of imminent blade failure, thus preventing the unexpected and catastrophic blade failure.
- The need of modelling uncertainty using probabilistic techniques is further investigated. Figure 1.13 indicates that the past research in C-AIM utilised stochastic analyses in order to quantify the uncertainty associated with various predictions.

BTT is regarded as one of the most promising techniques for blade VCM [Rigosi et al., 2017]. The reasons being that BTT offers the possibility of online and non-intrusive measurement capabilities [Diamond et al., 2015]. BTT further offers the possibility to monitor each blade in a particular stage of a turbine, therefore making this VCM technique very suitable for use in industry [Rigosi et al., 2017]. Diamond et al. [2015], however, mention that the processing of BTT data to find the associated vibration characteristics is a non-trivial task. These vibration characteristics are also difficult to validate, therefore resulting in a lack of consensus in published literature as to which BTT technique attains the greatest accuracy. Diamond et al. [2015] developed a new BTT algorithm which incorporates BLR to perform the curve-fitting of the blade response.

The scope of this research project incorporates the following points with regards to using BTT as a viable solution for the online and non-intrusive VCM of turbomachine blades:

- The use of a the BTT technique based on BLR is tested experimentally for the online and non-intrusive monitoring of test blades. Incremental discrete damage is introduced on a test blade during different BTT investigations and the proposed BTT technique is tested to sense changes in the vibrational characteristics of the blade due to this damage. It should be noted that the BLR post-processing in this study was done by Diamond [Diamond et al., 2015].
- The advantages of using the BTT based on BLR is practically demonstrated by noting that the parameters of the assumed SDOF response model of the blade are solved for as multivariate probabilistic quantities.
- The use of these multivariate probabilistic quantities to find the amplitude and phase values associated with the blade response is proposed. The natural frequencies of the blades are then determined by performing a feature extraction process on the corresponding amplitude and phase results.

The requirements of a proven reliability and simple implementation of a monitoring technique (as discussed by Rao and Dutta [2012]), however, also needs to be considered. Diamond et al. [2015] outlined scepticism surrounding the use of BTT as a VCM tool, mainly due to the aforementioned difficulty in determining its accuracy. Liao and Köttig [2014] and Mishra et al. [2014] documented extensive examples of hybrid methodologies for the use in diagnostic and prognostic applications. More so, the advantage of using a hybrid approach to improve the reliability of the proposed monitoring technique was noted. The use of a hybrid blade condition monitoring approach is therefore proposed in this research project. The scope and contributions of the research incorporates the following points with regards to using a hybrid approach for the VCM of turbomachine blades:

- A hybrid approach is proposed for the *identification* and *classification* of turbomachine blade damage. The proposed hybrid approach incorporates a stochastic FEM modal analysis (physics-based) in order to supplement the BTT (data-driven) results, while also offering the potential to project expected blade conditions. The decision of whether a turbomachine outage should be scheduled, based on a blade damage threshold being reached, is proposed as the output of the hybrid approach. The following is specifically proposed with regards to the blade damage *identification* and *classification* procedures:
  - *Damage identification:* The changes in the blade natural frequencies are tracked as relative quantities in order to keep this process as general as possible. It is further aimed to test the ability of the proposed hybrid approach to track small changes in the natural frequencies of the blades. This relative natural frequency tracking is done for both the BTT and FEM modal analysis results. The concept of a probabilistic blade damage threshold based on a stochastic hybrid approach is presented and demonstrated. This probabilistic damage threshold aims to provide sufficient evidence that a turbomachine outage should be scheduled for relevant maintenance operations to commence
  - *Damage classification:* An unsupervised clustering technique is proposed to classify BTT measurements into various damage severity groups. A fundamental feature of this method is the use of the FEM modal analysis results for cluster initialisation. The blade damage threshold for this implementation is proposed as purely an acceptable severity of blade damage based on the classification of the BTT results. Again, this is practically demonstrated in the research.
- Varying temperature effects are incorporated in the research in order to test the ability of the proposed hybrid approach to function under these conditions. The aforementioned damage *identification* and *classification* procedures are tested at the different temperatures. Various strategies are proposed for the damage classification procedure in an attempt to overcome the effects of the varying temperature, with regards to the clustering of the BTT results.

The author is aware that the literature review (Section 1.2) does not provide motivation for the consideration of varying temperature effects. This is partly due to BTT literature providing limited information with regards to the effects of varying temperatures on the performance of existing BTT techniques. The author therefore provides motivation for this consideration as part of the various stages in the experimental investigation. This is formally documented in Chapter 3 (specifically Section 3.5.3).

- The possibility of combining the BTT results is proposed for the long-term archiving of this data. This archiving strategy is demonstrated and the benefits of this strategy, in terms of its implementation in industry, are elaborated on.

The proposed hybrid approach is tested using an experimental rotor setup (used to acquire the BTT data) and a FEM modal analysis. The ability of the proposed hybrid approach to identify and classify turbomachine blade damage, therefore providing evidence of a damage threshold being reached, is specifically tested.

1.4 Limitations

The purpose of this research is to advance the state of the art in BTT technology into a stochastic hybrid approach, used for the identification and classification of turbomachine blade damage. This stands in stark contrast to the vast majority of current BTT research where purely data-driven approaches are used, most of them being deterministic in nature. It was therefore decided, before the commencement of this research, that Dawie Diamond (a study leader for this research), should perform the BLR analyses of all the experimental data obtained in this research. The results of the BLR analyses were then used as a starting point to propose, develop and test a hybrid approach. This decision was made for the following reasons:

1. The BLR technique and all related techniques used for the processing of raw BTT ToA data is currently being commercialised by the University of Pretoria and the South African power utility, Eskom. The methods and techniques are the subject of three Patent Cooperation Treaty (PCT) applications, with these patents not yet finalised. For this reason, a deliberate effort has been made to avoid the description of any sensitive information concerning BLR.
2. The fact that the BLR analyses were not part of the contribution of this study allowed the author to significantly advance towards a BTT stochastic hybrid approach. This further allowed the author to take into account the effects of varying temperature in BTT, something completely new to BTT research to the knowledge of the author. The potential to leverage existing and in-house expertise in BLR, to create advancements that would not have been possible otherwise, has therefore been fully exploited.

The BLR method, and related methods, have been implemented in the *Python* programming language in a software package referred to as *Vibrapy*. *Vibrapy* is currently not available to the public. Throughout this document, many of the outputs of the *Vibrapy* software are used in the form of figures and mathematical quantities.

1.5 Document Overview

The proposed stochastic hybrid BTT approach for the identification and classification of turbomachine blade damage is outlined in Chapter 2. This chapter gives an overview of the various processes used in this approach. This chapter further discusses the advantages and disadvantages of purely data-driven or physics-based approaches, therefore motivating why a hybrid approach is attractive solution for its intended use.

Chapter 3 gives a detailed overview of the experimental testing (procedure and setup), BTT signal processing and blade condition monitoring steps are further elaborated on. The BTT investigative process is discussed with regards to the various groups and stages of experimental testing. Initial BTT results are also presented in this chapter, thus providing an indication of the performance of the proposed BTT technique based on BLR. Recommendations are presented after each BTT investigative stage, therefore motivating why certain aspects were considered or neglected.

Chapter 4 describes the FEM modal analysis. More importantly, the intended use of the FEM results as part of the hybrid approach is discussed. Preliminary FEM modal analysis results are presented and various recommendations are made regarding the use of these results in the hybrid approach. This chapter therefore motivates the use of a FEM modal analysis in the hybrid approach.

Chapter 5 formally presents the results of the research with regards to its intended use in the proposed hybrid approach. The relative natural frequency tracking results are presented and discussed with regards to the blade damage identification procedure. The clustering implementation is discussed in greater detail and its intended use in the blade damage classification procedure is elaborated on. The results from this clustering implementation are presented, discussed and summarised.

The research is concluded in Chapter 6 and recommendations for future work are made. This dissertation includes two appendices. *Appendix A* provides logistical information about the research, specifically with regards to the naming convention used during the BTT experimental testing. *Appendix B* includes auxiliary information related to the BTT analysis. This includes further details of the experimental testing, setup and methodology. This appendix also provides supplementary results from the various BTT investigations.

Chapter 2

Hybrid Approach

2.1 Overview

The purpose of this research is to propose a stochastic hybrid BTT approach for the identification and classification of turbomachine blade damage. This chapter gives an overview of the proposed hybrid approach by introducing various aspects of the research. This is vital to give a clear overview of the intended approach before the specific topics are discussed in detail. Motivation for the intended approach stems from the literature review presented in Section 1.2 and the research scope outlined in Section 1.3. Figure 2.1 shows the process flow of the proposed hybrid approach.

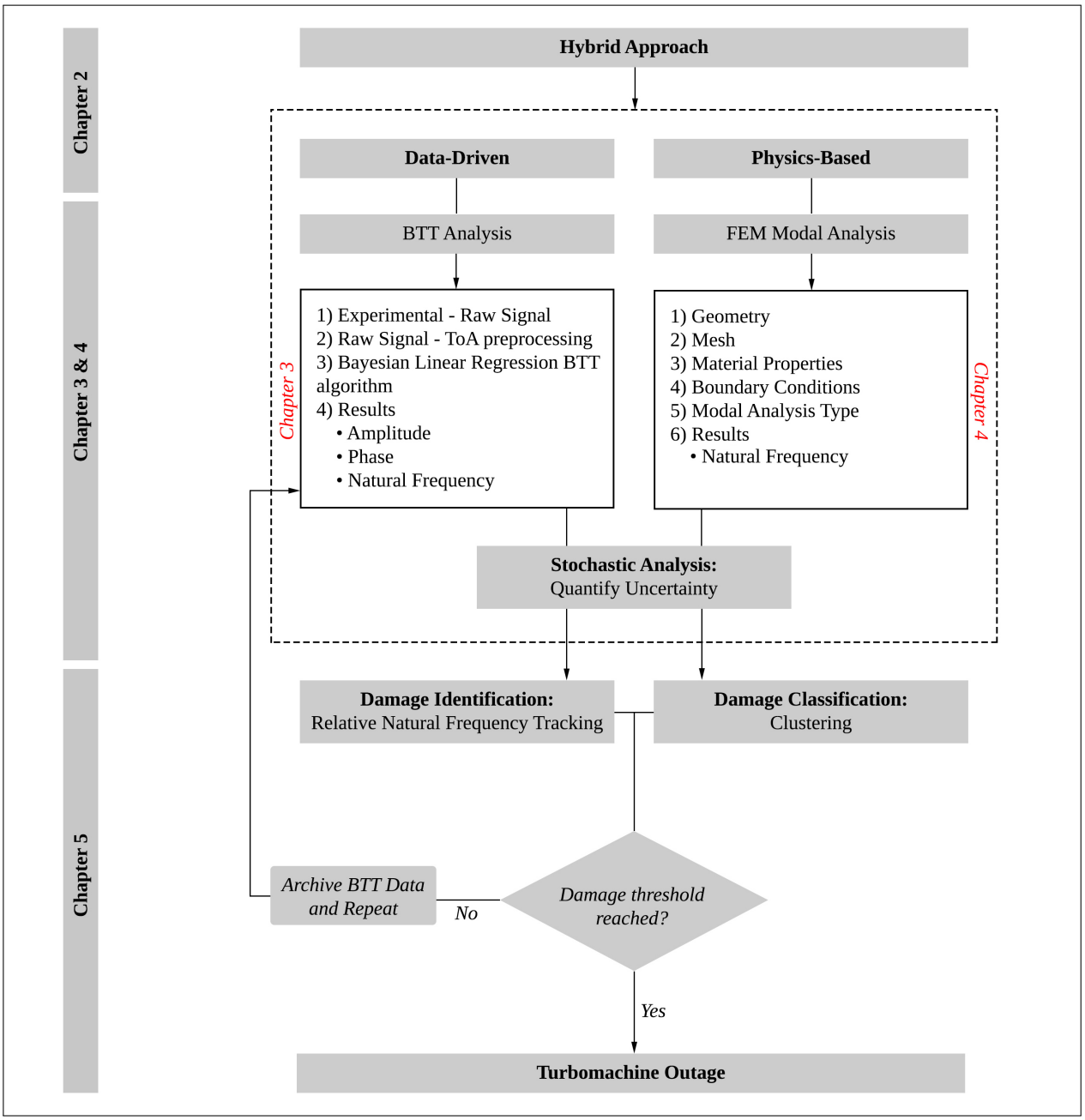

Figure 2.1: Proposed hybrid approach.

Figure 2.1 also relates the process flow of the hybrid approach to the detail discussed in each of the remaining chapters in this document. In Chapter 1 the problem of potentially unexpected and catastrophic blade failures, mainly due to HCF, is introduced. Section 1.2.2 specifically emphasised that poor maintenance strategies is part of this problem. Section 1.2.3 further highlights the need for a paradigm shift from SBM to NBM. It is identified that the online and non-intrusive monitoring of turbomachine blades using BTT would aid this paradigm shift. Adopting this VCM approach would in theory enable the early detection of blade damage, thus ensuring that the need for maintenance operations is justified in a more proactive way. However, purely detecting blade damage and scheduling a turbomachine outage as a result is not always a practical. There needs to be enough evidence to justify that the blade damage poses a risk of imminent failure.

The ideal scenario would incorporate the RUL estimation of each turbine blade and maintenance operations could then be scheduled according to this estimate. However, Mishra et al. [2014] highlighted that this is not always possible due to many complexities and uncertainties associated with such a prediction. Furthermore, the requirements outlined by Rao and Dutta [2012] dictate that a diagnostics / prognostics approach should be simple to implement, as well as reliable. For aforementioned reasons, the proposed hybrid approach for the purposes of this research will not estimate the RUL; however, this is certainly a desired outcome for future work. Again, it should be emphasised that the proposed hybrid approach aims to be reliable in terms of its outputs while also being relatively simple to implement in industry. The remaining sections in this chapter will briefly introduce the various aspects of the proposed hybrid approach. The hybrid approach output will also be discussed to give further perspective of the aim of this research project.

2.2 Hybrid Approach Output

Figure 2.1 shows that the output of the proposed hybrid approach will be to determine whether a turbomachine outage should be scheduled. Also shown in Figure 2.1 is that the decision to schedule this outage will be based on the indication of whether a blade damage threshold has been reached. Mishra et al. [2014] proposes a thresholds as part of an RUL estimate where the component health and associated degradation is tracked over time. For the purposes of the proposed hybrid approach, the damage threshold will be a measure of the uncertainty in the prediction or an *acceptable* severity of blade damage (detail discussed in Chapter 5). Naturally, the ability of the proposed approach to detect a fault precedes the indication of whether a damage threshold has been reached. Detecting a fault / damage specifically involves the detection of an abnormal vibration signature of a blade [Randall, 2011]. This vibration signature may include the amplitude, phase information and associated natural frequency of the blade vibration. The change in vibration signature is typically due to blade damage causing the decrease of the blade stiffness [Madhavan et al., 2014]. The two categories of information that will be used as evidence for the damage threshold are:

1. *Damage identification:* Sikorska et al. [2011] identified that fault identification is an important aspect of diagnostics following fault detection. Fault / damage identification specifically involves estimating the nature and extent of a fault. In the context of the proposed hybrid approach damage identification involves: tracking the relative change in the natural frequency of the blade in order to identify and infer the degree of discrete blade damage. The change in natural frequency from an initially undamaged state will in essence be quantified. More detail regarding this is discussed in Chapter 5 (Section 5.2).

2. *Damage classification:* The natural frequency and amplitude of the BTT results are clustered using predetermined mean values. These predetermined mean values are derived from a FEM modal analysis whereby possible blade conditions and corresponding vibration characteristics are simulated. The clustering of these *measured* BTT values thus enables the severity of the blade damage to be classified. According to Mishra et al. [2014] many classification techniques exist and more detail regarding this is discussed in Chapter 5 (Section 5.3).

This particular hybrid approach incorporates various aspects of the review presented by Mishra et al. [2014]. In this review it was highlighted that past CBM techniques heavily focus on traditional statistical approaches. The study by Jardine et al. [2006] gave a good overview of various statistical methods, where the detail of all the aspects from data-acquisition to maintenance decision making are discussed. However, Mishra et al. [2014] indicate that there have been a number of noteworthy advancements in the field of Artificial Intelligence (AI) and machine learning since 2006. Lee et al. [2014] acknowledge this hype in maintenance strategies incorporating AI approaches. These AI approaches intend to complement the traditional approaches by establishing a basis of comparison for the results. This may potentially result in a higher accuracy of the desired prediction. Many AI or machine learning approaches exist, thus the reader is referred to Mishra et al. [2014] for a thorough overview of examples of popular approaches.

The choice of AI or machine learning approach largely depends on the type of prediction that needs to be made. The output of the hybrid approach shown in Figure 2.1 requires information about the predicted severity of blade damage. In order to do so, the vibrational state of the blade during operation at resonant conditions will be considered. A feature extraction process of the measured data would be required to infer a change in the blade condition due to the change in the associated values of the features. Typical vibration-based features were outlined previously as the amplitude, phase information and the corresponding natural frequency (the detail of these features will be discussed in Chapter 3, Section 3.4.2). The proposed hybrid approach therefore incorporates a clustering based technique whereby features are grouped according to its associated level of blade damage severity. Some of the advantages and disadvantages of different clustering techniques are shown in Table 2.1. In the context of the desired output, the damage classification (clustering) results aim to complement the damage identification process. An in-depth explanation and motivation for the use of clustering is presented in Chapter 5, Section 5.3.

Table 2.1: Summary of the advantages and disadvantages of different types of clustering techniques, adapted from Mishra et al. [2014].

Advantages	**Disadvantages**
• There is an easy adaptation to new data by changing the clustering algorithm accordingly.	• Performance of the technique is highly dependent on the effectiveness of the clustering algorithm capability to capture normal instances.
• The unsupervised operation of the technique is possible.	• An anomaly may accidentally be added to a large cluster.
• A relatively fast testing phase of the algorithm is possible.	• Anomaly detection occurs as a by-product of clustering and is not optimised.

As previously mentioned, the main purpose of the current research is to propose a feasible hybrid approach to overcome the outlined problems related to turbomachines. However, determining the feasibility of the proposed hybrid approach largely depends on demonstrating its capabilities. What remains in this chapter is an overview of how the proposed hybrid approach will be tested, specifically by incorporating the data-driven and physics-based approaches. The basis of the investigation will therefore be to introduce discrete blade damage incrementally to an initially undamaged blade. In doing so, the performance of the hybrid approach in detecting, identifying and classifying the blade damage will be tested. The phases of the damage introduced will be as follows:

1. Collect vibrational data of the initially undamaged blades and use this as a reference.
2. Introduce discrete damage to a specific blade and collect new vibrational data.
3. Incrementally increase the size of the discrete damage, collect the new vibrational data and repeat this process until a damage threshold is identified. Figure 2.1 shows that this damage threshold is used to determine whether a turbomachine outage should be scheduled.

2.3 Data-Driven Approach

Figure 2.1 indicates that the data-driven approach incorporates the BTT analysis. The chosen BTT analysis incorporates the BLR based method introduced by Diamond et al. [2015] and is referred to as *Vibrapy* in this dissertation. This BTT method was chosen due to the advantages outlined in Section 1.2.7. The main advantage of this method is that BLR is specifically used to infer the values of the constants A, B and C (from the assumed SDOF blade response function shown in Equation 1.6) as probabilistic quantities. The fact that these values may be be calculated as probabilistic quantities enables further statistical analyses of the post-processed vibrational data. As indicated in Figure 2.1, this allows the BTT analysis to employ a stochastic analysis, therefore allowing uncertainty of the BTT results to be quantified by establishing confidence bounds.

In this study experimental tests are conducted using a bladed-rotor setup. This setup merely intends to facilitate the practical simulation of similar operating conditions expected in industry (although it is a recommendation to test the proposed hybrid approach in industry). The experimental tests are categorised according to various stages, where different aspects of the proposed BTT approach are tested. All the formal experimental tests, however, involve the incremental introduction of discrete blade damage in order to represent the possible consequence of HCF. A number of experimental tests are conducted for each stage of experimentation in order to obtain as much practical BTT data as possible. The post-processing of the measured BTT data aims to enable a number of features to be extracted and these features will be used as inputs in the remaining processes of the hybrid approach. Table 2.2 summarises some of the advantages and disadvantage of using a purely data-driven approach, as documented by Mishra et al. [2014]. More details of the experimental setup and BTT methodology (shown in Figure 2.1) follows in Chapter 3.

Table 2.2: Summary of possible advantages and disadvantages of data-driven approaches, adapted from Mishra et al. [2014].

Advantages	**Disadvantages**
• Relatively fast and simple implementation depending on the choice of technique.	• Large amounts of data is generally required and it is difficult to know when the data is sufficient.
• It may be difficult to form a balance between generalisations and *learning* specific trends in data.	• Expert knowledge or learning from field data may still be required for model parameter tuning.
• Anomalies may occur in certain instances and averaged past learning data may not help to predict this accurately.	• Models may be computationally expensive to run and therefore impractical for real-time applications.
• Evidence of what actually happened is present, which may be less apparent in theory.	• Specific physical cause-effect relationships are not utilised; different fault growths for example.

2.4 Physics-Based Approach

Diamond et al. [2015] highlight that there is no consensus in published literature as to which BTT method attains the greatest reliability or accuracy. The reason is partly due to the difficulty in validating turbomachine vibration measurements. Furthermore, the accuracy of experimental BTT results may also be difficult to determine without taking the physics of a particular blade into account. For these reasons it is proposed to utilise a physics-based approach in the hybrid model that supplements the BTT results. The use of a FEM modal analysis also aims to project expected blade conditions associated to the blade damage. By incorporating a Finite Element Analysis (FEA), the physics associated with the change in blade vibrational conditions will be considered.

Discrete blade damage will therefore also be introduced in this model and thereafter a FEM modal analysis will be performed to derive the vibrational characteristics of the damaged blade. This simulation intends to project the expected blade conditions, therefore allowing a further basis of comparison for the BTT results. Further indicated in Figure 2.1 is that the FEM modal analysis will incorporate a stochastic rather than deterministic approach by simulating uncertainty in the model parameters (this will be related to material properties, boundary conditions and the discrete blade damage). Table 2.3 summarises some of the advantages of using a purely physics-based approach, as documented by Mishra et al. [2014]. More details regarding the aforementioned FEA (shown in Figure 2.1) follows in Chapter 4.

Table 2.3: Summary of possible advantages and disadvantages of physics-based approaches, adapted from Mishra et al. [2014].

Advantages	**Disadvantages**
• Prediction results are generally intuitive and based on modelled case-effective relationships.	• Deviations may signify the need to add more fidelity for unmodelled effects to handle noise.
• Only model calibration is required to model different cases once a base model is established.	• Expert knowledge or learning from field data may still be required for model parameter tuning.
• Prediction results are highly accurate if the incorporated physics remains consistent across the systems.	• Models may be computationally expensive to run and therefore impractical for real-time applications.

2.5 Summary

The purpose of this research is to propose a stochastic hybrid approach utilising BTT for the identification and classification of turbomachine blade damage. The proposed methodology therefore needs to be tested in terms of its feasibility for practical implementation. In-doing so, it was highlighted that discrete blade damage will be introduced to a test blade. This will be done experimentally, during which the proposed BTT method incorporating BLR will be tested. The application of a hybrid approach aims to alleviate the disadvantages of an individual analysis type while conserving its advantages [Liao and Köttig, 2014]. The following points highlight the advantages of the proposed hybrid methodology:

1. The FEA establishes a basis for comparison for the BTT results.
2. The FEA makes it possible to project expected blade conditions, which may not be available from practical BTT measurements for quite some time.
3. The BTT analysis accounts for real measurements and aspects not considered using the FEA.
4. Combining the individual approaches may ultimately result in a higher prediction accuracy and a greater reliability.

The experimental BTT results and FEM results will be used in conjunction with one another to infer the test blade condition as part of the proposed damage identification and classification procedures. Figure 2.1 indicates that a blade damage threshold will be established for the aforementioned damage identification and classification analyses. If this threshold is met the operation of the turbomachine will be halted and relevant maintenance operations will commence. Furthermore, the BTT analysis will be repeated until this threshold is reached. Importantly, the measured BTT data will be archived in order to form a database of the individual blade conditions. The archived data is important in the sense that it establishes a reference condition for the damage identification and classification of the BTT data. The proposed methodology shown in Figure 2.1 was tested on a laboratory setup and will be discussed in detail in the remainder of the report.

Chapter 3

BTT Analysis

3.1 Overview

This chapter describes the detail of the chosen BTT analysis used in the proposed hybrid approach shown in Figure 2.1. The application of the chosen BTT analysis aims to provide practical data, thus enabling the chosen BTT technique to be tested. More so, the ability of the BTT technique to provide the relevant information for the blade damage identification and classification outcomes of the hybrid approach was tested. Incremental blade damage was introduced to selected blades during experimentation to test these outcomes. The detail of the experimental testing (setup and procedure), BTT signal processing and post-processing of the BTT data is therefore outlined in this chapter. Before the detailed discussion of this it is important to take note of the various groups and stages shown in Figure 3.1. Performing the experimental BTT tests in various stages assisted with initial feasibility checks and allowed increasing investigative complexity in consecutive stages. The basic overview of the various BTT investigative groups will be discussed in this section and the detail discussion will follow in the remaining sections of this chapter.

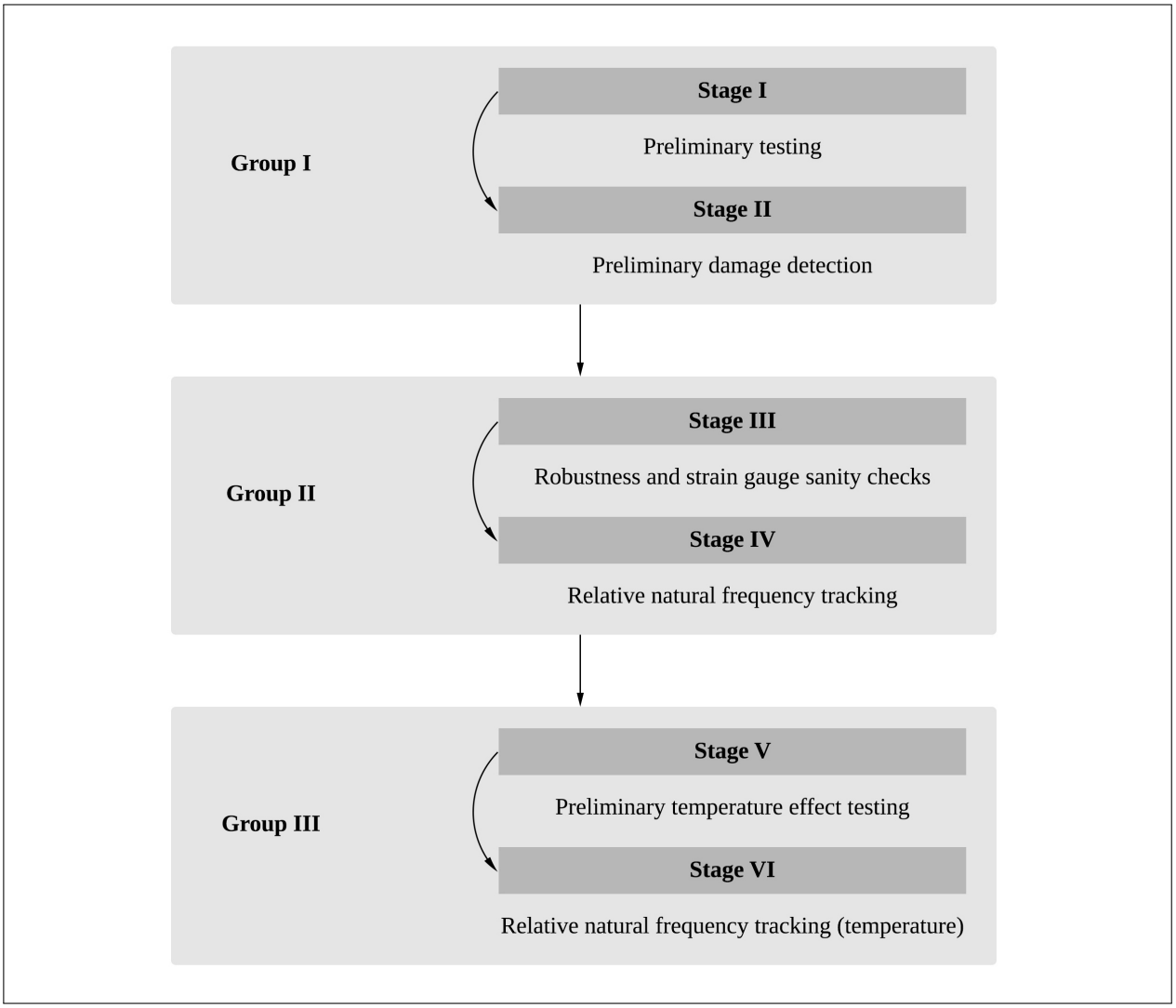

Figure 3.1: Stages of the BTT investigation.

A brief overview of the various BTT investigative groups and associated stages shown in Figure 3.1 follows (the detailed overview of the equipment used in these stages follows in Section 3.2):

- *Group I:* This group consists of the preliminary testing which improved the author's competence in BTT. The equipment was set up and the safety of the test-rig was improved.
  - *Stage I:* This stage comprised very general initial BTT tests. No blade damage was introduced during this stage and BTT data was captured for a constant shaft speed. Some signal processing algorithms used to extract the ToAs were developed. The desired investigation to use BTT for blade damage detection was also conceptualised during this stage of testing.
  - *Stage II:* The preliminary damage detection using the proposed BTT analysis was tested. In order to do so a varying speed profile was used to ramp the shaft speed up and down through predetermined critical speeds. As a result BTT measurements could be acquired for each blade at resonance (due to synchronous blade vibrations). This process was repeated a number of times, with all the blades in an initially undamaged state. Thereafter a blade was selected and a crude discrete crack was introduced. Various BTT signal processing algorithms were developed which enabled blade conditions to be determined from the derived blade vibration characteristics (more detail about this will be discussed in Section 3.3). The vibration characteristics of the undamaged and healthy blades were compared to determine whether a further blade condition investigation would be feasible.
- *Group II:* This group forms the bulk of the BTT investigation where discrete blade damage was introduced to a test blade and the changes in blade vibrational characteristics were tracked.
  - *Stage III:* A number of the same tests were performed to determine how robust the chosen BTT approach was for these tests. Furthermore, strain gauges were attached to a particular blade along with a slip ring on the rotor-hub. Signal processing of the strain gauge signal acted as a sanity check of the derived natural frequency results. More detail about this follows in Section 3.5.2.
  - *Stage IV:* Discrete blade damage was incrementally introduced to a particular blade and a number of BTT tests were performed. Repeated tests were performed for each damage increment and the relevant BTT signal processing followed. The details of this is discussed in Section 3.5.2.
- *Group III:* This group of testing incorporated the effects of varying blade temperature on the hybrid approach. This group of testing in essence replicated the investigation of *Group II*, however, the ambient air temperature surrounding the rotor was varied to heat the blades.
  - *Stage V:* Various methodologies to heat the blades in the rotor assembly were tested and the most feasible or practical solution was selected for further testing. Various troubleshooting issues resulting from the increased temperature were also addressed. More detail about these issues and associated recommendations follow in Section 3.5.3.
  - *Stage VI:* This stage is more or less a repeat of *Stage IV*. The only difference being that the testing was done for two blade temperatures. Incremental discrete cracks were introduced to a new blade and it was aimed to keep the size of the final crack similar to that of *Stage IV*. The detail regarding this is discussed in Section 3.5.3.

The details of the aforementioned investigations is discussed in Section 3.5. An overview of preliminary results is discussed in this section. Before the details of the various investigations are presented it is important to take note of the general BTT procedure that was implemented. The detailed overview of this procedure is shown in Figure 3.2. Three main categories are shown for this BTT procedure, namely: experimental testing, BTT signal processing and the determination of the blade condition from the resultant vibrational characteristics.

The details of the experimental testing, with regards to the signal generation and data acquisition, are discussed in Section 3.2. Thereafter, the various processes and algorithms used in the BTT signal processing are outlined in Section 3.3. An introduction of how the blade condition was determined from processed BTT data follows in Section 3.4. The specific contributions of the author, in line with the BTT signal processing and blade condition value-chain, is highlighted in the remaining sections of this chapter. Lastly, the detail of how the various BTT investigations incorporated the BTT procedure shown in Figure 3.2 will follow in Section 3.5.

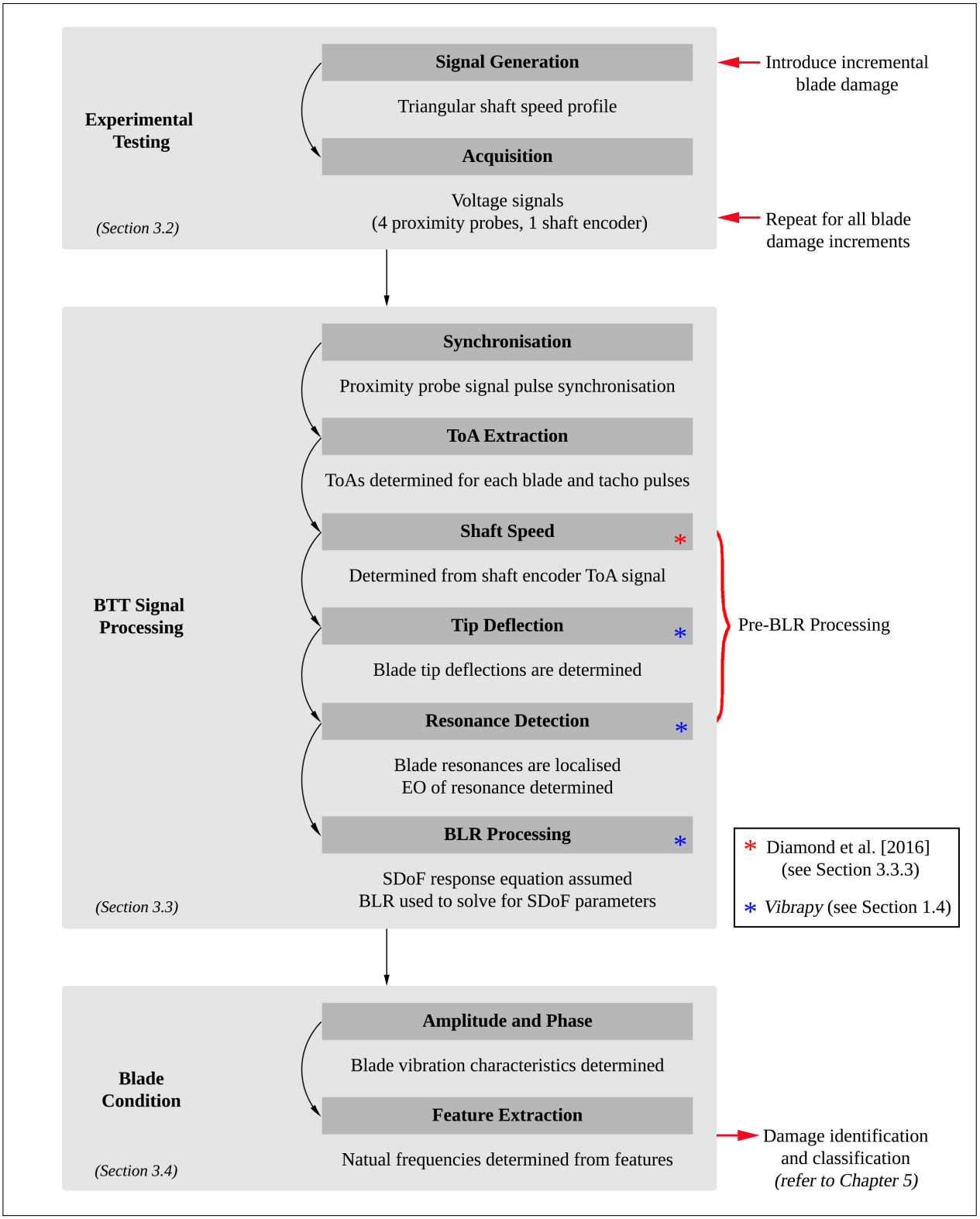

Figure 3.2: BTT procedure overview.

3.2 Experimental Testing

3.2.1 Overview

Figure 3.2 indicates that the experimental testing comprised two processes, namely: signal generation and acquisition. The details of these processes are discussed in the remainder of this section. Importantly, the BTT analysis is limited to purely synchronous blade vibrations, therefore requiring that the shaft speed profile induces these blade vibrations. Another requirement was the acquisition of only relevant data for further BTT signal processing. The appropriate sensors, acquisition equipment and software were used to meet these requirements. A comprehensive understanding of the experimental equipment was essential before any formal BTT tests were performed. This section therefore aims to give an in-depth overview of the experimental setup and BTT investigative procedures outlined in Figure 3.1. In short, the desired outcome of the experimental testing was to gather data to demonstrate the use of BTT for damage identification and classification. The details of the experimental testing follows.

3.2.2 Experimental Setup

Figure 3.3 shows a rendered diagram of the experimental rotor assembly used for the BTT testing. The setup is ideal for experimental testing, as it facilitates various sensors to be placed on the rotor housing / casing. Furthermore, the bladed assembly shown in Figure 3.3 may also be easily removed, therefore allowing a completely new set of blades to be tested. However, it was aimed to maintain a level of consistency between the various tests in an attempt to facilitate a control during the BTT investigations. For example, removing the bladed assembly and replacing it on the shaft runs the risk of changing the reference angle measured between a certain blade proximity probe pulse and a particular zebra strip shaft encoder pulse. The measured proximity probe signals, with reference to the shaft encoder signal, would therefore be inconsistent amongst the same tests. For this reason, the required blades on the bladed assembly were removed individually. This was done by removing the sensor mounting plates and detaching a single blade at a time. Also shown in Figure 3.3 is the slip ring attachment; the slip ring enabled strain gauges to function during the normal operation of the rotor without obstructing the rotational path. Strain gauges were only placed on a single blade during a particular batch of tests as a sanity check of the BTT results (the detailed discussion follows in Section 3.5.2).

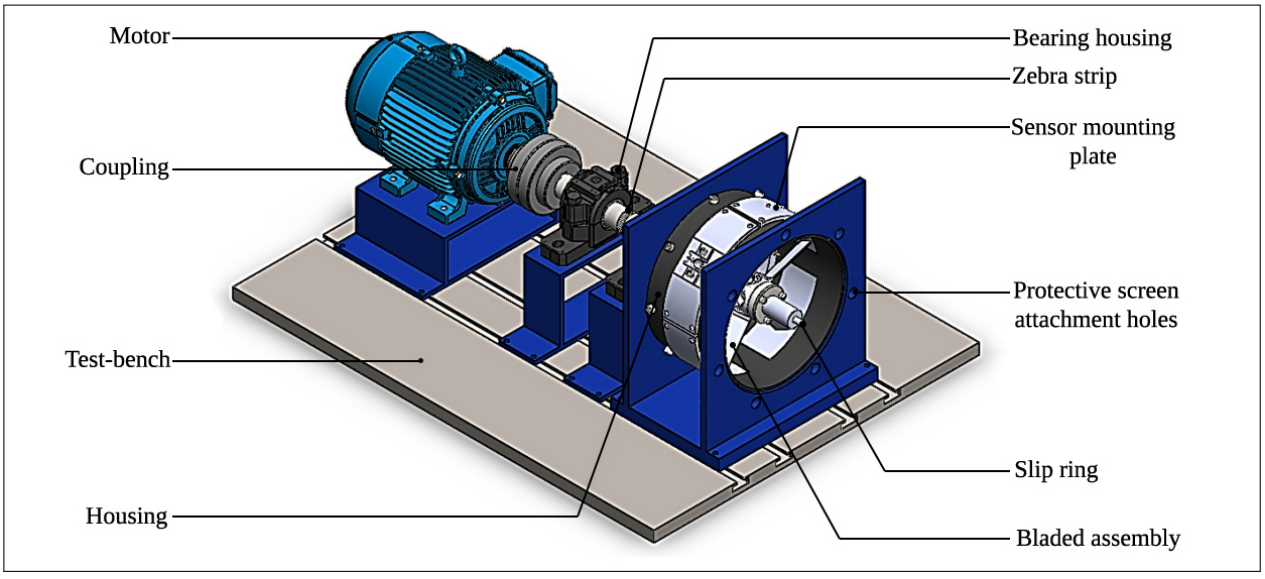

Figure 3.3: Rendered diagram of experimental rotor assembly, adapted from [Church, 2015].

Figure 3.4a shows a close-up photograph of the actual rotor assembly. Clearly shown in Figure 3.4a is the bladed assembly attached to the rotor hub. As previously noted, these blades are individually fastened to the hub and may be removed individually. Also shown in Figure 3.4a are the compressed air nozzles around the inner circumference of the rotor housing. Only the top and bottom compressed nozzles were used to excite the blades during rotation. The fact that the rotor casing is open at the back and front ensured that the blades were easily accessible during tests. However, this posed a safety concern at higher operational speeds, especially when a large discrete crack was introduced to a certain blade. For this reason, failure calculations were performed to determine if there is indeed a risk of a blade breaking off during operation at resonant conditions. During these calculations an acceptable / safe size for the discrete blade crack was determined according to a relevant stress-criteria. As an extra precaution, 8mm polycarbonate safety-screens were fitted to the front and back of the rotor housing, with the attachment sleeves shown in Figure 3.4a.

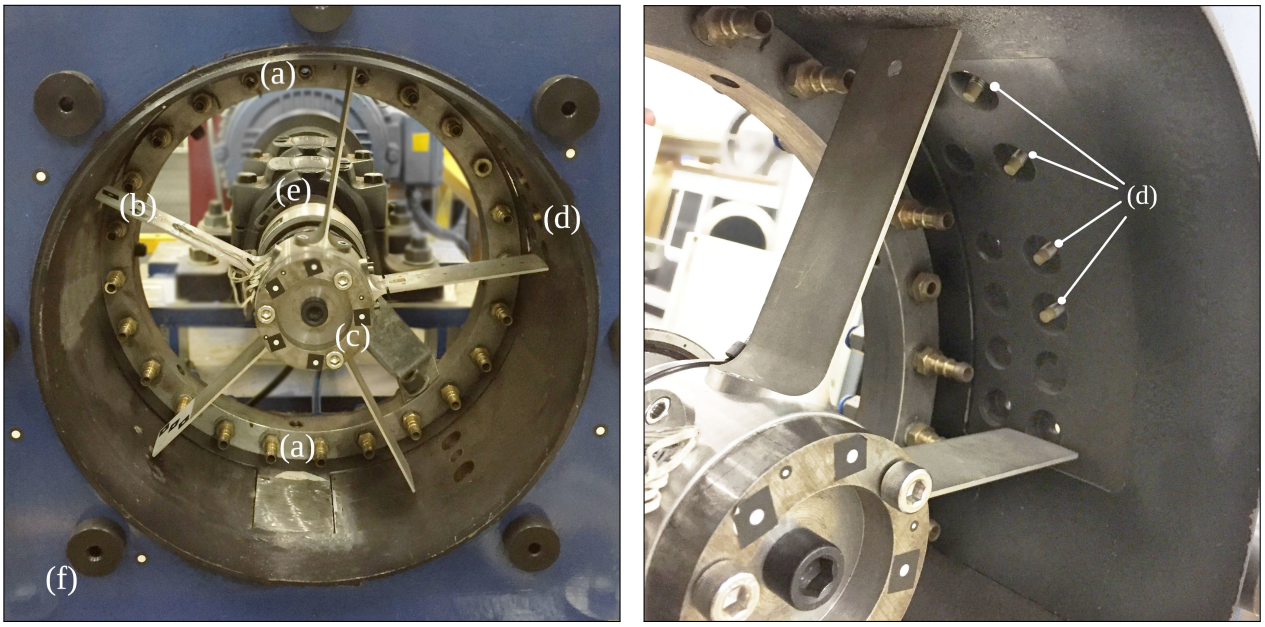

(a) Rotor assembly.

(b) Casing with proximity probes.

Figure 3.4: Experimental setup.

Figure 3.4b shows a close-up of the eddy current proximity probes used during experimentation. These proximity probes were placed so that the centre of the blade tips pass the probe. It was essential to fine-tune how far these proximity probes protrude from the rotor casing; too far-out would result in the blades scraping the probes and too far-in would result in undetectable blade passing pulses (these proximity probe have a maximum measuring range of 2mm). Also shown in this figure is the irregular spacing of the proximity probes around the circumference of the rotor housing. The reasons for the irregular spacing is discussed in Section 3.3. A summary of the main components of the experimental setup, with reference to the labels in Figure 3.4, is as follows:

a. Compressed air supply nozzles for blade excitation (top and bottom of casing).

b. Bladed assembly comprising 5 aluminium 6082 T6 blades; with a root-to-tip length of 132mm, a width of 40mm and a 2mm thickness at the aerofoil (as shown by Figure 3.6a).

c. Central blade hub with slip ring mounting holes (for strain gauge wiring). The strain gauges were used as an initial sanity check of the BTT results for the damaged blade.

d. Rotor casing with 4 irregularly spaced eddy current proximity probes.

e. Shaft connected to a motor with variable speed control.

f. Polycarbonate safety-screen's attachment sleeves.

The detailed design drawings of the rotor setup may be found in Appendix B.1.1. In short, the experimental setup broadly consisted of the following: rotor assembly, excitation mechanism, sensors, an acquisition system and a signal generation system. The signal generation and data acquisition systems are discussed in Section 3.2.3.

3.2.3 Experimental Procedure

Before the experimentation commenced the required shaft speed profile for blade resonance was determined. This profile was chosen by firstly determining which speeds were possible using the 5.5kW motor. The maximum motor speed was determined to be roughly 1400 RPM. Secondly, it was required to inspect the theoretical Campbell diagram of the undamaged blades. Figure B.4 in Appendix B.1.2 shows the derived Campbell diagram of the healthy blades. This Campbell diagram was generated by Church [2015] as part of a FEM modal analysis in the *ANSYS* commercial software environment. This diagram was specifically generated by performing a number of pre-stress analyses in order to determine the natural frequencies across the motor operational speed range of 0 RPM to 1400 RPM [Church, 2015]. More detail regarding the formulation of Figure B.4 is documented in Appendix B.1.2.

From the Campbell diagram (Figure B.4) it was determined that critical shaft rotational speeds of 1100 RPM and 1290 RPM would result in the first natural frequencies of vibration of the blades being excited. Also indicated in Figure B.4 is that the associated blade natural frequency is an integer multiple of the shaft speed (or EO). This is due to the occurrence of synchronous blade vibrations. An example of the general speed profile implemented during the experimental testing is shown in Figure 3.5 below. The triangular shaft speed profile passes through the critical speeds during acceleration and deceleration. This results in the blades vibrating at the first natural frequency when a critical speed is passed. An interesting observation from the Campbell diagram shown in Figure B.4 is the effect of blade stiffening (due to higher rotational speeds) on the resultant natural frequencies. When considering the theoretical blade natural frequencies at 0 RPM and 1400 RPM, a 2.3 Hz increase in natural frequency is noted for the higher speed. A blade increasingly stiffens, at an increasingly higher operational speed, due to the resultant centrifugal load being directly proportional to the square of the blade angular velocity. The effects of blade stiffening were observed during the BTT investigation and is elaborated on in Section 3.3.

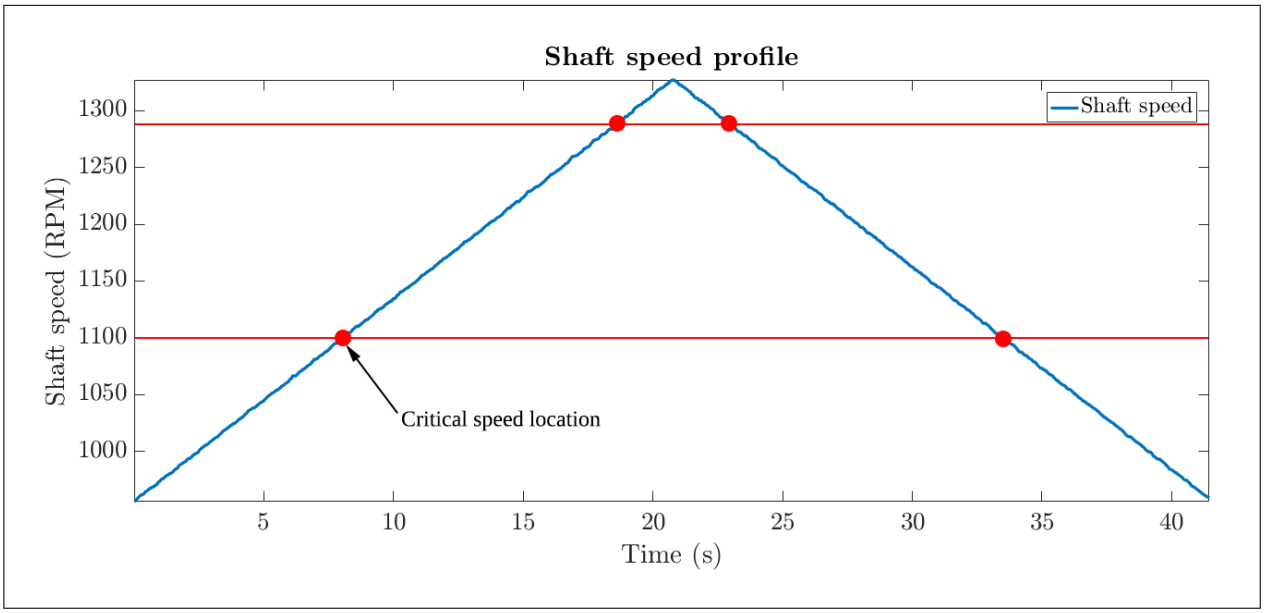

Figure 3.5: Chosen shaft speed profile as a result of the information derived from the Campbell diagram and motor speed capabilities.

The BTT investigations were initially performed with all the blades in an undamaged state, therefore providing a basis of comparison for the damaged blade. Thereafter a selected blade was damaged by machine a small discrete slot (referred to as *crack* in this dissertation) and incrementally increasing the size of the crack after a batch of tests. Figure 3.2 shows how this process was incorporated and repeated during the experimental testing procedure. An important prerequisite for the introduction of the discrete cracks was to determine a suitable location. *Suitable* in the sense that the chosen location would be where natural cracks due to HCF would most likely occur and a location where the introduction of the cracks would have a more noticeable effect on the vibration of the blade. In order to determine this location, an initial modal analysis was performed using an FEA to determine where the maximum stress concentration would occur for the first mode of excitation. Only the first mode was considered due to the reasons discussed in Section 1.2.5. The modal analysis was performed using the *MSC Marc Mentat 2016* commercial software and it should be noted that this does not form part of the FEM modal analysis proposed for the hybrid approach. This FEA was merely used to determine a suitable location for the discrete cracks. Figure 3.6a shows that the maximum stress concentration for the first mode occurs directly and slightly above the blade fillet. The discrete damage was therefore introduced in this region for two reasons:

1. Crack formation due to fatigue commonly occurs in maximum stress concentration regions [Budynas and Nisbett, 2011, Chapter 6].
2. A noticeable change in vibrational state of the blade is expected to occur due to damage in this region, as opposed to damage close to the tip of the blade.

The sizes of the discrete damage increments were specific to the type of investigation that was performed and these sizes are recorded in Section 3.5. It was further aimed to only increase the crack size by a small amount between the relevant damage increments. This was done to test the ability of the BTT technique to track small changes in the natural frequency of the blade as a consequence to the introduced damage. Figure 3.6b shows a close-up of the actual blade used during *Group II* of testing. The maximum discrete damage introduced to this blade during *Stage IV* of testing is also shown in Figure 3.6b. The strain gauges attached to this blade were used as an initial sanity check of the BTT results during *Stage III* of testing. The details of this BTT investigation follows in Section 3.5.2.

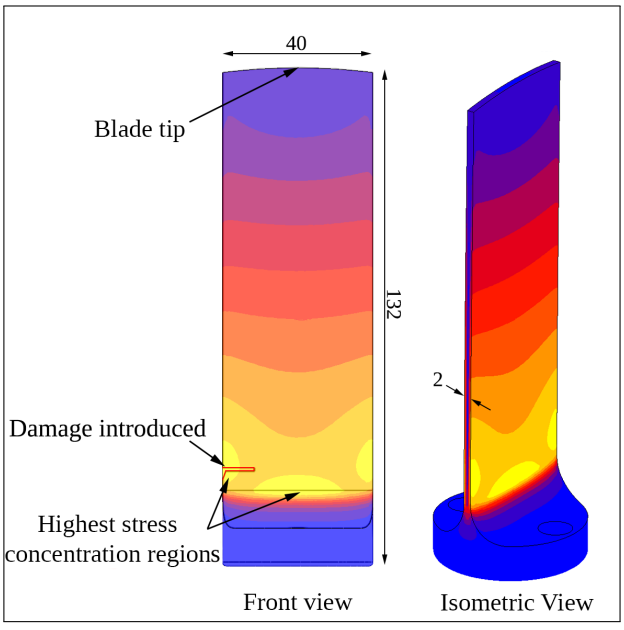

(a) Highest stress concentration region check for the first mode of vibration.

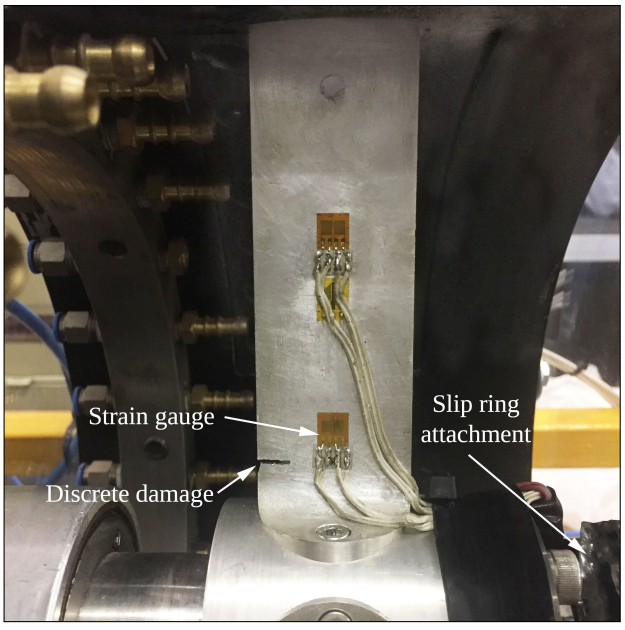

(b) Test blade with maximum incremental damage used for *Group II* of the BTT investigation.

Figure 3.6: Overview of test blade.

Another preliminary step for the experimental testing was to number the five blades in the rotor assembly. This helped to keep track of the blade specific results after the BTT signal processing. The details of the signal generation and acquisition during the various BTT investigations is an important topic of the experimental procedure and is discussed in detail in Section 3.5. The schematic shown in Figure 1.9 aids the discussion of this procedure, by highlighting the use of the relevant equipment during the respective processes. The descriptions of the items shown in this schematic are recorded in Table 3.1, with the item numbers in Table 3.1 corresponding to the labels shown in Figure 3.7.

The signal generation was done on the *LabVIEW* software interface along with a BNC voltage output *NI* card. The voltage signal output from this card was used to control the motor speed, therefore enabling the shaft speed profile to be controlled. Figure 3.7 shows this process with the associated outputs. As previously mentioned, it was required for the shaft speed profile to pass through a critical speed that would result in the resonance of the blades. The shaft speed was then ramped up and down in the chosen profile in order to initiate the blade resonances. A secondary voltage output is shown in Figure 3.7 as branching off from the *NI* analog card and into the Data Acquisition Device (DAQ). This voltage output was the same voltage output sent to the motor control unit and was used to trigger when the acquisition process should start or stop. The associated trigger level corresponded to a particular shaft speed that was calibrated using the voltage signal. The use of this voltage trigger enabled the data acquisition during the various BTT investigative tests to start and end at the same shaft speed. This aimed to keep the various tests in a particular investigation comparable over the chosen shaft speed profile.

The signal generation was initiated in *LabVIEW* and once the trigger level was reached the acquisition commenced. Diamond et al. [2015] identified that one of the greatest factors influencing BTT measurement accuracy is: data acquisition sampling frequency. For this reason, the sensitivity of the chosen BTT technique to sampling frequency was investigated by using two independent Data Acquisition Devices (DAQs) for *Group II* of testing (the details of this investigation are discussed in Section 3.5.2). However, the *OROS OR35* DAQ with *NVGate* software (with a sampling frequency limitation of 65.536 kHz for the required number of input channels) was used for the majority of tests. Figure 3.7 and Table 3.1 shows the various input channels used for acquisition. The various input channels and equipment are summarised as follows:

1. An *Optel-Thevon 152G8* optical shaft encoder along with a 79 strip zebra tape on a section of the shaft was used to measure the shaft speed. The sensitivity of the shaft encoder was adjusted to suit the distance that the probe was placed from the alternating black and white strips of the zebra tape.

2. Four eddy current proximity probes were used to capture the required voltage signal resulting from the passing blades. The proximity probe system also required signal conditioning and amplification before the resultant voltage signal was input into the DAQ.

3. Not shown in Figure 3.7 is the strain gauge system (power unit, analog amplifier and slip ring). The raw voltage signal of the strain gauge system was acquired for *Stage III* of testing for an initial sanity check of the BTT results. Furthermore, it was used to determine whether the change in discrete crack size would result in a noticeable change in natural frequency of the test blade.

After each test, the acquired voltage signal files from the various input channels were converted to a *.mat* format to be used in the BTT signal processing. The file sizes of the raw voltage signals was proportionate to the chosen DAQ sampling frequency. After the ToAs were extracted from the raw voltage signals the size of the files drastically decreased (more detail regarding this follows in Section 3.3). Figure 3.7 shows the placement of the compressed air nozzles used to excite the blades during rotation. The compressed air supply was opened to the maximum air-flow before each test. Also shown in Figure 3.7 are the commercial heaters used to heat the rotor blades during *Group III* of testing. The details of the specific investigative procedures follow in Section 3.5.

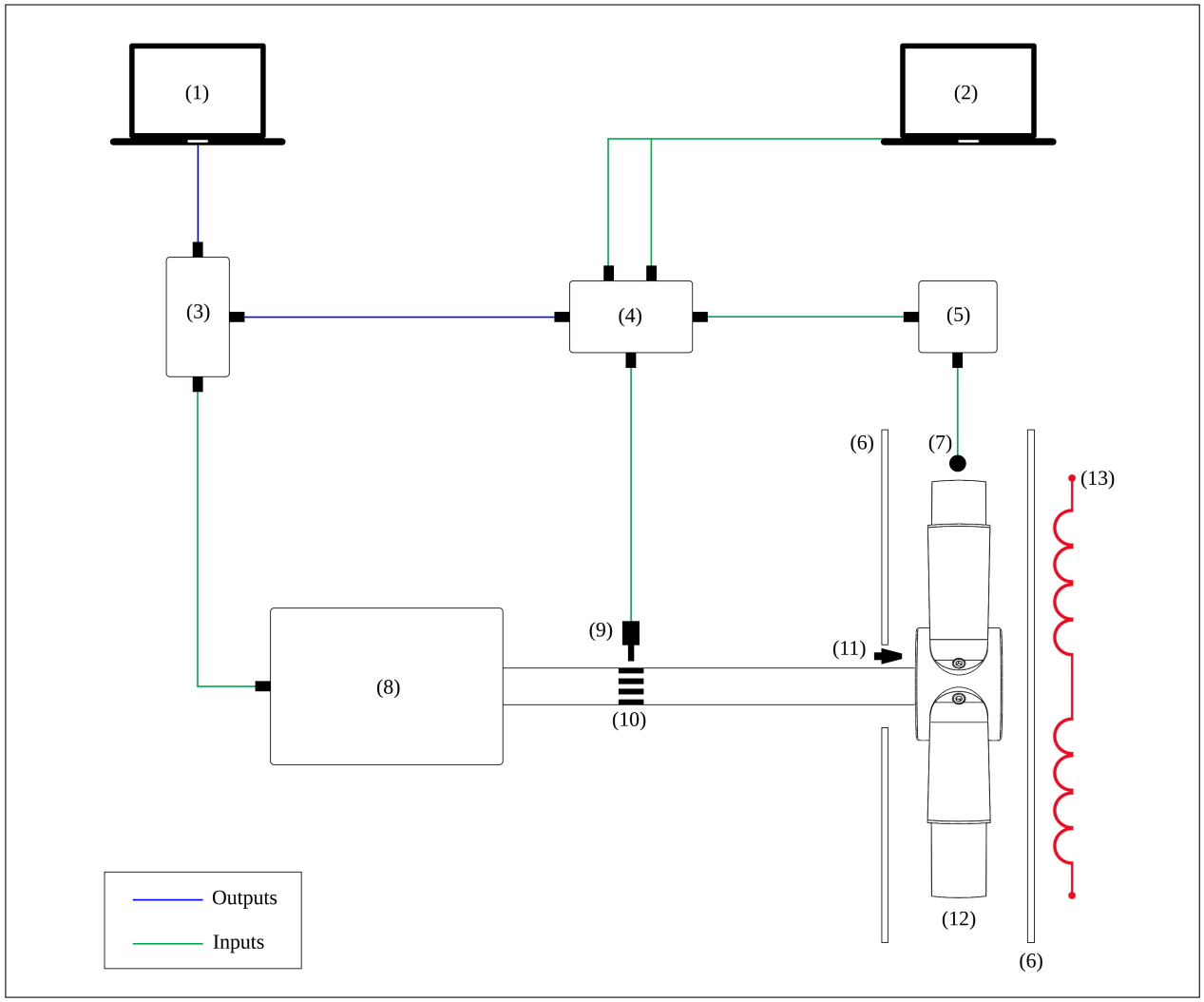

Figure 3.7: Schematic of the experimental setup, indicating the signal inputs and outputs used during experimentation (not drawn to scale).

Table 3.1: Item list of the experimental setup schematic shown in Figure 3.7.

Item number	Part description	Part quantity
1	PC with *LabVIEW* software used for signal generation	1
2	PC with DAQ software used to store raw voltage	1
3	NI analog voltage output card with BNC connections	1
4	DAQ used to capture raw voltage signals	1
5	Eddy current proximity probe amplifier	1
6	Polycarbonate safety screens	1
7	Eddy current proximity probes	4 probes
8	Electric motor (5.5kW)	1
9	Optical shaft encoder sensor	1
10	Zebra-strip tape for tachometer signal	79 strips
11	Compressed air supply nozzle	2 nozzles
12	Aluminium (6082 T6) bladed rotor assembly	5 blades
13	Commercial heaters for temperature tests	2 heaters (2kW each)

3.3 BTT Signal Processing

This section gives an overview of the BTT signal processing procedure used during the various investigations. The BTT signal processing procedure uses the acquired raw voltage signals from the experimental testing as an input. The BTT algorithm incorporating BLR, developed by Diamond et al. [2015], is then used to statistically infer the values of the constants in the assumed SDOF blade response model. Figure 3.2 shows that the processed data is lastly used to infer the blade condition as part of the proposed hybrid approach. The details of the signal processing procedure follows.

3.3.1 Synchronisation

Figure 3.8a gives an example of the measured voltage pulses at the four proximity probes. The raw proximity probe signals clearly indicate that a specific blade was slightly longer than the others; indicated by the voltage signal pulses of the corresponding proximity probes extending further down. This blade was used as a reference blade and referred to as *blade 1*. The reference was maintained for all the BTT investigations discussed in Section 3.5 with the intention of maintaining a consistent basis of comparison for the various tests during a particular investigative group. This reference was established for the following reasons:

1. To keep track of the blade specific BTT data. This was important when inferring the blade conditions from the derived vibrational characteristics.
2. Another important aspect was to synchronise all the raw voltage signals; i.e. ensure that all the raw voltage signals start on the same pulse. The pulse of the reference blade (blade 1) for proximity probe 1 was used as the reference pulse for all the raw voltage signals. The higher voltage range of the reference blade enabled a further trigger level to be established, thus allowing the first peak of the longer blade proximity probe data to be found. The sample number of this peak was used in the raw shaft encoder signal to find the sample number corresponding to the down-slope which was three tacho-pulses away. This sample number was then used as the starting-point for all the raw voltage signals. Figure 3.8b gives an example of this synchronisation process in terms of the shaft encoder and first proximity probe signals.

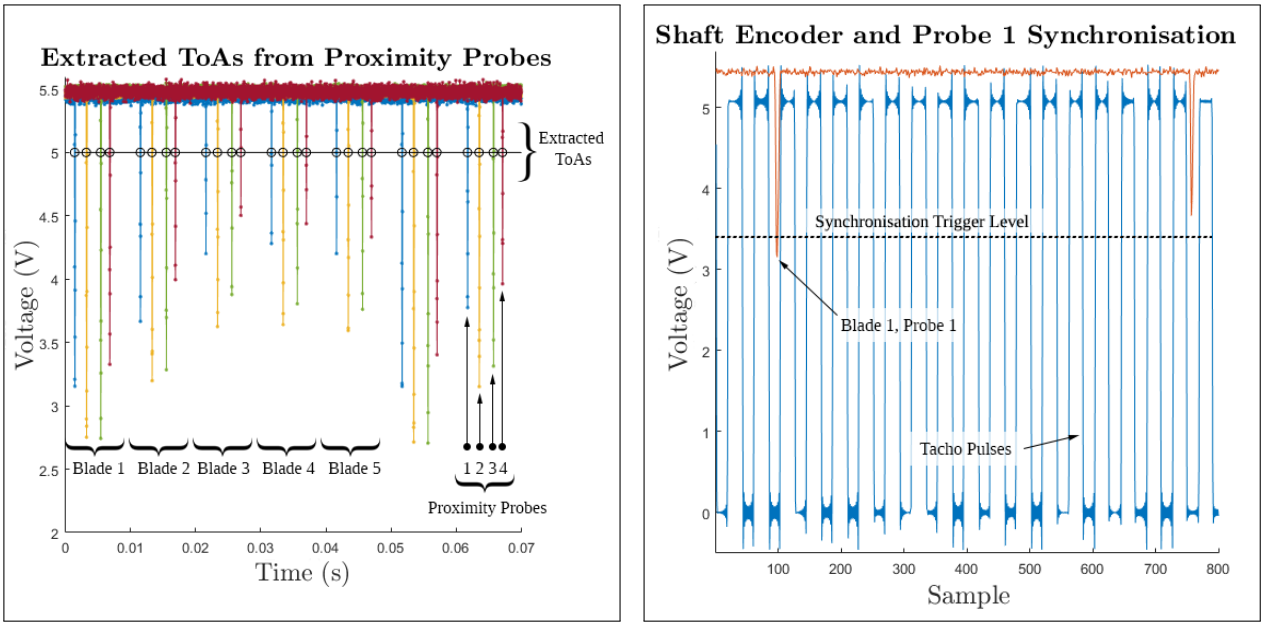

(a) Example of raw proximity probe signals.

(b) Synchronisation of raw proximity probe pulses.

Figure 3.8: Overview of the measured voltage signals.

3.3.2 ToA Extraction

The ToAs were extracted from the raw voltage shaft encoder and proximity probe signals at a chosen trigger level. Figure 3.8a gives an example of the extracted ToAs for the superimposed proximity probe data of the various blades. Figure 3.8a clearly indicates the grouping of five different raw voltage proximity probe signals, which is indicative of the blade specific acquired data. The proximity probes detect when a blade passes and this results in a pulse (measured from the base voltage signal) in the acquired voltage signal data. Upon close inspection of the various proximity probe pulses shown in Figure 3.8a, it is clear that the pulses are not uniformly spaced over time. The reason is that the eddy current proximity probes were irregularly spaced. For the detailed explanation of the reasons surrounding the irregular spacing, the reader is referred to Section 1.2.7 (*BTT Algorithm Overview*). In Figure 3.8a it is also clear that the range of the voltage pulses are not consistent for blade specific proximity probe data. The reason is that the proximity probes were not fastened at identical depths on the casing. Figure 3.9 shows the four steps used during the ToA extraction process for an arbitrary pulse. The steps corresponding to the labels shown in Figure 3.9 follows:

1. Establish a user-defined trigger level to be used in the ToA extraction algorithm.
2. Find the samples with voltage values above or below the chosen trigger level (above for the shaft encoder signal and below for the proximity probe signals). This was done on the positive slope for the shaft encoder pulses and the negative slope of the proximity probe pulses. The *MATLAB* built-in *find.m* function was used to find the indices of the first sample after the trigger level. The associated voltage and time values of the indexed samples were then recorded.
3. The sample located immediately before the trigger level is found as a single sample before the sample in step 3. The associated time and voltage of is also recorded for further use in step 4.
4. The ToA is then simply the time (t_{trig}) corresponding to when the trigger level voltage (V_{trig}) is reached. This time is calculated between the referenced samples of steps 3 and 4 using linear interpolation as shown in Equation 3.1 below.

$$\text{ToA} = t_{\text{trig}} = -\left(\frac{t_{\text{after}} - t_{\text{before}}}{V_{\text{after}} - V_{\text{before}}} \cdot (V_{\text{after}} - V_{\text{trig}}) - t_{\text{after}}\right) \tag{3.1}$$

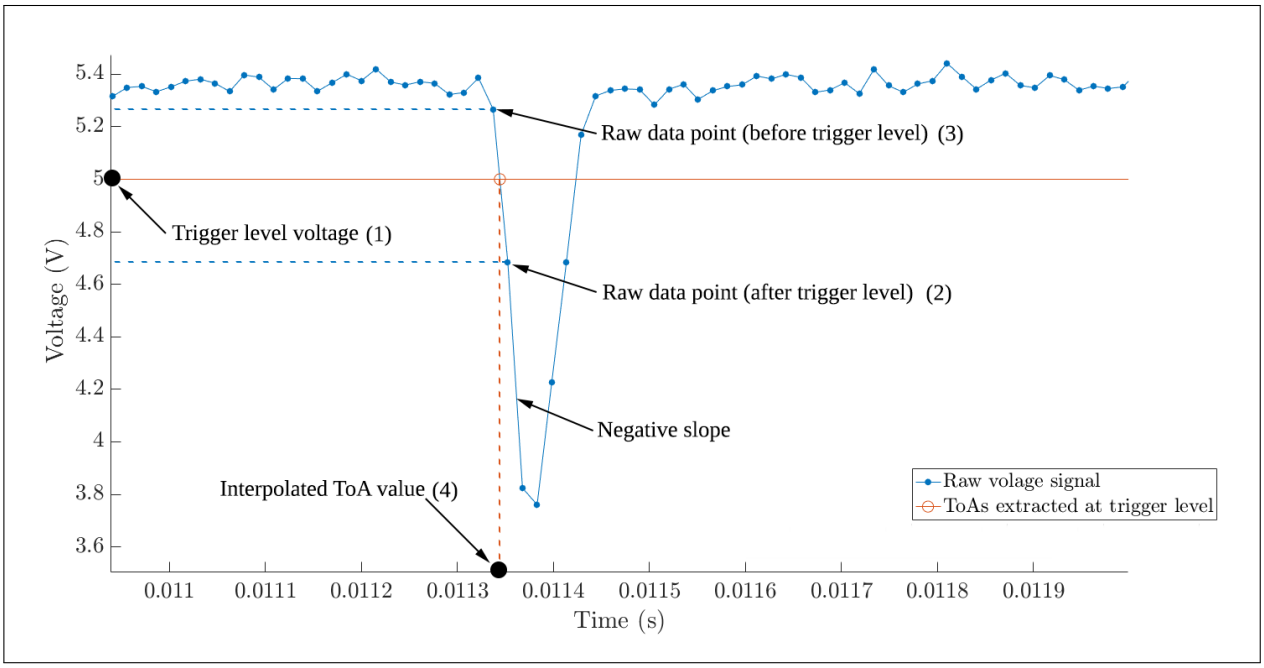

Figure 3.9: Illustration of the ToA extraction process for a particular proximity probe pulse.

The procedure used to extract the ToA associated with a particular pulse was implemented as a function. This enabled the extraction of all the ToAs associated with a particular BTT signal file. The extracted ToAs for the four eddy current proximity probes and shaft encoder were stored in separate vectors for further use in the BTT signal processing. An advantage of only using the extracted ToAs in the rest of the signal processing, was that the sizes of signal files drastically decreased when compared to the raw voltage signals.

3.3.3 Pre-BLR Processing

This section gives an overview of the pre-BLR processing procedures, namely: deriving the Instantaneous Angular Speed (IAS) from the extracted ToA values, thereafter determining the the resultant blade tip deflections and lastly detecting the blade resonances. All of these aspects are very important in the context of synchronous blade vibrations. Furthermore, these aspects are prerequisites for the BLR processing whereby the parameters shown in the assumed SDOF model (Equation 1.6) are solved for. The remainder of this section gives a brief overview of these processes.

Shaft Speed

Diamond et al. [2016] identified that the measurement of IAS is increasingly investigated for its diverse range of applications in condition monitoring and prognostics of rotating machinery. More so, using BTT for condition monitoring applications requires that the IAS is accurately measured and calculated. The reasons are that the BTT signal processing requires the IAS as a reference to ultimately derive the tip displacements and the associated blade resonant frequencies. The accuracy of the processed BTT data imminently relies on the accuracy of the measured IAS. The IAS is often measured using an incremental shaft encoder. The operating principles behind different incremental encoders are qualitatively similar [Diamond et al., 2016]. For the purposes of the research project, zebra strip tape with 79 alternating black and white sections was used as the incremental shaft encoder. This tape was stuck around the circumference of the shaft (as shown in Figure 3.7) and a stationary optical probe was used to measure the alternating sections as they passed the probe.

Figure 3.10 illustrates the operating principles of an incremental encoder (using gear teeth as opposed to zebra tape) as presented by Diamond et al. [2016]. Also indicated in Figure 3.10 is that the resultant voltage signal is directly dependent on the presence of the alternating sections of the incremental encoder passing the optical probe. In terms of the zebra tape; whenever a white strip passed the optical probe a high voltage would be measured and vice versa for the passing of a black strip. The result is the measurement of a wave-like nature similar to the signal seen in Figure 3.10. Diamond et al. [2016] mention that each rising edge of the resultant waveform indicates the precise time an alternating section arrives at the probe and refers to this as the zero-crossing times.

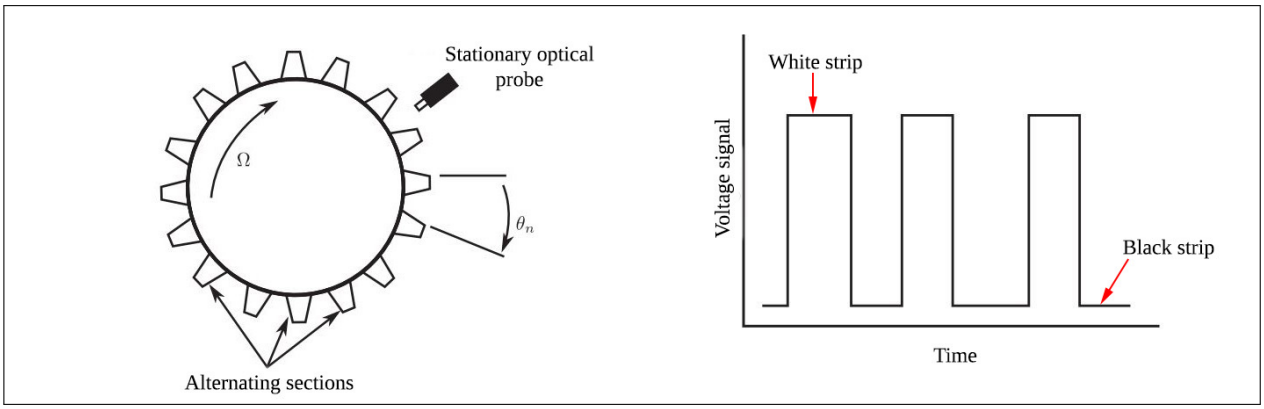

Figure 3.10: Operating principles behind incremental shaft encoders, from [Diamond et al., 2016].

Many different methods exist to determine the zero-crossing times and for an overview of these the reader is referred to [Diamond et al., 2016]. The IAS is calculated by using consecutive zero-crossing times and knowledge of the angular distance between successive alternating strips. In Section 3.3.2 the method used to extract the ToAs from the raw shaft encoder signal is elaborated on. These ToAs are in essence used as zero-crossing times to calculate the IAS. The conventional method of determining the IAS from two consecutive zero-crossing times or ToAs is shown in Equation 3.2. This method assumes a constant shaft speed between the two consecutive zero-crossing times [Andre et al., 2014]. In Equation 3.2 the IAS, $\dot{\theta}$, is calculated for an angular distance, θ, that represents a particular section of the zebra tape. Therefore only two consecutive zero-crossing times are used for this calculation.

$$\dot{\theta}_n(t) = \frac{\theta_n}{t_{n+1} - t_n} \quad t_n \leq t \leq t_{n+1} \tag{3.2}$$

Diamond et al. [2016], however, outline three factors that may affect the accuracy of the resultant IAS measurement. These factors ultimately contribute to the difficulty of accurately measuring the shaft IAS and are a consequence of invalid assumptions. The discussion of these factors and associated assumptions follows [Diamond et al., 2016]:

1. Assuming that the zero-crossing times of the encoder sections may be resolved to an infinitesimal precision. This occurs due to the raw shaft encoder signal being processed digitally, thus enforcing a discrete nature into the sampling of the signal. The acquisition system may therefore miss zero-crossing times and record the zero-crossing time as occurring at exactly the next sample. This is due to an inadequacy of the sampling rate during acquisition. Consequently, quantisation or quantification error may occur [Andre et al., 2014].
2. Assuming that the shaft speed is constant between two zero-crossing times. This assumption leads to discontinuities in the measured IAS. Infinitely large accelerations at the zero-crossing times may therefore occur as the measured IAS jumps from one value to the next (when using Equation 3.2). Figure 3.11 illustrates the discontinuities that result in the measured IAS for arbitrary zero-crossing times.

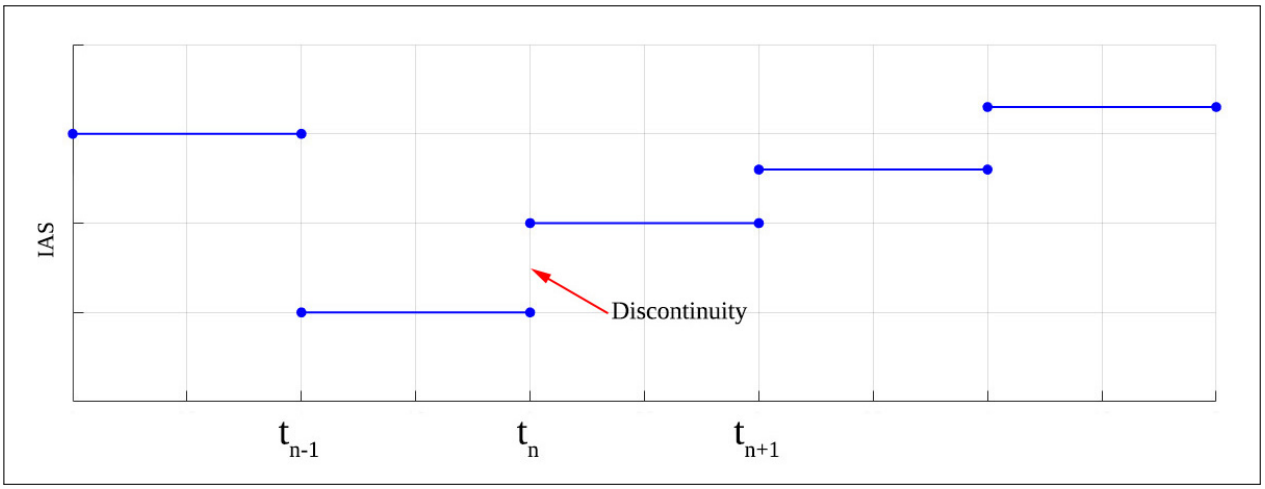

Figure 3.11: Discontinuities in the IAS due the assumption of a constant angular speed between zero-crossing times, adapted from [Diamond et al., 2016].

3. Assuming that all sections of the zebra strip shaft encoder have equal angular distances. The reality is that imperfections are inevitable. These imperfections occur in terms of how the strips are attached to the shaft and the actual increment imperfections. Rivola and Troncossi [2014] reported a 20% variation in the peak-to-peak incremental distance for specifically zebra shaft encoders. These geometric inconsistencies generally occur during the printing of the zebra strip tape and the misalignment during its fastening onto the shaft.

The butt joint, where both ends of the zebra strip tape meet, may also be another common geometric imperfection [Diamond et al., 2016]. Figure 3.12 illustrates a geometrically uniform zebra strip tape and a tape with exaggerated errors. Diamond et al. [2016] warn that these zebra strip geometric imperfections may result in high order content in the IAS if it is left uncompensated for. Thus, the errors in the IAS calculations may have a ripple effect on the accuracy of the processed BTT data.

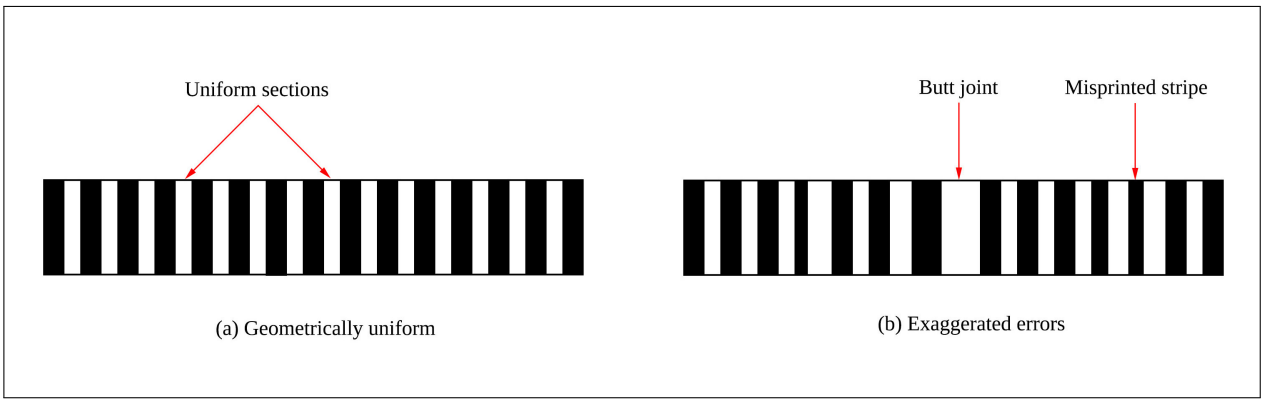

Figure 3.12: Examples of zebra tapes with and without errors, adapted from [Resor et al., 2005].

It is therefore essential to minimise the negative effects of the aforementioned assumptions. Diamond et al. [2016] propose a calibration method for the compensation of geometric inconsistencies between the shaft encoder sections. The novelty of the proposed method lies in the fact that it grants the shaft speed the flexibility of transient states and calculates every encoder section distance individually. The compensation method specifically uses BLR to calculate the encoder increment distances. Note that the BLR procedure used during the shaft encoder geometry compensation is completely independent of the BLR used during the BTT signal processing. Both approaches however incorporate the same fundamental statistical principles. The focus of this particular research project was not to develop or validate a method to calculate the shaft encoder geometry for arbitrary shaft speed profiles. Therefore, for further details regarding this approach and its derivation, the reader is referred to [Diamond et al., 2016]. The following assumptions were however deemed important for the shaft encoder and resultant IAS during this compensation incorporating BLR (for N sections and over M revolutions) [Diamond et al., 2016]:

1. The individual incremental shaft section distances remain constant for all M revolutions. This assumption implies that the printed sections and the alignment of the zebra strip tape remains constant during operation.

2. The sum of all N sections add up to 2π radians or an entire revolution. The zebra strip tape is attached around the entire circumference of the shaft during experimentation.

3. The assumption is made that the IAS may rather be expressed as a second order polynomial between two zero-crossing times, in contrast to the assumption of a constant IAS between these times (which is a zero order polynomial).

4. The IAS is assumed as a continuous function over time, therefore implying that no abrupt jumps are permitted for the IAS at the zero-crossing times. Figure 3.13 gives an example of the derived shaft speed after the shaft encoder geometry compensation was applied. This resultant signal is represented as a continuous function over the intended shaft speed profile. The shaft speed shown in Figure 3.13 is not smooth and this may be due to a number of reasons. The main reason may be related to the low resolution of the generated signal from the *NI* output card listed in Table 3.1.

The relevant IAS calculations (incorporating the BLR geometry compensation) directly utilised the extracted shaft encoder ToAs derived from the function described in Section 3.3.2.

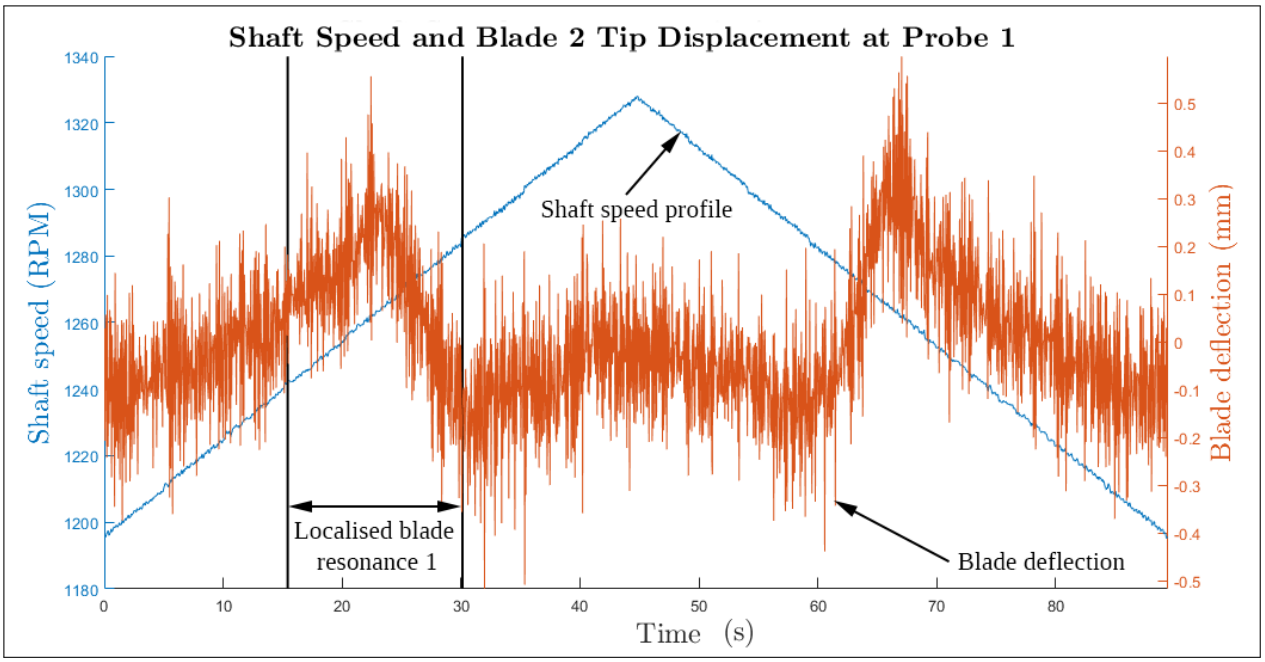

Figure 3.13: Tip displacement compared to the rotational shaft speed (blade 2, resonance 1).

Tip Deflection

At this stage of the signal processing it is important to recall the underlying principles of BTT as introduced in Section 1.2.7. The fundamental principles behind BTT are relatively straightforward: the measured ToA information of the blades passing a proximity probe may be analysed to indicate the vibrational state of each blade. The ToA of a non-vibrating blade is completely dependent on the shaft IAS. However, a vibrating blade arrives either earlier or later than expected at the proximity probe. This physically translates into the vibrating blade leading or lagging upon arrival at the proximity probe. The blade tip displacement may be calculated from the change in AoA (ΔAoA) of a vibrating blade which is derived by using an OPR pulse, or Multiple Per Revolution (MPR) pulses, as shaft reference positions. The change in AoA (ΔAoA) represents the difference between the measured AoA and the mean AoA, therefore indicative of the degree of vibration for a particular blade. The blade tip displacements are then derived by using an OPR reference pulse to determine the specific AoAs per revolution, for each blade passing a specific probe [Diamond et al., 2015]. The knowledge of the IAS and ToAs allows the angular distance of the blades to be calculated at the various proximity probes by establishing a reference. For the illustration of these underlying principles the reader is referred back to Figure 1.9. After the ΔAoAs are calculated for the various blades the tip displacements are found using Equation 3.3 below:

$$x_{tip} = r \cdot \theta_{tip} = r \cdot \Delta\text{AoA} \tag{3.3}$$

In Equation 3.3 the displacements and AoA refer to that of the blade tips. The radius (r) is also measured from the blade tip to the centre of the shaft. This radius is assumed to remain constant during the vibration of the blade. Figure 3.13 illustrates the derived blade tip displacement (x_{tip}) for the corresponding shaft speeds for proximity probe 1. Again, it is important to note that at this stage of the signal processing the data of the individual blades were independently processed. Referring back to Figure 3.13, it is clear that peaks in the tip displacement occur at two locations for this specific probe. The shaft speeds corresponding to these tip displacement peaks are roughly 1270 RPM. Figure 3.14 gives an example of the tip displacements at the corresponding shaft speeds versus time, for blade 2 measured at the various proximity probes. The derived blade tip displacements peaks occur more or less in the same location on the resultant shaft speed profile for the four probes; some peaks are indicative of a leading blade (positive deflection) while others are indicative of a lagging blade (negative deflection).

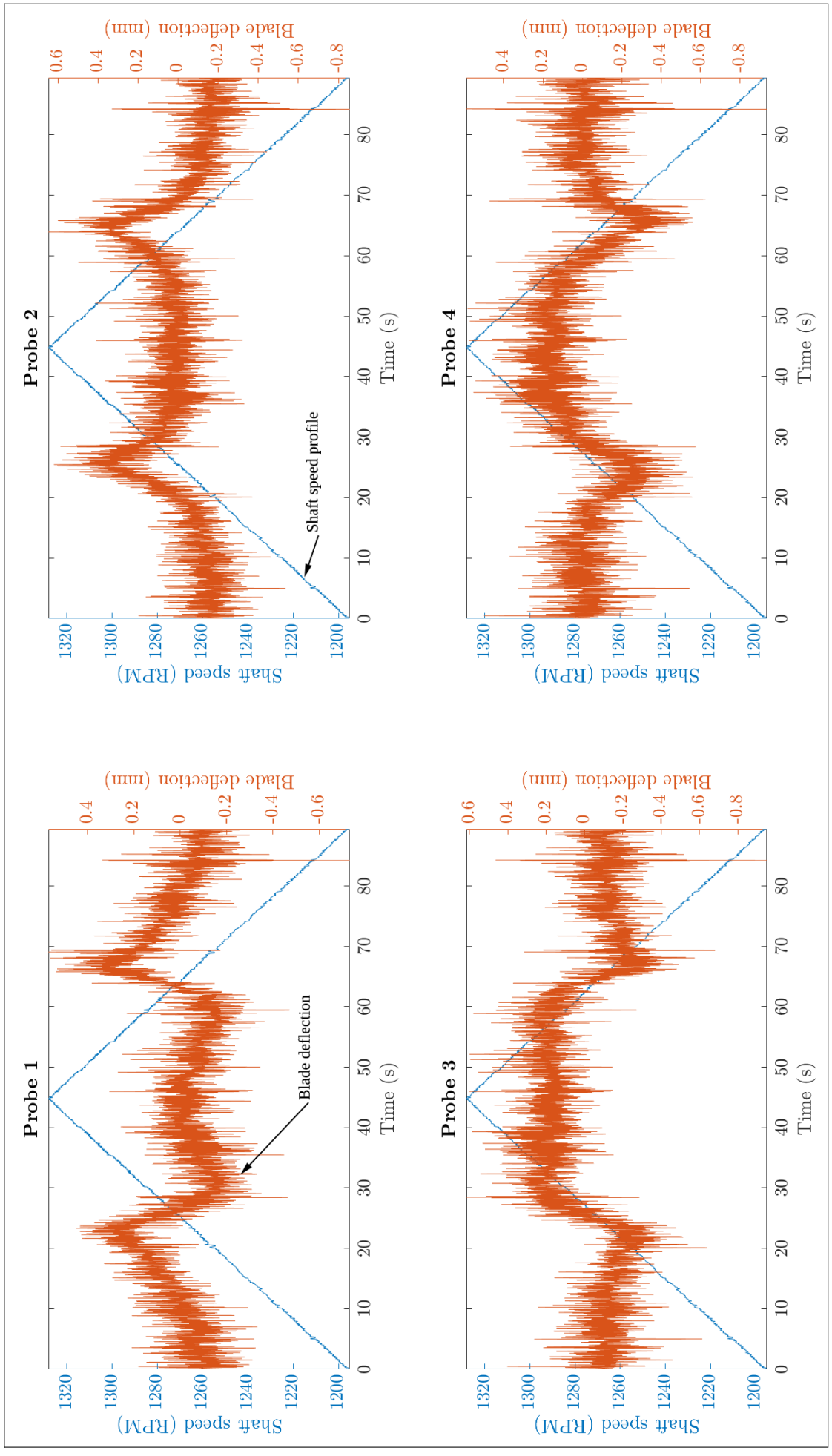

Figure 3.14: Tip displacement at corresponding shaft speeds versus time for the various proximity probes (blade 2, resonance 1).

The tip displacement data of all four probes for a specific blade are used collectively in the remaining procedures of the BTT signal processing. Due to the nature of the vibrations being synchronous or engine-ordered, the next step in the BTT signal processing involves resonance detection and the estimation of the EO of vibration.

Resonance Detection

Vibrapy is further used to detect the occurrence of blade resonance by localising the peaks of the blade tip displacements. This is done for all the probes independently. Figure 3.13 gives an example of the localised peak for blade 2 at probe 1. Similarly all the peaks corresponding to each probe are localised and are further used to derive the vibration characteristics of a specific blade. The starting and ending times for each localised peak are recorded for a specific blade. Thereafter, the corresponding tip displacement data is combined and later used to statistically infer the vibration characteristics using *Vibrapy*. What remains to be determined is the EO associated with the localised blade resonances.

The BTT method incorporating BLR relies on a probabilistic approach to determine the EOs, whereby a range of EOs are supplied to the algorithm. The probability, along with the associated variance, of each supplied EO to fit the blade tip displacement measurements are then computed. The EO with the highest probability is chosen for further use in the BLR processing. Figure 3.15 gives an example of the results from the probabilistic approach applied to estimate the EO of vibration. An integer of 6 was determined to be the most probable EO in this example.

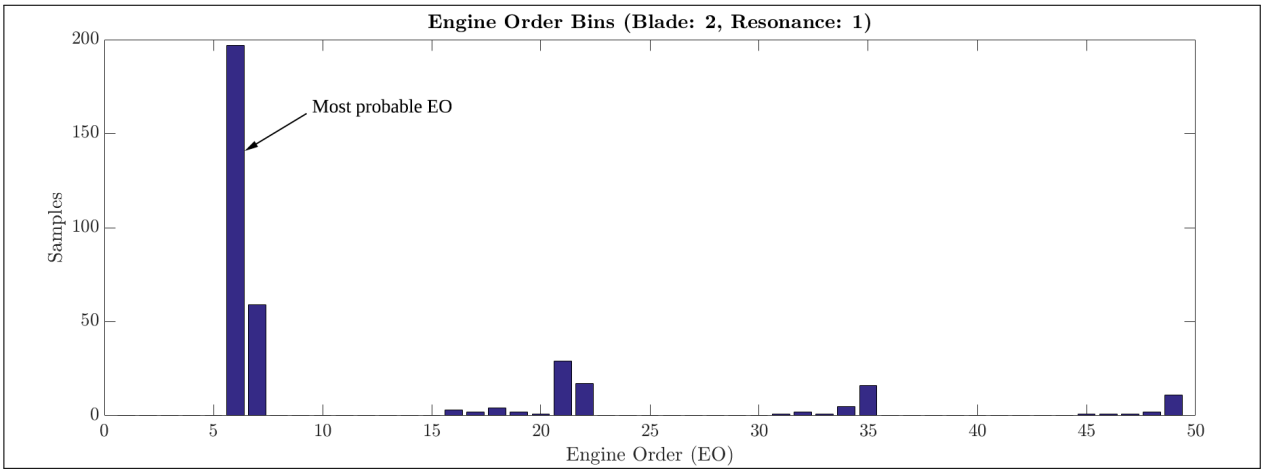

Figure 3.15: The results of the probabilistic approach used to determine which EO of blade vibration most likely occurred.

3.3.4 BLR Processing

This section describes a a fundamental step of the *Vibrapy* software (mentioned in Section 1.4), whereby the values of the parameters in the assumed SDOF model for the blade vibration are statistically inferred using BLR. Recall the SDOF model used to describe the blade response, shown in Equations 3.4 and 3.5. Parameters A, B and C are produced by the *Vibrapy* software and takes the form of a multivariate Gaussian distribution. Importantly, the parameters in Equation 3.4 are solved for each revolution (indicated by subscript i) in the localised resonance domain at a corresponding angular velocity or IAS (Ω). Equation 3.5 shows that the correct estimation of the EO is critical in order to infer the *true* vibrational characteristics of the blades.

$$x_i(t) = A \cdot \cos(\omega \cdot t_i) + B \cdot \sin(\omega \cdot t_i) + C \tag{3.4}$$

$$\text{where} \quad \omega = EO \cdot \Omega \tag{3.5}$$

Figure 3.16a gives an example of the entire domain of the localised blade resonance, where the four proximity probe data-points collectively represent an entire revolution. Note, Figure 3.16a merely gives an example of a single BTT experimental test. Figure 3.16b shows a magnified section of the entire blade resonance domain, hence a more detailed view of how the proximity probe data-points are used to fit a curve for the blade tip displacement. Importantly, four different proximity probe data-points are representative of a single revolution. Equation 3.6 highlights that the inferred SDOF model target parameter set, $\mathbf{w}$, is solved for each revolution, i, using *Vibrapy*. This parameter set forms part of a multivariate normal distribution with mean, $\boldsymbol{\mu}_i$, and covariance matrix, $\boldsymbol{\Sigma}_i$, as shown by Equation 3.6. The results of Equation 3.6 are used to derive the amplitude and phase for further use in the proposed hybrid approach (discussed in Section 3.4).

$$\mathbf{w}_i = \begin{pmatrix} A_i \\ B_i \\ C_i \end{pmatrix} \quad \boldsymbol{\mu}_i = \begin{pmatrix} \mu_{A_i} \\ \mu_{B_i} \\ \mu_{C_i} \end{pmatrix} \quad \boldsymbol{\Sigma}_i = \begin{pmatrix} \Sigma_{AA_i} & \Sigma_{AB_i} & \Sigma_{AC_i} \\ \Sigma_{BA_i} & \Sigma_{BB_i} & \Sigma_{BC_i} \\ \Sigma_{CA_i} & \Sigma_{CB_i} & \Sigma_{CC_i} \end{pmatrix} \tag{3.6}$$

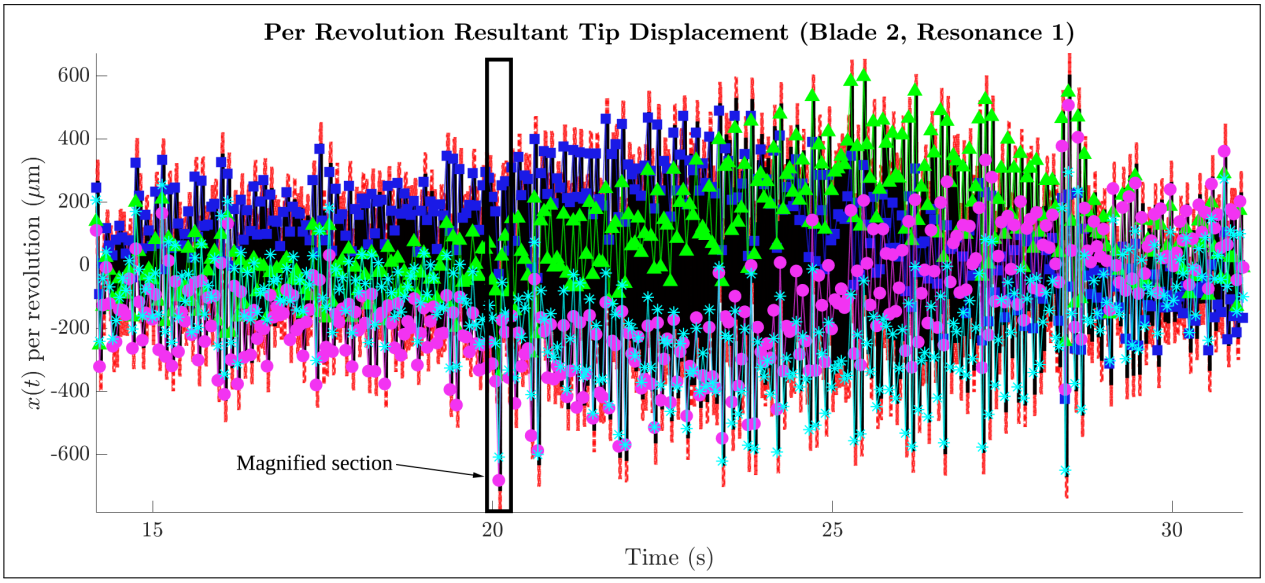

(a) Localised resonant tip displacement.

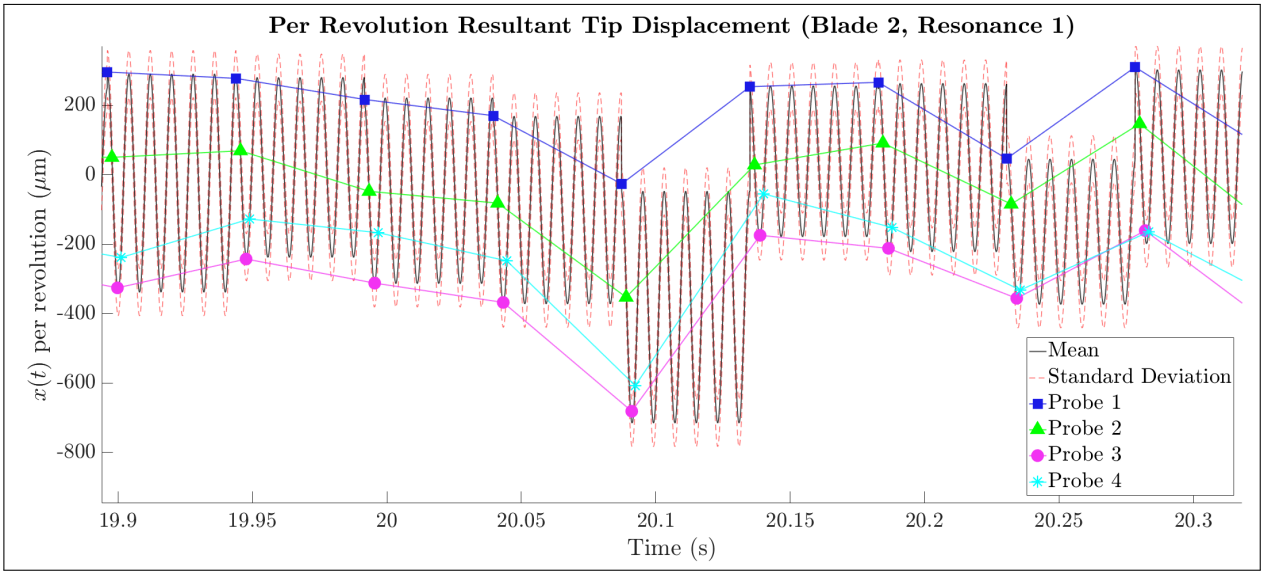

(b) Magnified localised resonant tip displacement.

Figure 3.16: Illustrations of the blade resonant tip displacement identification.

In Figure 3.16b the resultant fitted curves for the blade tip displacement have discontinuities. These discontinuities are indicative of the BLR being performed for each revolution. Figure 3.16b aims to give an example of the solution for Equation 3.4 with the upper and lower standard deviation from the mean solution also shown. It is clear from this figure that the superimposed tip deflection measurements result in aliasing which is present in the BTT data (for the shaft revolutions shown in Figure 3.16). An advantage of the BLR BTT method, as opposed to the more conventional AR method, is that equidistant probe spacing is not required. However, the major advantage of using the BLR BTT method is that uncertainty is incorporated in the derivation of the SDOF model parameters. This allows the amplitude and phase values to be determined stochastically rather than deterministically. Section 3.4 gives an overview of how a change in the blade condition is determined using these values.

3.4 Blade Condition

This section presents how the results from the BTT signal processing are used to infer the blade condition. Advantageously, the use of BLR for the curve-fitting allows the solution of this parameter set to form part of a multivariate normal distribution with an associated mean and covariance. The outputs of the *Vibrapy* software are directly used in the data-driven approach of the proposed stochastic hybrid methodology. This section therefore elaborates on how the stochastic solution of the SDOF parameter set may be used to derive the associated amplitude and phase. Furthermore, the feature extraction process used to derive the blade natural frequencies and how this may be used to indicate the blade conditions will be elaborated on. The details of these aspects follow.

3.4.1 Amplitude and Phase

The hybrid approach outlined in Figure 2.1 requires the amplitude and phase values to be calculated as stochastic quantities in order to quantify the uncertainty associated with the processed BTT data. Figure 3.17 summarises the procedure used to calculate the resultant stochastic amplitude and phase values incorporating a Monte-Carlo Simulation (MCS). Again, this is done for each shaft revolution of the localised resonance, as indicated by the subscript i.

The amplitude and phase values are specifically calculated using Equations 3.7 and 3.8 respectively [Gallego-Garrido et al., 2007a]. A flow diagram of this calculation is given in Figure 3.17. Figure 3.17 emphasises that the BLR solution set for each revolution, $\mathbf{w}_i$, has an associated multivariate normal distribution for each of the parameters. Using these normal distributions in a MCS enables the amplitude and phase results to also have an associated normal distribution, with a corresponding mean and standard deviation. This is done by using 10000 random samples for A, B and C associated with the respective multivariate normal distribution. These random values are substituted into Equations 3.7 and 3.8 to find equivalent MCS samples for the amplitude ($\hat{A}$) and phase ($\hat{\phi}$). The use of a MCS is a simple and effective process for calculating the probability distributions for the amplitude and the phase. In essence, the MCS is used as a tool for combining a number of statistical distributions, thus enabling the amplitude and phase results to be stochastic rather than deterministic [Herrador and González, 2004]. This allows the uncertainty of these results to be quantified with associated confidence intervals around the mean of the prediction. The fact that it is possible to establish these confidence intervals is a clear advantage of the BLR BTT method (*Vibrapy* software) used for the BTT signal processing.

$$\hat{A}_i = \sqrt{A_i^2 + B_i^2} \tag{3.7}$$

$$\hat{\phi}_i = \arctan\left(\frac{B_i}{A_i}\right) \tag{3.8}$$

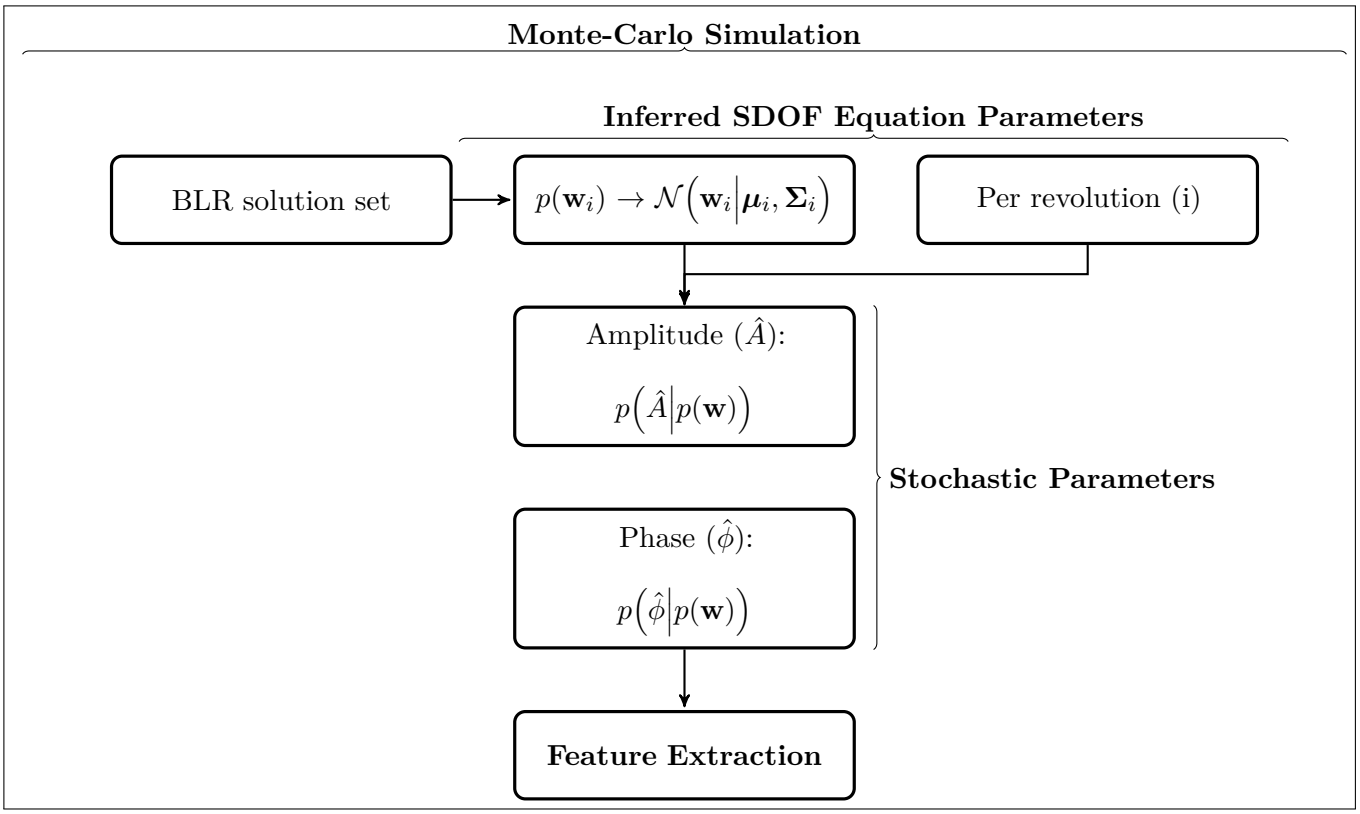

Figure 3.17: MCS overview.

Figure 3.18 gives an example of the MCS results for the amplitude and phase. The results are representative of a particular blade (blade 2) at the associated revolutions in the localised resonance domain in which the BLR is performed. As previously mentioned, 10000 random samples of the target parameter set ($\mathbf{w}$) with an associated multivariate normal distribution, is used for each revolution. The total number of random samples is chosen as 10000 due to a preliminary investigation indicating that a greater number of samples does not affect the accuracy of the results (this was determined in terms of the convergence of the values of the amplitude and phase for the corresponding number of samples used). Also imminent in Figures 3.18a to 3.18c is the fact that the derived amplitude and phase results have an associated normal distribution as a result of the MCS. Note, this normal distribution was not present for smaller amplitudes close to the blade resonance conditions. However for this research, the MCS was only performed for larger amplitude values corresponding to the localised blade resonance conditions. The mean values of these distributions are located at the highest concentration of samples resulting from the MCS. In addition, the following observations are made from the amplitude and phase results, namely:

1. As expected, the mean amplitude of vibration increases as the blade nears resonant operating conditions. Figure 3.18a shows a mean amplitude of approximately $135\mu m$ and Figure 3.18c shows a mean amplitude of approximately $430\mu m$. Revolution 203 (Figure 3.18b) is therefore more indicative of resonance conditions.
2. The standard deviation of the phase results tends to significantly decrease as the resonant operating conditions are neared. The much narrower normal distribution in Figure 3.18c, compared to that of Figure 3.18a, is indicative of this.

Figure 3.18 clearly shows a shift in the normal distribution of the amplitude results. This is evident as the revolutions increase from 3 to 103 and finally to what was determined to be resonance at 203 revolutions for this particular example.

During the various investigations, the normal distributions (amplitude and phase) for each revolution are represented collectively on plots as a function of excitation frequency. The frequency for a specific revolution is determined by multiplying the shaft IAS at that time of rotation with the EO of blade vibration. Examples of these plots are be shown in Section 3.5.

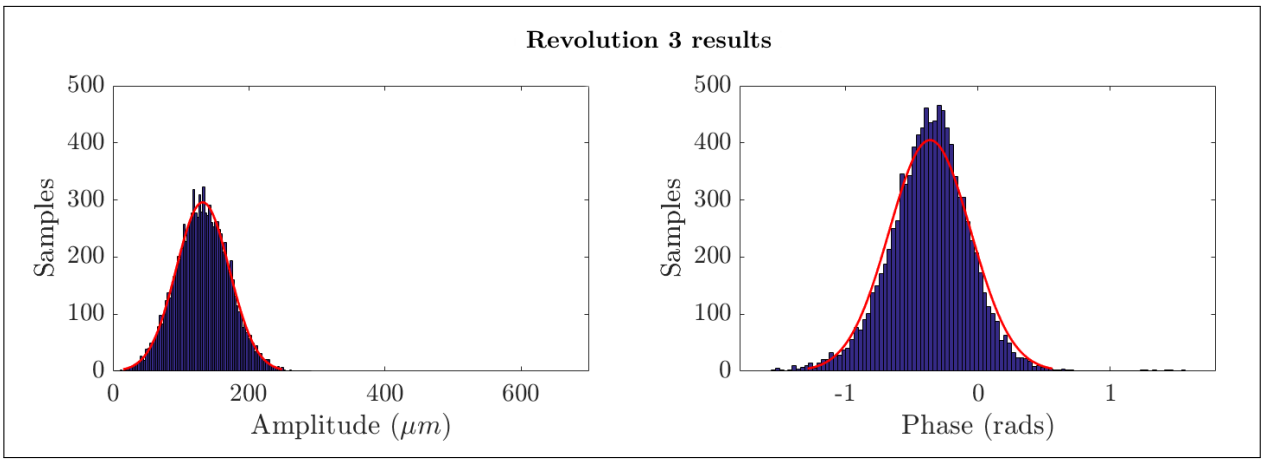

(a) Revolution 3 MCS results.

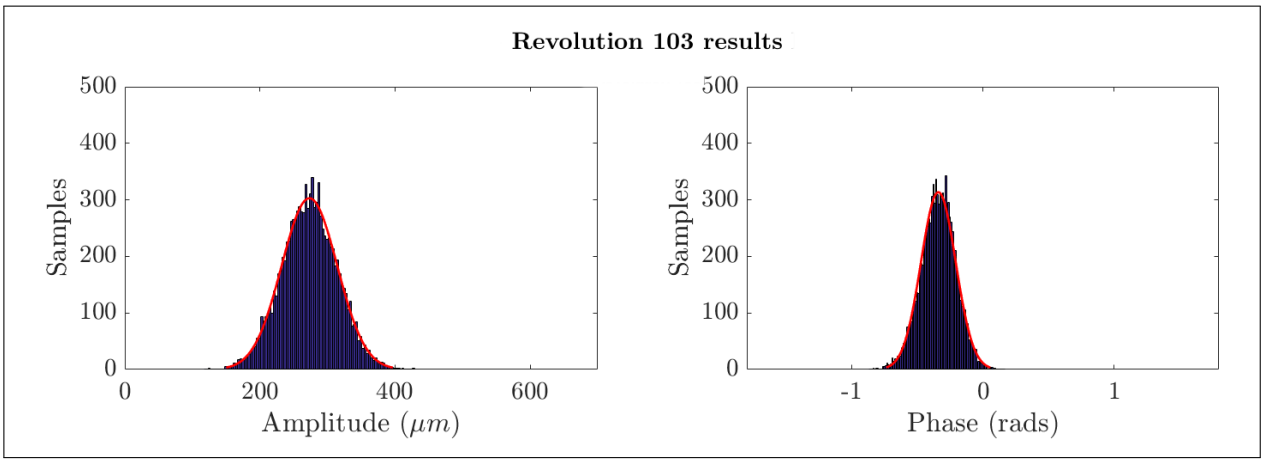

(b) Revolution 103 MCS results.

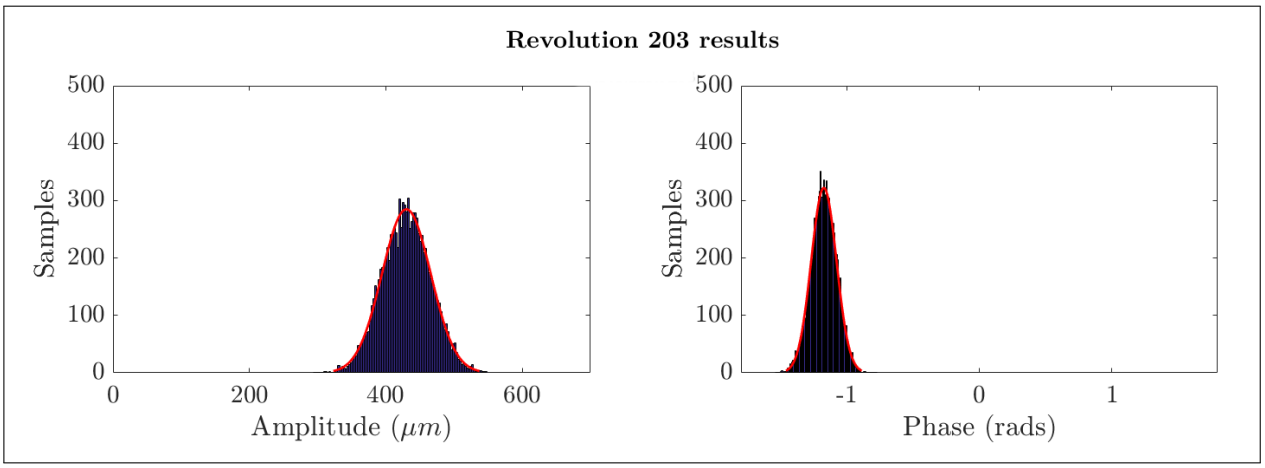

(c) Revolution 203 MCS results.

Figure 3.18: Amplitude and phase MCS results for blade 2 at particular shaft revolutions in the localised resonance domain.

3.4.2 Feature Extraction

Referring back to Figure 2.1, the desired outcomes are to track changes in the blade natural frequency and classify blade damage by using a clustering technique. These outcomes in essence culminate in a decision of whether a damage threshold is reached. Figure 3.17 shows that the next step in doing so is: *feature extraction*. For the discrete damage tracking it was proposed to observe the shift in the natural frequency of the blade [Tappert et al., 2001]. The feature extraction aimed to locate the natural frequency of the blade for a particular damage increment. The mean amplitude and phase values were considered for the feature extraction, however, confidence intervals of these values were also established in order to get a sense of the uncertainty associated present in the BTT measurements. The mean values over the localised resonant frequency domain were grouped together for the particular blade damage increments. This was done for the various BTT investigations outlined in Section 3.5 where discrete damage was introduced; more detail regarding this is discussed in this section. The extracted features are as follows:

1. The maximum amplitude and associated frequency as indicated by Equation 3.9. This natural frequency is referred to as the *the natural frequency based on amplitude* ($f_{n_{\hat{A}}}$) for the remainder of the report.

$$f_{n_{\hat{A}}} = f(\vartheta) \quad \text{where} \quad \vartheta = \max_{i \in N} \hat{A}_i \tag{3.9}$$

2. The mid-point of the 180° change in phase angle and associated frequency as indicated by Equation 3.10. This natural frequency is specifically calculated at the midpoint between the lower frequency (f_l) and upper frequency (f_u) where a 180° change in phase angle is located over the entire localised resonance domain. This is typically characterised by a sudden shift in the phase from -90° to +90° (or $-\frac{\pi}{2}$ to $+\frac{\pi}{2}$ in radians). This natural frequency is referred to as the *the natural frequency based on phase* ($f_{n_{\hat{\phi}}}$) for the remainder of the report.

$$f_{n_{\hat{\phi}}} = f(\varrho) \quad \text{where} \quad \varrho = \frac{f_u + f_l}{2} \quad \text{subject to} \quad \Delta\hat{\phi} \geq \pi \tag{3.10}$$

An example of this feature extraction process, or the visualisation thereof, is shown in Section 3.5. Furthermore, when considering the feature extraction procedure, it should be noted that two approaches are proposed. The choice of procedure depends on the desired outcomes of the post-processing, namely: the long-term archiving of the data or a more immediate indication of a particular blade condition by considering a single set of measurements. The proposed feature extraction approaches are as follows:

1. The features may be extracted for each of the individual signals of a particular test case. Consequently, the individual natural frequencies corresponding to the amplitude and phase features may be found for each test case. This approach is more realistic in terms of what may be expected in industry where successive BTT measurements may be months apart. The first approach, however, requires that the results of a single measurement set should be very accurate, therefore demanding a lot of confidence in this prediction.

2. The mean amplitude and phase signals may first be combined for a number of repeat tests in a particular investigation. The feature extraction is then performed on the combined signals. This approach, however, requires utmost consistency between the same measurements.

The aforementioned feature extraction process was relatively simple to execute, however, emphasis was placed on the utmost accuracy and consistency of the results. The robustness of the proposed BTT methodology was tested by repeating a number of the same tests for a particular damage increment during the experimental BTT investigations (this is discussed in Section 3.5). The synchronisation procedure discussed in Section 3.3.1 therefore played a vital role in ensuring that an experimental control was maintained during the acquisition of the relevant BTT signals.

3.5 BTT Investigations

The preceding sections in this chapter gave an in-depth discussion of the various steps involved in the BTT procedure (as shown in Figure 3.2). In summary, this included: an overview of the experimental testing, BTT signal processing and the methodology used to determine the blade condition. It was important to give an overview of the various processes used in the proposed BTT methodology before discussing the details of the actual investigations. The reason is that the various results presented after the investigations may seem quite rudimentary, however, the processes used to get to the point where the results could be presented in a simplified form was quite complex. The preceding section demonstrated the complexity of the BTT process, the co-dependence of the various steps involved in this process and, lastly, how an incorrect assumption or derivation in a step could lead to inaccuracies in the final outputs. The aim of this research project is also to present a CBM (or VCM) methodology that is simple to implement, yet robust in its functioning. The fact that the various BTT investigations were performed in groups aimed to progressively improve the proposed BTT methodology used for CBM, while also simplifying the methodology as far as possible. Each investigative group aimed to highlight different aspects and each stage in the groups aimed to build on the prior knowledge gained from the preceding groups. The various subsections presented in this section correspond to the investigative groups shown in Figure 3.1. The details of the various BTT investigations follow.

3.5.1 Group I: Preliminary Tests

The preliminary testing gave the researcher insight into the various aspects of BTT. This included the fine-tuning of the equipment used during experimental testing and the implementation of the various algorithms (ToA extraction, synchronisation, blade condition algorithms). For these reasons the results from the preliminary testing were informally documented and does not form part of the intended research outputs. The preliminary testing was done in two stages and the details follow.

Stage I

This stage of testing was very basic, with no damage introduced to the blades. The experimental equipment (signal generation and acquisition) was set up and, where necessary, fine-tuning was applied. The fine-tuning of the experimental equipment, for example, involved finding a suitable sensitivity level for the *Optel-Thevon 152G8* optical shaft encoder. An incorrect sensitivity resulted in a number of missing shaft encoder pulses during acquisition. The fine-tuning also, quite importantly, involved finding the correct depth at which the eddy current proximity probes needed to be fastened on the rotor casing. Fastening the eddy current proximity probes too deep resulted in contact with the blades during rotation. Fastening the eddy current proximity probes too shallow resulted in undetectable blade pulses during acquisition. The manufacturer's guide was consulted in order to seek recommendations of the correct fastening distance relative to a passing blade.

The next step was to gain competence in the various software suites used during experimentation. This included setting-up the triggered acquisition process in the *NVGate* software environment. Furthermore, the *LabVIEW* signal generation virtual interface was implemented and smaller investigations were performed in order to determine which shaft speed profile would be best suited for the desired study. It was concluded that a triangular waveform would be the most applicable as this profile ramps up and down at a constant rate, therefore allowing the blades to gradually pass through their respective resonances. During these investigations it was noted that the safety of the rotor rig should be improved. The relevant blade failure calculations were thus performed. Following this, safety recommendations were made for the experimental testing, as well as the design, manufacturing and installation of custom protective covers on the rotor assembly. Thereafter, a vast number of preliminary tests were performed at a constant shaft speed.

For this stage of testing all of the blades were kept undamaged in order to establish a baseline for the next stage of testing. The relevant BTT data was acquired and preliminary checks were conducted to determine whether the acquisition process was successful. The BTT signal processing procedure was discussed with the author of [Diamond et al., 2015] and following this the necessary algorithms were implemented. The following recommendations are made:

- The triangular shaft speed profile (as shown in Figure 3.5) should be used for the remainder of the investigations. The triangular shaft speed profile enabled the blades to pass through a critical shaft speed during acceleration and deceleration.
- A number of repeat tests should be performed for each stage of the investigation to determine the robustness of the proposed BTT methodology.
- The next stage of testing should preliminarily test the ability of the proposed BTT methodology to detect blade damage. A single blade should therefore be used as a test blade and damage should be introduced to this blade. The initial damage should be quite large in order to gauge whether smaller damage increments should be introduced for the remaining stages.

Stage II

Stage II of the BTT investigation specifically focusses on preliminarily testing the ability of the proposed BTT methodology to detect blade damage. The initial blade damage was machined to the dimensions indicated in Figure 3.19. This was only done on a single test blade (blade 5). For this discrete damage increment, six of the same tests were performed in order to determine the robustness of the BTT methodology. The other blades were left in an undamaged state for comparison. Once all the data was acquired for this damage increment, slightly larger damage was introduced to the test blade (this damage was measured to be approximately 1mm on either side of the test blade). Once all the experimental data was acquired, the various BTT signal processing procedures commenced (as presented in Section 3.3). Thereafter the vibrational characteristics of the blades were determined using the MCS and a feature extraction process was used to determine the blade natural frequencies for mode 1 of vibration (as presented in Section 3.4). Again, it should be emphasised that the results from the preliminary damage detection investigation is not part of the formal investigation. The preliminary results merely enabled further recommendations to be made, therefore allowing progressive improvements of the proposed BTT approach.

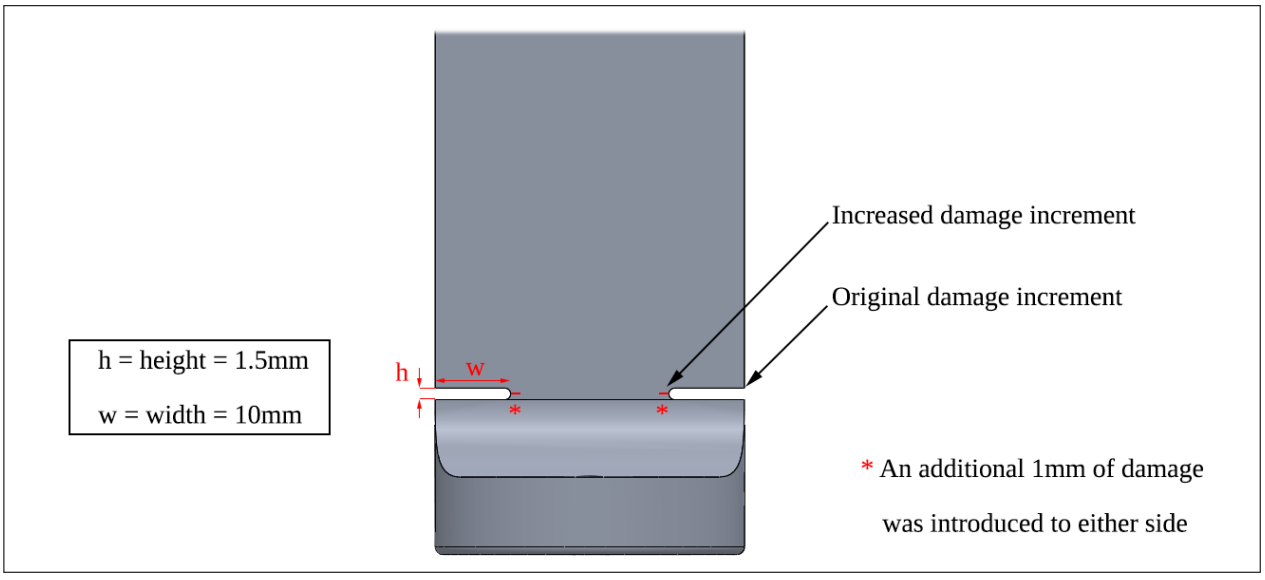

Figure 3.19: Bottom section of the test blade used for the preliminary testing; with the discrete damage dimensions indicated.

Figure 3.20 gives an example of the amplitude and phase results after the MCS was performed using the outputs of the BTT signal processing. The shaded regions in this figure are indicative of the 95% confidence intervals established from the normal distribution associated with each revolution of the localised resonance. Figure 3.20, in essence, represents the combination of the per blade and per revolution normal distribution results shown in Figure 3.18. Figure 3.20 clearly indicates a peak in the amplitude and a sudden shift in the phase results. Also quite evident from the phase results in Figure 3.20, are the narrower confidence intervals close to the excitation frequency of the maximum amplitude. Please note that this figure merely serves as a single example of the abundance of results derived from the BTT signal processing and by no means forms part of the formal results.

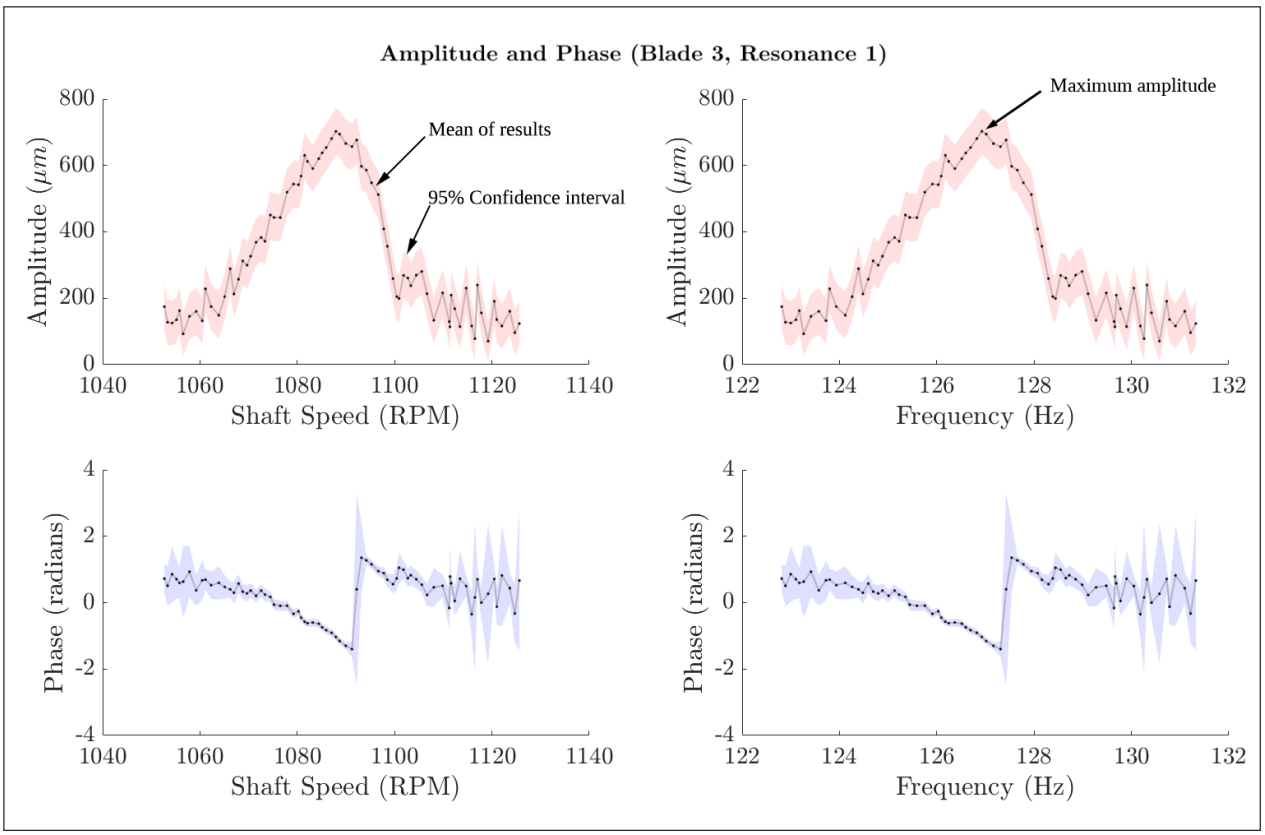

Figure 3.20: Example of the amplitude and phase results (blade 3, resonance 1) following the MCS.

Figure 3.21 gives an example of the natural frequencies derived from the amplitude and phase results (this figure shows the BTT results corresponding to blade 3 at resonance 1). For the preliminary testing the natural frequencies were found as the average frequency, $f_{n_{ave}}$, corresponding to the two features described by Equations 3.9 and 3.10. For clarity purposes, Equation 3.11 highlights this calculation below:

$$f_{n_{ave}} = \frac{f_{n_{\hat{\phi}}} + f_{n_{\hat{\phi}}}}{2} \tag{3.11}$$

The maximum amplitudes are marked by the unfilled marker in Figure 3.21. The filled markers indicate the derived natural frequencies for each of the tests for this particular investigation. The normal distribution for these natural frequencies is also shown; this distribution indicates a relatively small variance in the derived natural frequencies. Also shown in Figure 3.21 is an example of how the amplitude and phase signals may be combined. This combined signal was obtained by finding the average of the mean amplitude and phase signals corresponding to each of the six tests. The solid vertical line indicates the natural frequency of the combined signal. It was noted that quite a significant difference exists between the natural frequency resulting from the combined signal and the mean of the natural frequencies from the individual signals. This observation was used to make further recommendations for the remaining BTT investigations.

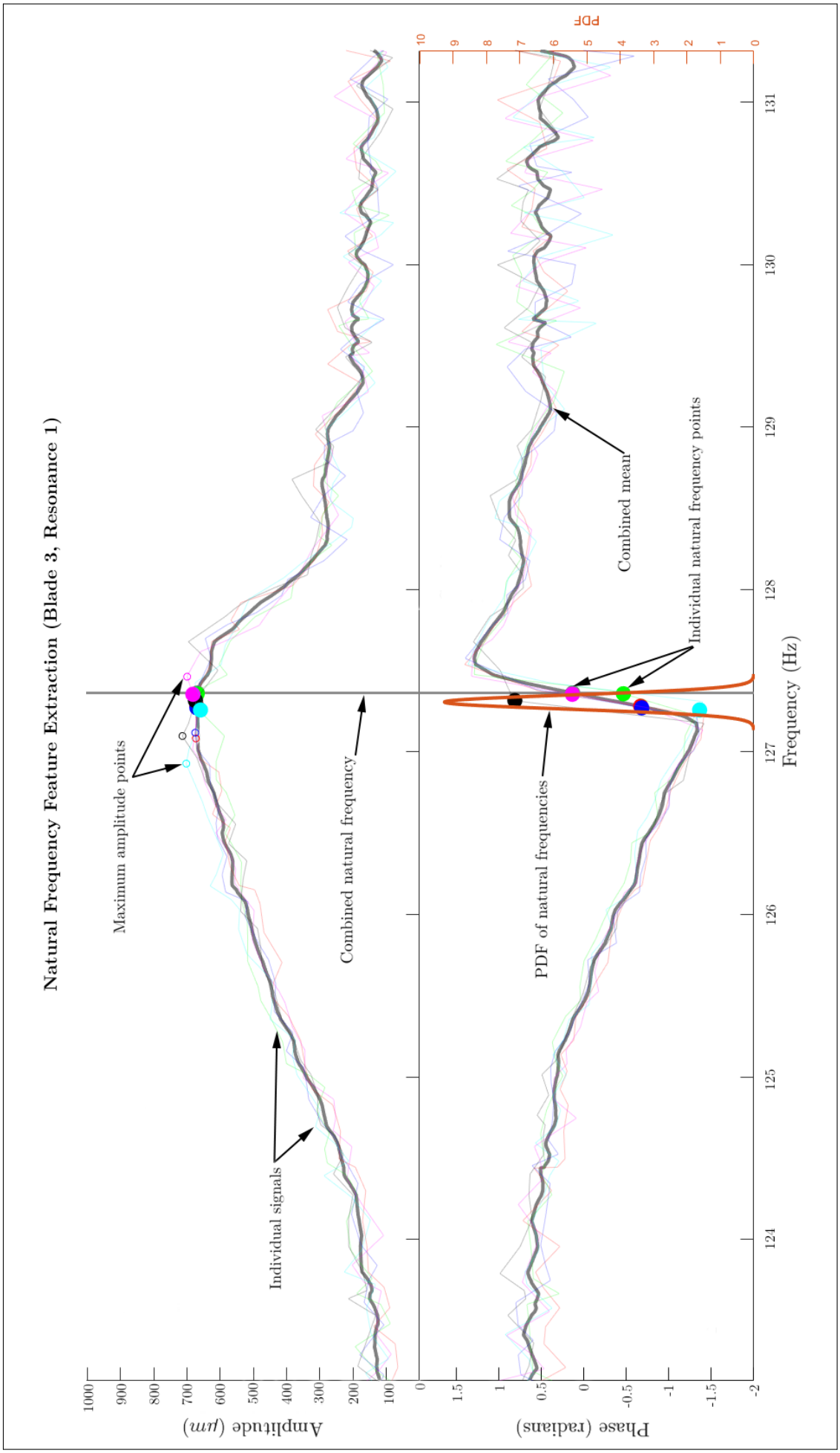

Figure 3.21: Example of the derived natural frequencies following the feature extraction process for *Stage II* of testing (blade 3, resonance 1).

The natural frequencies were similarly derived for the test blade (blade 5), where discrete damage was introduced to the blade. Table 3.2 compares the natural frequencies of the test blade for the two damage increments. The discrete cracks were introduced to both sides of the test blade as indicated in Figure 3.19. The dimensions of the discrete cracks correspond to the values shown in this figure. Table 3.2 indicates that the natural frequency of the test blade decreased by approximately 2Hz after increasing the crack size width by 1mm on either side of the blade. Figures B.5a and B.5b in the appendix (Section B.2.1) shows the complete amplitude and phase signals of this test blade, as well as the derived natural frequencies corresponding to the aforementioned feature extractions process.

Table 3.2: Natural frequencies at the various damage increments introduced to blade 5 for the preliminary tests.

Discrete crack size, w (mm)	**Natural Frequency, $f_{n_{ave}}$ (Hz)**
10	114.20
11	112.19

It was also important to get a sense of the accuracies of the derived natural frequencies of all the blades. In order to do this a static modal analysis was performed using a modal hammer, laser vibrometer and spectrum analyser. The resultant Frequency Response Function (FRF) of this modal analysis is shown in Figure 3.22. The natural frequencies of the various blades correspond to the frequency of the peaks in the signals. The natural frequencies of the undamaged blades are almost consistently higher at 15Hz for both the FRF and BTT results. The BTT results are represented by the vertical lines in Figure 3.22 and correspond to the averaged blade specific natural frequencies, $f_{n_{ave}}$, which are derived as demonstrated in Figure 3.21.

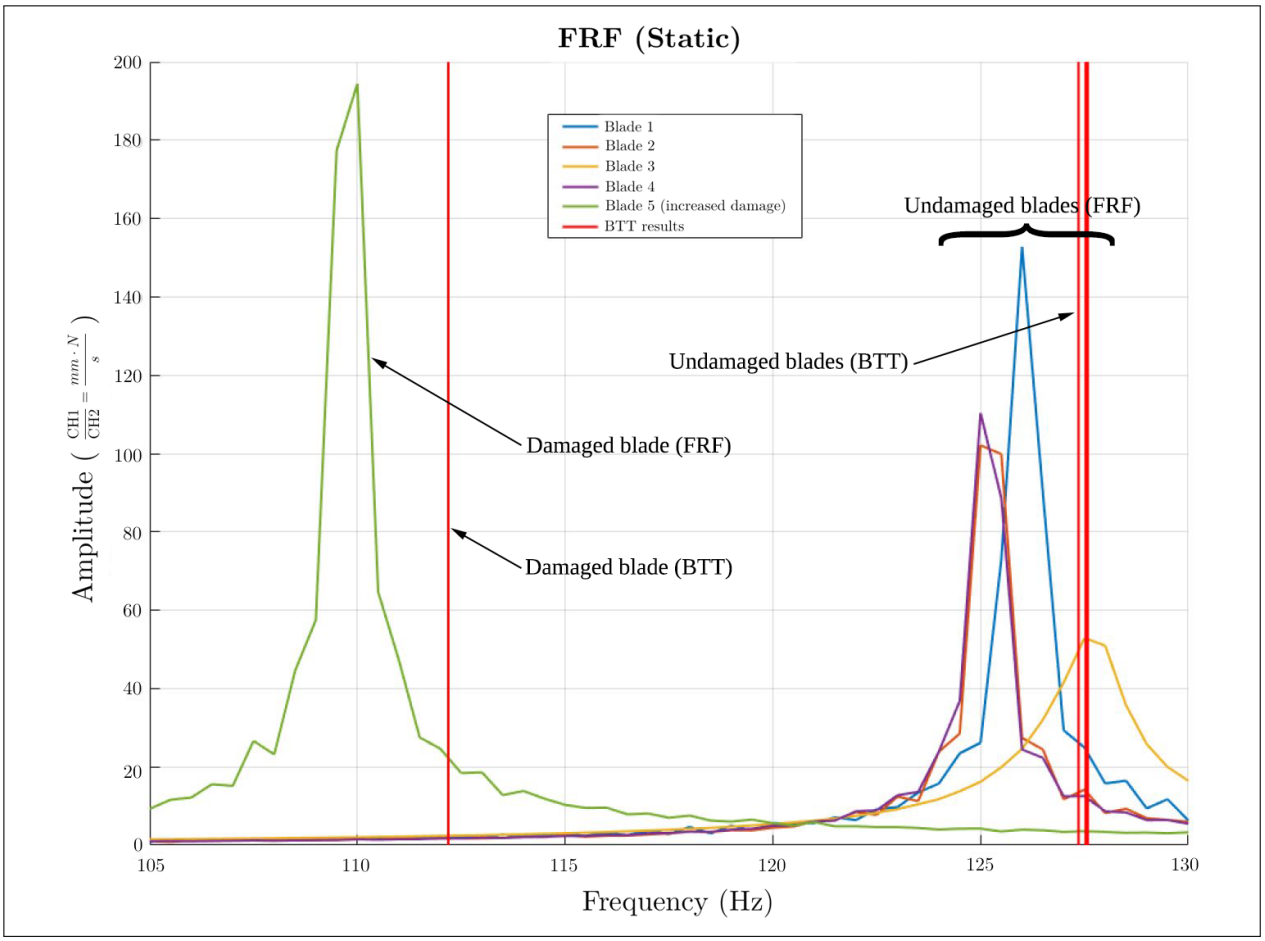

Figure 3.22: Preliminary FRF results of the static modal analysis.

The static modal analysis natural frequency results (shown in Figure 3.22) were consistently lower by approximately 2Hz compared to the BTT results. The reason is that blades were fastened to a static base during this modal analysis, therefore neglecting the effect of the centrifugal loads as a result of the shaft rotation. The static modal analysis in essence did not account for blade stiffening due to these centrifugal loads. The following recommendations are therefore made:

- For the sanity check of the BTT natural frequency results, blade stiffening should be accounted for. The measurement of blade natural frequency should therefore be performed dynamically while the rotor assembly is in operation. The proposed method to do so incorporates the use of strain gauges attached to selected blades. Acquiring the voltage signals and performing an FFT should result in a more accurate indication of the actual blade natural frequencies during rotation.
- A DAQ with a higher sampling frequency (greater than the 65.536kHz limitation of the *OROS OR35 DAQ*) should be used for acquisition. This should give an indication of the sensitivity of the BTT results to sampling frequency.
- More than six tests should be performed per discrete damage increment, since more of the same BTT results give a better indication of the robustness of the proposed method.
- The test blade should be tested in an initially undamaged state to be able to compare the relative changes in the natural frequency from this undamaged state. The discrete damage should then be introduced incrementally and each incremental increase in the damage size should then be less than 1mm. This should be done to test the ability of the proposed BTT methodology to detect small changes in the natural frequency of the test blade.

3.5.2 Group II: Relative Natural Frequency Tracking

This group of the BTT investigation formed the bulk of the formal research outputs. The results, of particularly *Stage IV*, are presented in Chapter 5. The aim of this investigative group was to test the ability of the proposed BTT methodology to track the relative changes in the natural frequency of the test blade due to the incremental introduction of discrete damage. It was further aimed to test whether the proposed BTT methodology is able to track small changes in the blade natural frequency; smaller than the 2Hz change reported for the preliminary testing and desirably less than 1Hz for practical purposes. The desired outputs of this investigative group correspond to the damage identification and classification outputs of the hybrid approach (as mentioned in Section 2.2). A summary of these desired outputs follows:

1. *Damage identification:* This involves tracking the relative change in the natural frequency of the blade to identify and infer the degree of blade damage. The reference state for this process is the natural frequency of the initially undamaged blade. A FEM modal analysis (the discussion of this analysis follows in Chapter 4) will also be used as a reference with expected blade conditions forming part of the simulation process.
2. *Damage classification:* The natural frequency and amplitude BTT results are clustered or grouped using predetermined mean values. The predetermined mean values are derived from a FEM modal analysis (the discussion of this analysis follows in Chapter 4). The damage classification process therefore aims to classify the severity of the blade damage based on the FEM modal analysis and BTT results.

As noted from the above outputs, the BTT data from this investigation is supplemented by data obtained from a FEM modal analysis, for reasons which will become more apparent in the remainder of this subsection. Again, it should be emphasised that this investigative group directly incorporated the recommendations from *Group I*. The investigation from this group did, however, start with a preliminary stage where the robustness of the proposed BTT method was tested more thoroughly.

Stage III

This stage of testing formed part of the preliminary testing of the associated investigative group. A number of the same BTT experimental tests were performed using the initially undamaged test blade (*blade 2*). Strain gauges were attached to this blade along with a slip ring on the rotor-hub. The shaft speed was maintained at a constant predetermined critical speed (approximately between 1280 - 1290 RPM) and the raw voltage signal of the strain gauge was captured. This was done using a sampling frequency of 8.192 kHz and acquiring this signal for around a minute. Signal processing of this raw voltage data (using an FFT) enabled the natural frequency of the test blade to be determined for this operational speed. This merely acted as a sanity check of the derived BTT natural frequency results and by no means intended to act as a thorough validation of the results. The choice to use strain gauges was largely due to the recommendations from *Stage II* of testing, where the static modal analysis was noted to not account for blade stiffening during rotation.

Figure 3.23 highlights the BTT results of a preliminary investigation whereby 30 of the same BTT measurements were taken of the undamaged blade. This investigation aimed to demonstrate what may be expected from a single BTT measurement. Figure 3.23 shows a Multivariate Probability Density Function (MPDF) of the natural frequencies of the test blade extracted from the BTT amplitude results. The results of this investigation are summarised in Table 3.3. The results from Figure 3.23 and Table 3.3 indicate that uncertainty exists for the individual measurements. This needs to be accounted for in the proposed hybrid approach. As previously mentioned, the use of a FEM modal analysis aims to supplement the BTT results. More specifically, the results from the FEM modal analysis intends to establish a preliminary reference for the blade vibrational characteristics derived from BTT investigation. As previously highlighted, one of the main advantages of using the BTT approach based on BLR is that it offers the ability to quantify the associated uncertainty in the predictions. Predictions are not merely deterministic but incorporate the uncertainty by establishing confidence intervals around the means. Figure 3.20 gives an example of the 95% confidence intervals which may be established around the mean amplitude and phase results.

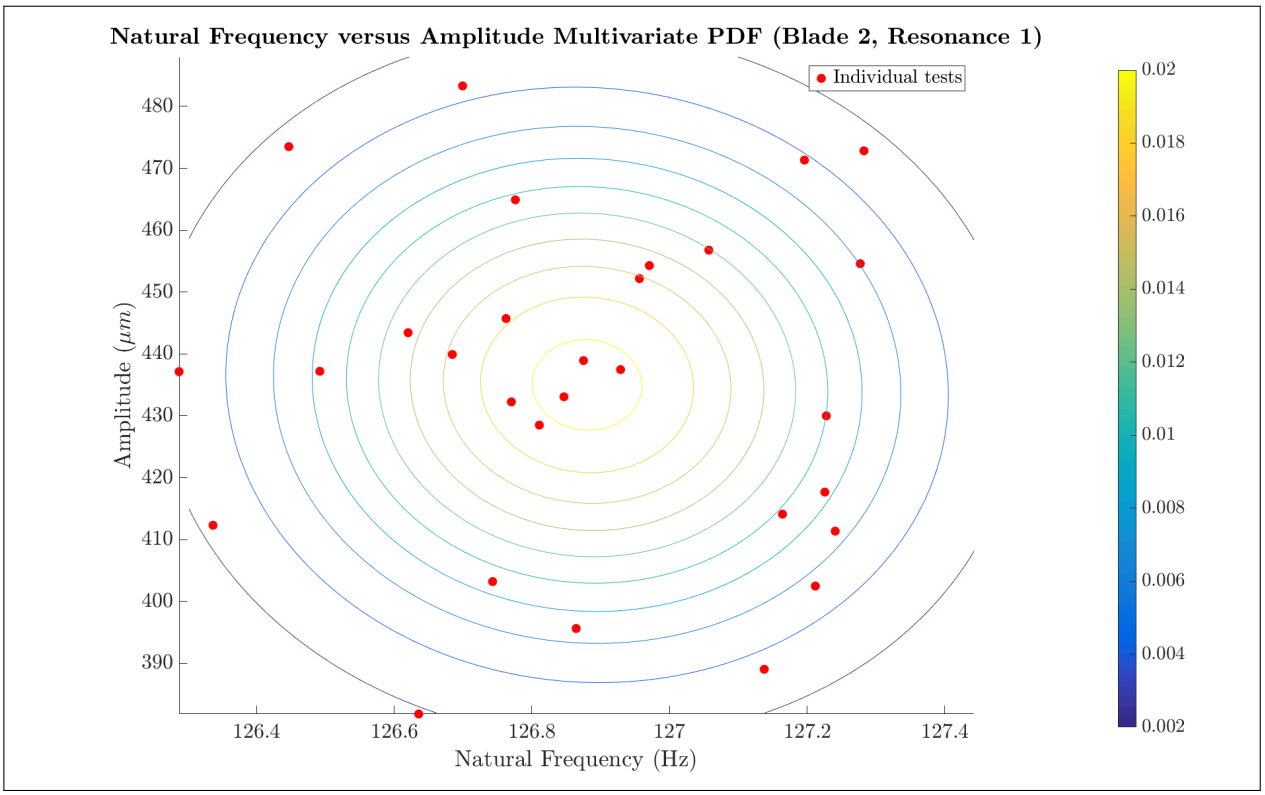

Figure 3.23: Scatter plot of BTT amplitude and natural frequency results for blade 2 at resonance 1 (preliminary investigation, *Stage III*).

Table 3.3: Amplitude and natural frequency results (as a result of a univariate analysis of these parameters).

Value	Amplitude ($\hat{A}$)	Natural Frequency ($f_{n_{\hat{A}}}$)
Mean	435	126.88
Standard Deviation	26.513	0.289

Figure 3.24 shows the strain gauge results for blade 2 in bending mode 1. It should be noted that the use of strain gauges in this preliminary investigation was merely a sanity check of the extracted natural frequencies of the BTT results. The mean natural frequency based on the amplitude results of the BTT investigation, shown in Table 3.3 is very close to what is shown for the strain gauge in Figure 3.24. It is clear that performing a number of the same tests and extracting the features does help establish a more confident indication of the natural frequencies. However, the option of performing the same tests will not always be available for more practical implementation in industry. Performing a number of the same tests is more feasible in a laboratory environment where the desired operational conditions may be controlled and closely monitored. In industry it may be more difficult to ensure that the operational conditions remain the same and it is thus impractical to perform a number of the same tests. A lot of confidence needs to be placed on a single BTT measurement. The following recommendations are therefore made:

- It is clear that the uncertainty of the BTT measurements need to be accounted for during the blade damage identification (relative natural frequency tracking) and damage classification (clustering). The proposed hybrid approach aims to account for the uncertainty of the single BTT measurements by incorporating a FEM modal analysis to project expected natural frequencies associated with a certain discrete damage increment.
- The proposed hybrid approach should account for the fact that a lot of confidence needs to be placed on a single BTT measurement. It is therefore desired that a single BTT measurement should have a high accuracy. However, Figure 3.23 indicates that there is the possibility that the derived natural frequency of a particular blade may vary by 1Hz between the two extremes (minimum and maximum). This proves that it is difficult to know with certainty what the actual natural frequency of the blade is, based on a single BTT measurement.

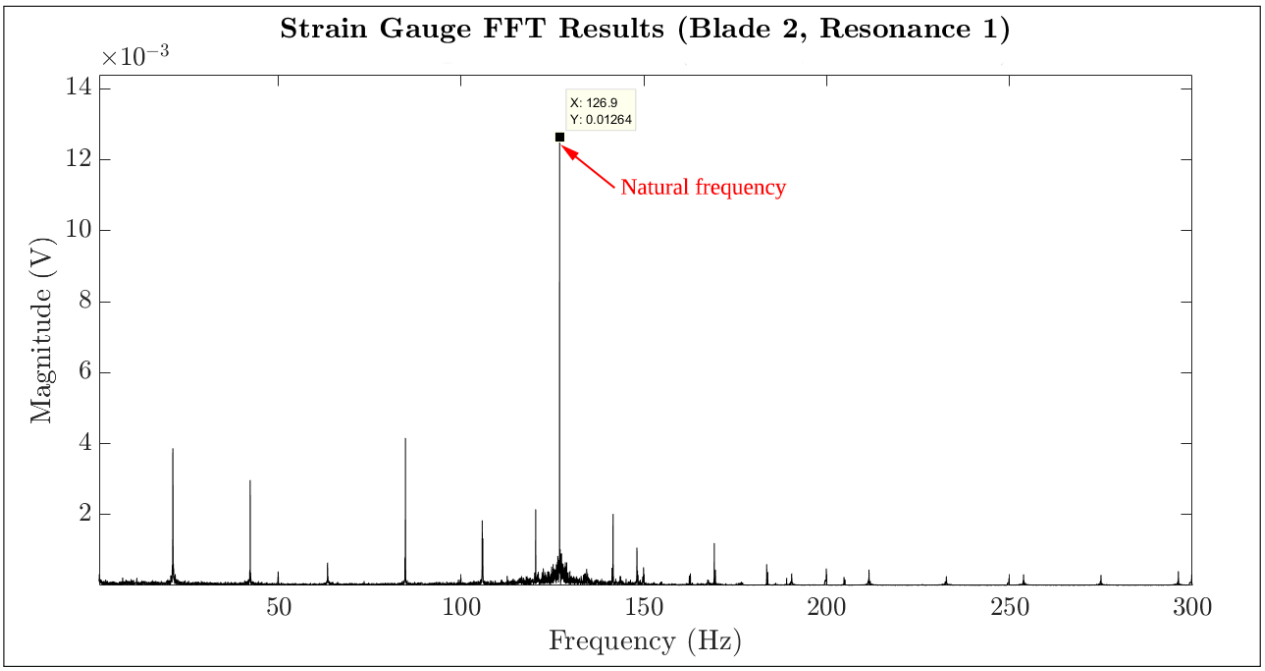

Figure 3.24: Strain gauge FFT results for blade 2 at resonance 1 (preliminary investigation, *Stage III*).

Stage IV

This stage formed the basis of the formal investigation in terms of the desired research outputs shown in Figure 2.1. The results of the investigation corresponding to *Stage IV* are therefore documented in Chapter 5. The overview of this stage starts off with a recapitulation of the experimental procedure relevant to this investigation. The details of this follow.

Figure 2.1 highlights that the results from the chosen BTT technique would be used to identify and classify blade damage. In order to do so, the ability of the proposed BTT method to detect a noticeable change in the blade natural frequency was first tested; done in the preliminary testing (*Group I*, *Stage II*). Discrete damage was introduced to a single blade as part of this preliminary testing. Distinct differences were noticed between the healthy blades and the damaged blade with regards to the resultant amplitude, phase characteristics and derived natural frequency. As expected, the natural frequency proved to decrease as the increased damage reduced the blade stiffness. Subsequent to this, a more controlled experimental procedure was followed to test the performance of proposed hybrid approach in identifying and classifying blade damage; this specifically forms part of *Stage IV* of testing. The following experimental procedure acts as a summary of the details outlined in Section 3.2.3, but adds the relevant detail for *Stage IV* of testing:

1. The blades in the rotor assembly were numbered in order to keep a record of the blade specific results. Figure 3.8a gives an example of the measured voltage pulses at the four proximity probes and the extracted ToAs at a chosen trigger level. The raw proximity probe signals clearly indicate that a specific blade was slightly longer than the others. This blade was used as a reference blade and referred to as *blade 1*. Blade 2 was selected as the test-blade.

2. An initial modal analysis was performed using an FEA to determine where the maximum stress concentration would occur for the first mode of excitation. Figure 3.6a shows that the maximum stress concentration for the first mode of vibration occurs directly and slightly above the blade fillet. The discrete damage was therefore introduced in this region for the reasons outlined in Section 3.2.3. It should be emphasised that this modal analysis does not form part of the proposed hybrid approach shown in Figure 2.1. This modal analysis was merely used for preliminary investigative purposes and to locate a region where cracks would most likely initiate *naturally* as a result of HCF.

3. The size of the incremental damage introduced to blade 2 for this stage corresponded to the values shown in Table 3.4. This damage was only introduced to a single side of the test blade. The relative crack sizes were computed as a percentage of the total width (40mm) of the blade. The small size of the discrete damage aimed to test the ability of the BTT technique to track small changes in the natural frequency of the blade due to the introduced damage.

4. The shaft speed was ramped up from 1195 RPM to 1330 RPM and down again in order to pass through the blade resonant frequencies. The resonant frequencies were predetermined from a simple FEM modal analysis. The FEM modal analysis at this stage does not form part of the proposed hybrid approach outlined in Figure 2.1. The strain gauges shown in Figure 3.6b were also used as an initial sanity check of the blade natural frequencies which were extracted using an FFT of the recorded time-voltage signal; as discussed for *Stage III* of testing. The compressed air supply (top and bottom of the rotor casing) excited the first mode of vibration of the blades during rotation.

5. The experimental BTT tests were repeated six times for each of the damage increments shown in Table 3.4 (72 tests in total). The repetition of the experiments aimed to determine the robustness of the chosen BTT technique. In order to control the comparison of the extracted blade phase results between tests, it was important to synchronise all the measured proximity probe signals with respect to a certain shaft encoder pulse. In essence, this synchronisation enabled all the proximity probe signals for all the tests to start on the same pulse. Figure 3.8b shows that blade 1 at probe 1 was used for this synchronisation.

6. Diamond identified that one of the largest factors influencing BTT measurement accuracy is: data acquisition sampling frequency. The sensitivity of the chosen BTT technique to sampling frequency was investigated by using two independent DAQs. The *OROS OR35* DAQ with *NVGate* software had a sampling frequency limitation 65.536 kHz for the required number of input channels. The *HBM Genesis High Speed* DAQ with *Perception* software had a much higher sampling frequency at 1 MHz as well as a higher resolution. The sensitivity of the BTT measurement accuracy to data acquisition sampling frequency was therefore investigated by performing three tests per DAQ for a particular damage increment shown in Table 3.4.

7. The ToAs were extracted from the raw voltage shaft encoder and proximity probe signals at a chosen trigger level. Figure 3.8a gives an example of the extracted proximity probe signal ToAs for the various blades. The extracted ToAs were then used directly in the remainder of the BTT signal processing. After the BTT signal processing, the blade conditions were inferred by deriving the amplitude, phase and associated natural frequencies (as discussed in Section 3.4).

In summary, a few important aspects of the BTT experimentation need to be noted. Discrete blade damage was introduced incrementally from an originally healthy state (the most severely damaged blade is shown in Figure 3.6b). For this stage of testing the incremental damage was only introduced to a single side of the blade, in contrast to what was done for *Stage II* of testing. The introduction of incremental damage aimed to test the ability of the proposed hybrid approach to identify changes in the natural frequency of the blade and to further classify this damage. Relative changes in blade natural frequencies therefore needed to be computed. The incremental change in the size of the introduced damage was kept small. This aimed to test the ability of the proposed BTT approach to track small changes in the natural frequency of the blade as the size of the damage was increased. The strain gauges, along with an FFT, were merely used as an indicator of what level of damage would result in the desired natural frequency change of the blade, as well as a sanity check of the natural frequencies derived from the BTT data. Furthermore, it should be reiterated that the initial FEM modal analysis does not form part of the hybrid approach. The FEM modal analysis essentially highlighted where the maximum stress concentration occurs for the first bending mode of vibration as well as the associated natural frequency to choose the required shaft speed profile. The introduced incremental damage is shown in Table 3.4. The sizes of the discrete cracks were measured by taking high resolution photographs of the damaged areas and then digitally measuring the cracks using the *Adobe Photoshop CC 2015* software suite. The relative crack size represents the percentage of the total width of the blade with a discrete crack and is computed using Equation 3.12 below:

$$\text{Relative crack size} = \frac{\text{Discrete crack size}}{\text{Blade total width}} \times 100 \tag{3.12}$$

Table 3.4: Incremental discrete damage introduced to blade 2.

Damage Increment	**Crack Size (mm)**	**Relative Crack Size (%)**
1	0	0
2	0.90	2.250
3	1.11	2.775
4	1.28	3.200
5	1.58	3.950
6	1.81	4.525
7	3.11	7.775
8	3.87	9.675
9	5.60	14.000
10	6.97	17.425
11	8.30	20.750
12	8.61	21.525

Figure 3.25 shows the superimposed amplitude and phase results for all for all 72 tests corresponding to *Stage IV*. These tests are colour-coded in Figure 3.25 according to the particular damage increment. Figure B.6 in Section B.2.2 of the Appendix shows only the superimposed amplitude and phase signals for clarity. Also shown in this Figure 3.25 are the mean extracted natural frequencies derived from the maximum amplitude feature, for all the tests in the particular damage increment. The mean was computed as the average of all the individual tests (three from the *OROS* DAQ and three from the *Genesis* DAQ). As expected, these natural frequencies decrease as the size of the discrete damage increases for the increments shown in Table 3.4. More detail about this follows in Chapter 5. Furthermore, linearly fitted curves are shown as an overlay on the phase results. These curves correspond to the locations of the phase shift feature from Equation 3.10 and locations after the phase shift. For clarity, the general form of of the linearly fitted curves is shown below:

$$y = m \cdot x + c \tag{3.13}$$

In Equation 3.13, y corresponds to the phase value at the frequency x, m is the associated gradient and c is the intercept on the phase axis. These fitted curves were merely used to demonstrate the, more or less, consistent nature of the gradients in these fitted curves. The fitted curves were placed in the location of the phase signal where the sudden 180° shift in phase was detected and immediately after this location. It was initially thought that the parameters of these fitted curves (gradients and intercepts) could be used as further features in the damage identification and classification process. The data of the intercepts and gradients are shown in Figure 3.26. However, upon closer inspection of the fitted curve data, the following is concluded:

1. There is almost no correlation between the intercepts of these fitted curves and the associated discrete damage increment; noted upon inspection of the data shown in Figure 3.26a.
2. The derived intercepts varied considerably amongst the tests of the same discrete damage increment. This is indicative of the fact that wide confidence bounds exist around the mean values; indicated by the shaded areas in Figure 3.26a.
3. Upon initial inspection, it is noted that both gradient-sets of the phase data shown in Figure 3.26b are more or less consistent over the entire discrete crack size domain. However, between 3.87mm and 8.61mm the gradients of the phase data starts to increase monotonically. The confidence bounds around the mean phase gradients in this localised domain are nonetheless wide, therefore implying that relatively large uncertainties exist.

For the above-mentioned reasons, the fitted curve data for the phase results were not used as features. Using too many features that are not distinguishable from one another may consequently result in predictions prone to large errors. Figure B.7 in Section B.2.2 of the Appendix shows the amplitude results versus discrete crack size and natural frequency in greater detail. A preliminary indication of the relative natural frequency tracking results (derived from the amplitude and phase data) is shown in Figure 3.27. From this figure the following is noted:

1. The mean natural frequencies derived from the amplitude results decrease monotonically as the discrete crack size increases. This is expected since a greater crack size would decrease the stiffness of the test blade.
2. The mean natural frequencies derived from the phase results decrease monotonically, only from a crack size of 1.28mm onwards, as the discrete crack size increases.
3. For both the natural frequency results (derived from the amplitude and phase) it is interesting to note that a relatively wide 95% confidence bound exists at the initially undamaged state. For the remainder of the damage increments, these confidence bounds tend to be narrower for the phase results where it widens for the amplitude results and vice versa.
4. The *Genesis* and *OROS DAQ*s performed similarly in terms of its consistency in derived natural frequencies. Both *DAQ*s exhibited a few derived natural frequencies far from mean natural frequency of the particular damage increment.

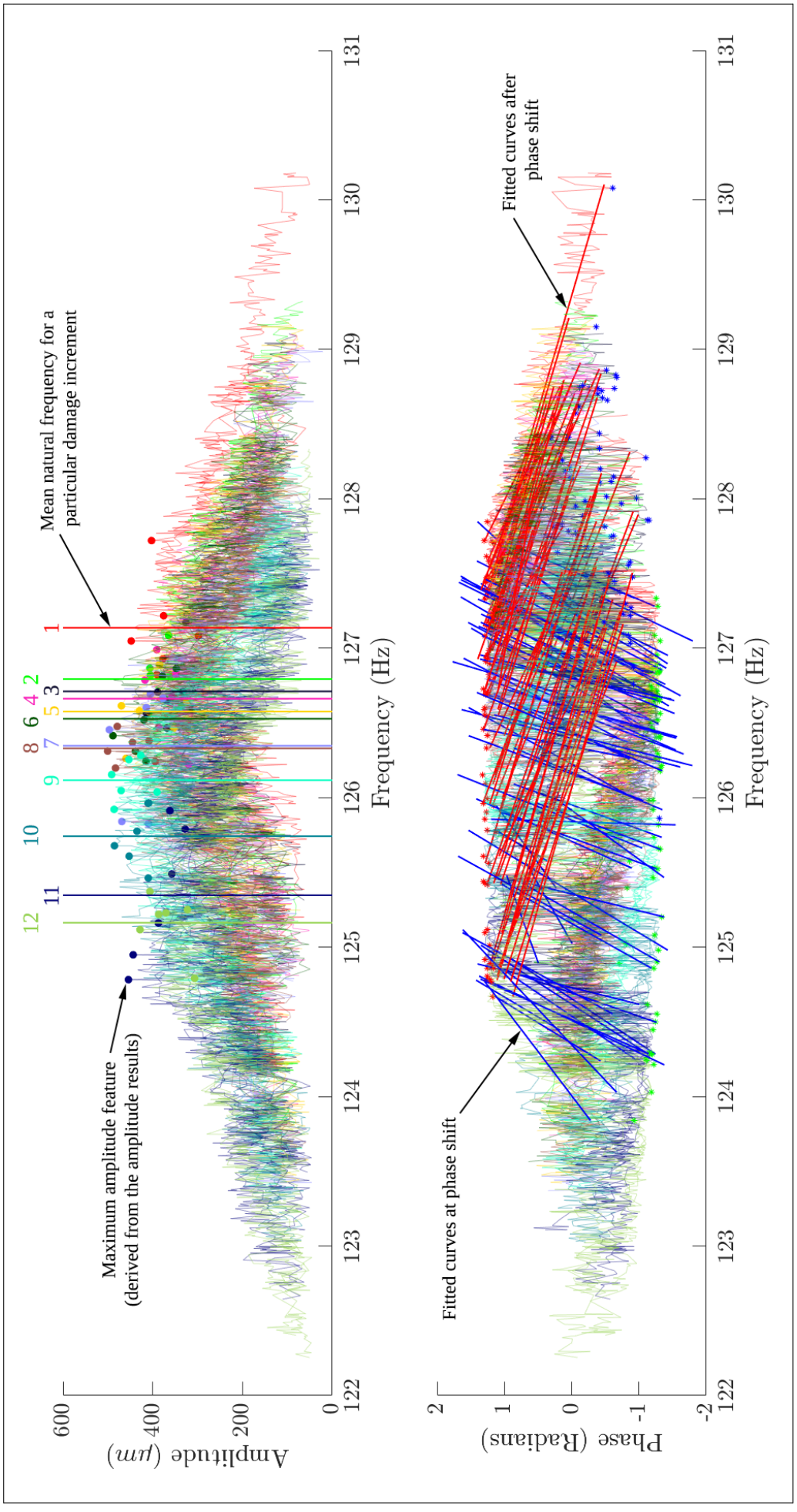

Figure 3.25: Amplitude and phase results of *Stage IV* of testing, superimposed for the various tests and damage increments (blade 2, resonance 1).

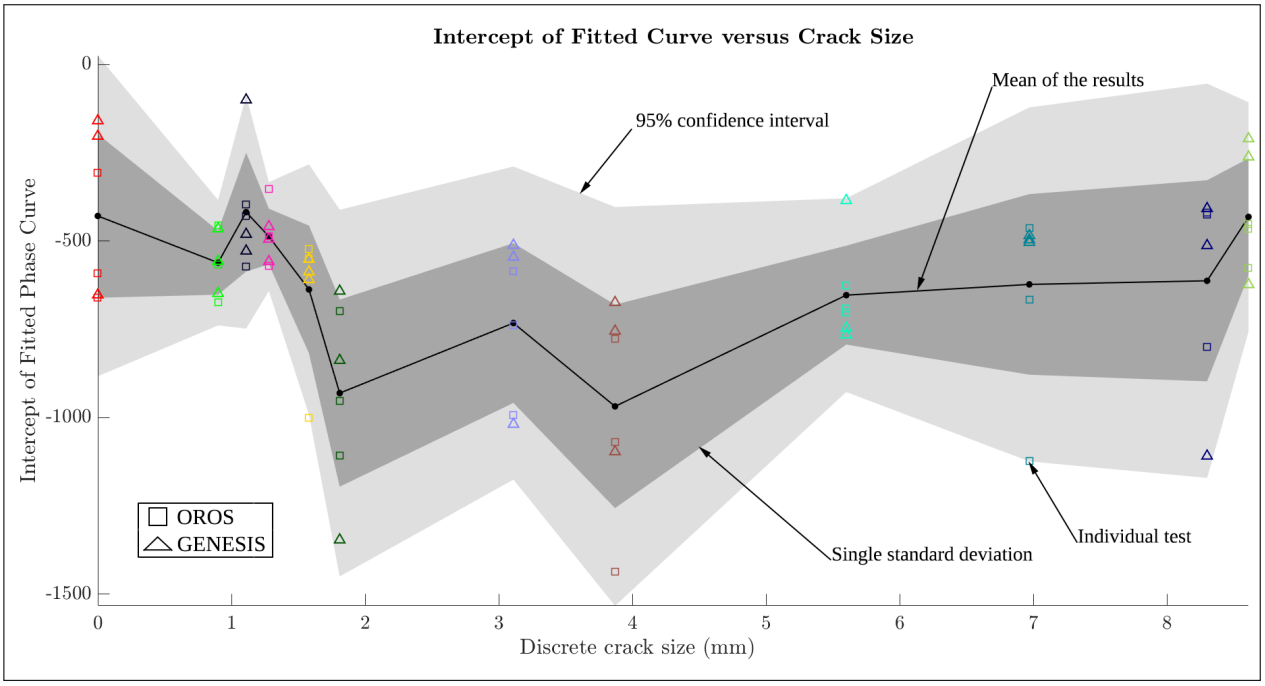

(a) Intercepts of the fitted curves for the phase data in *Stage IV* of testing.

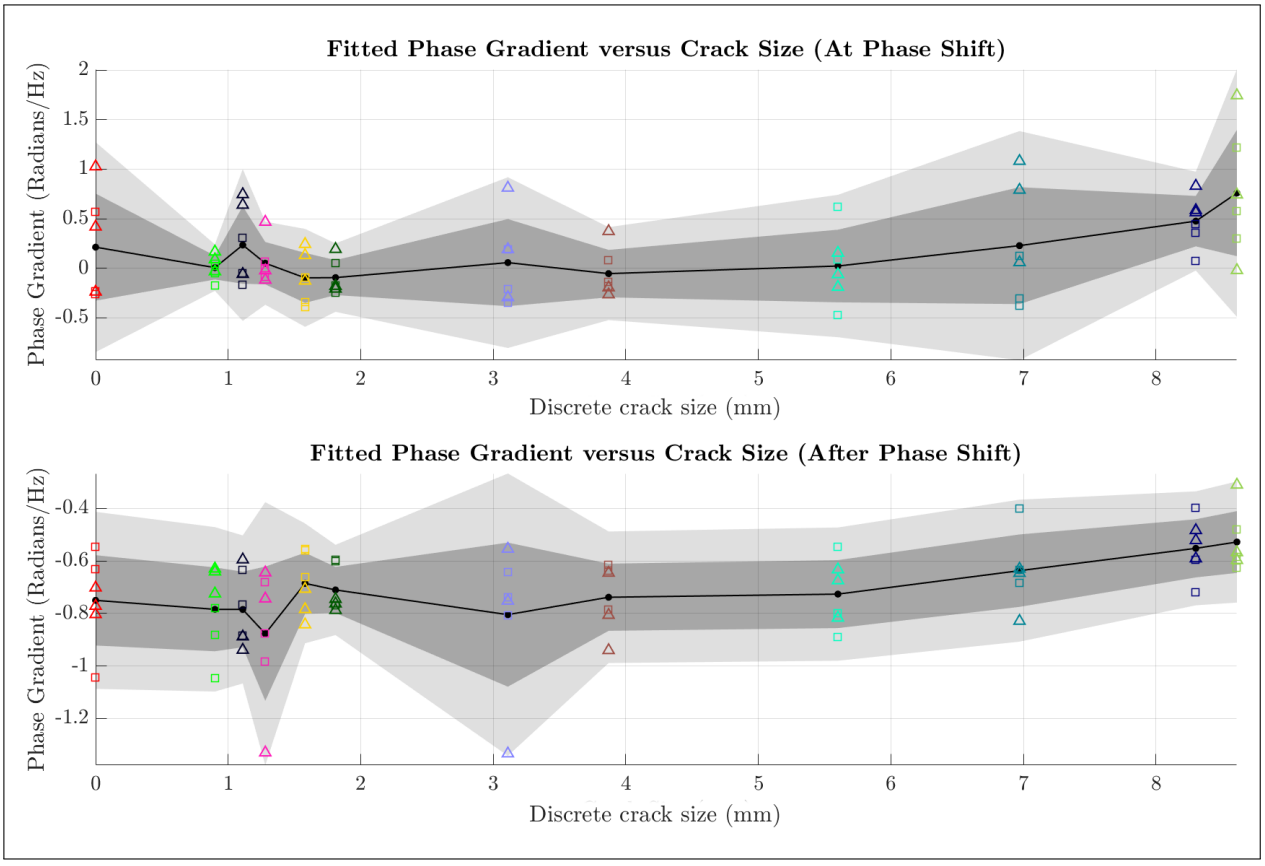

(b) Gradients of the fitted curves for the phase data in *Stage IV* of testing.

Figure 3.26: Fitted curve data for *Stage IV* of testing at the various discrete damage increments.

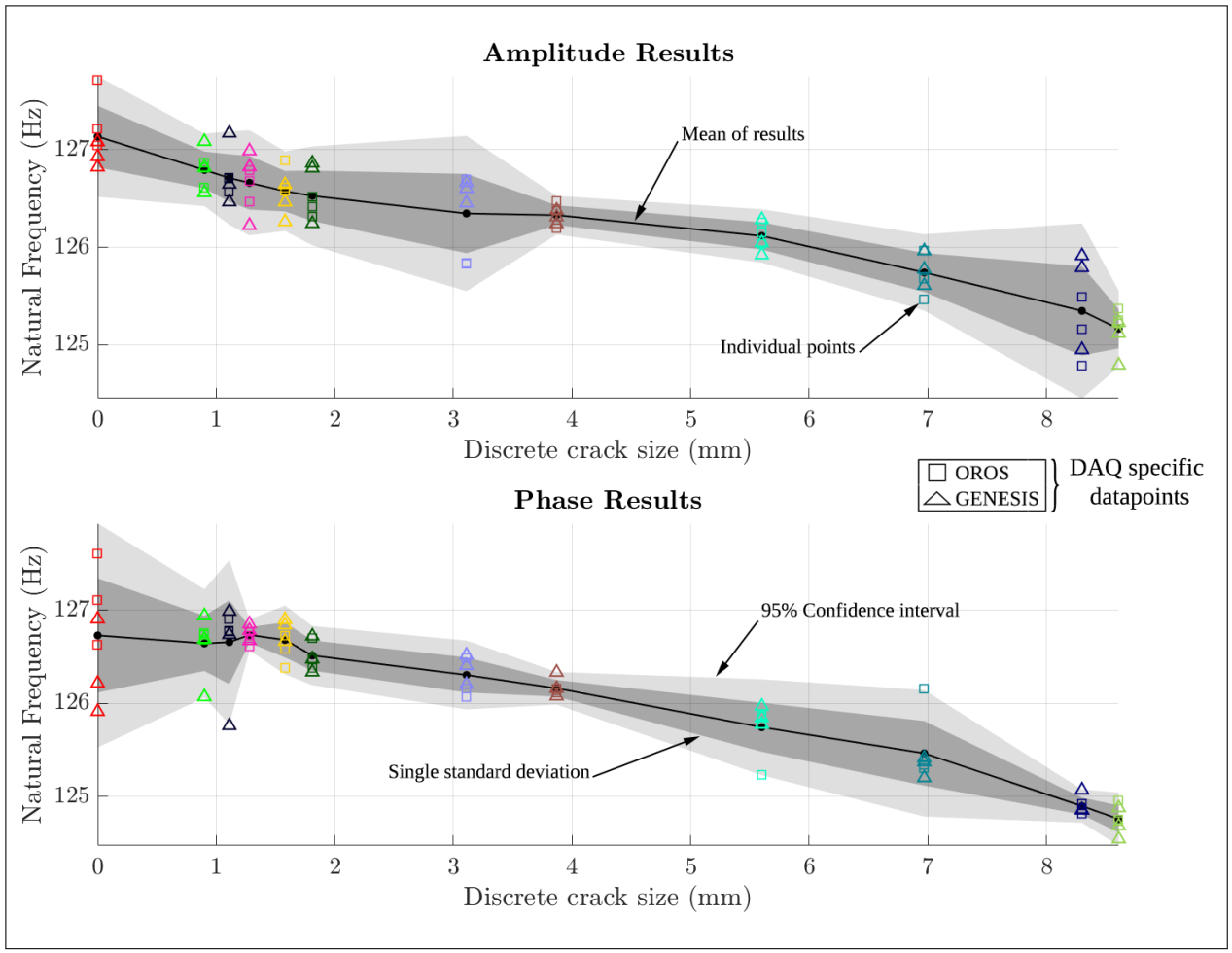

Figure 3.27: Derived natural frequency results for *Stage IV* for the amplitude and phase results (showing individual test points corresponding to a particular DAQ).

As previously mentioned, the results from *Stage IV* of testing form the bulk of the formal investigation. The detailed overview of these results are therefore presented in Chapter 5. The following recommendations and preliminary conclusions are made:

- A definite change in the mean natural frequency of the test blade (*blade 2*) was observed as the discrete crack size increased. For most instances, the mean natural frequency decreased monotonically as the discrete crack size increased. It was possible to derive the natural frequencies from both the amplitude and phase results. At first glance, the natural frequencies derived from these result-sets seem to be in agreement with one another. However, a more in-depth comparison of these result-sets will be presented in Chapter 5.
- There was no definite improvement in the performance of the chosen BTT methodology when comparing the natural frequency results of the higher sampling frequency *DAQ* to that of the lower sampling *DAQ* (65.536kHz for the *OROS* DAQ and *1MHz* for the *Genesis* DAQ). In essence, the 65.536kHz sampling frequency of the *OROS* DAQ was sufficient for the purposes of the investigation. However, this sampling frequency may be insufficient at higher operational speeds. The author therefore recommends that a higher DAQ sampling frequency is utilised during the implementation of this methodology in industry.
- All the tests up to this point have not considered varying temperature effects. The tests were all conducted at room temperature in order to purely consider the effect of the increase in the discrete crack size on the associated natural frequency of the test blade. The next investigative group therefore incorporates temperature effects during the investigation. The motivation for this recommendation will be discussed in Section 3.5.3.

3.5.3 Group III: Relative Natural Frequency Tracking with Temperature Effects

Group III of testing builds on the recommendations from *Stage IV*, specifically the consideration of varying temperatures and the effects this may have on the BTT results. Motivation for the temperature effects consideration on vibration-based damage detection results is presented by Kostić and Gül [2017]. In this study the importance of employing Structural Health Monitoring (SHM) for the evaluation of the integrity of bridges is emphasised. More so, it is stressed that an important issue to account for in continuous SHM is the variation of temperature and the effect this may have on measurement data. In order to account for these variations Kostić and Gül [2017] employed a sensor-clustering-based time-series analysis method which further integrates Artificial Neural Networks (ANNs). The concern with varying temperature effects for this specific research project is that it may in-turn result in varying BTT results. It is hypothesised that these varying temperature effects may produce bigger effects in the response compared to effects related to purely the introduction of incremental discrete blade damage. Section 4.2 in Chapter 4 outlines the relationship between various material properties and the change in temperature, therefore supporting the idea that an increase in temperature of the blade may result in a lower associated natural frequency. *Group III* of testing therefore sets out to determine the effects of varying temperature on the proposed BTT results.

Stage V

This stage of testing consisted of preliminary tests incorporating the effects of varying temperature in the BTT experimental setup. Commercial heaters were secured in front of the rotor setup, as shown in Figure 3.7. The maximum temperature setting was used to heat up the blades before the experimental testing commenced. Once the blades reached an equilibrium temperature an infrared thermography camera was used to measure the temperature of each blade (these temperature values were recorded independently for each blade). Thereafter, six BTT tests were performed, following the same procedure as previously discussed. After each test the temperatures of each blade in the rotor setup were measured again to determined to what extent the blades cooled during the testing. For these tests all the blades were in an undamaged state and the blades were all heated to an equilibrium temperature between tests.

Furthermore, the raw voltage signals from the eddy current proximity probes were analysed to quantify the cooling effect of the blades during testing. Figure 3.28 compares the raw eddy current proximity probe data captured for the blades at room temperatures to that of the blades with maximum temperature effects. The raw voltage signal seemed to decrease by approximately 0.3V at each proximity probe over the entire test period. This was directly related to the blades cooling during the test period, therefore resulting in a slight decrease in the lengths of the blades over this period. In contrast, Figure 3.28 showed that the raw proximity probe voltage signals remained fairly constant at room temperature. The initial voltages of the proximity probes at room temperature were almost 1V higher than the initial voltage for the tests with the maximum temperature effects. This change in voltage, along with the sensitivity specifications of the proximity probes, may be used to determine the change in the lengths of the blades due to the increased temperature. This was, however, not done due to the fact that this stage of testing merely intended to determine whether the variation in temperature influences the BTT results. Six further BTT tests were performed without the effects of an increased temperature. The blades were cooled using the compressed air supply until the temperatures of the blades returned to that of the ambient air. These six tests aimed to establish a basis of comparison, thus allowing the effect of the increased temperature on the blade natural frequencies to be quantified. After the BTT signal processing of the two result-sets (with and without the effects of temperature) it is concluded that the increased blade temperatures resulted in noticeably lower natural frequencies. The natural frequencies were again extracted from the amplitude and phase features extraction process discussed in Section 3.4.

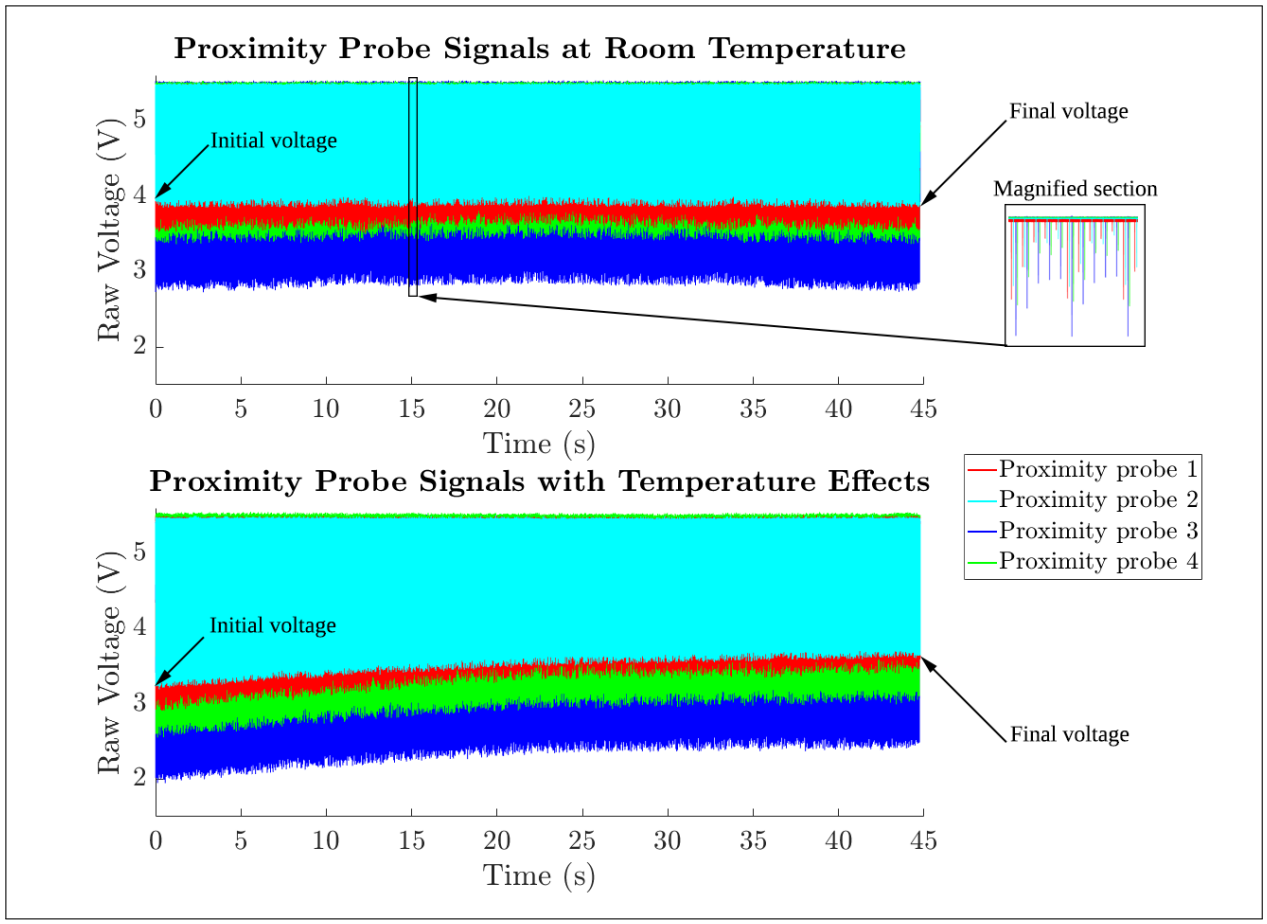

Figure 3.28: Raw proximity probe signals with and without temperature effects (*Stage V*).

The preliminary results for this investigation showed that the natural frequencies of the blades decreased by an average of just under 2.5Hz for the temperature range tested (approximately $98°C$ for the increased temperature tests and $22°C$ for the ambient air temperature tests). The increased temperature, however, resulted in a few complications during the experimental testing. These complications were addressed in a thorough troubleshooting procedure and resulted in the following recommendations for the next stage of testing:

- The increased temperatures of the blades caused the lengths of the blades to slightly increase. In-turn, this increased blade length resulted in a single blade making contact with the eddy current proximity probes during rotation (due to this blade being slightly longer than the others). Fine-tuning of the eddy current probe fastening depth was thus required. It was also important to test whether the fastening depth ensured that the proximity probe pulses were noticeable for the lower temperature testing; the lower temperature resulted in a shorter blade length, thus resulting in smaller proximity probe pulses as the blades passed.
- The effects of blade cooling during a particular test (as shown in Figure 3.28) should be accounted for. It is proposed that this cooling effect could be accounted for by estimating the time occurrence of the localised blade resonances in the time-period of testing. The blade temperatures could then be determined for this specific time by using the initial and final blade temperatures along with interpolation to find the associated resonance temperature.
- It was recommended that the next stage of testing should further consider the effects of introducing incremental discrete blade damage to a single blade (as was done in *Stage IV* of testing) along with the investigation of the effects of varying the temperature. This aimed to determine whether or not the proposed hybrid methodology shown in Figure 2.1 would still be applicable for different blade temperatures.

Stage VI

Stage VI was the final stage of the BTT testing. This stage of testing was also part of the formal investigative process and built-on the recommendations from *Stage IV*. Especially with regards to considering the effects of varying the temperature, along with the introduction of incremental discrete blade damage, and how this would affect the resultant blade natural frequencies. For this investigation incremental discrete blade damage was introduced to blade 3 and all the other blades were left undamaged (blade 2 was replaced with a new blade after *Stage IV* of testing). The various discrete damage increments and relative crack sizes are shown in Table 3.5 below. The same experimental procedure, as used for *Stage IV*, was used for this investigation. The only difference being that two batches of tests were conducted. The first batch of testing corresponded to a lower blade temperature and the second batch to a higher temperature. The blades were heated as discussed for *Stage V* of testing, using two commercial heaters placed in-front of the rotor assembly. For the high temperature tests, the blades were heated for approximately three minutes ensuring that all the blades were heated to the same temperature. The individual blade surface temperatures were regularly measured using an infrared thermographer during this heating process and the BTT tests were conducted once the temperatures reached equilibrium. The blades were allowed to cool for approximately three minutes for the lower temperature tests, the blade surface temperatures were measured, these values were recorded and thereafter the BTT tests were conducted.

Table 3.5: Incremental discrete damage introduced to blade 3.

Damage Increment	**Crack Size (mm)**	**Relative Crack Size (%)**
1	0	0
2	0.71	1.775
3	1.07	2.675
4	1.47	3.675
5	1.97	4.925
6	2.44	6.100
7	3.67	9.175
8	4.91	12.275
9	6.55	16.3750
10	9.11	22.7750

This stage of BTT consisted of a total of 200 tests; 10 tests for each temperature setting, corresponding to a particular discrete damage increment showed in Table 3.5. The surface temperatures of the individual blades were measured before and after each test and these temperatures were recorded. This was specifically done to take into account the cooling effect noticed in *Stage V* of testing (as illustrated in Figure 3.28). After all the tests were conducted these temperature values were analysed in detail. The change in temperature was also related to the location of the resonance area on the shaft speed profile. It was noticed that the resonance occurs more or less in the middle of the total ramp-up time period (at approximately 23 seconds) of this speed profile. The temperatures at resonance were therefore found for all the blades, corresponding to a particular test, using linear interpolation at this time and the two known temperature values for each blade. The temperature values for each blade at this interpolated time were noticeably very close to one another. It was thus decided to use the mean temperature values amongst all the blades for all the tests during the classification of the high and low temperatures. Based on this, the following distinctions are made:

- *Low temperature*: this temperature value was specifically $41°C$, nearly double the ambient temperature. It was decided to use a temperature value higher than the ambient temperature to provide a total of three temperature datasets for the entire research project, namely: ambient (*Stage IV*), low and high temperature (*Stage VI*).
- *High temperature*: this temperature value was specifically $98°C$.

After all the tests were conducted the BTT post-processing commenced to derive the natural frequencies using the proposed feature extraction process. Figure 3.29 illustrates the natural frequency results for the test blade (blade 3) at the low (Figure 3.29a) and high (Figure 3.29b) temperatures. These natural frequencies are based on the amplitude and phase features discussed in Section 3.4.2.

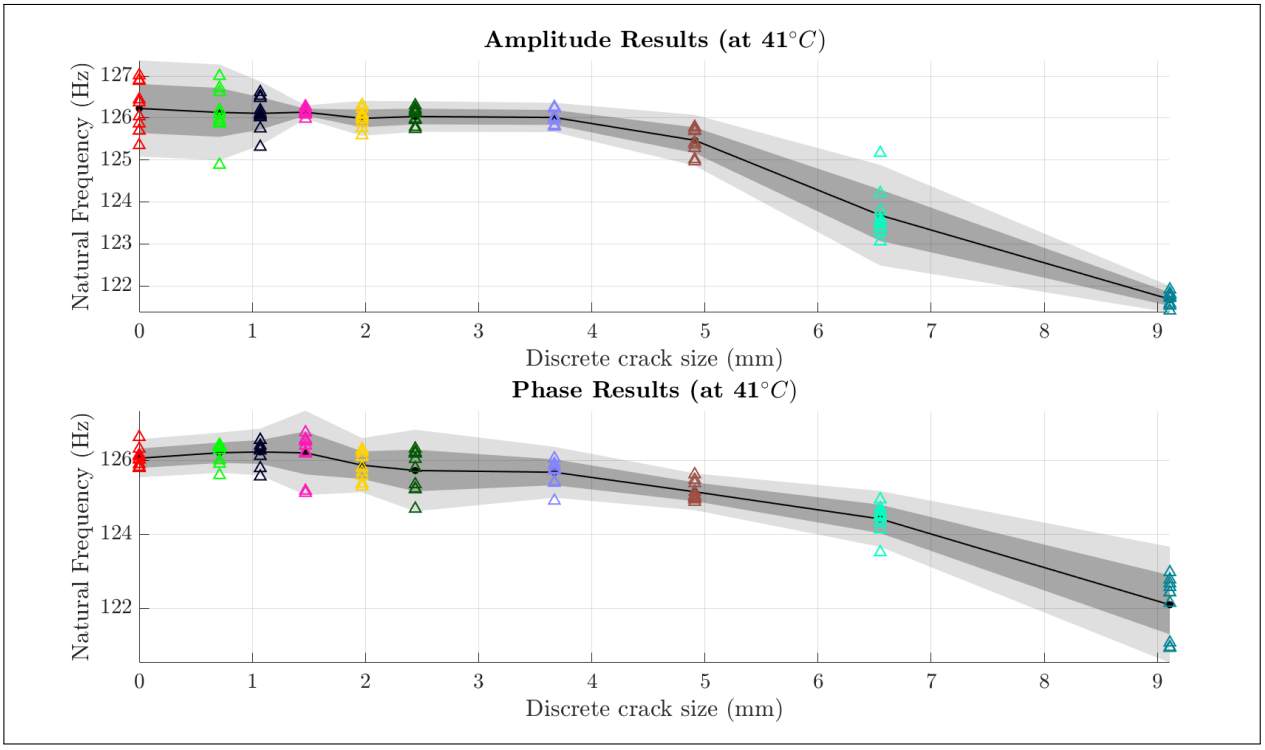

(a) *Stage VI* natural frequency tracking results (at 41°C).

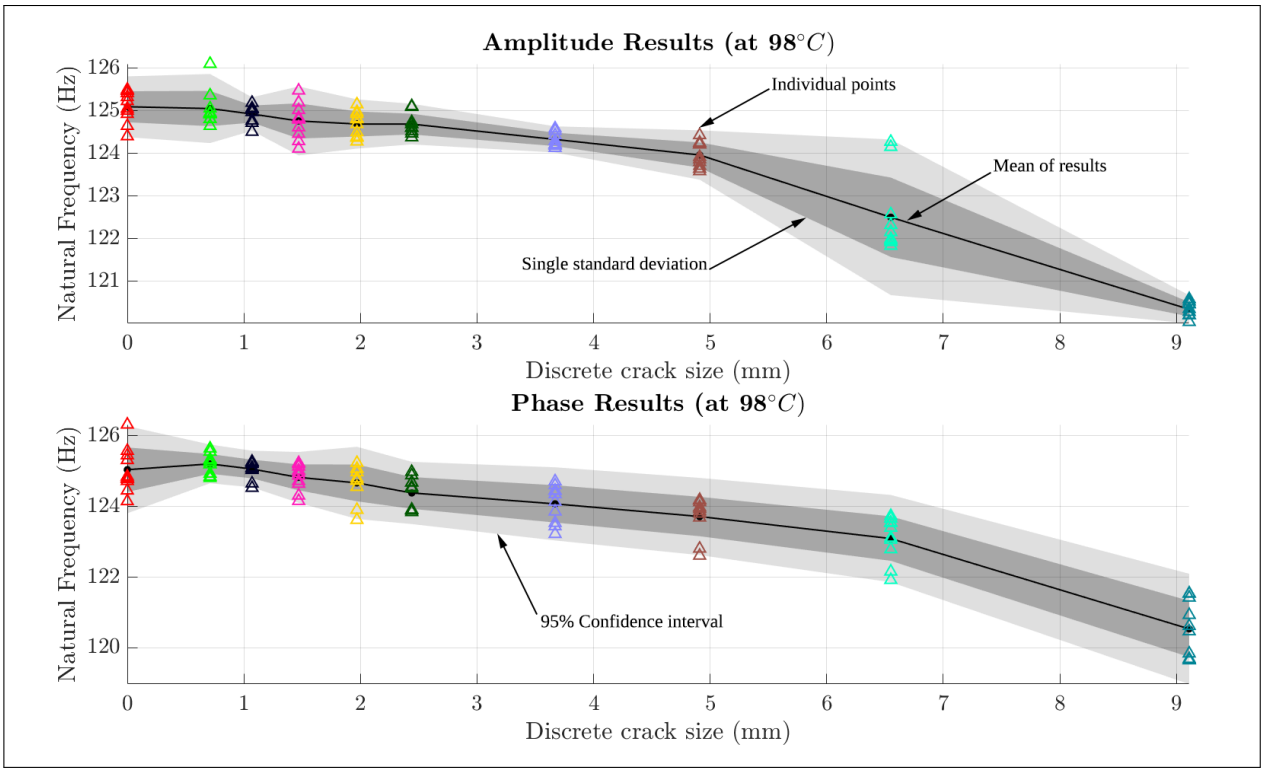

(b) *Stage VI* natural frequency tracking results (at 98°C).

Figure 3.29: *Stage VI* natural frequency tracking results for blade 3 at various temperatures using the amplitude and phase features.

Figure 3.29 shows that the natural frequencies decrease with an increase in the discrete crack size, as expected. The mean natural frequencies decrease almost monotonically for an increase in the associated damage. The mean natural frequencies of the higher temperature tests are noticeably and consistently lower than that of the lower temperature tests, again as expected. The confidence intervals, however, have a very similar profile amongst the various temperature tests, for example; the confidence intervals of the amplitude results for both temperature values have an area of greater uncertainty at 6.55mm of discrete blade damage. Upon inspection of the natural frequency versus blade tip displacement plots, it was noticed that tip displacements for the higher temperature tests were consistently higher when compared to the lower temperature tip displacement results. This makes sense, due to the fact that an increase in the temperature of the blade, results in a lower blade stiffness, consequently resulting in a lower natural frequency. The lower blade stiffness makes a blade more susceptible to greater tip displacements or amplitudes of vibrations as it is easier to deform this blade with the same excitation force. These natural frequency versus amplitude plots are associated with the plots shown in Figure 3.29 and may be found in the Appendix, Section B.2.3. The natural frequency results for *Stage VI* of testing is discussed in greater detail in Chapter 5. Figure 3.30 compares the change in natural frequency of the undamaged blade due to an increase in temperature from $41°C$ to $98°C$. The natural frequencies based on the phase are plotted against the natural frequencies based on the amplitude in this figure. This enabled a more accurate indication of the change in natural frequency due to purely temperature effects. The mean natural frequency locations, based on the phase and amplitude natural frequencies for all 100 tests (for each undamaged blade at the different temperatures), were computed and are also shown in this figure. The change in natural frequency between these mean values (based on the two temperatures) were computed as the norm distance in Euclidean space. These distance values or shift in natural frequency due to temperature effects are shown in Table 3.6.

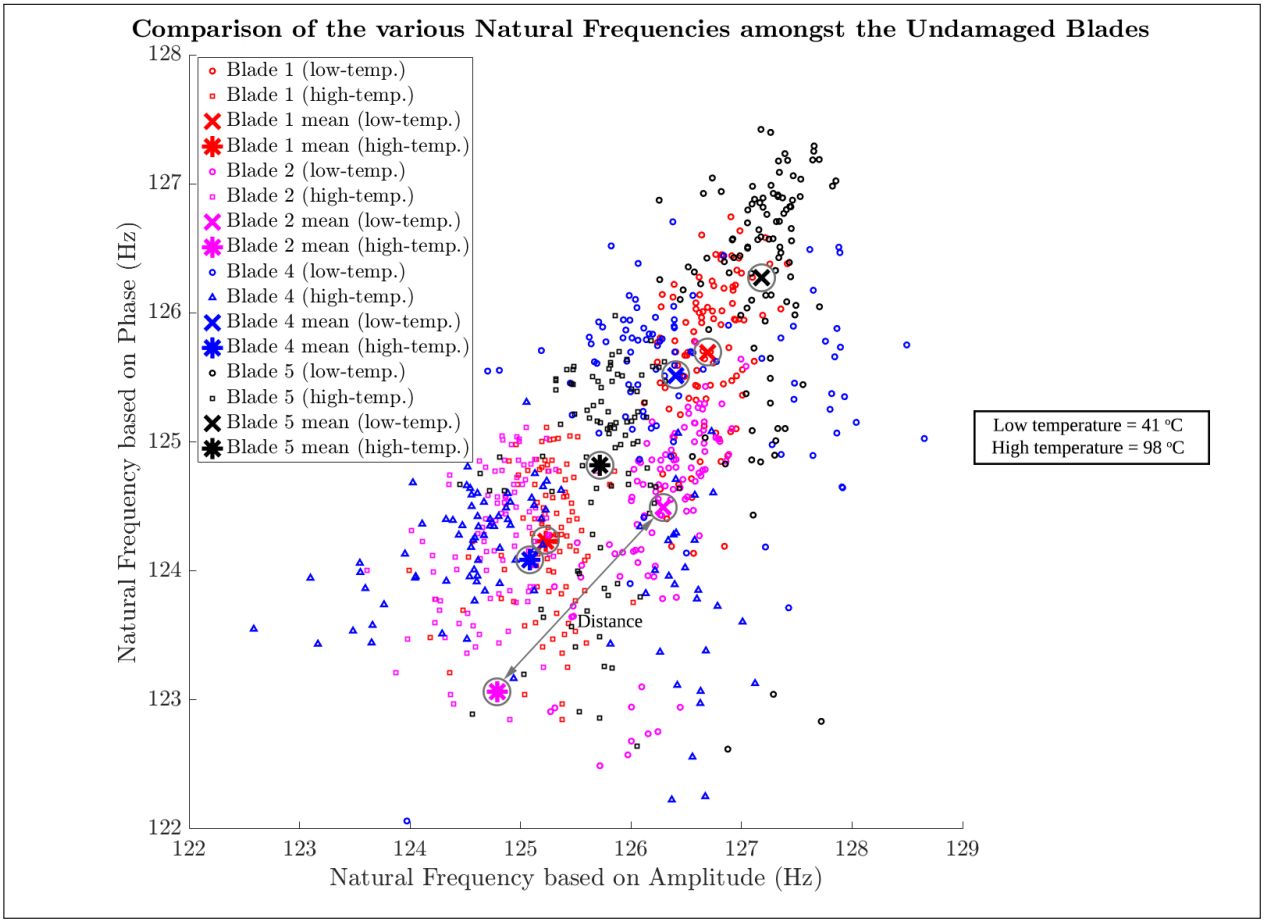

Figure 3.30: Comparison of the change in natural frequencies of the undamaged blades due to a change in temperature for *Stage VI* of testing.

Table 3.6: Change in natural frequency ($\|norm\|$ distance) due to temperature for the undamaged blades in *Stage VI* of testing.

Blade Number	Distance (Hz)
1	2.0710
2	2.0727
4	1.9449
5	2.0629
Mean	**2.0379**

Table 3.6 shows that the associated natural frequency of each blade shifted by approximately 2Hz due to the change in blade temperature from $41°C$ to $98°C$. It is quite interesting and satisfying to note that the various undamaged blade natural frequencies shifted by approximately the same amount. The consistency in this shift of the natural frequencies, to a certain extent, implies that the experimental testing was well controlled and that the employed BTT methodology based on BLR was quite robust. The robustness of this methodology was also maintained amongst the various blades, even though these blades were physically slightly different from one another. This in itself, provides motivation for why the proposed BTT methodology may be an attractive solution for VCM of turbomachines in industry. Chapter 5 further discusses the results from *Stage VI* of testing.

3.6 Summary

The proposed BTT methodology utilising the *Vibrapy* software (based on BLR) is presented in this chapter. This includes the thorough elaboration of the implemented BTT procedure with regards to the experimental testing, important aspects of the BTT signal processing and blade condition monitoring. It is highlighted that the experimental setup consisted of a five-bladed rotor setup, which mimics important aspects of the operation of turbomachines. The shaft operational speed was ramped up and down in a speed range where critical speeds or resonance due to synchronous vibrations occurred. A compressed air supply was further used to excite the blades during rotation, therefore enabling the blade vibrations to be detected using the proposed BTT methodology. With regards to the BTT sensory equipment, a total of four eddy current proximity probes were used for the BTT measurements. The importance of accurate shaft speed measurements (using a *tacho* signal) was also emphasised. The issue of geometric inconsistencies, of specifically a zebra strip shaft encoder, was highlighted and a method developed by Diamond et al. [2016] to overcome these effects was discussed. The remainder of the discussion about the BTT procedure focused on aspects the *Vibrapy* software (BTT processing based on BLR) and how the outputs of this software could be used in an MCS to derive the amplitude and phase as statistical quantities. A feature extraction process was lastly proposed to derive the associated blade natural frequencies from the amplitude and phase values. In doing so, the advantages of using the BLR curve-fitting technique were very clear, especially in terms of establishing confidence intervals around the mean BTT results.

The remainder of the chapter focused on the details of the BTT investigations. The progressive nature of this investigative process was elaborated on. Each stage of testing within an investigative group aimed to build-on the recommendations of the previous stage, therefore allowing more complex investigations to be performed in each stage. The preliminary testing in *Group I* enabled a thorough troubleshooting exercise to be completed before the formal BTT investigations commenced. *Group II* and *III* were very similar in terms of tracking the change in the natural frequency, associated with a specific test blade, due to the introduction of incremental discrete damage to this blade. *Group III*, however, only differed in the sense that it considered varying temperature effects. The preliminary discussion of the formal results seemed positive with regards to the objectives of the research project. Chapter 5 further discusses the formal BTT results and provides further motivation of why the proposed methodology may be a viable solution for its intended application.

Chapter 4

FEM Modal Analysis

4.1 Overview

A Three-dimensional (3D) FEM modal analysis was performed as part of the physics-based approach outlined in Section 2.4. The FEM modal analysis aimed to supplement the BTT (data-driven) results, therefore establishing the basis of a hybrid approach. Chapter 2 describes the proposed hybrid approach as consisting of a BTT analysis (Chapter 3) and an FEA (Chapter 4). Figure 2.1 outlines the details of the various inputs and outputs of the proposed hybrid methodology. Figure 2.1 further gives an overview of how the results of the data-driven and physics-based approaches would be used to determine whether a blade damage threshold has been reached. As a recapitulation, it is important to note that the application of a hybrid approach aims to alleviate the disadvantages of an individual analysis type while conserving its advantages [Liao and Köttig, 2014]. The following points highlight the advantages of the proposed hybrid methodology and gives an overview of what the application of the individual approaches aim to achieve:

1. The FEM modal analysis first and foremost aims to establish a basis for comparison for the BTT results. For practical applications, the FEA may be performed before any BTT tests are conducted. This gives a sense of what may be expected for the BTT results at a particular operational speed. The BTT results may also be used to update the FEA model to more accurately represent the *true* case. It is therefore clear that either result-set may be used to establish an initial reference.

2. Performing an FEA, however, creates the possibility to project expected blade conditions which may not be available for quite some time from the BTT measurements. For example, discrete damage of the desired size may be introduced in the FEA without the need to wait for a crack to propagate to this size due to HCF. Therefore, quick and relatively inexpensive estimations are possible from the use of a FEM modal analysis. The results from an FEA may be used to establish the damage threshold identified in Figure 2.1 (more details regarding the damage threshold is discussed in Chapter 5).

3. The noticeable disadvantage of the FEA is that it is deterministic. The same results are expected for the FEM modal analysis when all the model parameters are unchanged. The BTT analysis, however, accounts for *real* measurements and aspects not considered using the FEA. It may therefore be expected that each BTT analysis would output slightly different results. Slight variations were thus introduced in the FEA model to perform a more stochastic analysis (the details of this stochastic analysis follow in this chapter).

4. Combining the individual approaches as part of a hybrid approach may ultimately result in a higher prediction accuracy. The reason for this is simply related to the fact that two pieces of information are generally better than one [Mishra et al., 2014]. The agreement of the results from two independent analyses may act as supporting evidence, therefore establishing greater confidence in the hybrid prediction when compared to a single prediction.

The remainder of this chapter outlines the details of the FEM modal analysis as part of proposed hybrid approach shown in Figure 2.1. The FEM modal analysis should not be confused with the preliminary FEA performed to determine the likely blade resonances at the particular operational speeds (refer to Section 1.2.5) and preliminary FEA performed to determine the regions on the blade with the highest stress concentration for the first bending mode (refer to Section 3.2.3). The details discussed in this chapter specifically relate to the FEM modal analysis shown in Figure 2.1 for the proposed hybrid approach.

4.2 Background

Incremental discrete blade damage is introduced in the FEA model, corresponding to the blade damage introduced during *Stage IV* of the BTT investigation. Thereafter a FEM modal analysis will be performed to derive the vibrational characteristics of particular blade. As indicated in Figure 2.1, the FEM modal analysis incorporates a stochastic rather than deterministic approach by simulating uncertainty in the model parameters. These model parameters include the material properties (due to temperature and inconsistencies), centrifugal loading and geometry of the discrete blade damage. The slight variation in these model parameters aim to alleviate the disadvantage of FEM whereby an ideal or deterministic case is merely represented (a single result may be expected at a particular damage increment). Incorporating uncertainty in this analysis consequently enables the representation of a range of possible results. Furthermore, the sensitivity of the model to various conditions or changes in parameter values are determined. Lastly, a stochastic FEA enables confidence intervals to be established around the mean of a particular result corresponding to a certain damage increment (similar to what was done for the BTT results). As background to the proposed FEM modal analysis and motivation for the various aspects thereof, the reader is referred to the following literature:

1. Madhavan et al. [2014] performed an FEA similar to what is proposed in this research; on a low-pressure turbine bladed disk model, to estimate the blade natural frequencies and mode shapes in the speed range of operation. In this study, centrifugal loads were accounted for by applying angular velocities to all the elements. Furthermore, thermal loads were accounted for by varying the associated material properties. The temperature dependence of the material properties, for Young's modulus (E) and the density (ρ), is shown in Equations 4.1 and 4.2 respectively. The mathematical relationship for the dependence of the natural frequency on these material properties is shown in Equation 4.3 [Madhavan et al., 2014]. From these equations it is clear that Young's modulus and the density associated with the material decrease as the temperature increases. Consequently, the natural frequency of the blade is related to the combined effects that the temperature has on the material density and associated Young's modulus. Equation 4.3 shows this relationship.

$$E \propto \frac{1}{T} \tag{4.1}$$

$$\rho \propto \frac{1}{T} \tag{4.2}$$

$$f_n \propto \sqrt{\frac{E}{\rho}} \tag{4.3}$$

   The study presented by Madhavan et al. [2014], however, does not use the modal analysis results from the FEA to supplement the BTT results. The reason stated by Madhavan et al. [2014] is that the severity of blade resonance is almost impossible to predict from the FEA results, as it is affected by damping, the strength of the excitation source and blade mistuning effects. It is therefore suggested that the experimental evaluation of the operational vibratory characteristics of rotating blades is a crucial process to assess the criticality of these resonances.

2. The use of a commercial Blade Vibration Monitoring System (BVMS) on the final stage of the low-pressure steam turbine is shown in EPRI [2012]. This report mentions that BTT methods employed by commercial BVMSs offer a viable approach for managing risks associated with turbine blade vibrations. Importantly, it is noted that, although the use of BVMS offers a continuous monitoring capability of the blades, many of the effects of the blade vibration risks may only be noticed over long-term monitoring periods. It is therefore suggested that the blade modelling, crucial for the interpretation of the BVMS results (or similarly BTT results), needs to be performed using an FEA tool. This report therefore supports the concept of using the FEA results to project expected conditions in the blade, thus offering a viable means to supplement the BTT results.

3. Brits [2016] constructed and simulated a physics-based model of a turbomachinery blade in order to predict its associated fatigue crack life. Importantly, this was done by modelling uncertainties and varying the Paris Law material constants in the lifetime estimation. This research further incorporates a two-pronged approach as summarised below:

   (a) The first approach consists of an experimental setup designed to initiate and propagate a crack on an axial fan blade (this blade approximately represents the geometry of a turbomachine blade). The experimental procedure then utilises a base excitation applied to the test specimens to stimulate crack growth during resonance conditions. This process was measured with digital image correlation equipment. The relevant data was extracted from the aforementioned experimental procedure and used in post-processing of the fatigue crack life estimation.

   (b) The second approach consists of a physics-based model consisting of an FEA performed in the *MSC Marc Mentat* commercial software environment. This simulation was specifically used to estimate the fatigue crack life of the test blades. For this simulation a faceted surface was used to initiate a crack on a section of the blade. A 3D Virtual Crack Closure Technique (VCCT) was used to model the crack propagation and material fracture properties are applied to the crack. This simulation process relied on adaptive remeshing for each increment of the crack propagation due to fatigue blade damage. The FEA employed by Brits [2016] aimed to simulate the *natural* crack growth due to HCF, therefore allowing the RUL of the blade to be estimated. Importantly, uncertainties are modelled and variations in the material properties are accounted for. These uncertainties and material property variations in the input parameters were accounted for in an MCS, therefore ensuring that the reliability of predicted blade life was quantified.

The aforementioned references to the literature highlight important aspects related to the use of an FEA for the intended problem. This firstly includes, using an FEA in the preliminary stages of a BTT analysis to determine the likely blade resonances at the desired operational speeds. This secondly highlights that a FEM modal analysis could be performed to project expected blade conditions, therefore offering a viable possibility to supplement the BTT results as it becomes available. Lastly, the possibility of performing a more stochastic rather than deterministic FEA was discussed. It was attempted to implement all these aspects in the proposed FEA for this particular investigation. The details of this implementation follow in the remaining sections of this chapter.

4.3 Analysis principles

This section gives a brief overview of the main analysis principles incorporated in the proposed FEA. For the purposes of this research, the FEM modal analysis aims to establish a reference of expected natural frequencies. This was done for the specific operating conditions outlined in the BTT experimental investigation, specifically corresponding to *Group II* (Section 3.5.2). The commercial software, *MSC Marc Mentat 2016*, was used to perform the FEA. The *Lanczos* modal solution method was used to compute the desired natural frequencies of the simplified blade model in this commercial software. Figure 2.1 highlights that a stochastic rather than deterministic FEM modal analysis was performed to model uncertainty related to various aspects of the investigation. The discrete damage modelled in the FEA was also introduced in twelve incremental stages, which correspond to the damage of the experimental test blade for *Stage IV* of testing (Section 3.5.2). The discrete crack sizes and locations were in essence replicas of what was introduced experimentally for the various increments shown in Table 3.4. However, slight variations in the angle of the discrete cracks and the size (length, width and height) were introduced to the various increments. This was done to account for small inaccuracies of the *true* crack measurements. Furthermore, the slight variations aimed to account for uncertainties that would be present if the location of the blade damage is assumed.

The damage was only introduced to the location shown in Figure 3.6a as it was shown that this is where a *natural* crack would most likely form due to HCF. The study by Brits [2016] modelled a more *natural* crack growth due to HCF also using the *MSC Marc Mentat* commercial software. The modelling of a *natural* crack growth using the relevant crack propagation method is therefore certainly a possibility in this commercial FEM software environment. This was however not done for this particular research project, due to the fact that the FEA aimed to supplement the BTT results. For this reason, the FEA intended to replicate what was done experimentally in terms of the operating conditions and the discrete damage introduced to the test blade. Discrete blade damage was introduced on the experimental blade, as opposed to more *natural* damage as a result of HCF, due to the fact that a viable accelerated crack propagation mechanism was not found for the experimental testing. It was considered to remove the test blade and to place this blade on the shaker with a base excitation, similar to what Brits [2016] did experimentally. However, this was also not done on account of the fact that propagating a crack on a shaker would not be a true representation of the operating conditions for this investigation. The blade tip displacements would be difficult to replicate and at very low tip displacements the crack propagation would be a tedious process. It would also be difficult to control the rate of the crack growth to what was desired. Furthermore, the purpose of this research is to test the performance of the proposed hybrid approach in identifying and classifying blade damage. Thus, the introduction of relatively small incremental discrete blade damage was deemed the most feasible approach in doing so.

The recommendations from *Stage II* (Section 3.5.1) of testing suggest that another important aspect to consider in the FEA is blade stiffening. Blade stiffening was accounted for by applying a centrifugal load to the model (the details of this will be discussed in Section 4.4). The reference material properties corresponded to what was reported by the manufacturers of the blades for *Aluminium 6082 T6* at room temperature. Again, slight variations in the material properties and centrifugal load were introduced to the model in order to account for uncertainty. The details of all these aspects and relevant analysis principles incorporated in the FEM modal analysis follows in the next section, Section 4.4.

4.4 Modelling

This section describes the main components of the FEA modelling, namely: the geometry, mesh, material properties and applied boundary conditions. Figure 4.1 gives an overview of how the five-bladed rotor experimental setup was simplified in the FEM environment. The detailed model definition and FEA formulation follows.

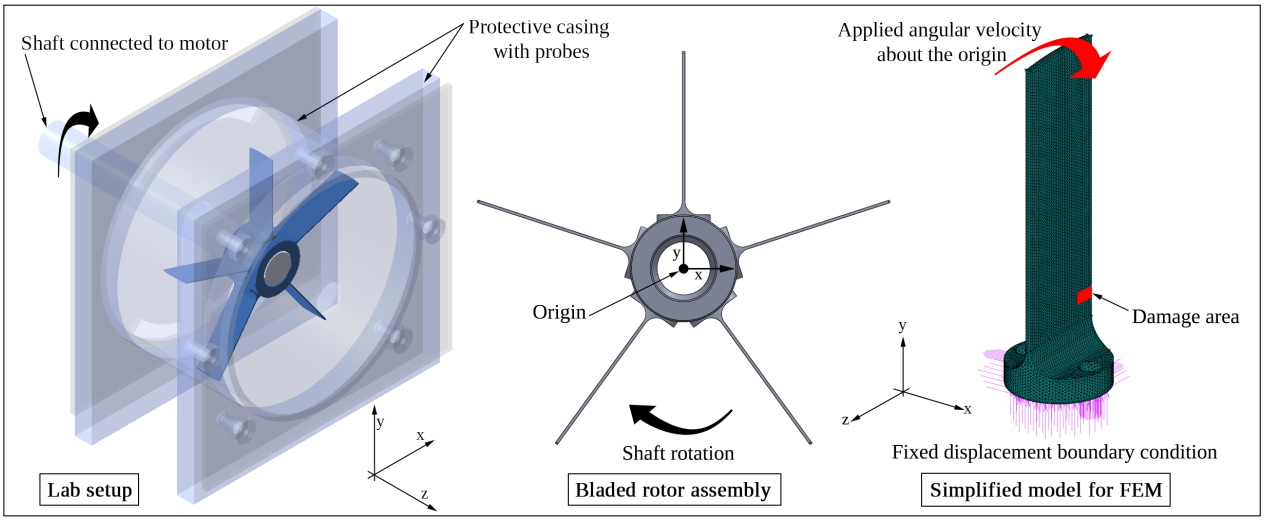

Figure 4.1: Overview of the simplified FEA model.

The FEA model shown in Figure 4.1 aims to represent the actual test blade as accurately as possible while also being relatively computationally inexpensive to solve (refer to Section 6.3 for recommendations). For this reason a few iterations of the simplification process shown in Figure 4.1 were performed; each iteration aimed to improve the accuracy of the FEM modal analysis. The aforementioned modelling process intended to maintain the requirements outlined by Rao and Dutta [2012] for a CBM technique to appeal to industry. The FEA therefore aims to effectively model aspects of the BTT analysis, while remaining as simple and accurate as possible.

Geometry and Mesh

Only a single blade was considered for the solid 3D FEA. The generated mesh consisted of at least 89885 elements for the most basic geometry (undamaged blade) and local mesh refinement was applied around the discrete crack for the damaged blades. Ten-noded tetrahedral elements (type 127) were used for all the analyses. The selected mesh and element types resulted after a thorough set of mesh convergence tests. This involved incrementally adjusting the coarseness of the mesh for specific element types and comparing the total computational times for convergence to expected blade vibrational characteristics. The discrete crack was introduced in the damage area shown in Figure 4.1, where the first increment corresponds to the healthy blade and the twelfth increment to the most severe damage. These discrete damage increments correspond to the values shown in Table 3.4 and the FEA results were grouped according to these increments. The reference discrete cracks were introduced to the blade as parallel to the z-axis (perfectly horizontal). For all the damage increment groups, the angle of the applied crack was varied by approximately 10° and the sizes of the cracks around 12% in order to model uncertainties or inaccuracies in measurements. Samples of these parameters were randomly selected from a uniform distribution within this 12% variation range (refer to Section 6.3 for more detail and further recommendations about these variations). For consistency, the same variations were applied for each successive damage increment of the FEA.

Material

The reference material properties for Aluminium 6082 T6 are shown in Table 4.1. The temperature in the laboratory where the experiments were conducted was monitored. It was reported that a more or less consistent ambient temperature (room temperature) was maintained due to the use of air-conditioning. Uncertainty was incorporated into the FEA by varying the material properties within 12% of the reference values. Ultimately, a number of analyses were conducted for each damage increment, therefore resulting in a stochastic rather than deterministic modal analysis.

Table 4.1: Aluminium 6082 T6 material properties at room temperature.

Temperature $T\ (°C)$	**Density** $\rho\ (\frac{kg}{m^3})$	**Elastic modulus** $E\ (GPa)$	**Poisson's ratio** ν
22	2710	71	0.33

Boundary Conditions

The applied boundary conditions were representative of the blade attachment to the hub. Structural fixed displacements were therefore applied at the contact points. Furthermore, the blade stiffening was accounted for by applying a structural centrifugal load to the model. This was done by applying an angular velocity to all the elements. The angular velocities were varied according to the shaft speed range shown in Figure 3.13 for all the blade damage increments. The reference axis for the centrifugal load corresponds to the origin depicted in Figure 4.1.

The FEA was implemented in such a way that it was possible to conduct an investigation similar to what was done during *Stage IV* of the BTT testing. Each damage increment in the FEM modal analysis also consisted of six independent tests. For each of these tests, the model parameters (discrete crack geometry, material properties, centrifugal load) were varied according to what was presented in Section 4.4. The variation of these model parameters resulted in a variation of the natural frequencies obtained for each test within a particular damage increment group. This further enabled a mean, with associated confidence intervals around the mean, of the natural frequencies to be found for each damage increment. Advantageously, this process enabled the uncertainties of the various parameters in the FEA model to be quantified, therefore being more representative of what may be expected from the BTT analysis. The remaining sections in this chapter give an overview of the results from the FEM modal analysis.

4.5 Post-processing

The natural frequencies and mode shapes of the first three modes were computed. Figure 4.2 gives an example of the contour band plots of these modes for the undamaged and most severely damaged blades using the reference model properties. Modes 1 and 3 clearly correspond to a bending mode shape. Mode 2 corresponds to a torsional mode shape. The changes in natural frequencies between these damage increment extremes are approximately 4Hz, 19.9Hz and 9.2Hz for modes 1, 2 and 3 respectively. All the undamaged blades have a symmetrical displacement contour band pattern. However, for the most severely introduced damage, only mode 1 shows contour band patterns which remain fairly symmetrical. Mode 3 shows a completely different contour band pattern, with the maximum displacement changing from the centre of the blade to the upper-left tip. The blade exhibits increased *twist* as the discrete damage is increased on a single side. However, for the purposes of this investigation only mode 1 was considered. This corresponds to what is suggested in Section 1.2.5 in terms of which mode would have the greatest contribution to fatigue blade damage.

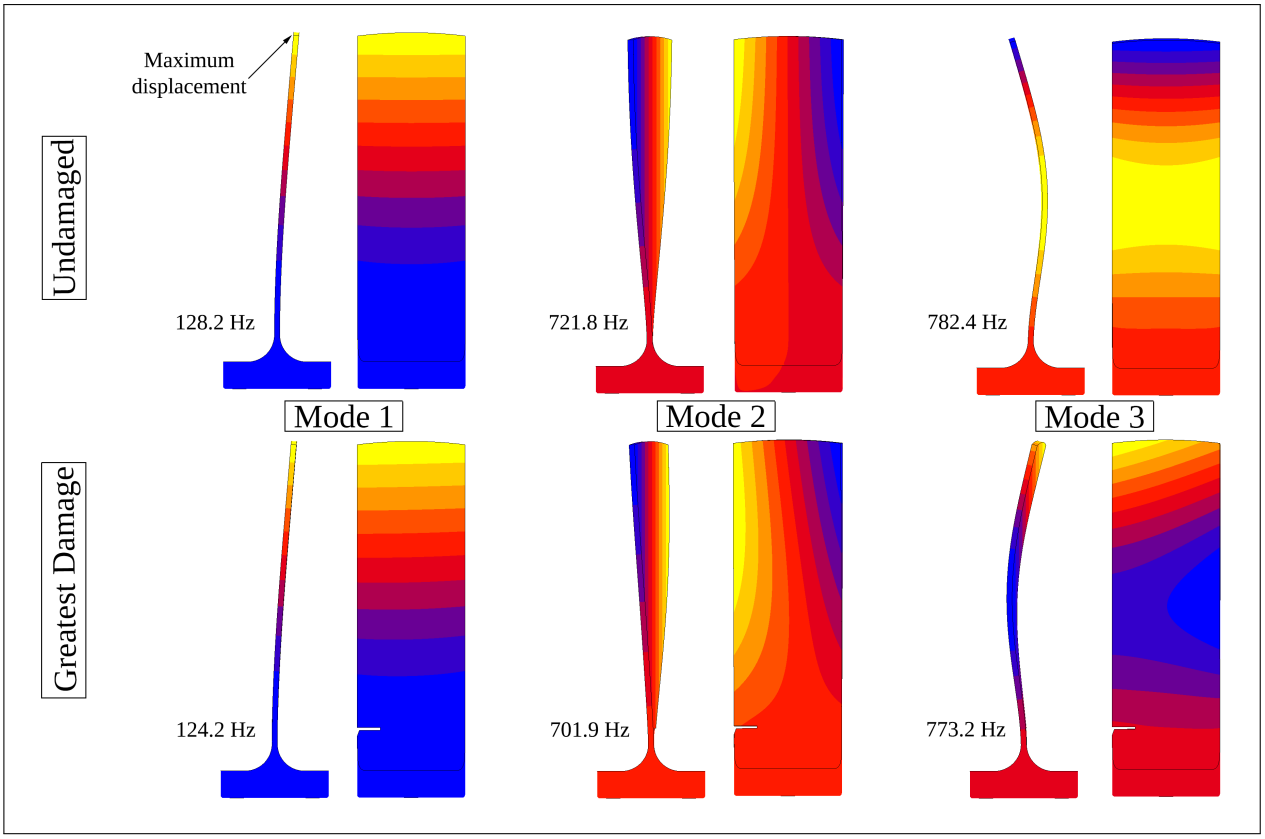

Figure 4.2: Mode shapes indicating the displacement contour bands.

4.6 Results

Figure 4.3 shows a plot of the natural frequency versus discrete crack size for the FEM modal analysis results. The natural frequency of the test blade clearly decreases monotonically as the discrete crack size increases. The FEM results are therefore in agreement with the BTT natural frequency results derived from the amplitude results for *Stage IV)*. Also shown in Figure 4.3 are the confidence intervals of the natural frequencies around the mean corresponding to a particular damage increment. The individual data-points, from each damage increment, are also plotted to gauge the sensitivity of the natural frequency of the blade to the variations in the model parameters. The following observations are made from Figure 4.3 for the various discrete damage increments:

1. For the undamaged blade (the first discrete damage increment), the material properties and boundary conditions (centrifugal loading) were varied according to what was outlined in Section 4.4. This resulted in quite a wide confidence interval, therefore implying that the natural frequency of the test blade is sensitive to the variation of these model parameters, specifically Young's modulus.

2. The next discrete damage region (from slightly under 1mm, to slightly under 2mm of damage) shown in Figure 4.3 resulted in quite a consistent change in the mean natural frequency. More so, this region illustrated a similar change for the individual data-points amongst the various discrete damage increments. The decrease in the natural frequency is also noticeably linear in this region. During the post-processing of these results it was noted that the displacement contour bands (Figure 4.2 for example) were all more or less symmetrical. The blade *twist* in this discrete damage region was therefore negligible.

3. The remaining discrete damage increments (from slightly over 3mm, to slightly under 9mm of damage) resulted in an increasing scatter of the individual data-points. This subsequently contributed to greater uncertainty as indicated by slightly wider confidence intervals. Furthermore, a somewhat non-linear decrease in the mean natural frequency is shown for an increase in the discrete crack size. During the post-processing of these results it was noted that the displacement contour bands (Figure 4.2 for example) were considerably asymmetrical. The blade *twist* in this discrete damage region was noticeable which may have been the cause of the slightly non-linear decrease in the mean blade natural frequencies.

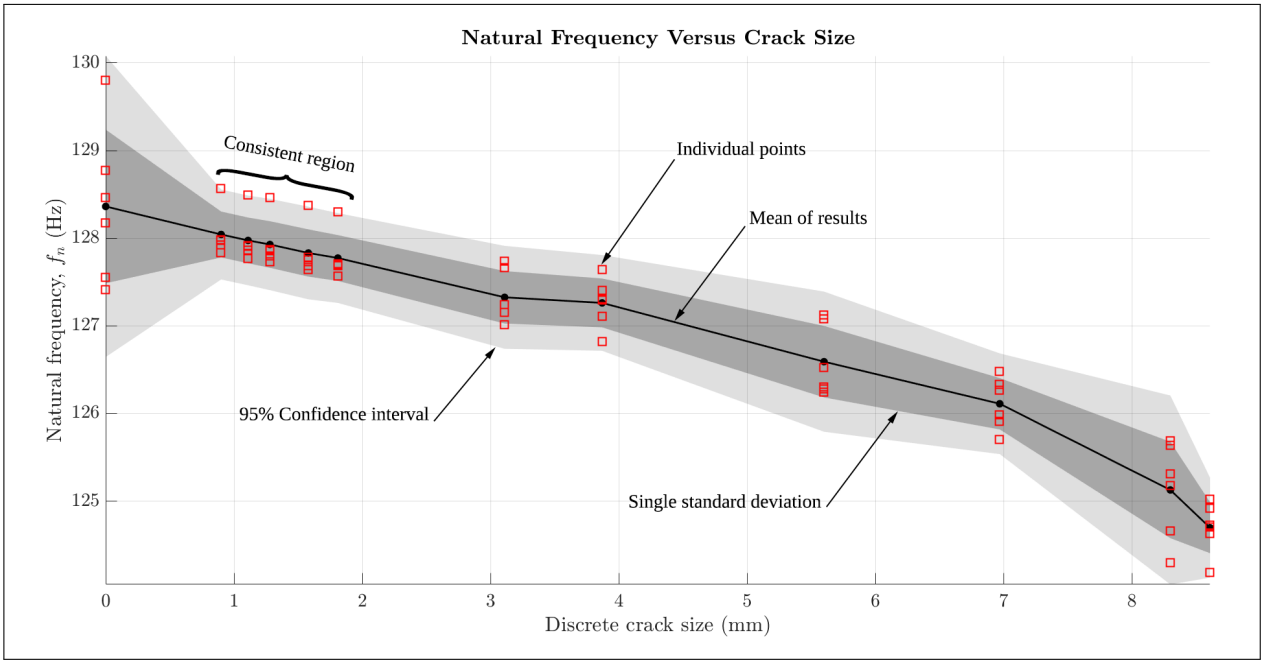

Figure 4.3: Natural frequency versus discrete crack size for the FEM modal analysis results.

Chapter 5 gives a more detailed comparison and discussion of the BTT and FEM results. Chapter 5 further presents how these results may be used to identify and classify the discrete blade damage, therefore indicating whether or not a damage threshold has been reached.

4.7 Summary

The FEM modal analysis aimed to account for the physics in the proposed hybrid approach shown in Figure 2.1. Furthermore, the use of an FEA aimed to project expected blade conditions, therefore allowing the BTT results to be compared as it becomes available. In essence, the BTT investigation accounts for the *real* measurements and the FEM modal analysis accounts for *simulated* conditions. It was noted, and emphasised that a major disadvantage of an FEA is that it is rather deterministic; for each set of model parameters used in a simulation a single outcome will result. Inevitably, considerable uncertainty exists for the various model parameters. For example, the exact material properties of the blades and the exact location or geometry of the blade damage may be unknown. For this reason, it was decided to perform a stochastic rather than deterministic FEA by accounting for the uncertainty in these model parameters. The output of the FEM modal analysis was therefore similar to what was seen for the BTT approach incorporating BLR. Hence, confidence intervals could be established around the mean FEM modal analysis results, therefore quantifying the uncertainty associated with a particular damage increment.

It is important to recapitulate that the FEM modal analysis was also performed for discrete damage increments that corresponded to what was done for *Stage IV* of the BTT investigation. This was done to establish a basis of comparison for the two result-sets, thus allowing the hybrid approach to be tested. A preliminary FEA was also performed to determine the likely operational speeds that would result in blade resonance. Another preliminary FEA enabled the regions of the highest stress concentration to be localised on the test blades during the first bending mode. The discrete blade damage was introduced on a single side of the blade with the highest stress concentration, purely due to the high likelihood that HCF damage would result in this region. These preliminary simulations were completely independent of the FEM investigation discussed in this chapter. However, these preliminary investigations were important for a number of reasons. The main reason being that it was essential to simulate realistic or expected conditions resulting from the operation of turbomachines, This emphasised the need for thorough preliminary checks. For this implementation of the hybrid approach shown in Figure 2.1, the FEM modal analysis was performed after the BTT investigation. For practical applications, this would typically be done the other way around. For this scenario much more emphasis would then be placed on the FEM modal analysis to simulate expected conditions. However, the purpose of this research project was to propose and demonstrate the implementation of a hybrid approach to identify and classify turbomachine blade damage. Discrete blade damage was introduced to a test blade and various investigations commenced to test the performance of the proposed hybrid approach.

It was mentioned in this chapter that it is possible to simulate a more *natural* crack propagation in the commercial *MSC Marc Mentat* FEM software. However, this was not done, due to the difficulty associated with propagating a crack experimentally in the rotor setup for a particular blade. This point is certainly noted for future work or recommendations of what may be tested in the next phases of the research. The FEA results presented in Sections 4.5 and 4.6 are informative, in the sense that the natural frequencies are associated with a corresponding mode shape. It is valuable to physically see the deformation of the blade associated with a particular mode shape. Larger discrete blade damage result in slight *twist* of the test blade for the first bending mode. This increasing *twist* is regarded as the possible cause of the less linear change in the natural frequency at larger discrete crack sizes. It may, however, be concluded that the FEM modal analysis achieved its desired purposes; it is relatively simple to implement, relatively efficient in its execution and it demonstrates the ability to project expected blade conditions.

Chapter 5

Results

5.1 Overview

This chapter presents the results obtained for the BTT and FEA methodologies. More importantly, the comparison of the results in terms of the hybrid approach shown in Figure 2.1 is discussed. Ultimately, the goal is to determine whether the practical BTT results are indicative of a damage threshold being reached. Figure 2.1 indicates that both damage identification (relative natural frequency tracking) and damage classification (clustering) will be employed to determine whether this threshold has been reached. The detailed discussion of these two approaches follows in this section. The following points summarise important aspects of the various investigations performed:

- Small incremental discrete cracks were physically introduced to a test blade during the BTT testing and FEM modal analysis. Discrete damage was introduced to the test blade, as opposed to more *naturally* propagated cracks, due to the difficulty associated with initiation and propagating this sort of crack during experimentation. It is possible to propagate cracks using a 3D VCCT technique in the commercial *MSC Marc Mentat* FEM software, as was done by Brits [2016] to determine the RUL of test blade. However, it was intended to replicate what was done experimentally in the FEM environment and the most effective way to do this was by introducing discrete blade damage. As mentioned in Section 4.7, it is recommended for future iterations of this research project to incorporate a more *natural* crack growth mechanism during the operation of the experimental setup.
- The changes in size of these discrete cracks were not constant for the various incremental steps used in the BTT analyses. It was, however, decided that a random change in the discrete crack size would be more indicative of what would happen in practice. The cracks corresponding to *Stage IV* of the BTT investigation were measured for each incremental step and these measurements were subsequently replicated in the geometry for the FEM modal analysis. Slight variations in the geometry of the discrete crack were introduced during the FEA. This was done to move away from a traditionally deterministic FEA and to rather model uncertainty in a range of model parameters. As a result, the analyses were more stochastic and enabled the uncertainty to be quantified for the proposed hybrid implementation.
- The BTT tests were performed a number of times at each discrete damage increment. For *Stage IV* of testing, the sensitivity of the BLR BTT technique to the sampling frequency was determined by using the *OROS* DAQ (65.536 kHz) for half of the tests in the particular damage increment and the other half using the *Genesis* DAQ (1 MHz). There was no noticeable improvement in using the higher sampling frequency DAQ within the set of operational conditions utilised during the BTT investigation. For this reason, the remaining BTT tests used the *OROS* DAQ. It is, nevertheless, recommended that the sensitivity of the proposed BTT methodology to the sampling frequency is tested for a specific implementation.
- Feature extraction, based on the amplitude and phase features, was performed on the processed BTT measurements to determine the blade natural frequencies. An advantage of the BTT approach incorporating BLR (*Vibrapy* software) is that it facilitates a stochastic analysis. This enabled a MCS to be used to further determine the amplitude and phase associated with the vibration of the blade. The natural frequencies derived from the FEA were also recorded (also corresponding to the first bending mode and a particular discrete damage increment). These two data-sets form the basis of the data-driven and physics-based approaches in the proposed hybrid approach.

This chapter further elaborates on how the results from the proposed hybrid approach are used to determine whether a blade damage threshold is reached. As outlined in Figure 1.9, relative natural frequency tracking (*damage identification*) and clustering (*damage classification*) is proposed to give evidence with regards to whether this damage threshold is reached. This chapter presents the results from the proposed hybrid approach and discusses these two approaches in detail. The details specifically *Stage IV* (*Group II*) and the temperature effect results from *Stage VI* (*Group III*) of the BTT investigative groups are presented.

5.2 Damage Identification

Section 2.2 mentions that damage identification involves: tracking the relative change in the natural frequency of the blade in order to identify and infer the degree of discrete blade damage. The change in natural frequency from a reference state (in this case an undamaged state) is quantified during the blade damage identification. The aim of the damage identification is to determine whether a blade damage threshold has been reached. Figure 2.1 shows that this decision is made using the outputs of the proposed stochastic hybrid approach and consequently results in a decision of whether a turbomachine outage should be scheduled. The challenge is that the discrete crack sizes of the blades are not known while online BTT measurements are made. It is also impractical to schedule a turbomachine outage and to inspect the individual blades, unless there is sufficient evidence that suggests that a certain blade has reached a critical level of damage; i.e. a *damage threshold*. It is therefore essential to infer the degree of blade damage from the processed BTT results. This section presents the damage identification process by discussing two procedures, namely:

- *Procedure 1* (Section 5.2.1) is purely used to demonstrate the relative natural frequency tracking results of the BTT analysis and FEM modal analysis. In doing so, the ability of the proposed hybrid approach to track small changes in the blade natural frequency, due to the changes in the size of the discrete blade damage, is demonstrated.
- *Procedure 2* (Section 5.2.2) is a sensible approach used to identify and infer the degree of discrete blade damage based on a probabilistic blade damage threshold criterion.

5.2.1 Procedure 1

The relative natural frequency tracking is demonstrated in this section by presenting the results from *Group II* and *Group III* of testing. The results in this section do not demonstrate the proposed damage identification process, but rather demonstrates the ability of the proposed stochastic hybrid approach to track small changes in the natural frequencies of the test blades. The BTT results and FEM modal analysis results are therefore directly compared to one another in this section.

Group II Results

The results presented in this subsection correspond to *Stage IV* of the BTT investigation (discussed in Section 3.5.2). This stage of testing followed directly after the various preliminary BTT investigations where troubleshooting commenced, the performance of the BTT methodology based on BLR was determined and the feasibility of detecting discrete blade damage using the proposed BTT technique was tested. The damage increments shown in Table 3.4 in Section 3.5.2 apply to what was done in both the FEM modal analysis and BTT investigation. The FEA was used to simulate the effect of the cracks imparted experimentally on the blade natural frequency. This correspondence between the FEA and the experiments ensures that the results are directly comparable. This group of testing was conducted in such a way that the damage identification and classification outputs of the proposed hybrid approach (Figure 2.1) could ultimately be tested.

As stated in Section 3.5.2, the relative change in the natural frequency of the test blade (blade 2) was tracked for changes in the size of the discrete blade damage. The remainder of this subsection presents and discusses the results from the relative natural frequency tracking for this particular blade (blade 2). Figure 5.1 shows the change in the natural frequency at the various discrete crack sizes as determined from the amplitude and phase results. This figure also shows a logarithmic scale plot in order to visualise the change in the mean natural frequencies versus discrete crack size slightly differently; indicating where there is a more linear change (based on a logarithmic-scaled domain) in the natural frequency versus discrete crack size and vice versa. The 95% confidence intervals indicate that there is a reasonable amount of uncertainty for the phase results of the healthy blade. In contrast, the greatest uncertainty of the amplitude results occurs close to the greatest damage increment. The mean natural frequencies of the amplitude results decrease monotonically as the crack size increases. The mean of the amplitude results exhibit a decrease in the natural frequency of smaller than 0.2Hz for the smaller damage increments; therefore demonstrating the ability of this stochastic approach to track small changes in the natural frequency while incorporating uncertainty. The phase results, however, show a slight hump in the mean natural frequencies at the smaller damage increments. This hump may be indicative of the greater uncertainty of the phase results for the smaller damage increments.

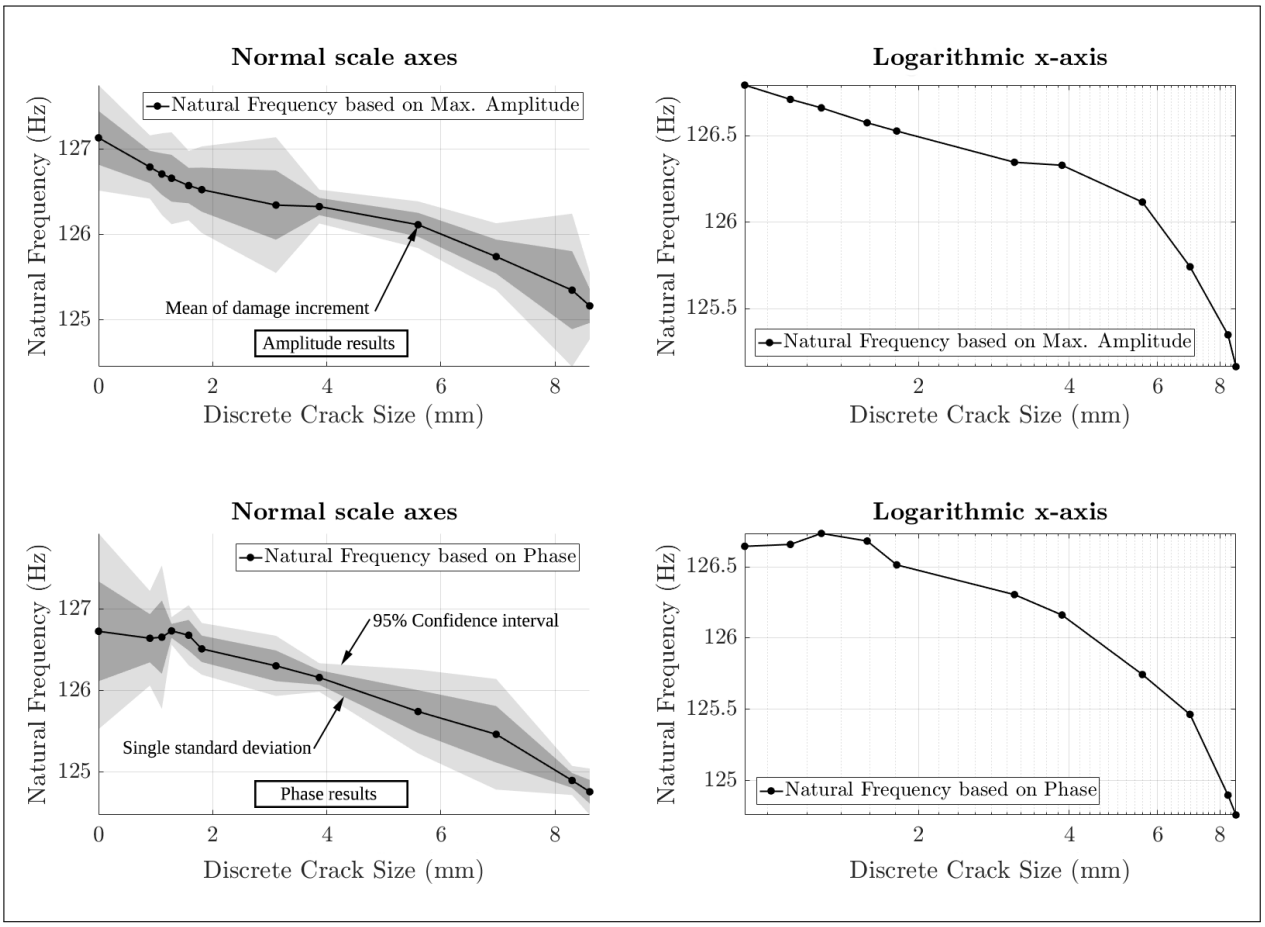

Figure 5.1: BTT natural frequencies derived from the amplitude and phase results.

When comparing the results from the individual measurements (shown in Figure 3.27 in Section 3.5.2) it is unclear whether the *OROS* or *Genesis* DAQ performs better. There is a reasonable amount of scatter in both sets of results and outliers occurred for both DAQs. As previously discussed, it was therefore decided to use the *OROS* DAQ for the remaining tests. However, it was also proposed that the sensitivity of the proposed BTT methodology to the sampling frequency is tested for a specific future implementation. Figure 5.2 compares the natural frequencies determined from the FEA and BTT methodologies.

The relative error between the mean natural frequency results at the various damage increments are also shown. The following is deduced from Figure 5.2:

- The mean BTT natural frequency results derived from amplitude and phase features indicate a maximum relative error between the two approaches of just under 0.4%. In essence, the mean results are a very close match. The confidence intervals around the means of these result sets, nonetheless, vary somewhat. This suggests that these result sets may work well in tandem; i.e. the phase results may give a more confident indication of the natural frequency when there is greater uncertainty for the same set of natural frequencies derived from the amplitude results and vice versa.
- The FEM results similarly (to the BTT natural frequencies derived from the phase results) indicate a greater degree of uncertainty for the natural frequency of the undamaged blade. The confidence intervals remain more or less uniform around the mean results thereafter, as indicated by the dotted-lines around the mean results in Figure 5.2.
- The relative error plots indicate that the FEM and BTT amplitude results are more often or consistently a closer match (with a maximum relative error of approximately 0.95%) when compared to the BTT phase results. The FEM natural frequencies also decrease monotonically, as would be expected for greater blade damage. The BTT phase results perform better for the largest damage increments when compared to the FEM results (indicated by narrower confidence intervals in this region).
- The FEM results give a good projection of what may be expected in terms of the natural frequencies at the various damage increments. The natural frequencies from the FEM modal analysis do, however, decrease more rapidly (as the discrete damage size increases) when compared to the natural frequencies derived from the BTT results. This difference in tempo may be due to a number of reasons. A possible reason may be related to the fact that a simplified FEA model was used (this was intentionally done as a simplistic implementation of the proposed hybrid approach was outlined as a requirement). There may have been a number of aspects that were not adequately modelled in the FEM modal analysis. However, the stochastic nature of the FEA modelled some of the uncertainty present in this analysis.

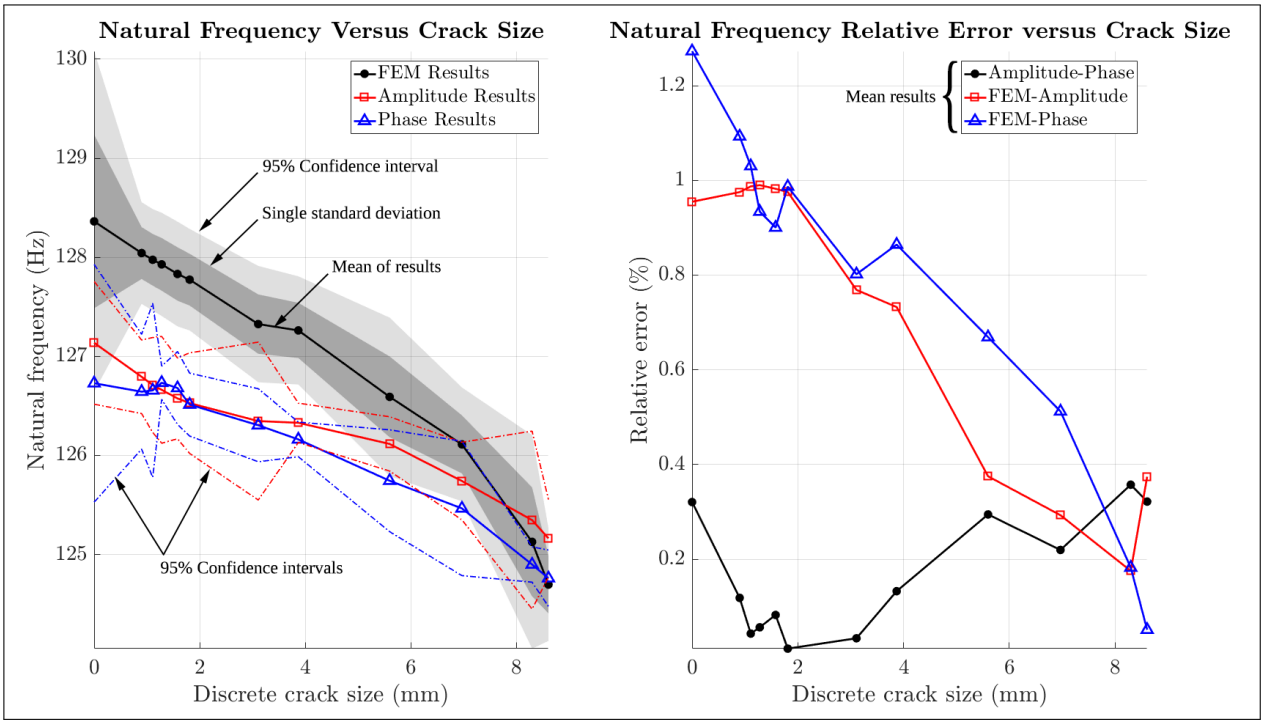

Figure 5.2: Comparison of the natural frequencies at the various discrete damage increments.

It was further decided that it is more sensible to track the change in the natural frequencies for the various result-sets as a relative change, hence the term: *relative natural frequency tracking*. The implementation of the relative natural tracking aimed to give a more general indication of the blade condition, thus enabling a better basis of comparison between the various result-sets. The reference condition for this investigation was the natural frequency of the undamaged blade for the FEM modal analysis results and the BTT results (natural frequencies derived from the amplitude and phase). Figure 5.3 shows the relative change in the natural frequency at the various discrete crack sizes. The relative discrete crack sizes are indicative of the fraction of the total width of the blade that is damaged. The calculation of the relative change in natural frequency (Δf_{n_i}) from the original natural frequency (f_{n_0}) to the current natural frequency (f_{n_i}) is shown in Equation 5.1 below:

$$\Delta f_{n_i} = \frac{f_{n_0} - f_{n_i}}{f_{n_0}} \times 100 \tag{5.1}$$

Figure 5.3 compares this relative change in the natural frequency of the test blade for the various approaches. These relative changes in the natural frequencies are plotted against the relative discrete crack size (the fraction of the width of the blade with discrete damage). It was further decided that fitting a curve through the mean data-points would give a clearer indication of relationship between the relative change in the natural frequency and the relative discrete crack size of the blade. This fitted curve does not intend to generalise the relationship of the change in the natural frequency versus the relative discrete crack size, but is rather used to simplify the hybrid approach, in accordance with the requirements of simplicity mentioned previously. A number of different polynomials were tested in order to find the best fit without resulting in over-fitting. Fitting a quadratic curve to mean data-points resulted in a lower Root-Mean-Square Error (RMSE) compared to a linear fit and fitting a cubic polynomial resulted in slight over-fitting. The quadratic polynomial was then selected and fitted through the mean data-points. However, up to approximately 5% relative change in discrete crack size, the mean natural frequency appears to decrease almost linearly as the discrete damage increases. Figure 5.3 shows that the relative FEM and BTT amplitude results are a close match up to this point. The fitted curve for the phase results follows a similar path to that of the FEM results, but exhibits a slight offset.

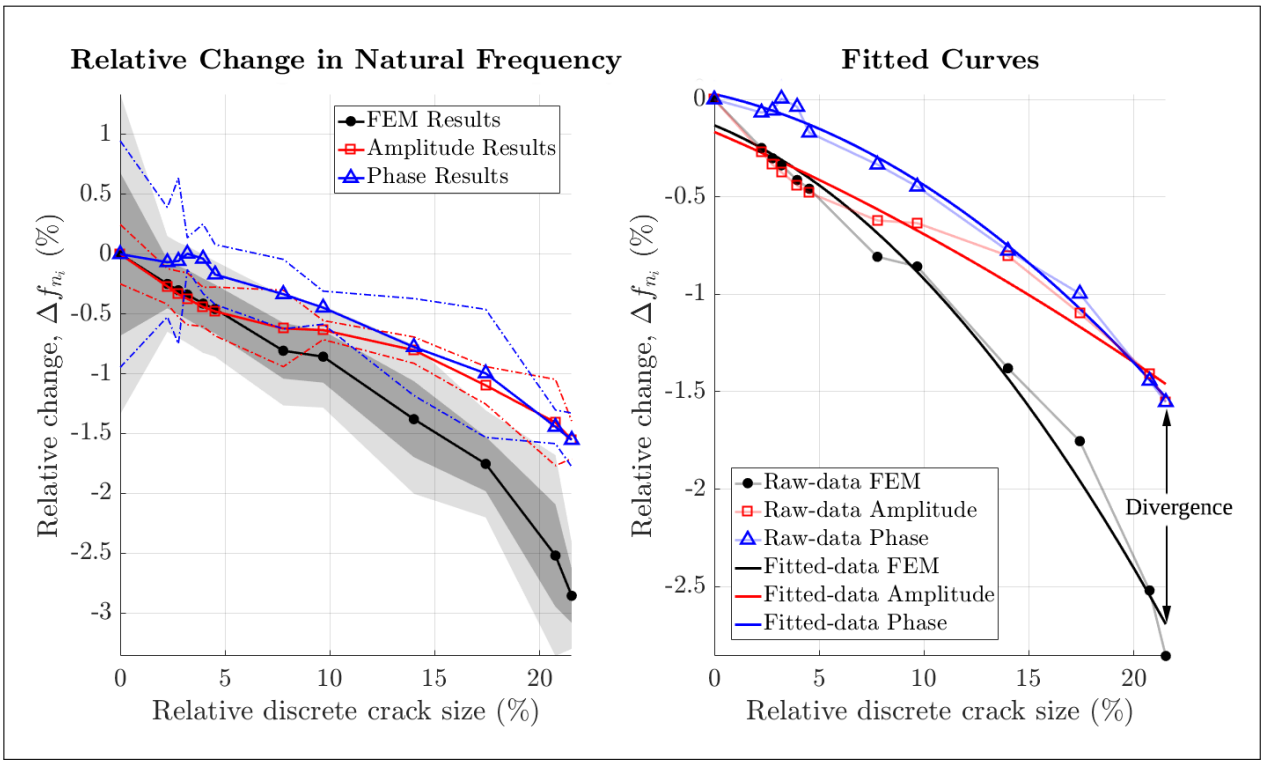

Figure 5.3: Relative natural frequency tracking results for the test blade (blade 2).

Figure 5.3, however, shows that beyond approximately 5% relative change in discrete crack size the mean BTT results start to diverge from the mean FEM results. Furthermore, at the largest damage increments for this investigation, the 95% confidence intervals of the BTT results no longer intersect the corresponding confidence intervals of the FEM results. This divergence needs to be accounted for in the damage identification process. This may possibly be done by being more conservative during the damage identification process; i.e. being more conservative when deciding whether a blade damage threshold has been reached. Another possibility is to perform model updating in the FEM modal analysis. However, this would require an inspection of the actual turbomachine blades to incorporate more complex aspects in the FEM modal analysis. More suggestions are presented in Section 5.2.2 alongside the demonstration of the damage identification process.

Section 3.4.2 discusses the possibility of combining the BTT mean amplitude and phase signals at the respective frequencies. This differs to the preceding relative natural frequency tracking results in the sense that; once the complete range of amplitude and phase signals were combined or averaged, only then the associated natural frequencies were extracted using the features outlined in Section 3.4.2. Figure 5.4 shows these combined mean amplitude and phase signals for the six corresponding tests at each damage increment. The features (represented by Equations 3.9 and 3.10) were extracted from the combined results and the associated natural frequencies, as shown in Figure 5.4, were found. The trace of the natural frequency indicates a decrease in the derived natural frequencies as the discrete damage increases. The derived natural frequency values using this approach tend to be slightly higher than the preceding approach where the natural frequencies were independently calculated. It was however noted that the natural frequencies using this combined approach was a closer match to the FEM results. This approach demonstrates the capabilities of using periodic BTT measurements to construct an *archive* of BTT data over time. This would enable relative changes in the vibrational states of the blades to be tracked after similar signals are grouped together. For example, if a number of successive BTT measurements do not indicate a noticeable change in the derived natural frequencies, then these measurements may be grouped together and combined in this *archiving* scheme. Evidently, the amplitude and phase signals need to match more or less, as was shown for the various discrete damage increments in Figure 3.25 (Section 3.5.2). The combined results shown in Figure 5.4 merely demonstrates the further potential of the BTT technique incorporating BLR. It is a major advantage of this BTT technique that the possibility exists to plot the entire range of amplitude and phase results over the local resonance domain; with the further possibility of establishing confidence intervals around the means of these results.

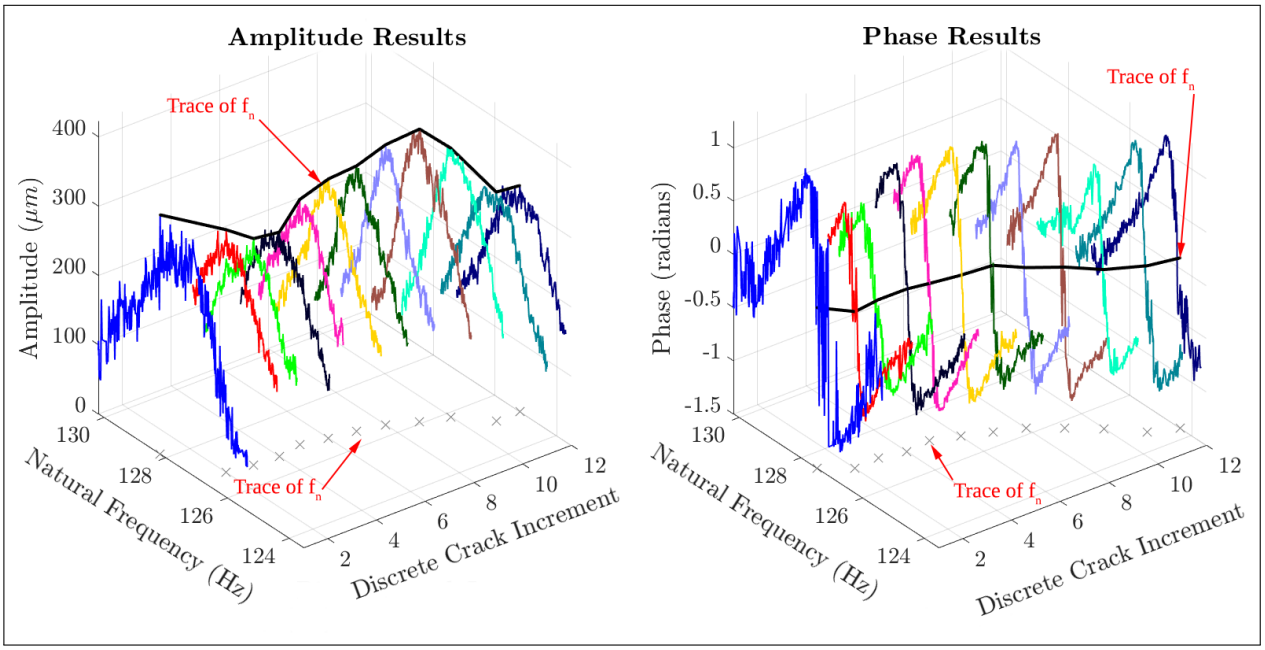

Figure 5.4: Demonstration of the archiving scheme for all the damage increments.

The results from both the relative natural tracking approaches indicate that very small changes in the natural frequency may be tracked. In some instances, relative changes of less than 0.2Hz were reported for the test blade due to small changes in the discrete damage size. The FEM modal analysis results provided a basis of comparison for the small relative changes in the natural frequency associated with a particular damage increment. This suggests that the proposed hybrid approach incorporating relative natural frequency tracking may be utilised for relatively small damage identification.

Group III Results

The results presented in this subsection correspond to *Stage VI* of the BTT investigation (Section 3.5.3). This stage of testing built-on the investigation from *Stage IV* by also considering the effects of varying temperature and how this affects the performance of the proposed hybrid methodology shown in Figure 2.1. The results from *Stage VI* (*Group III*) are representative of BTT tests performed at $41°C$ and $98°C$, as opposed to the ambient temperature used for *Stage IV* of testing.

Figure 5.5 compares the natural frequencies at the various discrete crack sizes of the BTT results (at the two temperatures) to the FEM modal analysis results. The FEM modal analysis results in this plot are the same results as used for *Group II*. The reason for the same FEA results being used corresponds to its objectives in the hybrid approach; specifically with regards to projecting expected conditions while remaining as general and non-case specific as possible. Figure 5.5 shows that quite a substantial difference exists between the BTT derived natural frequencies and FEA natural frequencies. This difference is larger than what is seen in Figure 5.2 for the BTT *Group II* results at ambient temperature. This was however expected, due to the *Group III* results being indicative of a substantially higher blade surface temperature. In Figure 5.5 a noticeable difference exists between the BTT natural frequency results at $41°C$ and $98°C$ respectively. The natural frequencies derived from the amplitude and phase of the BTT results for the $98°C$ surface temperature are almost consistently 1.2Hz to 1.5Hz lower than the corresponding values for a surface temperature of $41°C$.

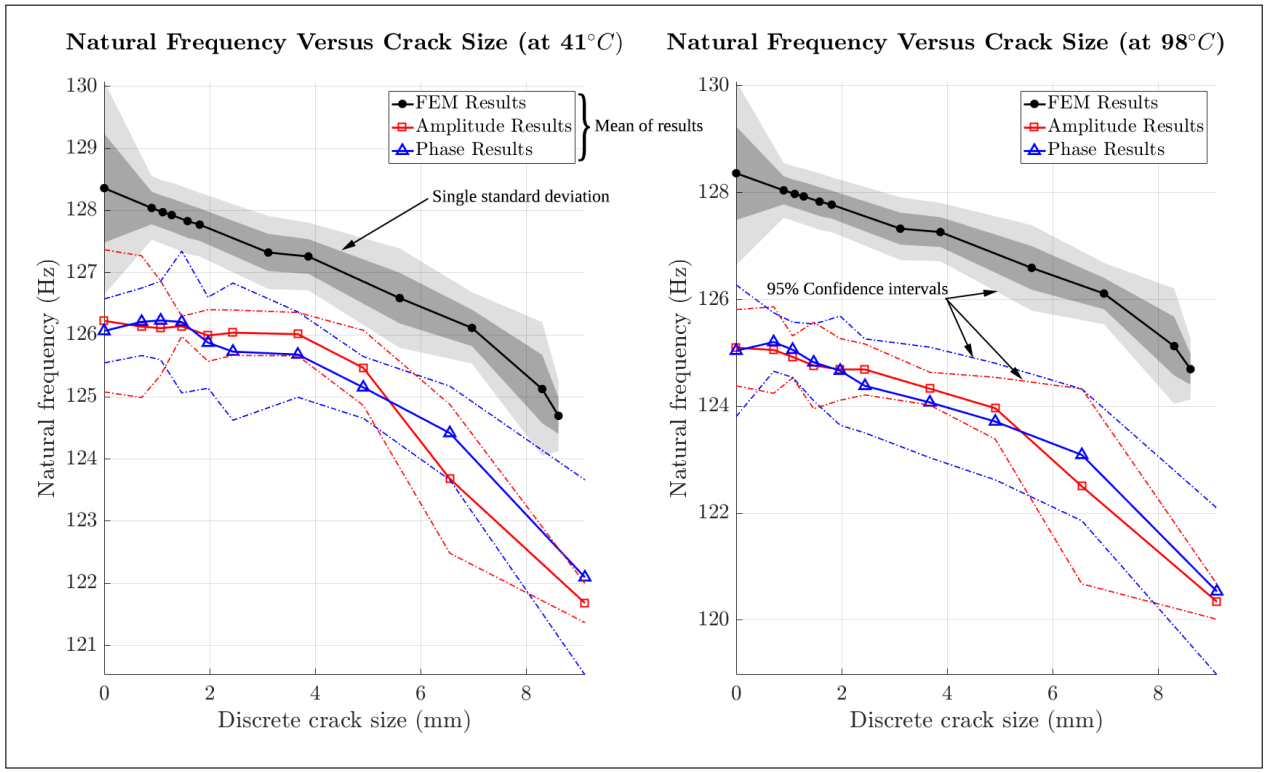

Figure 5.5: Change in the natural frequency versus discrete crack size for the test blade (blade 3) at various temperatures.

It is interesting to note that the shift in the natural frequencies between these temperatures for the damaged blade (*blade 3*) was lower than the mean of about 2Hz recorded in Table 3.6 (Section 3.5.3) for the undamaged blades. The reason for this difference may be due to the fact that each damage increment in Figure 5.5 consists of a total of 10 tests and the data of the undamaged blades comprises a total of 200 tests, thus resulting in a more accurate mean value. However, it is anticipated that this is not the case, due to the mean natural frequencies at each damage increment being consistently lower by approximately the same amount for these two temperatures. The difference may therefore possibly be due to the combined effects of the temperature and introduction of discrete blade damage. It was, however, always intended to track the natural frequencies as relative quantities, thus making the *specific* natural frequency values in the tracking process null and void. Equation 5.1 is used to calculate these relative changes in the natural frequencies and the relative discrete crack sizes represented the portion of the blade width with a discrete crack. The results for the relative natural frequency tracking, at the two different temperatures, are shown in Figure 5.6 below.

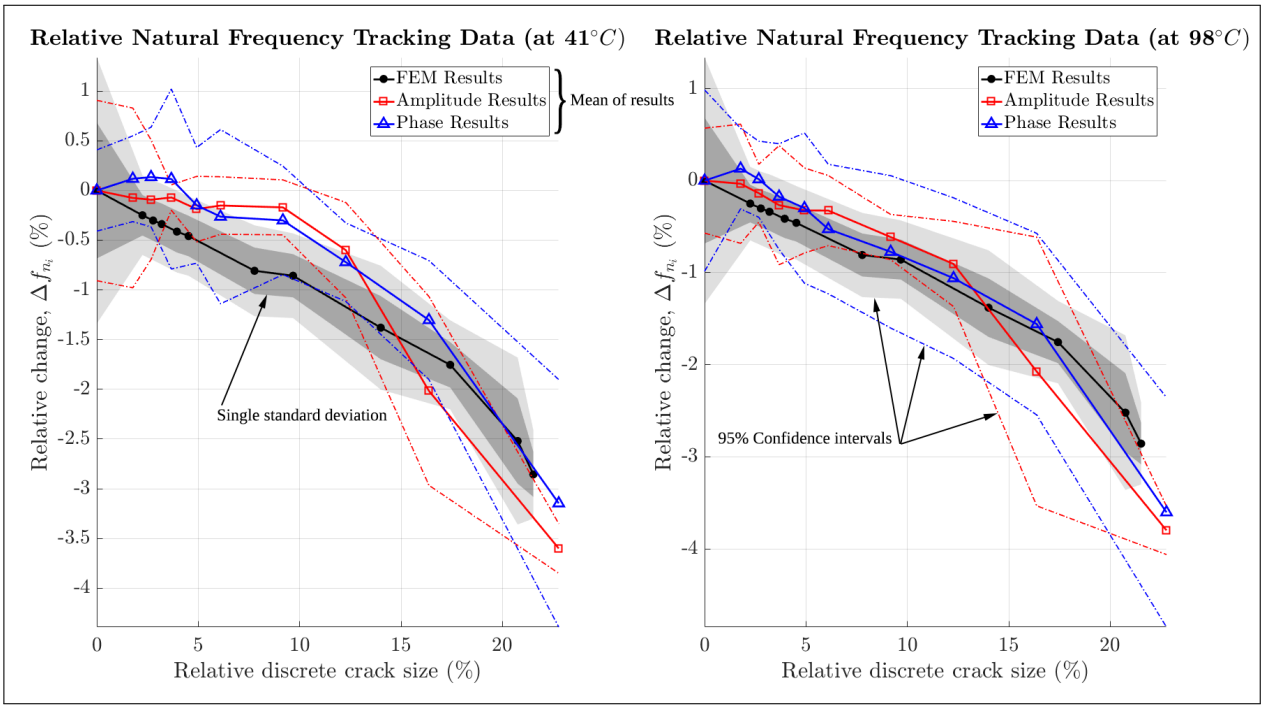

Figure 5.6: Relative natural frequency results for the test blade (blade 3) at various temperatures.

It is also interesting to note that the confidence intervals of both result-sets (41°C and 98°C) are in contact with the confidence intervals of the FEM modal analysis results over the entire relative discrete damage domain. The 41°C relative natural frequency results based on the amplitude, however, indicate slight divergence close to 9% relative discrete damage. The phase relative natural frequency results at this temperature are a better match in this region when compared to the FEM results. The relative natural frequencies based on the phase for the 41°C also have wider confidence intervals, however, this is indicative of more uncertainty in this data. The 98°C relative natural frequency results exhibit a closer match when compared to the FEM results to a relative discrete crack size of about 12.4%. Thereafter, both the 41°C and 98°C result-sets perform quite similarly. These results do not show distinct divergence from the FEM modal analysis results, as was seen in Figure 5.3, for the *Group II* results. However, it would be wise to always be more conservative when performing the damage identification process.

Section 5.2.2 further defines and demonstrates the proposed damage identification process. It was important to demonstrate the relative natural frequency tracking process for *known* changes in the size of the discrete blade damage. This essentially demonstrated the ability of the proposed stochastic hybrid approach to track small changes in the blade natural frequencies, while incorporating uncertainty in the relative natural frequency tracking.

5.2.2 Procedure 2

The results in Section 5.2.1 showed that it is possible to track small changes in the natural frequencies of the test blades using the proposed BTT methodology based on BLR (*Vibrapy*). The stochastic hybrid analysis advantageously allows confidence intervals to be established around the mean FEM and BTT results, therefore allowing the uncertainty in the results to be quantified. Section 5.2.1 also compared the relative natural frequency results of the BTT investigations and FEM modal analysis. It is generally noted that the relative natural frequency tracking results (at the corresponding relative discrete crack sizes) of the FEM modal analysis are in agreement with the corresponding BTT results (with and without the effects of temperature). The results from the FEM modal analysis may therefore be used to project the expected change in natural frequency for a particular degree of discrete blade damage. This section demonstrates how the relative natural frequency tracking results may be used to identify and infer the degree of discrete blade damage based on a predetermined blade damage threshold criterion. Consequently, this section demonstrates the use of a blade damage identification procedure (based on a stochastic hybrid approach) used to determine whether a turbomachine outage should be scheduled.

Group II Results

The damage identification procedure is presented and demonstrated in this subsection, specifically for *Group II* (*Stage IV*) of the BTT investigation. It should be emphasised that *Procedure 2* assumes that the actual discrete damage sizes of the blades are not known. *Procedure 2* therefore relies on the tracking of the relative changes of the derived natural frequency BTT results to infer the degree of discrete blade damage. The FEM modal analysis facilitates the estimation of expected blade conditions (relative change in natural frequency) corresponding to a particular discrete damage size that is deemed critical. This set of FEM modal analysis results may then be used to establish a *damage threshold*. The aim of the damage identification procedure is to determine whether there is sufficient evidence from the stochastic hybrid approach to suggest that this damage threshold has been reached, thus resulting in a turbomachine outage.

Figure 5.7 shows two iterations of the proposed identification procedure. Only the BTT relative natural frequency tracking results are plotted (based on the amplitude and phase results). The BTT relative natural frequency results in Figure 5.7 correspond to the BTT results in Figure 5.3. Very important to note is that the BTT relative natural frequency results are no longer plotted against the relative discrete crack size in Figure 5.7. These results are now simply plotted according to the BTT test number; in industry this could be a date or time. Also note that the FEA relative natural frequency results are not used directly. Instead, a predetermined damage threshold is established using the FEM modal analysis results. The following steps describe the proposed damage identification procedure:

1. Define a level of discrete blade damage that would justify a turbomachine outage / inspection. In Figure 5.7 this is indicated by *Level 1*. This level corresponds to increment 5 of the FEA results or 1.58mm of discrete blade damage (3.95% relative discrete crack size). This level is arbitrarily chosen for the purposes of the damage identification demonstration.
2. The FEM modal analysis was performed stochastically at this discrete crack size in order to quantify uncertainty. It is therefore essential to record the mean (μ_{FEM_1}) and standard deviation (σ_{FEM_1}) of the FEM results corresponding to this damage increment (*Level 1*).
3. A new variable, δ_{damage}, is defined as shown in Equation 5.2. This variable represents the difference between the relative change in the natural frequency of the BTT results (for a particular batch of tests) and the relative change in natural frequency of the FEM results at a particular discrete damage size (represented by *Level 1* in Figure 5.7).

$$\delta_{damage} = \Delta f_{n_{BTT}} - \Delta f_{n_{FEM}}(K) \tag{5.2}$$

In Equation 5.2, K denotes the predetermined crack size of the FEM modal analysis. It is very important to note that δ_{damage} is not a deterministic value, but rather a normal probability distribution. The reason being that both $\Delta f_{n_{BTT}}$ and $\Delta f_{n_{FEM}}(K)$ have associated normal distributions, summarised as follows:

$$\Delta f_{n_{BTT}} \sim \mathcal{N}\Big(\mu_{_{BTT}}, \sigma^2_{_{BTT}}\Big) \tag{5.3}$$

$$\Delta f_{n_{FEM}}(K) \sim \mathcal{N}\Big(\mu_{_{FEM}}, \sigma^2_{_{FEM}}\Big) \tag{5.4}$$

The associated normal probability distribution of δ_{damage} is the difference between the independent normal distributions of the BTT results (Equation 5.3) and FEM results (Equation 5.4). The formulation of the normal probability distribution of δ_{damage} is shown in Equation 5.5 [Cross Validated, 2015]:

$$\delta_{damage} \sim \mathcal{N}\Big(\mu_{_{BTT}} - \mu_{_{FEM}}, \sigma^2_{_{BTT}} + \sigma^2_{_{FEM}}\Big) \tag{5.5}$$

4. The calculation of the mean and variance of δ_{damage} (as shown in Equation 5.5) requires that a number of repetitive BTT tests are performed. Repetitive tests essentially enable the mean, $\mu_{_{BTT}}$, and standard deviation, $\sigma_{_{BTT}}$, of a certain batch of BTT tests to be determined.

5. The probability, $P(\delta_{damage} \leq 0)$, is determined for a particular batch of BTT tests and chosen $\Delta f_{n_{FEM}}$ (*Level 1* in this case). This probability is found from the Cumulative Distribution Function (CDF) of δ_{damage}, with associated mean and variance as shown in Equation 5.5. $P(\delta_{damage} \leq 0)$ is the probability that the relative change in the natural frequency derived from the BTT measurements ($\Delta f_{n_{BTT}}$) equals or exceeds the permissible relative change in the natural frequency derived from the FEM analysis ($\Delta f_{n_{FEM}}(K)$). The detailed interpretations of various probability ranges of $P(\delta_{damage} \leq 0)$ are discussed in the Appendix, Section B.3.

6. The damage threshold (X_{dt}) is based on a selected probability, $P(\delta_{damage} \leq 0) > X_{dt}$. It is up to the user to decide what an *acceptable* probability is to justify a turbomachine outage. Repetitive BTT tests are conducted in intervals until this probability value (damage threshold) is reached. Once this damage threshold is reached a turbomachine outage will be scheduled and the necessary inspections of the damaged blade will commence. If necessary, this blade may be replaced if the damage on the blade is deemed critical. It is important to note that the damage threshold (X_{dt}) may be selected as a conservative value. The choice of the value of the damage threshold may differ depending on the particular application of this procedure; it is entirely up to the user to decide what this value should be.

7. Steps 1 - 6 is repeated after every inspection or maintenance operation, until a blade needs to be replaced. After each inspection a new *damage level*, based on the FEM results will be prescribed to determine a new blade damage threshold.

Figure 5.7 demonstrates two iterations of the damage identification process. In this figure, *Level 1* corresponds to a relative discrete crack size of 3.95% (1.58mm) and *Level 2* corresponds to a relative discrete crack size of 9.675% (3.87mm). These levels were arbitrarily chosen and are merely used to demonstrate the damage identification process. Table 5.1 shows the derived probability, $P(\delta_{damage} \leq 0)$, for each batch of the BTT tests. In Table 5.1, P_{Amp} and P_{Phase} refers to the probabilities based on the BTT amplitude and phase results respectively. The following points summarise the outputs of the damage identification process for *Group II*:

- The first damage threshold is defined as $X_{dt_1} = P(\delta_{damage_1} \leq 0) > 0.5$ and relates to *Level 1*. This damage threshold implies that a turbomachine outage will be scheduled if there is a probability greater than 50% that $\Delta f_{n_{BTT}}$ exceeds $\Delta f_{n_{FEM}}(K_{Level_1})$. Based on the results in Figure 5.7 and Table 5.1, inspection 1 is performed after batch 5 of the BTT testing. According to Figure 5.3 (Section 5.2.1), the actual discrete blade damage is also 1.58mm (3.95% relative discrete crack size).

- After the first inspection a new reference position is established. The second damage threshold is defined as $X_{dt_2} = P(\delta_{damage_2} \leq 0) > 0.4$ and relates to *Level 2*. This damage threshold is chosen to be more conservative due to inspection 1 indicating that the blade is already damaged (close to 4%) and the fact that *Level 2* corresponds to approximately 10% discrete blade damage. It is advised to be more conservative with increasing blade damage. Based on the results in Figure 5.7 and Table 5.1, inspection 2 is performed after batch 9 of the BTT testing. According to Figures 5.2 and 5.3 (Section 5.2.1), the actual discrete blade damage is 5.6mm (14% relative discrete crack size) at this batch of BTT results. *Level 2*, however, represents 3.87mm of discrete blade damage in the FEA. Inspection 2 therefore proves that the FEM modal analysis and BTT relative natural frequency tracking results diverged for this discrete damage size. In practice, model updating would need to be performed in the FEA to correct this divergence.
- Table 5.1 shows that the probabilities, $P(\delta_{damage_2} \leq 0)$, for batch 10 - 12 are greater than 0.5. These values were merely computed for interest-sake. According to the detailed interpretation of X_{dt} in the Appendix (Section B.3), these probabilities imply that the mean of the relative natural frequencies of the BTT results have crossed-over the mean of *Level 2*. Figure 5.7 shows that this is indeed the case. For batch 12 the probabilities are very close to 1; the reason being that the 95% confidence intervals of the BTT results and *Level 2* no longer cross-over.

Table 5.1: Probabilities, $P(\delta_{damage} \leq 0)$, for the BTT relative natural frequencies based on the amplitude and phase results for blade 2 (*Procedure 2*, *Group II*).

BTT Test	$\boldsymbol{P_{Amp_1}}$	$\boldsymbol{P_{Phase_1}}$	$\boldsymbol{P_{Amp_2}}$	$\boldsymbol{P_{Phase_2}}$	
1	0.0458	0.2162			
2	0.2597	0.1350			
3	0.3665	0.1930			
4	0.4326	0.0292			
5	**0.5485**	**0.0719**	**Inspection 1**		
6			0.0579	0.0032	
7			0.1922	0.0234	
8			0.1569	0.0362	
9			**0.4035**	**0.3939**	**Inspection 2**
10			0.8501	0.6555	
11			0.9734	0.9948	
12			0.9987	0.9977	

Group III Results

Two iterations of the damage identification procedure are demonstrated in this subsection, specifically for *Group III* (*Stage VI*) of the BTT investigation. This subsection therefore presents the damage identification results whereby the effects of varying blade temperatures are considered. The same damage identification procedure, as previously documented, was used to formulate these results. The following discrete blade damage levels are defined for this demonstration, as indicated in Figures 5.8a and 5.8b:

- *Level 1* corresponds to increment 8 of the FEA results; 3.87mm of discrete blade damage or 9.675% relative discrete crack size.
- *Level 2* corresponds to increment 11 of the FEA results; 8.3mm of discrete blade damage or 20.75% relative discrete crack size.

Note, the damage identification results shown in Figure 5.8 correspond to the relative natural frequency tracking results shown in Figure 5.6.

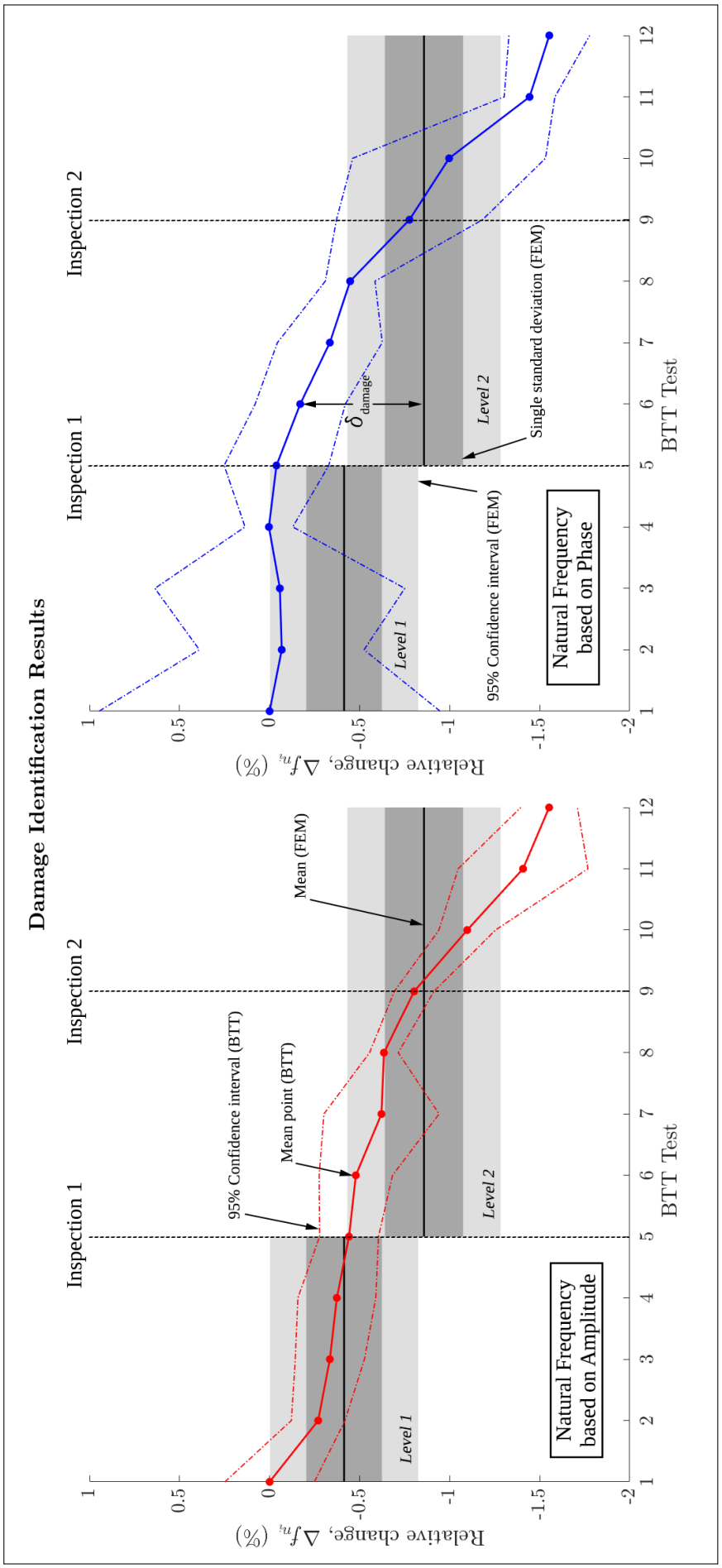

Figure 5.7: Damage identification results for blade 2 (*Procedure 2, Group II*).

The damage threshold for both sets of temperature tests, and at both levels, is defined as $X_{dt_{1,2}} = P(\delta_{damage_{1,2}} \leq 0) > 0.8$. It was decided to make this damage threshold a less conservative probabilistic value in order to demonstrate the implications of this choice. Tables 5.2 and 5.3 show the probabilities for the $41°C$ and $98°C$ BTT results respectively. Based on the chosen damage threshold inspection 1 would be performed after batch 9 of the BTT tests and inspection 2 would be performed after batch 10 of the BTT tests for both sets of temperature results. These inspections are also marked on Figures 5.8a and 5.8b. The following points summarise the damage identification results of *Group III* based on the aforementioned damage thresholds:

- According to Figures 5.5 and 5.6 (Section 5.2.1), the actual discrete blade damage is 6.55mm (16.38% relative discrete crack size) at inspection 1. This is the case for both sets of temperature results. *Level 1*, however, represents 3.87mm of discrete blade damage. This big difference in the predicted discrete blade damage is related to the fact that the probabilistic damage threshold (X_{dt_1}) was chosen as quite a high, less conservative value. The damage threshold, $X_{dt_1} = P(\delta_{damage_1} \leq 0) > 0.32$, would have resulted in a more accurate and conservative prediction of the discrete crack size.
- Inspection 2, however, shows that the actual discrete crack size of the blade and predicted values based on *Level 2* are very close. The actual damage, according to Figures 5.5 and 5.6, are 9.11mm actual damage (22.77% relative discrete crack size) as opposed to the 8.3mm predicted discrete crack size (20.75% relative discrete crack size) based on *Level 2*.

Table 5.2: Probabilities, $P(\delta_{damage} \leq 0)$, for the BTT relative natural frequencies based on the amplitude and phase results for blade 3 at $41°C$(*Procedure 2*, *Group III*).

BTT Test	$\boldsymbol{P_{Amp_1}}$	$\boldsymbol{P_{Phase_1}}$	$\boldsymbol{P_{Amp_2}}$	$\boldsymbol{P_{Phase_2}}$	
1	0.0467	0.0022			
2	0.0624	0.0008			
3	0.0209	0.0015			
4	0.0003	0.0283			
5	0.0073	0.0270			
6	0.0036	0.1161			
7	0.0040	0.0574			
8	0.2154	0.3222			
9	**0.9854**	**0.8830**	**Inspection 1**		
10			**0.9922**	**0.7934**	**Inspection 2**

Table 5.3: Probabilities, $P(\delta_{damage} \leq 0)$, for the BTT relative natural frequencies based on the amplitude and phase results for blade 3 at $98°C$ (*Procedure 2*, *Group III*).

BTT Test	$\boldsymbol{P_{Amp_1}}$	$\boldsymbol{P_{Phase_1}}$	$\boldsymbol{P_{Amp_2}}$	$\boldsymbol{P_{Phase_2}}$	
1	0.0091	0.0588			
2	0.0185	0.0010			
3	0.0038	0.0001			
4	0.0672	0.0001			
5	0.0477	0.0396			
6	0.0337	0.0288			
7	0.1644	0.0245			
8	0.5587	0.3474			
9	**0.9415**	**0.8492**	**Inspection 1**		
10			**0.9978**	**0.8564**	**Inspection 2**

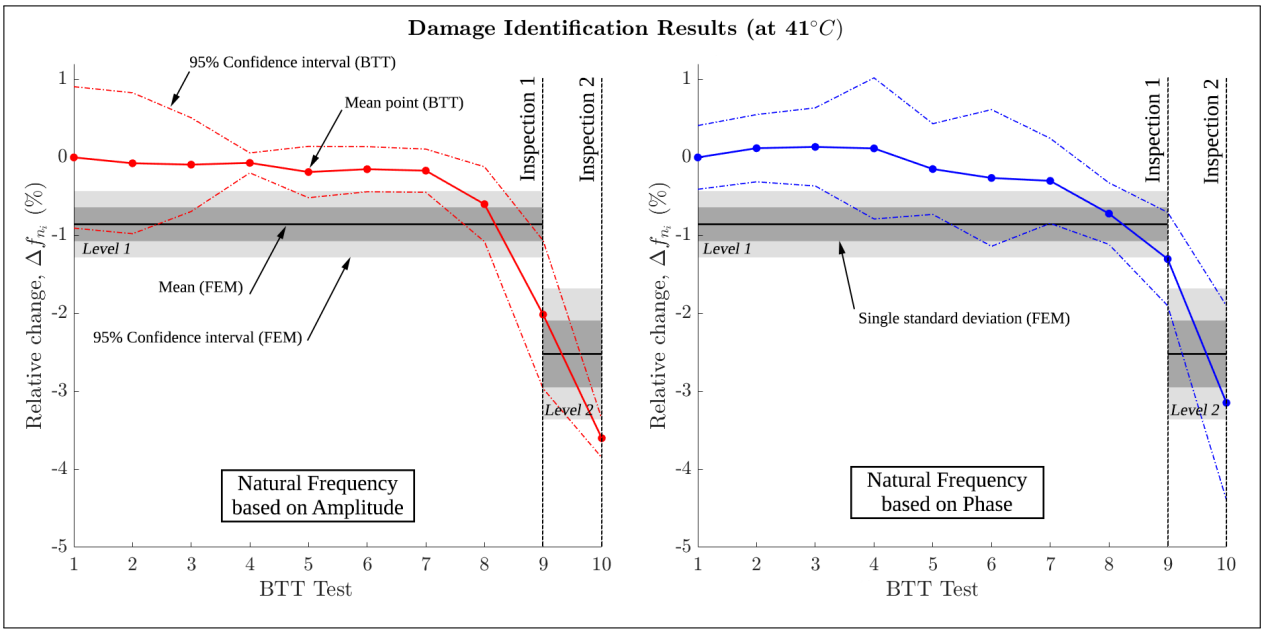

(a) Damage identification results at 41°C (blade 3).

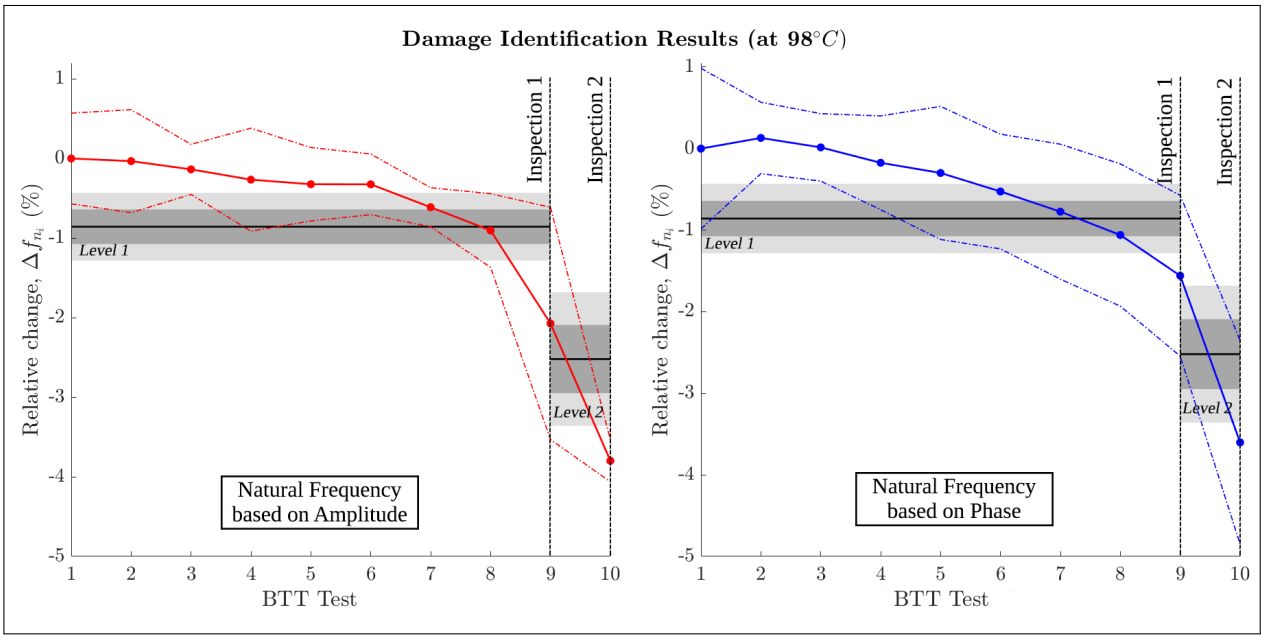

(b) Damage identification results at 98°C (blade 3).

Figure 5.8: Damage identification results (*Procedure 2*, *Group III*).

Summary

The damage identification approach presented in Section 5.2.2 demonstrated that the relative natural frequency tracking results may be used to identify and infer the degree of discrete blade damage. This is achieved by defining a predetermined and probabilistic blade damage threshold criterion. Importantly, this approach uses the results from a stochastic FEM modal analysis to project the expected change in natural frequency for a particular discrete crack size. The BTT tests are performed in batches (time intervals) with no prior knowledge of the *actual* blade damage. This enables the associated normal distributions of the relative change in natural frequency of a specific blade to be determined for a certain batch of tests. Consequently, this section demonstrated the use of a stochastic hybrid damage identification approach to determine whether a turbomachine outage should be scheduled.

5.3 Damage Classification

Section 5.2.2 presents a sensible approach for tracking the relative changes in the natural frequency of a blade as the discrete damage for this blade increases. This approach consists of FEM modal analysis, BTT amplitude and BTT phase results. Furthermore, this approach relies on repetitive or frequent measurements to be available for the use in a practical implementation. The archiving ability of the proposed BTT methodology was further elaborated on and the use of these approaches proved to have a practical benefit in a hybrid CBM scheme. The question as to *what happens if multiple and frequent BTT measurements are not practically possible*, however still remains. For this scenario the mean of particular BTT measurements (the mean of repetitive measurements corresponding to a particular discrete damage interval) would not be established, therefore requiring much confidence to be placed on a single measurement. Section 2.2 proposes a second approach to determine whether a damage threshold of a blade is reached, namely: clustering. Clustering forms part of a damage classification technique and allows a single measurement to be assigned to a cluster. Many of these techniques exist, with each technique ranging in complexity and functionality [Mishra et al., 2014]. The proposed clustering technique for the hybrid approach shown in Figure 2.1 is *K-means clustering*. K-means clustering is a mature and popular technique whereby observations with the nearest mean are assigned to a certain cluster of data-points [Wagstaff et al., 2001]. This physically translates into vibrational characteristics of a blade, from a specific BTT measurement, being assigned to an existing cluster of vibrational characteristics with the nearest mean.

5.3.1 Group II Results

The aim of this K-means clustering approach is to classify the severity of the blade damage according to which group the vibrational characteristics of a particular BTT measurement are assigned to. Consequently, the severity of the blade damage may be determined from these clusters. The following points summarise this process as used in the hybrid approach shown in Figure 2.1:

- The vibrational characteristics of a certain blade were extracted and used further in the clustering process. For the purposes of this research, the maximum amplitudes and associated natural frequencies (of the BTT data) were used.
- The clustering of the natural frequency and amplitude results using predetermined mean values is proposed. The predetermined mean values correspond to the natural frequency results from the FEM modal analysis, particularly for the first bending mode. Importantly, the amplitudes of vibration were not computed during the FEM modal analysis. A Computational Fluid Dynamics (CFD) analysis would be required to simulate the fluid-flow interaction on the the blades used during experimentation. From this CFD analysis an indication of the amplitudes of blade vibration could be determined. This CFD analysis was not performed for a number of reasons, namely:
  - The proposed approach aims to meet the requirement of a simple implementation.
  - Figure 1.13 shows that the Centre for Asset Integrity Management is doing further research related to the fluid-flow interaction of turbomachine blades using a CFD analysis. This topic therefore falls outside of the scope of this dissertation.
  - Further investigations of the *K-means clustering* implementation used in this research showed that it would be sensible to assign *zero* amplitude values to these predetermined mean values (more detail about this follows in the remainder of this sub-section).

  As previously discussed, the use of an FEA allows expected blade conditions to be projected, therefore enabling this data to be used as predetermined mean values. Chapter 4 describes the detail of using a FEM modal analysis to project expected conditions and how this may be done stochastically.

- For the purposes of this research it was decided to partition the data of *Group II* of testing into three initial clusters (*k mean clusters*, hence the name *K-means clustering*). These initial clusters correspond to the assigned zero amplitude values and predetermined mean natural frequencies from the FEA. The partitioning of the data corresponds to the discrete damage increments shown in Table 5.4 below. Each partition was classified according to severity of the blade damage it represented, thus indicating the non-severe damage increments, mid-severity damage increments and most severe damage increments respectively (also indicated in Table 5.4). These partitions correspond to thirds of the total damage introduced to the blade and are further shown in Figure 5.9. It is important to note that these partitions were not enforced on the BTT data before the K-means clustering commenced. However, after the clustering was completed the individual points shown in Figure 5.9 were used to determine the accuracy of the final classification into the various damage regions. More detail about this will be discussed later in this sub-section.
- The initial cluster centres corresponded to the zero amplitude values and the mean natural frequency values of the FEA results partitioned using the aforementioned scheme. This resulted in three amplitude and natural frequency combinations / locations used as a starting point of the centroids. These initial cluster centres thus enabled individual BTT measurements (according to the amplitude and derived natural frequency) to be classified to the closest partition. The detail of the K-means formulation and the results for this particular implementation will be discussed in the remainder of this sub-section.

Table 5.4: Incremental discrete damage segmentations or partitions used for clustering.

Damage Increment	Crack Size (mm)	Damage Severity Classification
1	0	Non-severe *(Region I)*
2	0.90	
3	1.11	
4	1.28	
5	1.58	
6	1.81	
7	3.11	Mid-severity *(Region II)*
8	3.87	
9	5.60	
10	6.97	Severe *(Region III)*
11	8.30	
12	8.61	

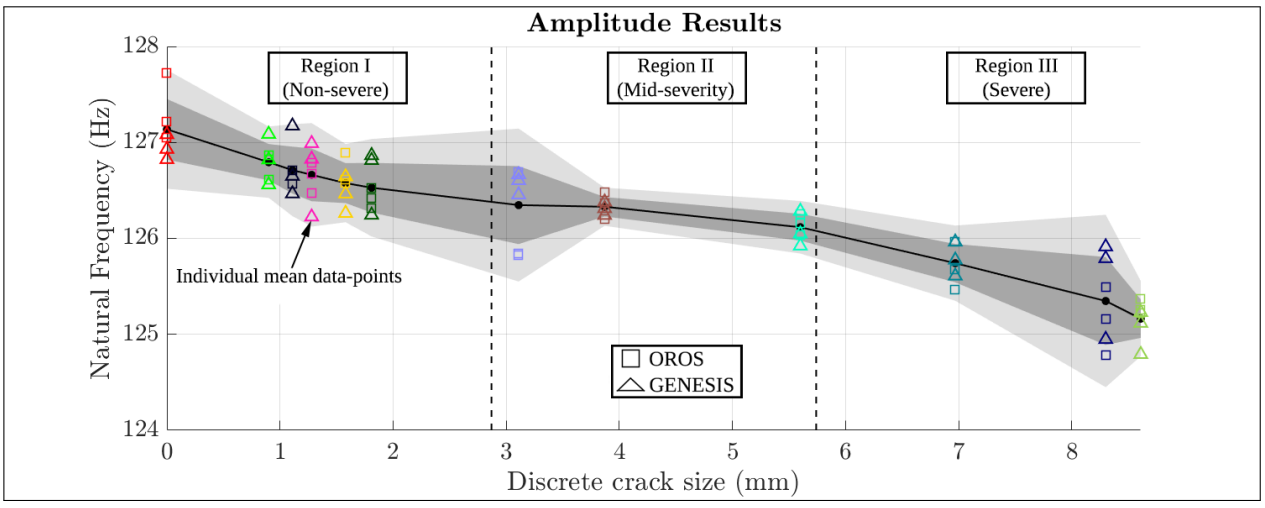

Figure 5.9: Partitions used to classify the BTT data.

Arthur and Vassilvitskii [2007] summarised the K-means clustering problem in terms of the goal of the algorithm. Given an integer k and a set of n data points in $\mathbb{R}^d$, the goal is to choose k centres to minimise the potential function, ϕ_{k-mean}. This potential function is in essence the Euclidean distance measure; the total squared distance between each point, x, and its closest centre, c, as shown in Equation 5.6 below [Arthur and Vassilvitskii, 2007]:

$$\phi_{k-mean} = \sum_{x \in \mathcal{X}} \min_{c \in \mathcal{C}} \|x - c\|^2 \tag{5.6}$$

In Equation 5.6 $\mathcal{X}$ refers to all the data-points and $\mathcal{C}$ refers to all the possible k centres in the set. As previously mentioned, the goal is to choose k centres, $\mathcal{C}$ so that the potential function shown in Equation 5.6 is minimised. Clustering is then achieved by grouping the data-points according to which centre a specific point is assigned to. The following points summarise the initialisation and working-principles of the K-means clustering algorithm specific to the implementation of this study [Arthur and Vassilvitskii, 2007; MathWorks, 2017; Seber, 1984]:

1. k initial cluster centres ($\mathcal{C} = \{c_1, c_2, c_3 \ldots, c_k\}$) are chosen. Many possible techniques exist for the cluster centre initialisation, however, it was decided to use the FEM modal analysis data for this initialisation. This was particularly done by using the mean natural frequency data from the FEM modal analysis corresponding to each damage partition shown in Table 5.4. Zero amplitude values were assigned to the initial cluster centres for the reasons mentioned previously. It was determined that it would be the most sensible to assign zero amplitude values to these initial cluster centres. The main reason for this being that preliminary investigations of the cluster initialisation showed that the classification accuracy of the K-means clustering is not sensitive to the initial values of the amplitude. These preliminary investigations of the clustering initialisation considered very large and small amplitude values (relative to the amplitudes derived from the BTT data); the performance for the various cases remained consistent. Furthermore, uncertainty of the actual amplitude values due to vibration related to the fluid-flow interaction would exist even when using a CFD analysis.

2. The details of aforementioned point resulted in three initial centres corresponding to the three partitioned damage increments shown in Table 5.4. The advantage of performing an FEA becomes clear; initialisation or clustering data may be available independent of any BTT tests conducted in practical implementations, therefore enabling initial clusters to be formulated or projected data to be generated.

3. The point-to-cluster-centroid distances are then computed for all of the individual points of the BTT data-set as they become available (as shown in Equation 5.6 above). This step would have been difficult to accurately execute if only a single BTT measurement was available. The results from the FEM modal analysis advantageously enabled initial centres to be formulated to overcome this.

4. The BTT points are in essence treated as a *black-box*, with no indication of which damage increment the points belong to. The K-means clustering algorithm then assigns these points to a suitable centre. This is done using one of the following update schemes [MathWorks, 2017]:

   (a) *Batch update*: Each new observation is assigned to the cluster with the closest centroid / centre. This *batch update* is the default of the built-in K-means clustering algorithm used in *MATLAB*.

   (b) *Online update*: Observations are individually assigned to a different centroid if the reassignment causes a change related to the sum of the within-cluster, sum-of-squares point-to-cluster-centroid distances.

5. The overall averages of the points in the clusters are then calculated (in terms of the natural frequencies and amplitudes) to find k new centroid locations.

6. Steps 2, 3 and 4 are repeated until there is no change in the cluster assignment or the maximum number of iterations is reached for the computation. For this particular implementation the computations are run until the change in the centroid locations, $\mathcal{C}$, are smaller than a chosen tolerance.

7. As a result, the BTT points are classified into the associated group (most likely damage region) that the amplitude and natural frequency would be representative of. The computation of this is quite efficient in terms of speed and simplicity.

It was important to scale the BTT amplitude and natural frequency data for the use in the K-means clustering; i.e. normalise the data so that the values of both the amplitudes and natural frequencies ranged between 0 and 1. This normalisation was done according to the minimum (assigned to 0) and maximum (assigned to 1) of these data-points. The initial cluster centroids (FEM natural frequency data) was also scaled using this scheme. The amplitudes of the initial cluster centroids were already zero and therefore did not require scaling. This was an important step before the K-means clustering commenced as it ensured that neither of these values (amplitude or natural frequency) dominated the Euclidean distance formulation. The results of the K-means clustering implementation for this particular investigation are shown in Figure 5.10. In Figure 5.10 *Region I*, *Region II* and *Region III* represent the new averaged clusters for the non-severe, mid-severity and severe damage increments respectively. The incorrectly classified BTT points are also shown in Figure 5.10; the correct classification for these incorrectly classified points are indicated by a Roman Numeral above the marker. These corrections were possible due to the fact that the actual BTT measurements were available before the classification commenced. In practise, these corrections may rely on the results from the *damage identification* procedure, where a certain discrete crack size is inferred from the procedure outlined in Section 5.2.2. Refer to Figure 5.9 and Figure B.7 (Appendix, Section B.2.2) for the mean BTT data-points which were used to determine the accuracy of the prediction. The following points should be noted regarding the accuracy of the K-means clustering implementation:

- The the overall classification accuracy is 78% (56 out of the 72 points were correctly classified) according to the imposed partitions of the damage increments shown in Table 5.4.
- If only the *Region III* (severe classification) is considered as important for determining whether a damage threshold has been reached, then this classification accuracy would be 94% accurate (4 out of the 72 points were incorrectly classified for this particular partition). This specific partition would put a greater emphasis on *Region III*, therefore grouping *Region I* and *Region II* together. It is, however, a great concern when an actual *Region III* (severe) point is classified as a *Region I* (non-severe) point. This, however, only occurred for a single data-point.
- When considering the damage increments or regions independently, the following is reported about the resultant K-means clustering accuracy for this implementation:
  - *Region I*: Only 26 out of the 36 possible points are correctly classified, therefore resulting in a 72% accuracy when this damage region is considered independently.
  - *Region II* and *Region III*: For both these regions 15 out of the 18 possible points are correctly classified, therefore resulting in a 83% accuracy when these damage regions are considered independently.

The above-mentioned points highlight important aspects of the K-means classification results. Different ways of interpreting the accuracy of the clustering prediction were discussed. It should be reiterated that an incorrect classification of an actual *Region III* point would be regarded as critical, especially when a data-point from this region is incorrectly classified as *Region I* point. This, however, only occurred once in the particular implementation and was as a result of the amplitude and natural frequency of this point not being completely distinguishable as a *Region III* point. It is hypothesised that the accuracy of the classifications may improve if additional features, resulting in more definitive cluster locations, are implemented.

It is recommended for future iterations of the proposed clustering approach to considering additional features. The consideration of additional features may be possible when a more complex CFD fluid-flow interaction analysis for a particular blade is implemented. The phase information could possibly be incorporated along with the natural frequencies associated with this phase information. For the hybrid approach to still be applicable, the additional features should be measurable in both the BTT analysis and FEM modal analysis. It should, however, be noted that additional features do not necessarily imply greater accuracy. If these additional features do not result in more definitive cluster locations, the accuracy of the final prediction may decrease drastically. Further investigations are therefore necessary to make this judgement-call.

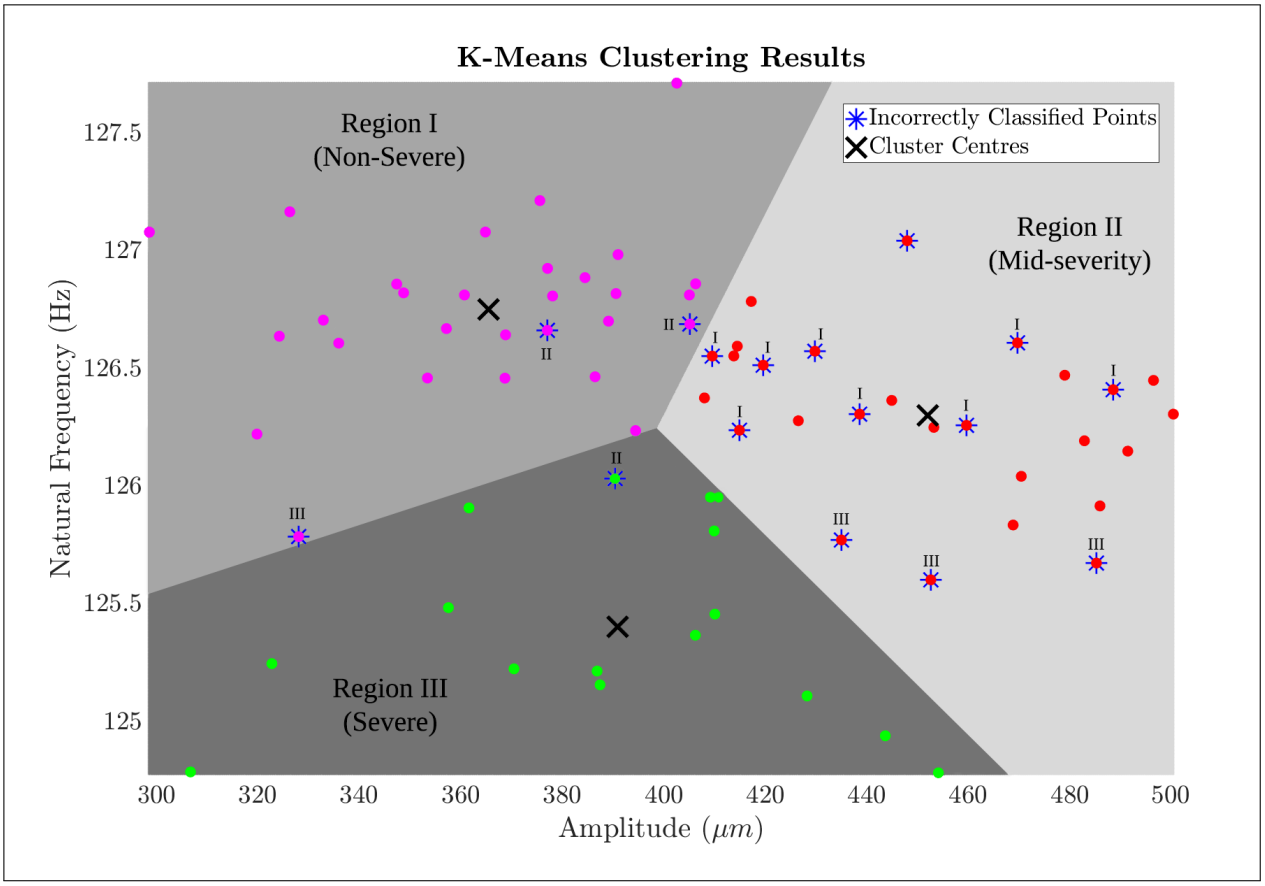

Figure 5.10: Illustration of the *Stage IV* K-means clustering results.

For practical applications, it is proposed that the K-means clustering implementation should supplement the hybrid approach outlined in Figure 2.1. The clustering of the BTT results to predetermined centres would allow the blade damage to be classified according to k-partitions imposed on the data. The damage threshold may be chosen based on these damage classifications. The following outcomes are possible for this proposed blade damage classification strategy:

1. The derived amplitude and natural frequency results are classified as *non-severe* (*Region I* in Figure 5.10). This could potentially signify that the blade is still in good condition. As indicated in Figure 5.10, numerous points were incorrectly classified as *Region I*. This may be a concern, especially if a *Region III* point is incorrectly assigned to *Region I*.
2. If these values are classified as *mid-severity* damage (*Region II* in Figure 5.10) then this would give an indication that the condition of the blade is potentially deteriorating.
3. Lastly, if these values are classified as *severe* damage (*Region III* in Figure 5.10) then this would indicate that the blade damage is immense, therefore signifying a damage threshold being reached and resulting in a turbomachine outage being scheduled.

5.3.2 Group III Results

The clustering approach presented in this section corresponds to what was done in Section 5.3.1. Again, this clustering approach is specifically based on K-means clustering and uses the FEM modal analysis results to initialise centres. It should be reiterated that the use of a clustering methodology aims to classify the severity of the discrete blade damage by grouping the derived vibrational characteristics. The advantage of the clustering (damage classification), as opposed to the relative natural frequency tracking (damage identification), is that it allows a single point to be used to make a prediction rather than a number of the same tests used to find a mean. The only difference between the results presented in this section and those presented in Section 5.3.1 is that the clustering approach now incorporates the effects of temperature in the implementation. This in itself results in a slight complication related to how the K-means clustering should be performed. Two options are therefore available on how to approach the clustering:

1. *Combined:* The data from both result-sets ($41°C$ and $98°C$ temperature tests) could be analysed jointly. This would require further normalisation (between 0 and 1) of the amplitude and natural frequency data in order to take into account the initial values corresponding to the specific temperature. This normalisation would in essence ensure that the various points corresponding to a certain temperature are scaled, therefore enabling the results from the different temperatures to be comparable during the execution of the K-means clustering. The data would then be scaled back to the original values once the clustering is completed. The data is in essence clustered as a *relative* quantity; a measure of how much the amplitude and natural frequency values changed with regards to the initial value corresponding to a specific temperature group. When these relative values are, however, scaled back to the original domain the representation of the cluster centres becomes tricky due to the fact that the data was scaled using different schemes.
2. *Separately:* The result-sets corresponding a specific temperature could be analysed separately. The $41°C$ natural frequency and amplitude results could be used in a completely separate K-means clustering implementation. Similarly, the $98°C$ results would be analysed independently. The results of the K-means clustering would ultimately remain independent amongst the various temperature ranges that were tested. It would not be practical to group the BTT data in specific temperature increments ($1°C$ increments for example), but rather in temperature range increments where a noticeable change in the blade natural frequencies or vibrational characteristics occur. For the purposes of this research project, only two temperature ranges, approximately $56°C$ apart, were investigated and used in the clustering. A smaller temperature ranges could have been considered for this investigation, however, this required a more controlled way to heat the blades and is certainly a recommendation for future work.

Both of the aforementioned approaches has its advantages and disadvantages. Clustering the data as part of a combined scheme seems a lot more practical and realistic in terms of what may be expected in industry. For example, it is much more appealing to be able to look at *all* the data that is representative of a specific blade, rather than looking at further groupings of data according to the temperature of testing. Clustering the data separately according to the temperature ranges that were used during testing, however, enables the different results to be more easily distinguishable from one another. It would also be somewhat easier to notice fundamental differences in the amplitude and natural frequencies with regards to how these are clustered. Furthermore, issues related to scaling the resultant centroids back into the original domain would not be present when analysing the data separately. For both of these approaches the assumption needs to be made that an indication of the temperatures of the blades will be present for the use in industry. If the temperature of testing remains fairly constant during the operation of turbomachines this would be more ideal, but it is certainly still recommended that at least the internal temperatures of the turbomachines are recorded for the rotor stage of interest when the BTT tests are performed. This would at least result in supporting evidence as to why there may be discrepancies in the processed data.

This section aims to demonstrate the capabilities of a rudimentary classification implementation. It is also intended to determine whether the proposed hybrid approach shown in Figure 2.1 would still be applicable when temperature effects are introduced. The two proposed approaches for the clustering are therefore tested with regards to its use in this hybrid approach. The results and a discussion of the clustering approaches are presented in the subsections which follow.

Combined Clustering

Figure 5.11 shows the results of the combined K-means clustering implementation, as scaled back to the original amplitude and natural frequency domain. The amplitude and natural frequency points of this implementation corresponds to the values shown in Figure B.10 in Section B.2.3 of the Appendix. Only two damage regions are allocated to this implementation as it was determined that this would ultimately improve the prediction accuracy of the clustering implementation; as is recommended in the concluding remarks of the initial clustering implementation in Section 5.3.1. The allocated damage regions are *Region I* (non-severe damage) and *Region II* (severe damage). Thus splitting the introduced discrete damage associated with blade 3 into two distinct regions (please refer to Table 3.5 for the complete record of the discrete blade damage). The first region consists of all the introduced discrete blade damage ranging from 0mm to 4.55mm and the second region from 4.55mm up to 9.11mm the greatest damage. The following points summarise the performance of this classification implementation:

- Figure 5.11 indicates that 29 out of a possible 200 points are incorrectly classified. The overall classification accuracy of this implementation is therefore 85.5%.
- Figure 5.11, however, shows that 14 out of the 29 incorrectly classified points lie in a region of *overlap*, where there is not a distinct difference in the natural frequency and associated amplitude values. This classification overlap corresponds to the region close to the border of the two damage severity regions. This region is not a direct output of the K-means clustering implementation. The author merely identified this region to emphasise that points in this region are prone to an incorrect classification. It would therefore be sensible to treat these points with a bit more caution when interpreting their resultant classification.

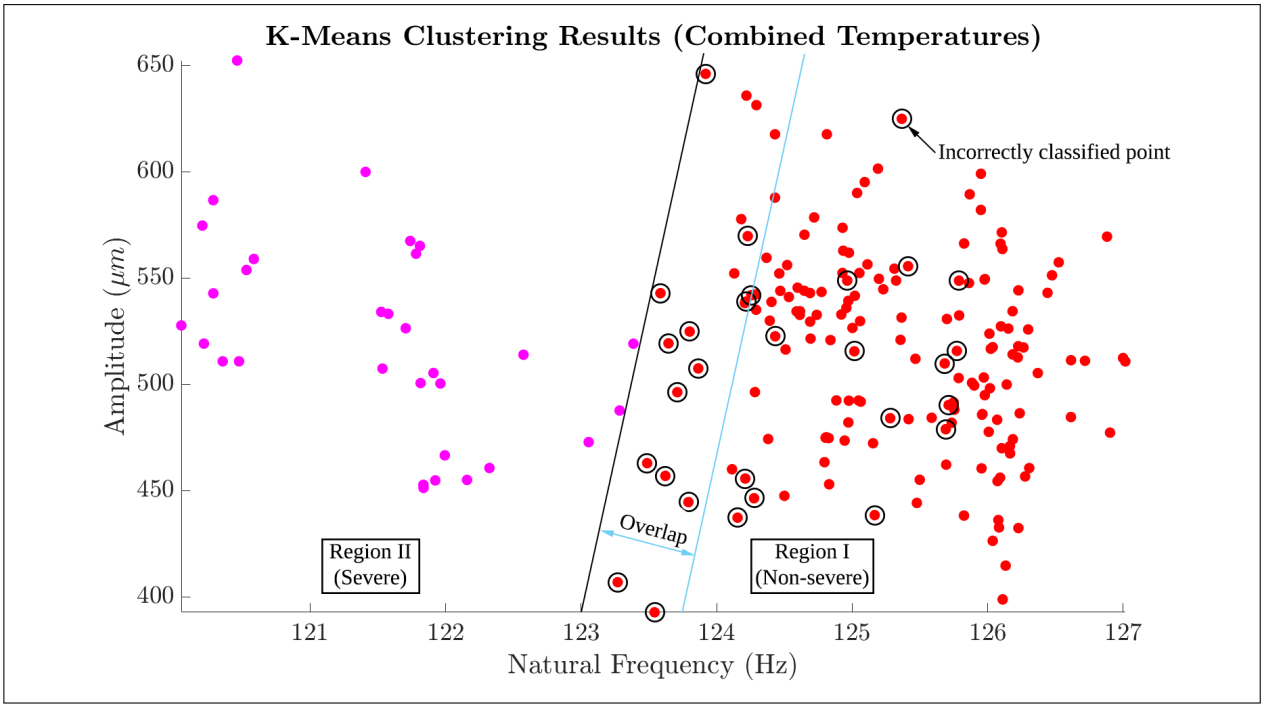

Figure 5.11: Illustration of the *Stage VI* K-means clustering combined temperature results (blade 3).

Separate Clustering

Figure 5.12 shows the results of performing the K-means clustering separately for the $41°C$ (Figure 5.12a) and $98°C$ (Figure 5.12b) temperature tests. It was initially attempted to perform the K-means clustering using three centroids, however, this decreased the accuracy considerably due to the selected features not being distinguishable enough amongst the discrete damage segmentations (the results for the centroid implementation is shown in Figure B.9 in Section B.2.3 of the Appendix). The same damage segmentations regions used for the combined clustering implementation were therefore also employed for the separate tests. The brief discussion of these results follows.

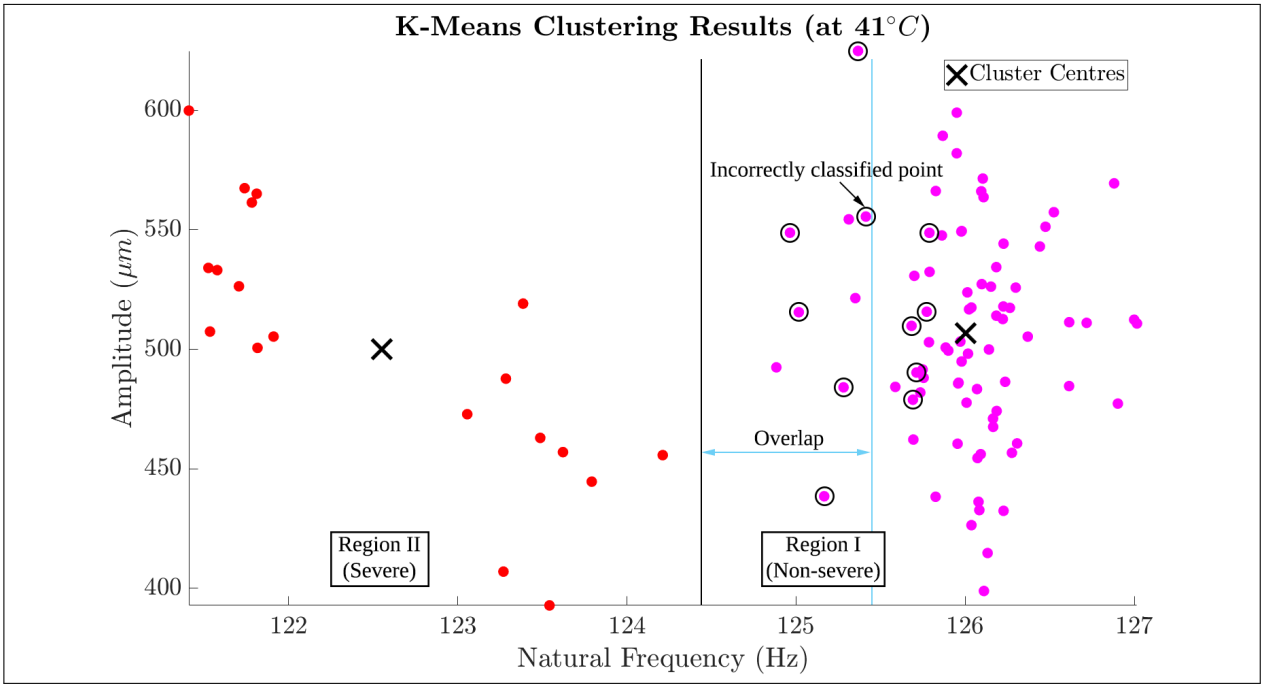

(a) *Stage VI* K-means clustering results at $41°C$ (blade 3).

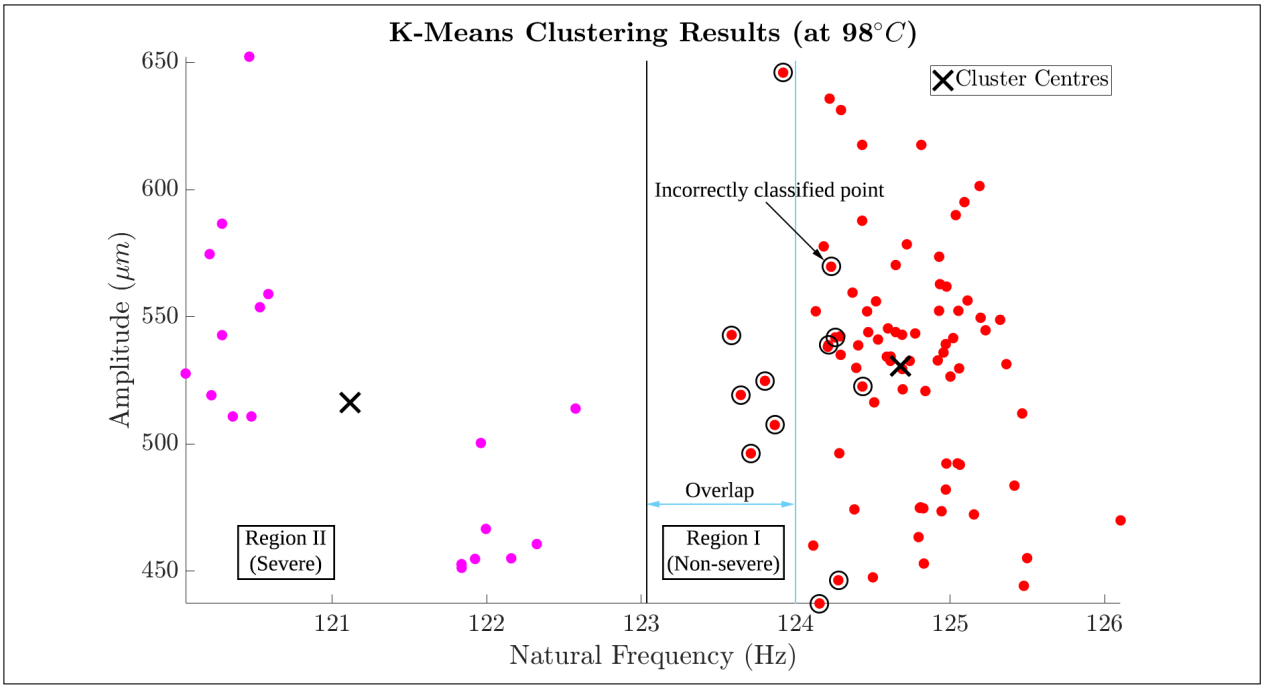

(b) *Stage VI* K-means clustering results at $98°C$ (blade 3).

Figure 5.12: Illustration of the *Stage VI* K-means clustering results at various temperatures.

In Figures 5.12a and 5.12b margins are indicated. Again, these margins correspond to sort of a *grey-area* where a high density of incorrectly classified points occurred. The incorrectly classified points in this region, however, never included points from the greatest damage increment (9.11mm of discrete blade damage) and seldom included points from the second greatest damage increment (6.55mm of discrete blade damage). The following points summarise the performance of the K-means clustering implementation for the separate temperature clustering approach:

- Figure 5.12a indicates that 11 out of a possible 100 points are incorrectly classified, therefore resulting in an overall classification accuracy 89% for the $41°C$ results.
- Figure 5.12b indicates that 12 out of a possible 100 points are incorrectly classified, therefore resulting in an overall classification accuracy 88% for the $98°C$ results.

The two sets of temperature results therefore perform very similarly in the classification process. It is also clear that the average *separate* classification accuracy, of 88.5%, is a definite improvement of the 85.5% classification accuracy of the *combined* approach. It is therefore up to the user to decide which clustering scheme is more appealing for the use in a practical implementation. Care needs to be taken when deciding how to categorise the temperature data according to temperature ranges of testing, thus being a recommendation for future work. Furthermore, for both clustering investigations (with and without the effects of temperature) it was seen that using two classifications or damage regions (non-severe and severe blade damage) damage resulted in a better classification accuracy. The choice with regards to the number of damage regions therefore also depends on the user requirements. The desired outcome of the hybrid approach is, however, only concerned with the information of whether a damage threshold is reached, therefore suggesting that two damage regions may be sufficient to do so. A *severe* blade damage classification would signal a damage threshold being reached. The advantage of having a further classification (*mid-severity*), as discussed in Section 5.3.1, would be that an earlier warning of imminent and severe blade damage could be possible. Section 5.4 summarises and discussed all the results presented in this chapter, therefore highlighting important aspects of the proposed hybrid approach.

5.4 Discussion and Summary

Two formal sets of results were presented and discussed in this chapter. The first set of results corresponded to *Group II* of testing where discrete incremental blade damage was introduced to a test blade. The details of this BTT investigative group may be found in Section 3.5.2 of the main report. The second set of results corresponded to *Group III* of testing as presented in Section 3.5.3 of the main report. Discrete incremental blade damage was also introduced to another test blade in this BTT investigative group, however, effects of varying the blade temperatures were also investigated. During this investigation the blade temperatures were varied between approximately $41°C$ and $98°C$. For both these investigative groups, the aim was to test the functioning of the proposed hybrid approach illustrated in Figure 2.1. The output of this hybrid approach entailed determining whether a blade damage threshold had been reached, therefore indicating whether a turbomachine outage should be scheduled. In order to answer this question two separate processes were considered, namely: damage identification (based on relative natural frequency tracking) and damage classification (based on clustering using a K-means implementation). The relative natural frequency tracking relied on a number of the same tests in a damage increment to be available, therefore allowing the mean of the relative change in the natural frequency to be tracked as the relative discrete blade damage increased. The results from a stochastic FEM modal analysis enabled expected blade conditions or damage increments to be projected, therefore creating a basis of comparison as the BTT results become available. The damage threshold for the damage identification procedure is based on the following question: *What is the probability that the relative change in the natural frequency of the test blade is as large as what the FEM modal analysis (at a chosen discrete damage size) projected it to be?* Various scenarios of this damage identification process were demonstrated.

The proposed hybrid methodology, consisting of a data-driven (BTT incorporating BLR) and physics-based approach (stochastic FEM modal analysis), performed well in this probabilistic damage identification scheme. This probabilistic damage identification scheme was, however, merely demonstrated. It is certainly a recommendation to test this procedure in the relevant industry. When considering specifically the relative natural frequency tracking process, it is quite satisfactory to note that the proposed BTT method could track very small changes in the blade natural frequency. In some instances natural frequency changes smaller than 0.2Hz were tracked, depending on the change in the incremental discrete damage size. The relative natural frequency results based on the phase and amplitude results for both BTT investigative groups were in general very close to the projected FEM results. The relative natural frequency tracking results for *Group II* (specifically the confidence bounds around the mean) did diverge in the largest discrete damage region, indicating that there may be a need for a model updating scheme in the FEA (this is a recommendation for future work, refer to Section 6.3). In contrast, the relative natural frequency results from *Group III* at both temperatures remained within an acceptable range from the projected FEM results.

The K-means clustering process enables individual BTT data-points to be grouped to a cluster which is indicative of a specific damage region or segmentation. The BTT amplitude and natural frequency results were used during this clustering process. A point (based on its amplitude and natural frequency) was allocated to a particular cluster if it was closest to its cluster centroid. Importantly, the FEM modal analysis natural frequency results enabled the initialisation of the K-means clustering process, therefore allowing a scarcity of data to be used for practical purposes. It would be pointless to not be able to use the clustering implementation when only a few BTT data-points are available, therefore demonstrating the immense advantage of performing the clustering as part of a hybrid approach. The damage threshold for the clustering implementation corresponded to the classification of the data, for example: severe or non-severe blade damage. The incorrect classification of a particular point may have dire consequences, however, it is proposed that the relative natural frequency tracking and clustering is always performed in tandem. This results in supporting evidence of what the severity of the actual discrete blade damage is.

The results of the K-means clustering implementation are promising. Again, it should be emphasised that numerous clustering methods exist (refer to the review by Mishra et al. [2014] for an overview of various other implementations). It was nevertheless attempted to keep the hybrid approach as simple as possible without compromising its performance, therefore justifying why the relatively rudimentary K-means implementation was opted for. For *Group II*, the overall accuracy using three damage regions (corresponding to non-severe, mid-severity and severe damage) was 78%. Fusing the non-severe and mid-severity damage regions together resulted in a much higher accuracy of 94%. The clustering of the *Group III* BTT results was done using two approaches. The first approach considered all the results regardless of the associated temperatures and required further scaling of the results, therefore allowing the clustering of relative quantities. Only two centroids or cluster groups were allocated for this implementation (non-severe and severe blade damage) and resulted in an overall classification accuracy of 85.5%. It was, however, recommended to perform the clustering separately; i.e. perform the clustering for groups of data that corresponds to a specific temperature range. The second approach for the clustering of the data for *Group III* therefore considered the $41°C$ and $98°C$ temperature results separately. The overall classification accuracy of this data into the two damage regions was 89% and 88% for the $41°C$ and $98°C$ temperature results respectively.

It was further demonstrated that periodic BTT results may be archived, allowing the relevant blade condition to be monitored over extended periods of time. This archiving approach relies on individual results that are similarly classified to be combined over time as more BTT results become available. All the aforementioned implementations demonstrate the extensive possibilities of the proposed hybrid approach, therefore motivating why this may be an attractive solution in for the use in industry. Determining whether a blade damage threshold has been reached adopting this approach may certainly assist with the CBM of turbomachines, therefore avoiding unnecessary downtime while also ensuring that a more accurate indication of blade specific conditions are known.

Chapter 6

Conclusion and Recommendations

6.1 Conclusion

Industry is increasingly confronted by ageing turbomachines prone to unexpected and catastrophic failure. This raises questions with regards to the safety and optimal outage planning of these turbomachines. LP turbomachine blades were recognised as a particularly high risk component due to its susceptibility to fatigue blade damage and the possibility of unexpected failure. BTT was noted as a promising VCM technique to monitor these blades and provide an early warning of critical blade conditions. BTT offers the ability to monitor all the blades in a stage of a turbomachine while also being a non-intrusive and non-contact methodology. Diamond et al. [2015], however, highlighted that there is no consensus in published literature as to which BTT attains the highest accuracy, mainly due to the utmost difficulty associated with validating these results. The purpose of this research is therefore to advance the state of the art in BTT technology into a stochastic hybrid approach, used for the identification and classification of turbomachine blade damage. This stands in stark contrast to the vast majority of current BTT research where purely data-driven approaches are used, most of them being deterministic in nature. This hybrid approach uses the outputs of a recently developed BTT technique based on BLR and a FEM modal analysis. The hybrid implementation thus consists of a data-driven (BTT) and a physics-based approach (FEA) as proposed by Mishra et al. [2014]. The use of a hybrid approach aims to alleviate the disadvantages of the individual analysis types while conserving their advantages. The aim of this research was therefore to implement and test the performance of the proposed hybrid approach in identifying and classifying blade damage. The detailed summary and conclusion of the research outputs follows.

An experimental rotor setup was used during the BTT investigations, therefore providing *authentic* data for the use in the proposed hybrid approach. Two main categories of formal BTT investigations were performed, namely: relative natural frequency tracking with and without the effects of temperature. The constant temperature tests were performed at ambient temperature and merely consisted of the introduction of incremental discrete blade damage to a particular rotor blade. The variable temperature tests were performed at $41°C$ and $98°C$ blade surface temperatures respectively. These tests aimed to determine to what extent the effects of temperature would affect the performance of the proposed BTT technique and therefore the performance of the hybrid approach. The temperature tests also relied on incremental discrete blade damage being introduced to a test blade. For both these categories of BTT investigations, the operational conditions of the rotor setup induced the first resonance (bending mode shape) of the blades. This enabled the BTT data to be captured for a number of the same tests corresponding to the same discrete damage increment. The stochastic nature of the BTT technique based on BLR allowed confidence intervals to be established, thus permitting uncertainty to be quantified for the resultant vibrational characteristics. The natural frequencies of the blades were computed after performing the feature extraction of the associated blade amplitude and phase information. Tracking the changes in the mean natural frequencies between each damage increment enabled a certain level of blade damage to be associated with a particular natural frequency. In some instances, the mean change in the natural frequency between two damage increments was reported as less than 0.2Hz, therefore indicating that small changes in the blade condition could be detected using the proposed BTT technique. It was, however, discussed that tracking the change in the natural frequency of a particular blade this way presented a few challenges. Firstly, tracking the changes in the natural frequencies this way results in a blade-specific analysis, therefore lacking generality when comparing different blades to one another. Secondly, this natural frequency tracking process relied on a number of the same tests to be performed at the same damage increment in order to establish a mean of the results.

The implementation of a stochastic FEM modal analysis aimed to address the first issue associated with the natural frequency tracking process. The use of the FEM modal analysis enabled a projection of the possible blade conditions to be established. The variation in the material properties, discrete crack geometry and centrifugal load parameters resulted in a stochastic analysis. It was shown that blade *twist* occurred for bending modes 2 and 3 as the discrete damage was increased. However, the research only focused on bending mode 1. For both categories of BTT tests (with and without the effects of temperature) it was found that these results were in agreement with regards to how the natural frequencies decreased as the discrete blade damage increased. As expected, the natural frequencies extracted from the BTT temperature tests were substantially lower at the higher temperatures. It was therefore decided that it would be sensible to track the changes in the natural frequencies as relative quantities. Performing the natural frequency tracking as relative quantities further proved to ensure the generality of the *damage identification* process. The relative changes in the natural frequencies from the undamaged, or reference states, of the relevant blades were computed to infer the degree discrete damage as part of a probabilistic damage identification procedure. A probabilistic damage threshold for the damage identification procedure was proposed based on the following question: *What is the probability that the relative change in the natural frequency of the test blade is as large as what the FEM modal analysis (at a chosen discrete damage size) projected it to be?* This probabilistic damage identification procedure was demonstrated for various scenarios, therefore demonstrating the ability of the hybrid approach to infer the degree of blade damage for various scenarios.

The fact, however, still remained that only a single BTT measurement may be possible at a time for practical applications. A lot of confidence needed to be placed on this single measurement to determine the blade conditions. The direct comparison of this single point to the FEM results may give a rough indication of where this point lies on the relative damage tracking projection. The implementation of a *damage classification* process, therefore aimed to address the second aforementioned issue associated with the natural frequency tracking. The use of a *K-means clustering* implementation was proposed to classify the blade damage according to the associated amplitude and natural frequency values. Again, it should be reiterated that a number of these clustering methodologies exist. The K-means clustering implementation was merely used to demonstrate the intended classification process [Mishra et al., 2014]. It was discussed that the projected FEM natural frequency results could be used to initiate clusters and cluster centroids as part of this K-means clustering implementation. The BTT amplitude and natural frequency results were then classified to a cluster with the nearest centroid. This enabled distinct clusters of points to be formed which corresponded to a certain damage region. This allowed the individual BTT points to be classified according to its associated level of damage. The decision whether a damage threshold was reached, was then solely based on the classification of the individual points in their associated clusters.

The results of the BTT investigation that did not consider the effects of temperature were clustered according to non-severe, mid-severity and severe damage classification regions. The overall accuracy of this implementation was found to be 78%. However, it was concluded that the accuracy would improve significantly if only two damage regions were considered. The results of the BTT investigation that considered the effects of temperature were thus clustered according to non-severe and severe damage classification regions. It was further discussed that this clustering could be done by *combining* the various temperature results (this required further scaling) or *separately*. The overall classification accuracies for the BTT temperature investigation were 85.5%, 89% and 88% for the combined, $41°C$ and $98°C$ results respectively. As previously mentioned, the choice of whether a damage threshold was reached was based on the damage classification of a specific BTT measurement. However, as indicated by the overall accuracies of the clustering, there is certainly a chance that the classification of a particular measurement could be incorrect. For this reason, it was proposed that the *damage classification* should be done in tandem with the *damage identification* process. The proposed hybrid approach intentionally ensures that multiple pieces of evidence are always available in order to determine whether a blade damage threshold is reached. Furthermore, the prediction accuracy of the hybrid approach could potentially improve as more BTT data becomes available.

Overall, it may be concluded that the use of BTT for blade condition monitoring has many advantages. The proposed BTT technique based on BLR overcomes some of the difficulties involved with processing BTT data and the use of an FEA may further alleviate a degree of uncertainty with regards to some of these difficulties. Throughout this research, the fusion of the results from the various analyses consistently provided a more confident indication of the condition of the test blade, resulting in supporting evidence of whether a practical maintenance decision should be made. An inspection of blades that are most likely damaged may thus be a good initial starting point for the hybrid approach in industry. This inspection will assist in establishing a known reference condition that BTT measurements may be compared to. Thereafter the proposed hybrid approach aims to provide evidence, with foreseeable confidence, of whether a turbomachine outage should be scheduled. Ultimately, the use of this hybrid approach aims to provide a road-map to inch a step closer to the much eluded topic of the RUL estimation of turbomachines.

6.2 Contributions

This study consists of various investigations and implementations as part of a hybrid CBM approach. It is therefore important to clearly define the contributions of this study. The following points recapitulate the main contributions of this research:

- A hybrid approach is proposed for the identification and classification of turbomachine blade damage. This hybrid approach uses the outputs of a recently developed BTT technique based on BLR and a FEM modal analysis. The main contributions of this study are therefore related to the implementation of this hybrid approach. This hybrid approach offers the following potential with regards to the damage identification and classification of turbomachine blades:
  - *Damage identification:* Small changes in the blade natural frequencies were tracked as relative quantities. The results from the FEM modal analysis were used to project expected blade conditions, therefore enabling a probabilistic damage threshold to be established, which corresponds to a certain size of discrete blade damage. The proposed relative natural frequency tracking process demonstrated that it was general enough to still be applicable under the effects of varying temperature. The idea that the blade damage threshold could be a probabilistic quantity based on a stochastic hybrid approach was presented and demonstrated.
  - *Damage classification:* An unsupervised clustering technique (K-means clustering) was used to classify the BTT measurements into various damage severity groups. The use of the FEM modal analysis natural frequency results for the initialisation of this clustering approach was proposed and demonstrated. This initialisation enabled a single BTT measurement to be used in the clustering, as opposed to performing BTT tests in batches. The damage classification procedure also considered the effects of varying blade temperatures. Various strategies were tested to account for these effects. The proposed K-means clustering technique demonstrated that it was possible to distinguish between result-sets with different temperatures.
- The possibility of combining the BTT results was proposed and demonstrated for the long-term archiving of this data. This archiving proved that the proposed hybrid approach could be used for the long-term condition monitoring of turbomachine blades.
- Although the BTT BLR analyses were not part of the contribution of this study, various functions / algorithms needed to be implemented for the BTT pre- and post-processing. This included: the ToA extraction, synchronisation and the use of a MCS to derive the amplitude and phase of the blade during a specific revolution, therefore enabling these values to be calculated as probabilistic quantities. Furthermore, a feature extraction process was proposed and implemented in order to derive the natural frequencies of the blades.

6.3 Recommendations and Future Work

This research project demonstrated the use of a hybrid and stochastic approach for the identification and classification of discrete blade damage. However, a number of recommendations need to be made for future work. These recommendations are discussed below:

- The proposed hybrid methodology should be tested on *natural* cracks resulting from fatigue blade damage. This applies to the FEM modal analysis and BTT testing. It was mentioned that it would be difficult to initiate and propagate cracks in an experimental setup, however, future work could possibly consider implementing and testing the hybrid approach on actual turbomachines in the relevant industry.
- The proposed methodology should be tested on a wider range of operating conditions. This includes different operating speeds and a more in-depth investigation of the temperature effects. Further investigations of the temperature effects should consider a greater range of temperatures and propose how the data should be categorised according to different temperature ranges. A more controlled procedure to heat the blades is therefore required. This procedure would require the experimental setup to be modified. It is proposed that the compressed air supply should also be heated to minimise the cooling effect of the blades during testing.
- Different blades should also be tested in future work. This will help to further establish the robustness and generality of the proposed hybrid methodology. Again, it is recommended that the proposed hybrid methodology should be implemented and tested on an actual turbomachine where each stage of the turbine has different blades.
- Different clustering or machine learning techniques should be tested as possible blade damage classification techniques. The possibility of extracting more distinguishable features from the BTT data and the FEM modal analysis should be investigated. This would require a CFD analysis where the fluid-flow interaction on the turbomachine blade is accounted for. The damage classification should also incorporate anomaly detection schemes.
- The sensitivity of the performance of the proposed BTT technique to the DAQ sampling frequency was briefly discussed in this dissertation. Future work should investigate this in greater detail and make further recommendations as to what the minimum sampling frequency should be with regards to the rotor design (total number of blades) and operational speeds.
- Model updating should be incorporated in the FEM modal analysis, specifically for the use in industry where more complex considerations need to be incorporated. Model updating should be performed to take into account the effects of specific operating conditions, for example: temperatures, operational speeds and other loading conditions not considered during this research. The model updating will ensure that the FEA model accurately represents the actual operating conditions. This was not done for the particular FEM modal analysis in this study, due to the aim of ensuring that the hybrid approach is as simple and general as possible.
- Section 4.4 proposed variations in the model parameters to incorporate uncertainty in the FEM modal analysis. These parameters were varied according to random samples drawn from a chosen variation range. In practise, it is recommended that this variation range is determined in a more controlled manner. For example, the material of the specific turbomachine blades should be exposed to different operating conditions (for example, temperatures). The variation of the material properties under these conditions could then be quantified and incorporated in the FEM modal analysis to model uncertainty.

The aforementioned recommendations clearly put a lot of emphasis on testing the proposed hybrid methodology on actual turbomachines. The author believes that this will be the best way to test the performance of the proposed hybrid methodology as well as gaining further insight into specific areas where the methodology could be improved.

References

B. Al-Bedoor. Blade vibration measurement in turbo-machinery: Current status. *The Shock and Vibration Digest*, 34(6):455–461, 2002.

B. Al-Najjar. A maintenance model for identification, quantification and elimination of losses in companies profitability: Application examples. In *22nd International Congress Condition Monitoring and Diagnostic Engineering Management*. Fundación Tekniker, 2009.

B. Al-Najjar and I. Alsyouf. Enhancing a company's profitability and competitiveness using integrated vibration-based maintenance: A case study. *European Journal of Operational Research*, 157(3): 643–657, 2004.

H. Andre, F. Girardin, A. Bourdon, J. Antoni, and D. Rémond. Precision of the IAS monitoring system based on the elapsed time method in the spectral domain. *Mechanical Systems and Signal Processing*, 44(1):14–30, 2014.

D. Arthur and S. Vassilvitskii. K-means++: The advantages of careful seeding. In *Proceedings of the Eighteenth Annual ACM-SIAM Aymposium on Discrete Algorithms*, pages 1027–1035. Society for Industrial and Applied Mathematics, 2007.

G. Battiato, C. M. Firrone, and T. M. Berruti. Forced response of rotating bladed disks: Blade tip-timing measurements. *Mechanical Systems and Signal Processing*, 85:912–926, 2017.

C. Booysen. Fatigue life prediction of steam turbine blades during start-up operation using probabilistic concepts. Masters dissertation, University of Pretoria, Pretoria (SA), 2014.

C. Booysen, P. S. Heyns, M. P. Hindley, and R. Scheepers. Fatigue life assessment of a low pressure steam turbine blade during transient resonant conditions using a probabilistic approach. *International Journal of Fatigue*, 73:17–26, 2015.

R. Branco, F. Antunes, and J. Costa. A review on 3D-FE adaptive remeshing techniques for crack growth modelling. *Engineering Fracture Mechanics*, 141:170–195, 2015.

J. C. Brits. An experimental and stochastic approach to estimate the fatigue crack life of a turbomachinery blade using finite element modelling. Masters dissertation, University of Pretoria, Pretoria (SA), 2016.

R. G. Budynas and J. K. Nisbett. *Shigley's Mechanical Engineering Design*. McGraw-Hill, New York, 9th edition, 2011.

I. B. Carrington, J. R. Wright, J. E. Cooper, and G. Dimitriadis. A comparison of blade tip timing data analysis methods. *Proceedings of the Institution of Mechanical Engineers, Part G: Journal of Aerospace Engineering*, 215(5):301–312, 2001.

C. Church. Turbomachine internal pressure and blade response modelling. Masters dissertation, University of Pretoria, Pretoria (SA), 2015.

R. Cookson, K. Armstrong, M. Howard, P. Pilidis, and K. Ramsden. Mechanical integrity of gas turbines. Technical report, Cranfield, England, 2001. doi:SME/PPA/RAC/0937.

J. Cooper. Comparison of some time-domain-system identification techniques using approximate data correlations. *International Journal of Analytical and Experimental Modal Analysis*, 4:51–57, 1989.

Cross Validated. Distribution of difference between two normal distributions, 2015. URL https://stats.stackexchange.com/questions/186463/distribution-of-difference-between-two-normal-distributions.

G. Das, S. G. Chowdhury, A. K. Ray, S. K. Das, and D. K. Bhattacharya. Turbine blade failure in a thermal power plant. *Engineering Failure Analysis*, 10(1):85–91, 2003.

D. H. Diamond, P. S. Heyns, and A. J. Oberholster. A novel technique for estimating synchronous turbomachinery blade vibration from blade tip timing data. Master's thesis, University of Pretoria, 2014.

D. H. Diamond, P. S. Heyns, and A. J. Oberholster. A comparison between three blade tip timing algorithms for estimating synchronous turbomachine blade vibration. pages 215–225. Springer, 2015.

D. H. Diamond, P. S. Heyns, and A. J. Oberholster. Online shaft encoder geometry compensation for arbitrary shaft speed profiles using Bayesian regression. *Mechanical Systems and Signal Processing*, 81:402–418, 2016.

EPRI. Survey of steam turbine blade failures. Technical report CS-3891, Palo Alto, CA, 1985.

EPRI. Steam turbine blade failure root cause analysis guide. Technical Report 1014137, Palo Alto, CA, 2008.

EPRI. Field demonstration of low-pressure turbine blade stress monitoring. Technical Report 1024665, Palo Alto, CA, 2012.

G. Forbes and R. Randall. Simulated gas turbine casing response to rotor blade pressure excitation. In *5th Australasian Congress on Applied Mechanics (ACAM 2007)*, volume 1. Engineers Australia, 2007.

G. Forbes and R. Randall. Non-contact gas turbine blade vibration measurment from casing pressure and vibration signals-a review. In *Proceedings of the 8th IFToMM International Conference on Rotordynamics*. TBA, 2010.

G. L. Forbes and R. B. Randall. Estimation of turbine blade natural frequencies from casing pressure and vibration measurements. *Mechanical Systems and Signal Processing*, 36(2):549–561, 2013.

J. Gallego-Garrido, G. Dimitriadis, I. B. Carrington, and J. Wright. A class of methods for the analysis of blade tip timing data from bladed assemblies undergoing simultaneous resonances—Part II: Experimental validation. *International Journal of Rotating Machinery*, 2007, 2007a.

J. Gallego-Garrido, G. Dimitriadis, and J. R. Wright. A class of methods for the analysis of blade tip timing data from bladed assemblies undergoing simultaneous resonances—Part I: theoretical development. *International Journal of Rotating Machinery*, 2007, 2007b.

A. A. Gubran and J. K. Sinha. Shaft instantaneous angular speed for blade vibration in rotating machine. *Mechanical Systems and Signal Processing*, 44(1):47–59, 2014.

S. Heath. A new technique for identifying synchronous resonances using tip-timing. *Rolls-Royce PLC-Report*, 1999.

M. Á. Herrador and A. G. González. Evaluation of measurement uncertainty in analytical assays by means of Monte-Carlo simulation. *Talanta*, 64(2):415–422, 2004.

A. K. Jardine, D. Lin, and D. Banjevic. A review on machinery diagnostics and prognostics implementing condition-based maintenance. *Mechanical Systems and Signal Processing*, 20(7): 1483–1510, 2006.

M. Jono. Fatigue damage and crack growth under variable amplitude loading with reference to the counting methods of stress–strain ranges. *International Journal of Fatigue*, 27(8):1006–1015, 2005.

B. Kostić and M. Gül. Vibration-based damage detection of bridges under varying temperature effects using time-series analysis and artificial neural networks. *Journal of Bridge Engineering*, 22 (10):04017065, 2017.

R. Kudelski and R. Szczepanik. In-flight early detection of cracks in turbine aero-engine compressor blades. In *12th World Conference on Non-Destructive Testing, Amsterdam, April*, pages 23–28, 1989.

A. Kurkov and H. Dhadwal. Simultaneous optical measurements of axial and tangential steady-state blade deflections. 1999.

C. P. Lawson and P. C. Ivey. Tubomachinery blade vibration amplitude measurement through tip timing with capacitance tip clearance probes. *Sensors and Actuators A: Physical*, 118(1):14–24, 2005.

J. Lee, F. Wu, W. Zhao, M. Ghaffari, L. Liao, and D. Siegel. Prognostics and health management design for rotary machinery systems—reviews, methodology and applications. *Mechanical Systems and Signal Processing*, 42(1):314–334, 2014.

L. Liao and F. Köttig. Review of hybrid prognostics approaches for remaining useful life prediction of engineered systems, and an application to battery life prediction. *Transactions on Reliability*, 63(1):191–207, 2014.

S. Madhavan, R. Jain, C. Sujatha, and A. S. Sekhar. Vibration based damage detection of rotor blades in a gas turbine engine. *Engineering Failure Analysis*, 46:26–39, 2014.

MathWorks. Kmeans, 2017. URL https://www.mathworks.com/help/stats/kmeans.html.

T. H. McCloskey, R. B. Dooley, and W. P. McNaughton. Turbine steam path damage: Theory and practice. *Palo Alto, California*, 94304:8–13, 1999.

M. Mishra, J. Saari, D. Galar, and U. Leturiondo. Hybrid models for rotating machinery diagnosis and prognosis estimation of remaining useful life. Technical report, Luleå University of Technology, May 2014.

Y. Murakami and K. Miller. What is fatigue damage? A view point from the observation of low cycle fatigue process. *International Journal of Fatigue*, 27(8):991–1005, 2005.

M. Neale and B. Woodley. A guide to the condition monitoring of machinery. Report, British Department of Industry, 1978.

A. J. Oberholster and P. S. Heyns. Online condition monitoring of axial-flow turbomachinery blades using rotor-axial Eulerian laser Doppler vibrometry. *Mechanical Systems and Signal Processing*, 23(5):1634–1643, 2009.

R. B. Randall. *Vibration-based condition monitoring: industrial, aerospace and automotive applications*. John Wiley & Sons, 2011.

A. R. Rao and B. Dutta. In situ detection of turbine blade vibration and prevention. *Journal of Failure Analysis and Prevention*, 12(5):567–574, 2012.

A. R. Rao and B. Dutta. Blade vibration triggered by low load and high back pressure. *Engineering Failure Analysis*, 46:40–48, 2014.

J. Rao. Application of fracture mechanics in the failure analysis of a last stage steam turbine blade. *Mechanism and Machine Theory*, 33(5):599–610, 1998.

J. Rao. *Turbomachine blade vibration*. New Age International, 2010.

B. R. Resor, M. W. Trethewey, and K. P. Maynard. Compensation for encoder geometry and shaft speed variation in time interval torsional vibration measurement. *Journal of Sound and Vibration*, 286(4):897–920, 2005.

G. Rigosi, G. Battiato, and T. M. Berruti. Synchronous vibration parameters identification by tip timing measurements. *Mechanics Research Communications*, 79:7–14, 2017.

A. Rivola and M. Troncossi. Zebra tape identification for the instantaneous angular speed computation and angular resampling of motorbike valve train measurements. *Mechanical Systems and Signal Processing*, 44(1):5–13, 2014.

R. Robinson. System for measuring rotor vibration. Patent US Patent No. 3654803, 1970.

P. Russhard. The rise and fall of the rotor blade strain gauge. In *Vibration Engineering and Technology of Machinery*. Springer, 2015.

R. Rzadkowski, E. Rokicki, L. Piechowski, and R. Szczepanik. Analysis of middle bearing failure in rotor jet engine using tip-timing and tip-clearance techniques. *Mechanical Systems and Signal Processing*, 76:213–227, 2016.

D. Sabbatini, B. Peeters, T. Martens, and K. Janssens. Data acquisition and processing for tip timing and operational modal analysis of turbomachinery blades. In *AIP Conference Proceedings*, volume 1457, pages 52–60. AIP, 2012.

B. Salhi, J. Lardies, and M. Berthillier. Identification of modal parameters and aeroelastic coefficients in bladed disk assemblies. *Mechanical Systems and Signal Processing*, 23(6):1894–1908, 2009.

G. A. Seber. *Multivariate observations*. John Wiley & Sons Inc, Hoboken, NJ, 1984.

J. Sikorska, M. Hodkiewicz, and L. Ma. Prognostic modelling options for remaining useful life estimation by industry. *Mechanical Systems and Signal Processing*, 25(5):1803–1836, 2011.

P. Sundin, N. Montgomery, and A. Jardine. Pulp mill on-site implementation of CBM decision support software. In *Proceedings of International Conference of Maintenance Societies*, Melbourne, Australia, 2007.

P. Tappert, A. von Flotow, and M. Mercadal. Autonomous PHM with blade-tip-sensors: algorithms and seeded fault experience. In *Aerospace Conference*, volume 7, pages 7–3295. IEEE, 2001.

D. A. Tobon-Mejia, K. Medjaher, and N. Zerhouni. The ISO 13381-1 standard's failure prognostics process through an example. In *Prognostics and System Health Management Conference*, pages 1–12, Macau, China, 2010. IEEE.

P. Vlok, J. Coetzee, D. Banjevic, A. Jardine, and V. Makis. Optimal component replacement decisions using vibration monitoring and the proportional-hazards model. *Journal of the Operational Research Society*, 53(2):193–202, 2002.

K. Wagstaff, C. Cardie, S. Rogers, S. Schrödl, et al. Constrained k-means clustering with background knowledge. In *ICML*, volume 1, pages 577–584, 2001.

I. Y. Zablotskiy and Y. A. Korostelev. Measurement of resonance vibrations of turbine blades with the ELURA device. *Energomashinostroneniye,(USSR)*, (2):36–39, 1970.

M. Zielinski and G. Ziller. Noncontact vibration measurements on compressor rotor blades. *Measurement Science and Technology*, 11(7):847, 2000.

Appendix A

Logistics

A.1 Overview

The importance of recording specific information of the various stages of testing was noticed during this research. This was especially evident during the BTT experimental testing where an abundance of data-files were recorded for each stage of testing. It was therefore crucial to implement a sensible naming convention for the various data-sets. Appendix A elaborates on this naming convention while also giving a summary of the various BTT tests and the logistics surrounding these tests.

A.2 Project Logistics

Table A.1 shows the record of the various BTT investigative groups. This table highlights the logic behind progression of the various stages of BTT investigations. The dates of the tests were used in the naming convention of the various stages of testing. It is proposed to also use the dates in the naming convention in the practical implementation of the methodology in order to easily match certain measurements to a particular day's operational log.

Table A.1: Logistics of the BTT investigations.

Group	Stage	Type	Number of Tests	Date of Tests
Group I	I	Preliminary	14	23-02-2017
	II	Preliminary	12	06-03-2017
Group II	III	Preliminary	30	30-03-2017
	IV	Formal	72	04-04-2017
Group III	V	Preliminary	20	05-05-2017
	VI	Formal	200	13-06-2017

- *Group I:* This group of testing was essentially used for troubleshooting purposes. This preliminary testing was done over approximately two weeks, thus enabling further recommendations to be made with regards to the formal stages of testing. This also made the author familiar with various aspects of the BTT methodology, therefore assisting in formulating a road-map for further investigations.
- *Group II:* This group of testing commenced almost a month after *Group I*. The reason being that the hybrid methodology was conceptualised in this period, therefore giving a sense of what the formal investigative stages should consider. The various BTT signal processing and feature extraction algorithms were further refined during this period. The robustness of the chosen BTT technique was also tested.
- *Group III:* This group of testing specifically considered temperature effects and how these may affect the BTT results. The heating of the blades presented a few complications with regards to the experimental setup. As the blades were heated, they expanded and this resulted in contact between the blades and eddy current proximity probes. This group of testing therefore started with troubleshooting and a number of preliminary tests. For the formal stage of testing, a much greater number of BTT tests were conducted due to the fact that two temperature ranges were tested.

Appendix B

BTT Analysis

B.1 Experimental Testing

B.1.1 Experimental Setup

This section presents detailed design drawings (with corresponding labels and dimensions where necessary). Figure B.1 shows a detailed side-view of the experimental rotor setup, with the corresponding descriptions to the labels shown in Table B.1.

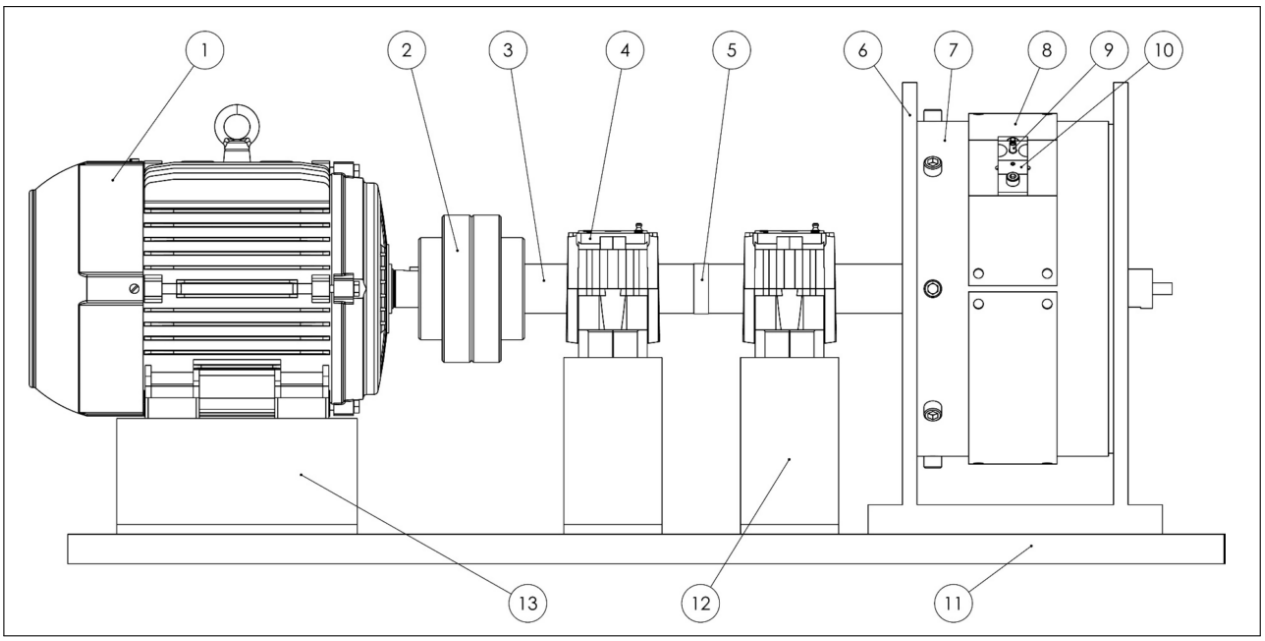

Figure B.1: Experimental rotor setup, adapted from [Church, 2015].

Table B.1: Part list of the experimental setup.

Part number	Part description
1	Electric motor (5.5kW)
2	Flexible shaft coupling
3	Tapered shaft
4	Plumber block with bearing
5	Zebra tape
6	Drum housing
7	Drum
8	Sensor mounting plate
9	Mounted sensor
10	Sensor mounting block
11	Test bench
12	Bearing mount
13	Motor mounting

Figure B.2 shows a detailed cross-sectional view of the rotor assembly, with the corresponding descriptions to the labels shown in Table B.2. This figure shows the attachment of the slip ring that was for the cabling of the strain gauges (power and acquisition) during *Stage III* of testing. The attachment of the rotor-hub to the tapered shaft is also shown. The compressed air supply nozzles, used to excite the blades during rotation, are shown in the upper left-hand corner.

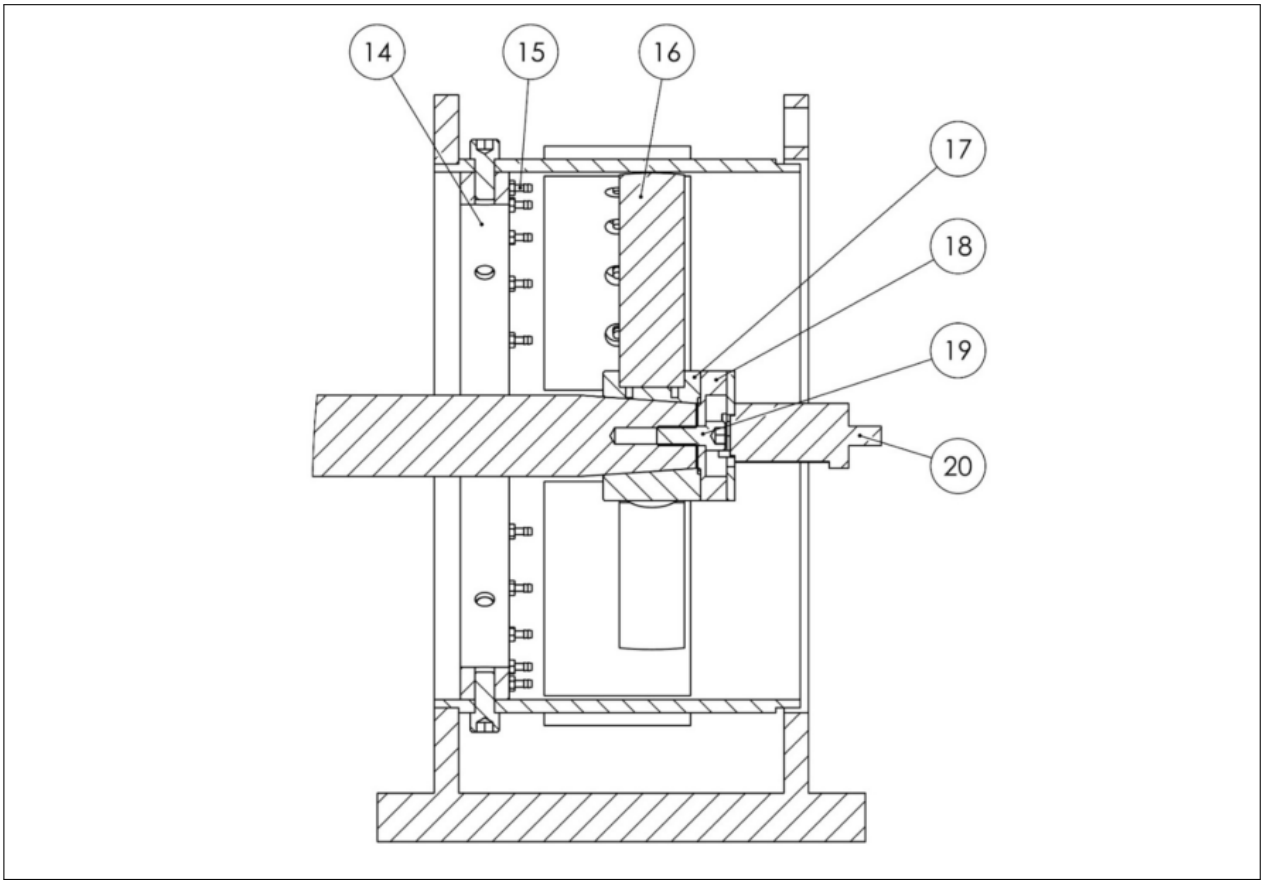

Figure B.2: Rotor cross-section with slip-ring, adapted from [Church, 2015].

Table B.2: Part list of the experimental setup.

Part number	Part description
14	Air jet attachment ring
15	Air jet nozzle
16	Rotor blade
17	Rotor blade attachment hub
18	Slip ring coupling
19	Slip ring coupling attachment bolt
20	Slip ring assembly

Figure B.3 shows the dimensions of the blades used during experimental testing. The blades were certainly not as large as some turbomachine blades, however, it was quite satisfying that the proposed BTT technique was able to track small changes in the natural frequencies of these blades. It is, however, recommended that future work should test the proposed BTT approach on different blades (different sizes, materials and damage properties).

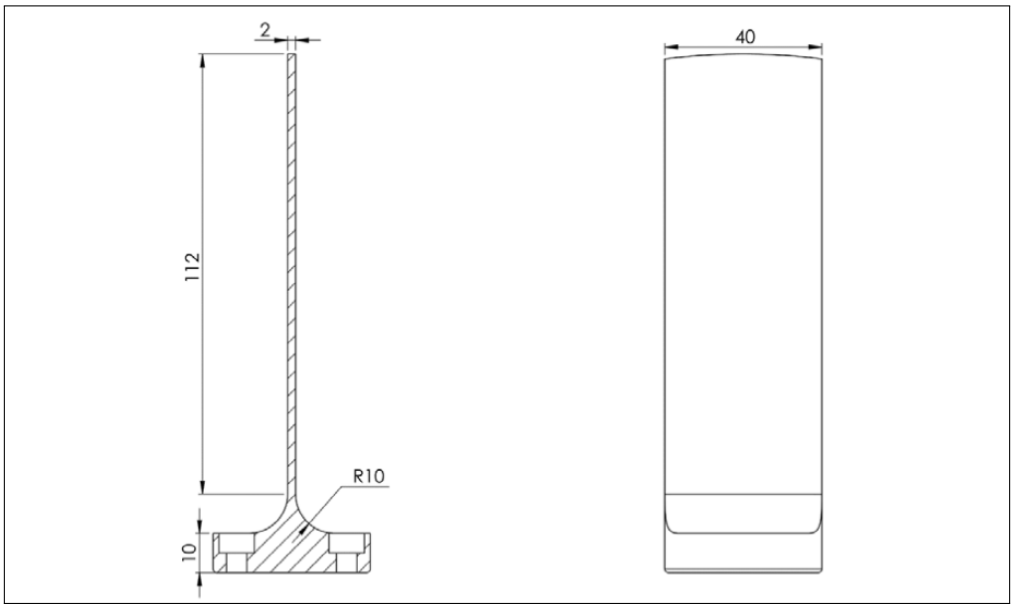

Figure B.3: Rotor blade dimensions, adapted from [Church, 2015].

B.1.2 Experimental Methodology

Campbell Diagram

Church [2015] stipulated that the Campbell diagram shown in Figure B.4 was generated using 11 pre-stress analyses as part of FEM modal analyses in the *ANSYS* commercial software environment. These analyses were done in order to determine the natural frequencies across the motor operational speed range of 0 RPM to 1400 RPM. Church [2015] further specified that a rotational speed boundary condition about the center of rotation was defined in these analyses. After the application of a pre-stress condition a FEM modal analysis could be performed, therefore allowing the blade natural frequencies to be determined at a particular speed.

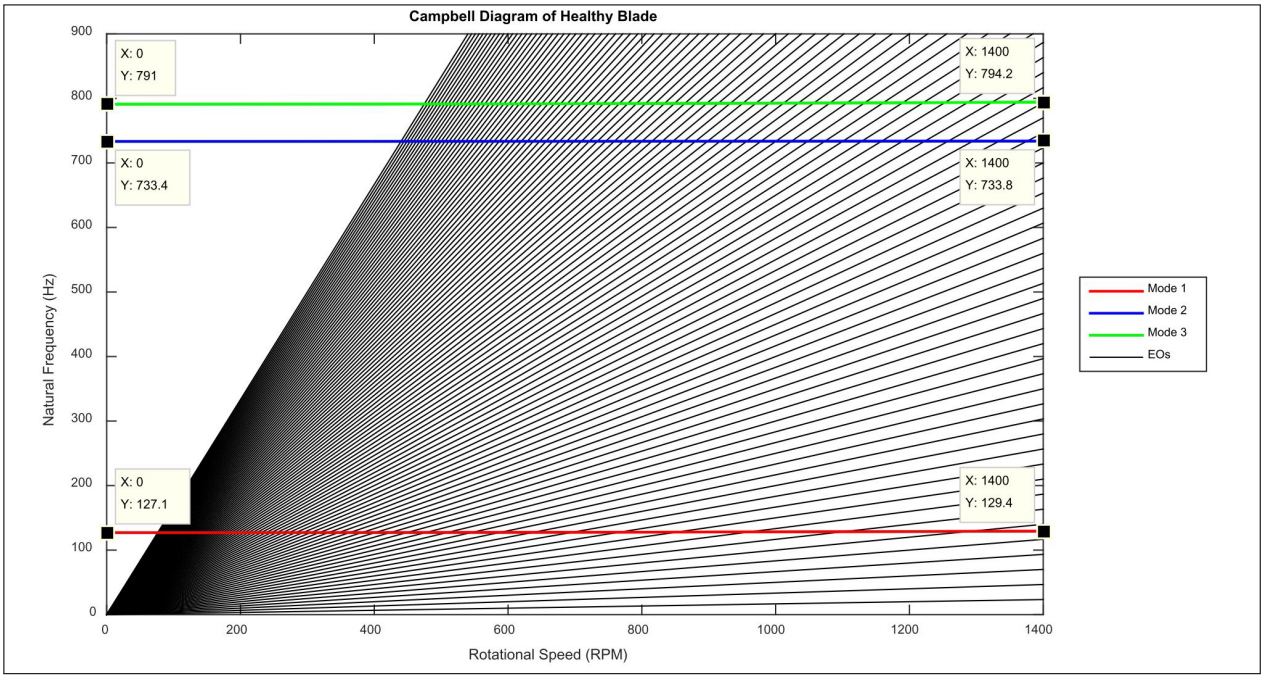

Figure B.4: Campbell diagram for a healthy blade showing the 100 EO lines, from [Church, 2015].

B.2 BTT Investigations

In this section a number of detailed figures from the BTT investigations are presented. These figures were omitted from the main report as they were considered to merely supplement the formal results from the various BTT investigative stages. These figures are presented according to the investigate group they represent and are summarised as follows:

- *Group I:* Preliminary Tests (as shown in Section B.2.1 of the Appendix and corresponds to Section 3.5.1 of the main report).
  - Figure B.5 shows the two-sets of results for the preliminary testing (*Stage II*) where discrete blade damage was introduced. This stage of testing aimed to determine whether the proposed BTT methodology was able to detect the increase in discrete blade damage.
  - Figure B.5a shows the natural frequency of the blade derived from the amplitude and phase features for each test. The solid vertical line indicates that the average natural frequency from these two features amongst all the tests was 114.2Hz. Figure B.5b indicates that the new average natural frequency of the test blade, due to a slight increase in the discrete damage, is 112.19Hz.
- *Group II:* Relative Natural Frequency Tracking (as shown in Section B.2.2 of the Appendix and corresponds to Section 3.5.2 of the main report).
  - Figure B.6 corresponds to Figure 3.25 in Section 3.5.2 of the main report. The purpose of this figure is to purely show all 72 derived amplitude and phase BTT result-sets from *Stage IV* of testing. Figure 3.25 showed the detail of how the mean natural frequencies due to the amplitude changed with an increase in the discrete crack size and where the associated amplitude features were. Figure 3.25 further indicated the locations of the extracted phase features for the various damage increments of blade 2 at resonance 1.
  - Figure B.7 shows the amplitude and natural frequency results of blade 2 at resonance 1. These features are plotted against one another to demonstrate how the blade amplitude or tip displacement changes as the natural frequency changes. The amplitude versus natural frequency plot in this figure corresponds to the points used in the clustering from Section 5.3.1. The amplitude versus discrete blade damage is also shown in Figure B.7
- *Group III:* Relative Natural Frequency Tracking with Temperature Effects (as shown in Section B.2.3 of the Appendix and corresponds to Section 3.5.3 of the main report).
  - Figure B.8 shows the various amplitude and natural frequency results for blade 3 at resonance 1. These results correspond to the BTT temperature tests outlined in Section 3.5.3 and the clustering results documented in Section 5.3.2 of the main report.
  - Figure B.8a shows the natural frequency and amplitude points specifically corresponding to the $41°C$ result-set. Figure B.8b shows the natural frequency and amplitude points specifically corresponding to the $98°C$ result-set. Both these figures indicate the multivariate normal distribution of these points for an increase in discrete blade damage.
  - Figure B.9 indicates the resultant classifications from the K-means clustering using three centroids for blade 3, at resonance 1 and at $98°C$. When comparing these points to the points shown in Figure B.9 it becomes clear that the overall performance of the K-means clustering using three centroids was poor. For this reason only two centroids were used to classify the blade damage as either non-severe or severe.
  - Figure B.10 shows the combined temperature results from *Stage VI* of BTT testing used to formulate Figure 5.11 (in Section 5.3.2) for the combined K-means clustering approach. Figure 5.11 clearly shows a large density of points grouped very close to one another in the higher natural frequency region.

B.2.1 Group I: Preliminary Tests

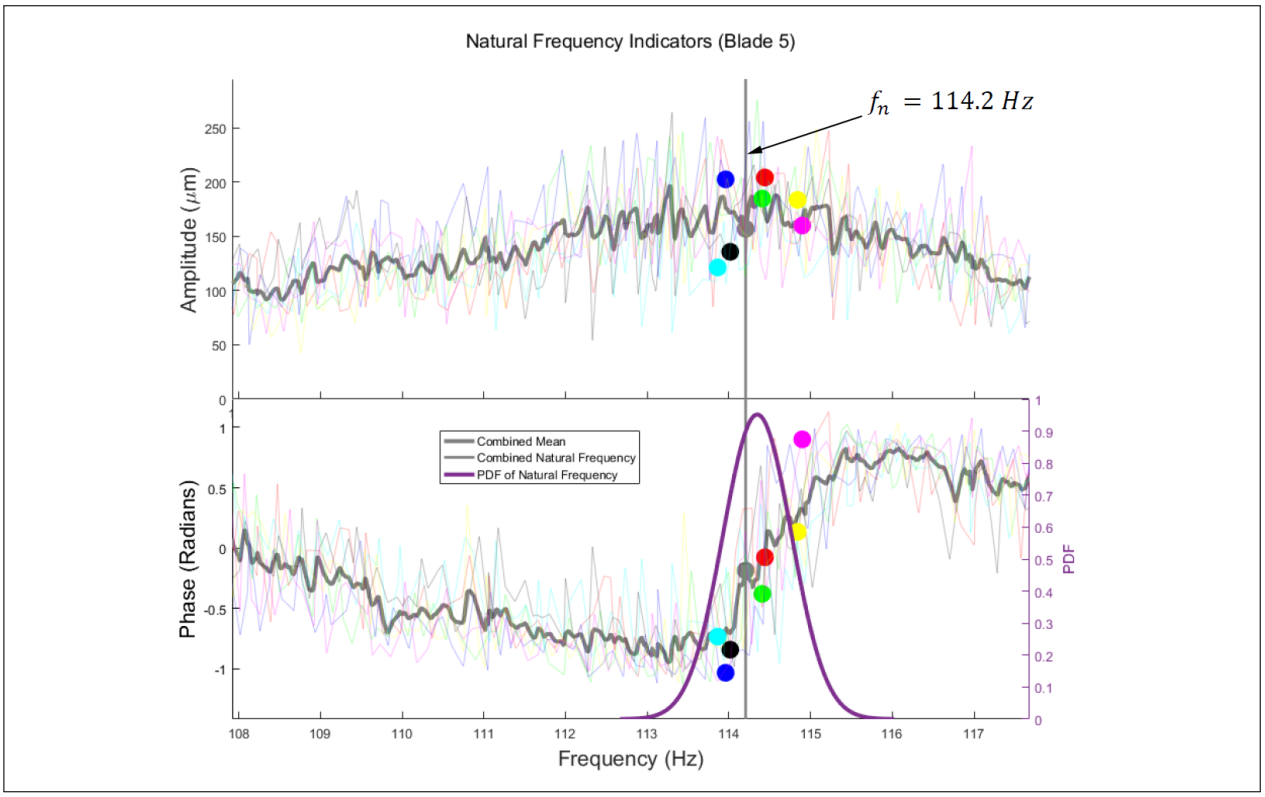

(a) Discrete blade damage at 10mm on either side of the test blade.

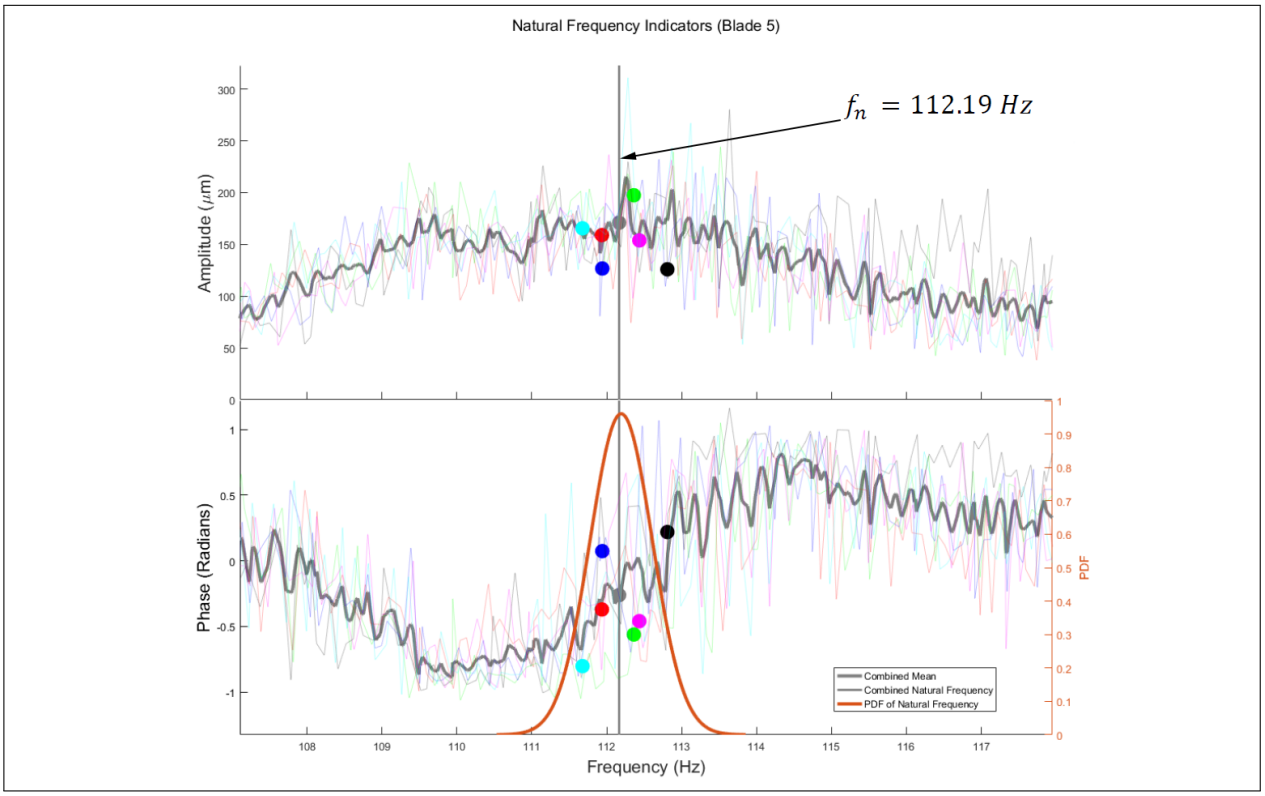

(b) Increased discrete blade damage at 11mm on either side of the test blade.

Figure B.5: Derived natural frequencies of the damaged test blade for the preliminary testing.

B.2.2 Group II: Relative Natural Frequency Tracking

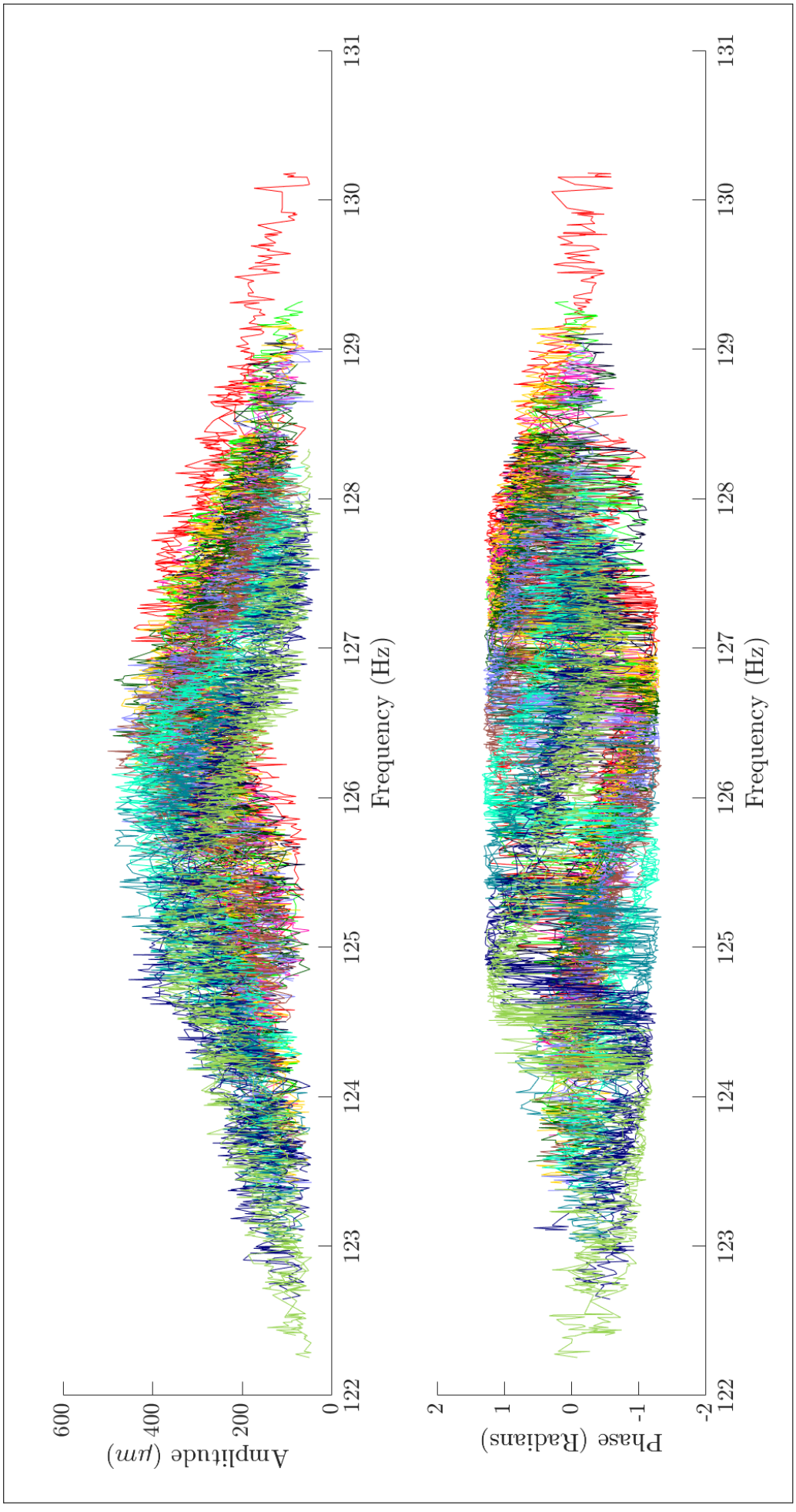

Figure B.6: Amplitude and phase results of *Stage IV* of testing, superimposed for the various tests and damage increments (blade 2, resonance 1).

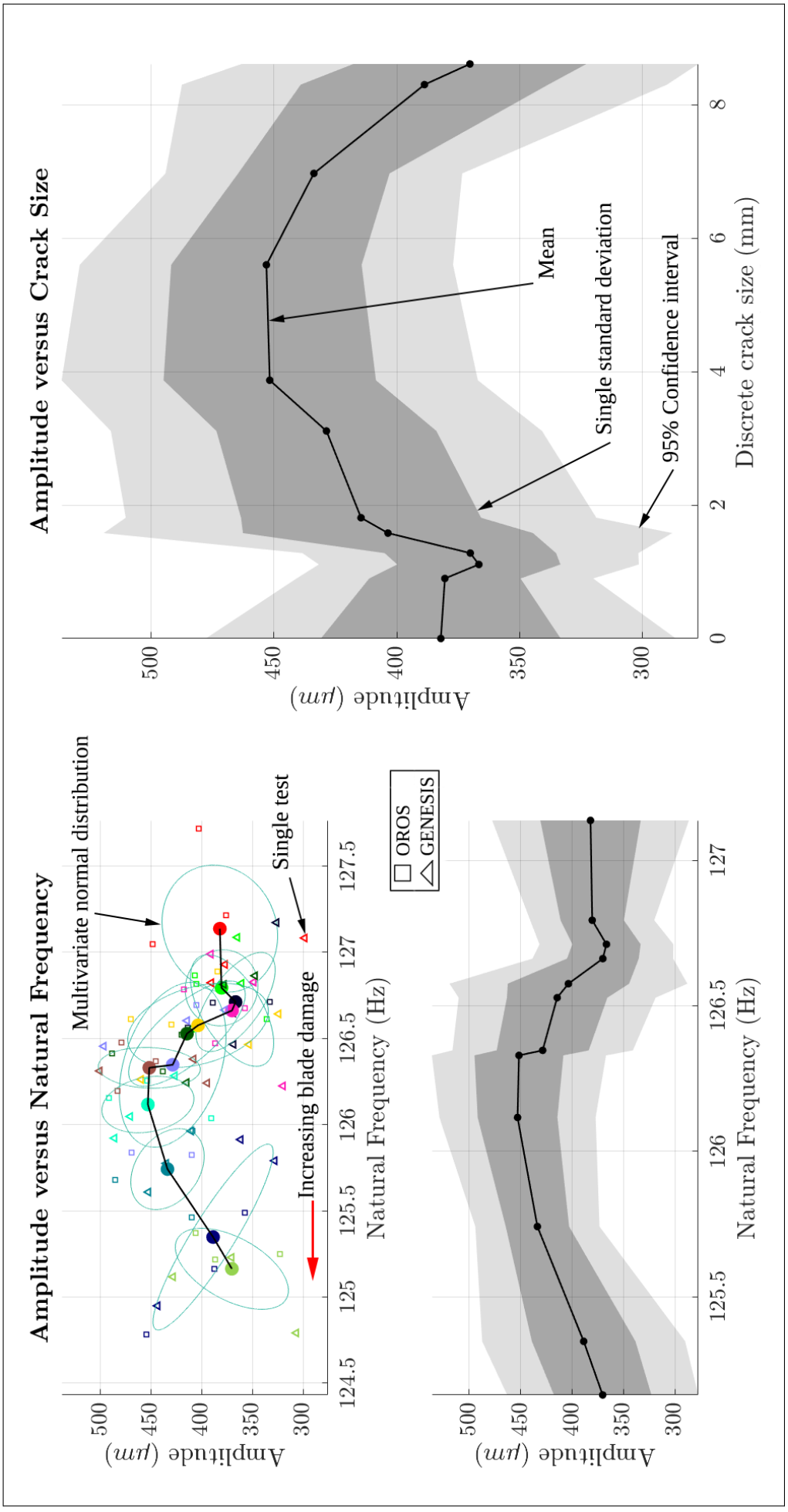

Figure B.7: Amplitude and natural frequency results of *Stage IV* of testing (blade 2, resonance 1).

B.2.3 Group III: Relative Natural Frequency Tracking with Temperature Effects

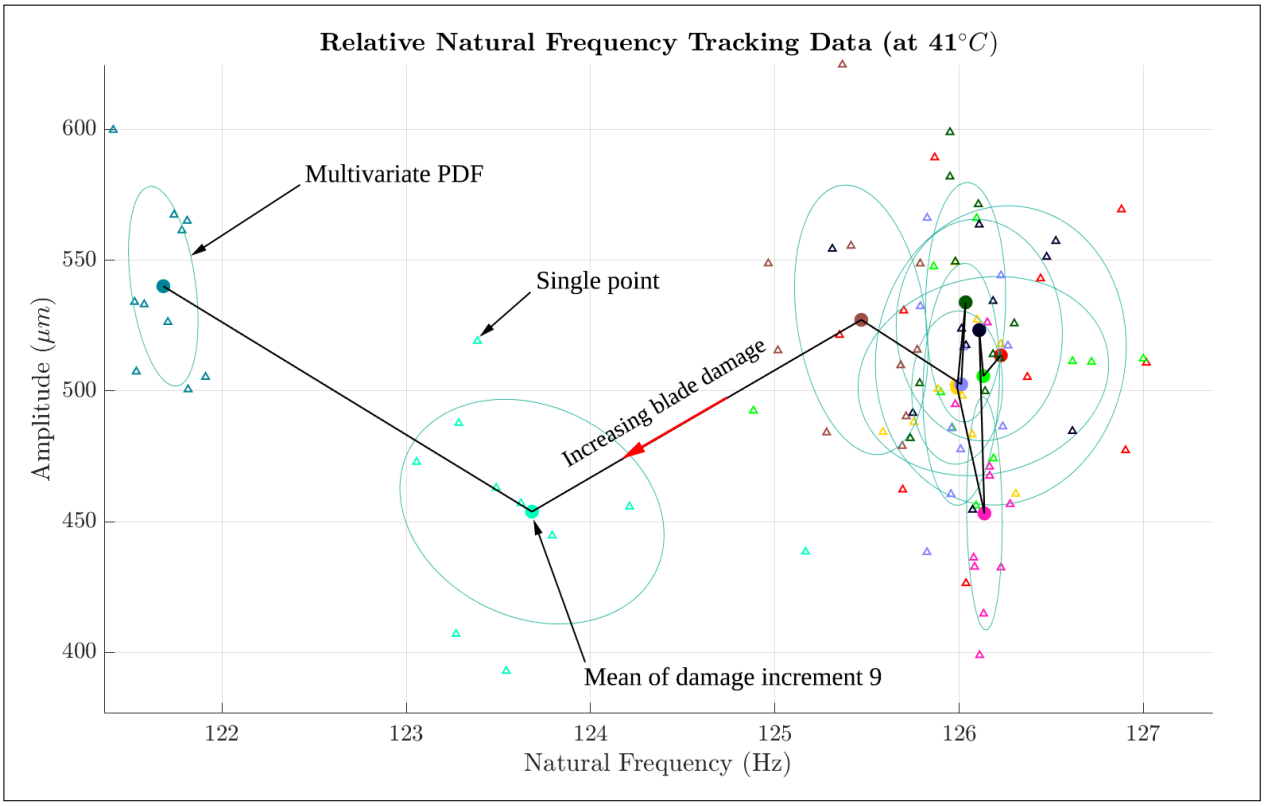

(a) *Stage VI* amplitude and natural frequency results (at 41°C).

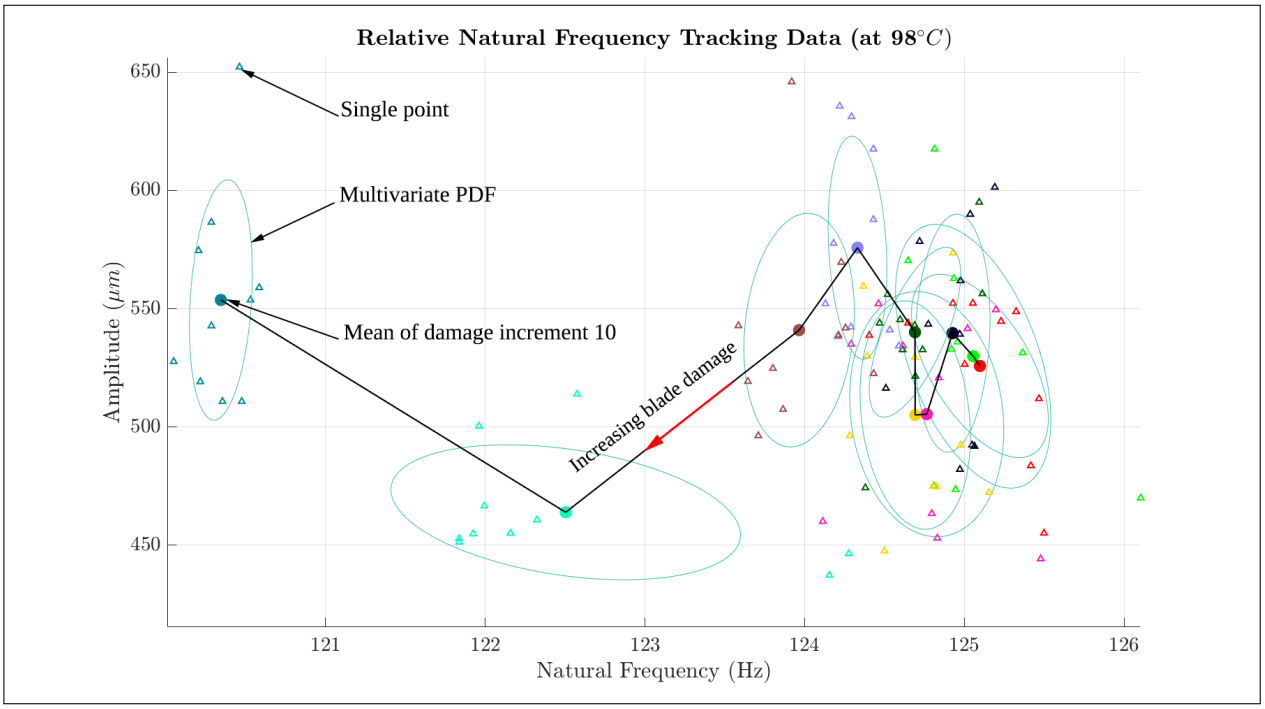

(b) *Stage VI* amplitude and natural frequency results (at 98°C).

Figure B.8: Amplitude and natural frequency results of *Stage VI* of testing (blade 3, resonance 1).

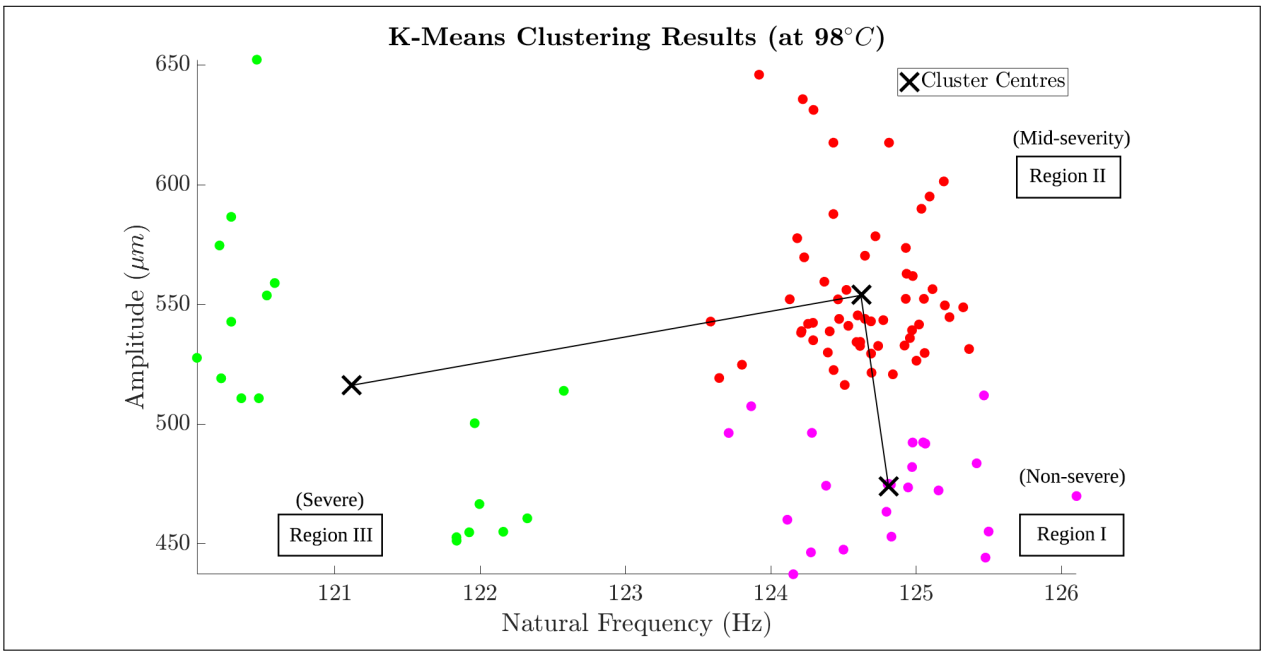

Figure B.9: *Stage VI* K-means clustering results using three centroids results (blade 3, resonance 1, at 98°C).

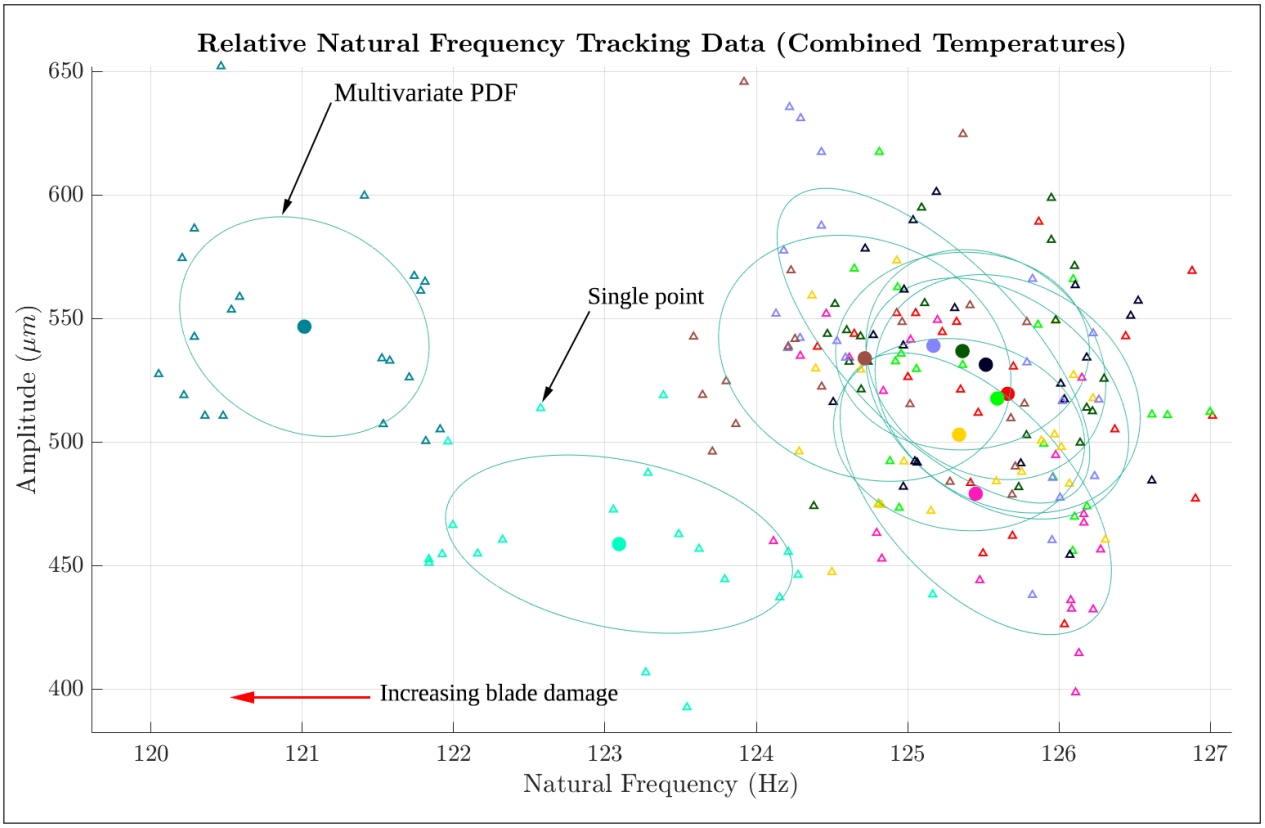

Figure B.10: *Stage VI* amplitude and natural frequency results for the combined temperatures (blade 3, resonance 1).

B.3 Damage Identification Probability Interpretations

This section provides further interpretations of the probabilistic damage threshold value, $X_{dt} = P(\delta_{damage} \leq 0)$, used in the damage identification procedure (Section 5.2.2, Chapter 5). As mentioned in Section 5.2.2, this probability is found from the CDF of δ_{damage}, with associated mean and variance as shown in Equation 5.5. The following detailed interpretations are given for different values / ranges of the probability derived from this CDF:

- $0 \leq P(\delta_{damage} \leq 0) < 0.5$: This range implies that the mean of the particular BTT batch has not crossed-over the mean of the prescribed FEM level. A very small probability, very close to 0, indicates that the predominant areas (within the 95% confidence intervals) of the two independent normal distributions are not close to one another. A probability that approaches 0.5 indicates that the predominant areas of the two independent normal distributions are close to one another (given that the mean of the BTT batch has not crossed-over the mean of the prescribed FEM level).
- $P(\delta_{damage} \leq 0) = 0.5$: This probability value implies that the two independent normal distributions are identical; i.e. the normal distribution of the BTT batch lies exactly on-top of the FEM normal distribution.
- $0.5 < P(\delta_{damage} \leq 0) \leq 1$: This range implies that the mean of the particular BTT batch has crossed-over the mean of the prescribed FEM level. A large probability, very close to 1, indicates that the predominant areas of the two independent normal distributions are not close to one another (given that the mean of the BTT batch has crossed-over the mean of the prescribed FEM level).